University of Southampton

Faculty of Environmental and Life Sciences

Ocean and Earth Science

Particle Flux, Carbon Sequestration and the Role of Mesoscale Spatial Variability in the Iceland Basin

by

Chelsey Adrianne Baker

ORCID ID 0000-0002-0840-2333

Thesis for the degree of Doctor of Philosophy

October 2019

University of Southampton

Abstract

Faculty of Environmental and Life Sciences

Ocean and Earth Science

Thesis for the degree of Doctor of Philosophy

Particle Flux, Carbon Sequestration and the Role of Mesoscale Spatial Variability in the Iceland Basin

by

Chelsey Adrianne Baker

Organic carbon sequestration is driven by the biological carbon pump (BCP), which transfers organic-rich biomass and detritus to the deep ocean, storing carbon on climatically significant timescales. The BCP exports 5 – 11 Gt C yr^{-1} globally into the interior ocean and 0.33 – 0.66 Gt C yr^{-1} reaches 2000 m depth. Understanding the functioning of the BCP, and the factors controlling the magnitude and composition of particle flux to the deep ocean in the current climate system, is crucial to detecting and predicting future changes. Records of deep ocean particle flux are usually limited to a single mooring in one location. Uniquely, this study utilises four sediment traps deployed below 2000 m in a mesoscale spatial array in the Iceland Basin (60 °N, 20 °W) from November 2006 to June 2008. In this thesis, the effects of spatial variability and particle flux composition on the magnitude of carbon sequestered in the deep ocean Iceland Basin will be investigated and the observed spatial variability in the context of upper ocean biological and physical processes will be explored.

In the first results chapter of this thesis, the flux of organic carbon to the deep ocean Iceland Basin is quantified for the first time. The mean annual particulate organic carbon (POC) flux to 2000 m in the Iceland Basin is 101.7 (± 12.3) mmol m^{-2} yr^{-1}, which is lower than the global average. The data indicate considerable mesoscale spatial variability, evidenced by differences in POC flux captured by the 4 sediment traps. Averaging POC fluxes over increasingly long temporal scales, decreases the magnitude of the observed mesoscale spatial variability, particularly for time scales > 1 month. The influence of localised spatial variability on observed POC fluxes should be considered when investigating particle fluxes at given locations, or using individual traps, for less than annual timescales. However, reassuringly, mesoscale spatial processes likely do not impact deep ocean annual carbon budgets derived from long-term time-series, such as at sustained observatories.

In the second results chapter of this thesis, I explore what controls spatial and intra-annual variability in carbon sequestration to the deep ocean Iceland Basin. The particle source regions of each sediment trap were estimated and used to explore how upper ocean biological spatial variability relates to deep ocean particle flux. Increases in POC flux coincide with increased biogenic silica fluxes and upper ocean diatom abundance, in line with previous literature, suggesting diatoms are a major contributor to deep ocean particle flux. The role of eddies on deep ocean particle flux is explored for periods with the greatest observed mesoscale variability. Four of the five case studies were found to be associated with periods of high eddy kinetic energy in the surface ocean above the trap location and increased biogenic silica fluxes suggesting deep ocean carbon fluxes may be influenced by mesoscale eddies.

In the third results chapter, I confirm the hypothesis that there is a regular annual sedimentation of Acantharian cysts to the deep ocean Iceland Basin in spring. Extremely high cyst fluxes were sampled, which allowed for improved estimates of cyst sinking rates, and POC and Strontium cyst content. Acantharian cysts can contribute significantly to the pre-spring bloom POC flux, and dominate the annual particulate Strontium flux in the Iceland Basin, with fluxes up to 2.50 mmol m^{-2} yr^{-1}. The role of celestite, rapid sedimentation and the viability of the Acantharian cysts in the Iceland Basin is explored to further the current understanding of the cyst reproductive strategy, as well as discussing the implications for deep ocean carbon sequestration and the Strontium cycle.

The composition of deep ocean particle flux, especially in terms of biomineral content and plankton community, is key to furthering our understanding of the factors controlling carbon sequestration in the deep ocean and can have important implications for other elemental cycles, such as Strontium. Further work is needed to determine the exact role of mesoscale eddies on deep ocean particle flux using data with greater spatial, temporal and vertical resolution.

Table of Contents

Table of Tables

Table of Figures

Research Thesis: Declaration of Authorship

Print name:	Chelsey Adrianne Baker

Title of thesis:	Particle Flux, Carbon Sequestration and the Role of Mesoscale Spatial Variability in the Iceland Basin

I declare that this thesis and the work presented in it are my own and has been generated by me as the result of my own original research.

I confirm that:

1. This work was done wholly or mainly while in candidature for a research degree at this University;
2. Where any part of this thesis has previously been submitted for a degree or any other qualification at this University or any other institution, this has been clearly stated;
3. Where I have consulted the published work of others, this is always clearly attributed;
4. Where I have quoted from the work of others, the source is always given. With the exception of such quotations, this thesis is entirely my own work;
5. I have acknowledged all main sources of help;
6. Where the thesis is based on work done by myself jointly with others, I have made clear exactly what was done by others and what I have contributed myself;
7. None of this work has been published before submission;

Signature:		Date:	

Acknowledgements

This work was funded by the Natural Environment Research Council (grant NE/L002531/1) and the Graduate School at the National Oceanography Centre.

I would like to express my gratitude to Richard Lampitt, Stephanie Henson and Anna Hickman for their excellent supervision, support and advice during my PhD and for allowing me to have the freedom explore different scientific avenues over the last four years. To Corinne P., Katsia P., Ed M., Matt C., Matt O., Bastian H. and Megan W. I would like to express my sincere thanks for training and assisting me with my PhD lab work. To Patrick M. for making an invaluable start to this project and for helpful discussions about the project. To Benoit E. for improving the backtracking code and helping me to run it. Thank you to all the people I have been on research cruises with who made them fun and enjoyable experiences, with a special mention to Rachel R. and our time in the container of fun!

I would also like to thank Kyle M. for introducing me to the UK Polar Network and providing me with the opportunity to grow as a leader and a person alongside my incredible co-president Anna B. To my wonderful office mates, Vlad M., Lucie D., Amber C. and Kyle M., thank you for filling the last few years with relentless laughter, weirdness and encouragement – stay fresh cheese bags! A special mention to Vlad for being a constant source of support, friendship and memes over the past four years – NOCS is not the same without you. To the members of the 'BE SOCIAL!' group for providing excellent distractions from PhD work, with a special mention to Callum F. and Manon D. To Charl, Bec and other friends and family, thank you for always supporting and encouraging me and reminding me that there is life outside of the ocean!

Thank you to my Auntie Lil and Uncle Graham who unknowingly started my journey into oceanography with a magazine article and who have supported me throughout my studies. To my mum and dad thank you for the continued love, support and encouragement. I owe much of my success to learning from your work ethic and conscientious nature – I hope I can continue to make you proud.

Finally, to Mike for being a source of unwavering support, love and companionship over the last five and a half years. It is impossible to express how much you have helped me through the process of my PhD but I can say with confidence that I have come out of the other side smiling because of you. One day I will convince you that the ocean is way cooler than space!

Definitions and Abbreviations

Ar	Argon
BATS	Bermuda Atlantic Time-series Study
Be	Beryllium
BOFS	Biogeochemical Ocean Flux Study
BSi	Biogenic Silica
Chl *a*	Chlorophyll *a*
CPR	Continuous Plankton Recorder
CMEMS	Copernicus Marine Environment Monitoring Service
CRM	Certified Reference Material
DIC	Dissolved Inorganic Carbon
DOC	Dissolved Organic Carbon
DUACS	Data Unification and Altimeter Combination System
DW	Dry Weight
EKE	Eddy Kinetic Energy
GF/F	Glass Fibre Filter
HNLC	High Nutrient Low Chlorophyll
IB	Iceland Basin
ICP/MS	Inductively Coupled Plasma Mass Spectrometry
In	Indium
IPCC	Intergovernmental Panel of Climate Change
JGOFS	Joint Global Ocean Flux Study
HNO_3	Nitric Acid
Milli-Q	Ultra-pure water (18.2 cm^{-1})
MLD	Mixed Layer Depth
NAB08	North Atlantic Spring Bloom Experiment in 2008
NABE	North Atlantic Bloom Experiment

NAC	North Atlantic Current
NaCl	Sodium Chloride
NaOH	Sodium Hydroxide
NAO	North Atlantic Oscillation
NPP	Net Primary Productivity
O_2	Oxygen
OOI	Ocean Observatories Initiative
OWSI	Ocean Weather Station India
PAP	Porcupine Abyssal Plain
PAP-SO	Porcupine Abyssal Plain Sustained Observatory
PIC	Particulate Inorganic Carbon
PIP	Particle Injection Pump
POC	Particulate Organic Carbon
POMME	Programme Océan Multidisciplinaire Méso Echelle
PON	Particulate Organic Nitrogen
PP	Primary Production
ppm	Parts per Million
Re	Rhenium
RSD	Relative Standard Deviation
SiO_2	Silicon Dioxide
SLA	Sea Level Anomaly
Sr	Strontium
SST	Sea Surface Temperature
σ	Standard Deviation
T_{eff}	Transfer Efficiency
TEP	Transparent Expolymer Particle
u	Zonal Velocity Component
v	Meridional Velocity Component
z*	Remineralisation Depth

Chapter 1 Introduction

1.1 The Carbon Cycle

The global carbon cycle consists of four major carbon reservoirs: the lithosphere, the hydrosphere, the atmosphere and the biosphere. In the natural carbon cycle the largest reservoir, the lithosphere, has the longest residence time of many millennia, whereas the three smaller reservoirs have shorter residence times, from years to millennia (Ciais et al., 2013). Anthropogenic activities, such as burning fossils fuels, have released a significant portion of the carbon stored in the lithospheric reservoir perturbing the global carbon cycle away from steady state (Archer et al., 2009; Ciais et al., 2013). The release of fossil fuel carbon dioxide (CO_2) into the atmosphere is the predominant cause of climate change (Denman et al., 2007) and has led to almost 1°C of global warming (Millar et al., 2017).

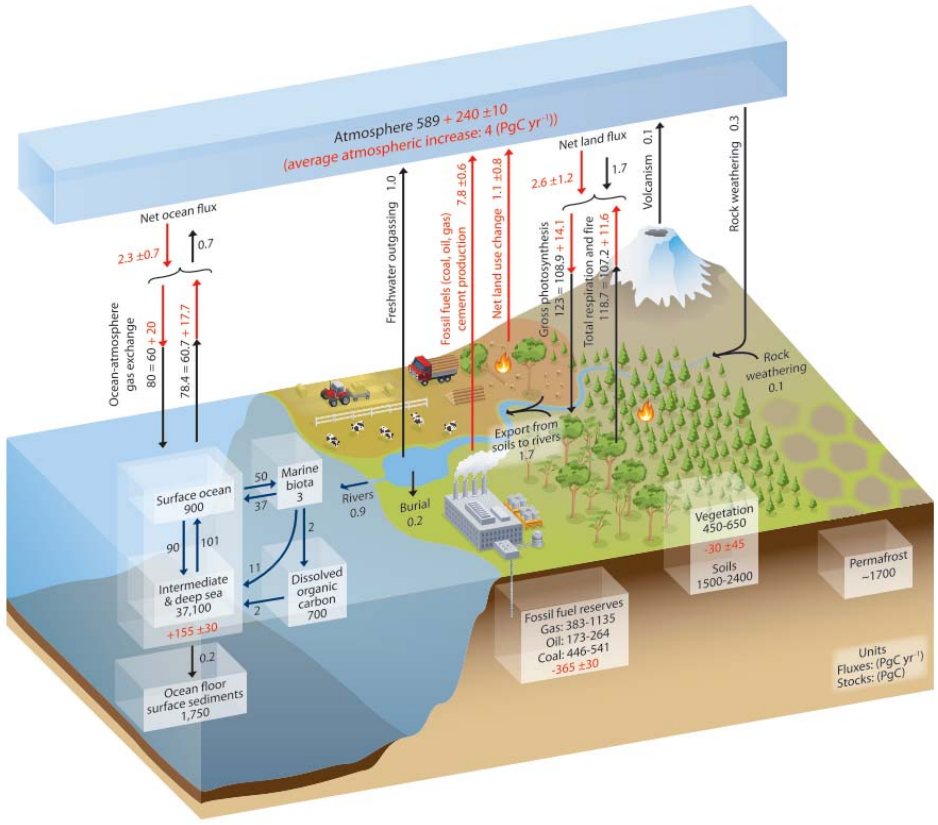

Figure 1.1 The global carbon cycle with the natural magnitude of carbon reservoirs and annual fluxes in black and anthropogenic driven changes in red. Figure reproduced from Ciais et al. (2013). Fluxes are in Pg C yr^{-1} and stocks are in Pg C.

The atmospheric concentration of CO_2 has significantly increased above the natural interglacial concentration of 280 parts per million (ppm) during the industrial era to 408.12 ppm (recorded on

the 29th September 2019; The Keeling Curve, 2019). The anthropogenic perturbations of the global carbon sinks and fluxes are shown in Figure 1.1, reproduced from the 5th Intergovernmental Panel on Climate Change (IPCC) report in 2013. The schematic highlights the importance of the oceanic dissolved inorganic carbon sink, which has stored 155 ± 30 petagrams (Pg) of anthropogenic carbon since 1750 (Ciais et al., 2013; Khatiwala et al., 2013; Le Quéré et al., 2016; Sabine & Tanhua, 2010). A recent estimate reported that between 1994 and 2007 31 % of anthropogenic CO_2 emissions have been absorbed by the oceanic sink (Gruber et al., 2019).

1.2 The Biological Carbon Pump

Atmospheric CO_2 is sequestered in the ocean via two main pumps, the solubility pump and the biological carbon pump (BCP), the latter of which consists of the soft tissue pump and the carbonate pump (Volk & Hoffert, 1985). The solubility pump is driven by the diffusion of CO_2 from the atmosphere into the surface ocean down a concentration gradient. The magnitude of CO_2 absorbed is determined by the saturation and temperature of the surface waters, with greater CO_2 absorption in colder surface waters (Volk & Hoffert, 1985).

The BCP stores organic carbon, initially formed as plankton biomass in the upper ocean, in the interior and deep ocean on timescales relevant to climate change. In an abiotic ocean, without the BCP, atmospheric CO_2 concentrations would likely be 170 – 200 ppm higher (Kwon et al., 2009; Parekh et al., 2006). The amount of carbon sequestered in the interior ocean via the BCP has been estimated as 6 - 13 Pg C yr^{-1} (Laws et al., 2011; Siegel et al., 2014), whilst the solubility pump absorbs 2.6 ± 0.5 Pg C yr^{-1} from the atmosphere (Gruber & Sarmiento, 2002; Passow & Carlson, 2012; Le Quéré et al., 2016; Reid et al., 2009). This means that minor perturbations in the BCP may have climatically-relevant implications (Kwon et al., 2009; Palevsky & Nicholson, 2018).

The BCP is driven by the photosynthetic production of organic carbon as phytoplankton biomass, which either remains within the euphotic zone or is exported to the interior ocean, usually via sinking detritus and subsequently remineralised back to inorganic carbon. Exported organic material supports the carbon demand of biota in the water column (Giering et al., 2014) and at the seafloor, whilst contributing to carbon storage in the bathypelagic zone (> 1000 m; Billett et al., 1983; Jahnke, 1996; Lampitt, 1985). The magnitude of carbon storage in the interior ocean is controlled by the stock of particulate organic carbon (POC) exported out of the surface ocean and the balance between sinking speed and remineralisation rate of the particles (Boyd & Trull, 2007; Kwon et al., 2009; De La Rocha & Passow, 2007). The sinking rate of organic material has been observed to increase with depth and is controlled by the characteristics of the particles (size, shape, density etc.), the seawater temperature, and subsequent processing during transit through

the water column (Alldredge & Gotschalk, 1989; Bach et al., 2012; Berelson, 2001; Fischer & Karakaş, 2009; Villa-Alfageme et al., 2016). This balance between sinking rate and remineralisation determines the remineralisation depth (z*; Boyd & Trull, 2007; Lutz, 2002). Modelling studies have indicated that a global shoaling of z* of 24 m can have considerable impacts of atmospheric CO_2 concentrations with predicted increases of 10 – 27 ppm (Kwon et al., 2009).

The predecessor to z*, and the most commonly used parameterisation of carbon flux attenuation in the ocean, is Martin's *b* (Boyd & Trull, 2007; Martin et al., 1987). Drifting sediment traps were deployed at six stations in the Pacific Ocean during the VERTEX (Vertical Transport and Exchange) study and the observed attenuation in carbon flux with depth was fitted to a normalised power function using Equation 1.1 (Martin et al., 1987). In Equation 1.1, *F* is the flux, Z_0 is the export depth, z is the depth of the flux measurement in meters and *b* is the log-log slope. The average *b* value from the VERTEX study was 0.858, which has been used in numerous subsequent studies and models to parameterise the flux of carbon out of the euphotic zone to the deep ocean (Berelson, 2001; Henson et al., 2012; Primeau, 2006; Sarmiento et al., 1993). *b* values between 0.6 and 2.0 have been calculated from upper ocean export measurements and deep ocean sediment trap studies and there is considerable regional variability and temporal variability during an annual cycle (Berelson, 2001; Francois et al., 2002; Primeau, 2006).

[Equation 1.1] $$F = Z_0(\frac{z}{100})^b$$

1.2.1 Drivers of Carbon Flux

Carbon flux out of the euphotic zone is driven by several biological processes and is also mediated by physical mechanisms (Boyd et al., 2019). The most well studied mechanism is the gravitational sinking of organic material from the surface ocean, known as the biological gravitational pump (BGP; Boyd et al., 2019; Buesseler et al., 2007). Other biological and physical mechanisms for transferring organic carbon efficiently from the euphotic zone to the interior ocean have been less well studied and are challenging to quantify due to a lack of high spatial, temporal and vertical resolution sampling. A recent review article of particle injection pumps (PIPs; both biological and physical) by Boyd et al. (2019) suggested that they may contribute up to 40 % of the total particle export and likely sequester as much carbon as the BGP.

Zooplankton play an important role in carbon fluxes via three main mechanisms, with the role of grazing and faecal pellet production discussed in more detail in Section 1.3.2.2. The mass movement of zooplankton into the surface waters for feeding at night, and subsequent mass descent into the mesopelagic zone during the day, is known as diel vertical migration, which is an

important carbon export pathway known as active transport (Steinberg et al., 2000; Steinberg & Landry, 2017). Active transport allows organic material to bypass remineralisation in the upper ocean and transfers carbon and nutrients to depth. Zooplankton in the mesopelagic zone release CO_2 via respiration, excrete dissolved organic carbon (DOC) and produce faecal pellets containing POC (Steinberg & Landry, 2017). A recent modelling study found that active transport in the North Atlantic contributes to 27 % of the organic carbon transported below the mixed layer by the BCP, highlighting the importance of understanding zooplankton processing of organic material (Hansen & Visser, 2016). The third zooplankton mediated process is the seasonal lipid pump, in which overwintering zooplankton migrate to depth and transport lipid rich organic material below the permanent thermocline, efficiently transferring organic carbon to the deep ocean. The seasonal lipid pump is possibly of similar magnitude to carbon sequestration by the BGP (Jónasdóttir et al., 2015).

Microorganisms also act on the flux of organic material to transform labile dissolved organic matter into recalcitrant dissolved organic matter that can be stored for millennia, termed the microbial carbon pump (Jiao et al., 2010). The microbial carbon pump has been estimated to sequester 0.2 Pg C yr^{-1} of recalcitrant DOC globally on timescales of more than 100 years (Legendre et al., 2015).

Physical processes mediate the BCP and may increase the amount of organic carbon that reaches in the interior ocean (Boyd et al., 2019). Physical processes that may act as PIPs are mesoscale eddies, which can penetrate down to 2000 m (Klein & Lapeyre, 2009; Waite et al., 2016), and the mixed layer pump, which may shorten the transit time of particles to the deep ocean via detrainment (Dall'Olmo et al., 2016; McGillicuddy, 2016). The mixed layer pump at high latitudes was found to contribute to > 100 % of the carbon supplied to the mesopelagic zone via fast sinking particles and is thought to sustain mesopelagic biota prior to the spring bloom in the Subpolar North Atlantic (Dall'Olmo et al., 2016; Gardner et al., 1995; Giering et al., 2016; Lacour et al., 2019).

There have been several studies that explore the effect of mesoscale eddies on carbon export down to 1000 m (Guidi et al., 2008; Omand et al., 2015; Stukel et al., 2018; Waite et al., 2016). Waite et al. (2016) observed up to a sevenfold increase in carbon flux in eddy centres compared to eddy flanks, termed the 'wineglass effect', in which sinking particles are concentrated in the centre of an eddy. The wineglass effect may either promote loss processes by creating a 'hotspot' for remineralisation or may promote aggregation of particles and increase export rates (Waite et al., 2016). Eddy subduction was also observed to export POC in the Subpolar North Atlantic during

the spring bloom on submesoscales (1 - 10 km) down to 350 m and contributed to half of the springtime flux of POC out of the surface ocean (Omand et al., 2015).

The North Atlantic ocean is a strong sink of atmospheric CO_2 with a pCO_2 uptake spatial range of 0 to -108 grams C m^{-2} yr^{-1} (Takahashi et al., 2009) and is an important area for anthropogenic CO_2 absorption, via the solubility pump, as it is an area of deep water formation and an area of efficient carbon storage via the biological carbon pump (Figure 1.2; Khatiwala et al., 2013; Sanders et al., 2014; Takahashi et al., 2009; Volk & Hoffert, 1985).

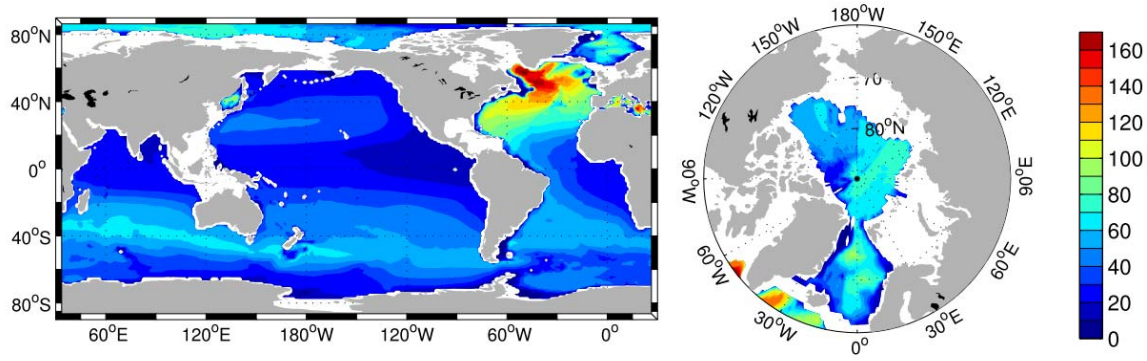

Figure 1.2 Water column inventories for 2010 in mol m^{-2} of anthropogenic CO_2 reproduced from Khatiwala et al. (2013).

1.2.2 Future Feedbacks on the Biological Carbon Pump

The BCP can have a global impact on the climate as shown by modern and palaeoceanographic studies (Kwon et al., 2009; Martinez-Garcia et al., 2014). The drivers of the BCP have been predicted to change under future climate conditions, such as decreases in PP, particularly in the North Atlantic and the tropics, and decreases in export production (Bopp et al., 2001; Levy et al., 2013; Moore et al., 2018). Moore et al. (2018) suggests that increasing greenhouse gas emissions in the atmosphere could subdue marine biological production for a millennium. Biogeochemical model studies have predicted that under future climate changes scenarios there is likely to be a floristic shift in the phytoplankton community from larger phytoplankton groups, such as large diatoms, to smaller phytoplankton groups, which may be less efficiently exported (Bopp et al., 2005). On the other hand, several recent studies have observed small phytoplankton (< 20 µm) and small particles can be efficiently exported out of the euphotic zone, especially prior to the spring bloom (Daniels et al., 2015; Giering et al., 2016), and may be able to reach the seafloor due to high sinking rates (Leblanc et al., 2018).

The impact of ocean acidification on the BCP has been predicted to occur in decades rather than centuries, for example by negatively impacting marine calcifiers (Orr et al., 2005). The ultimate

effect of ocean acidification on the global BCP is uncertain, as the increased acidity of the ocean may increase the bioavailability of iron which could stimulate productivity in high nutrient low chlorophyll (HNLC) regions (Breitbarth et al., 2010; Hoffmann et al., 2012). A further complexity in understanding how key phytoplankton types will adapt to climate change is that, under present day conditions, coccolithophores may be carbon limited, whereas diatoms are likely already at their maximal photosynthetic carbon fixation rates (Rost & Riebesell, 2013).

Predicting, identifying and understanding positive and negatives feedbacks on the BCP relies on a mechanistic understanding and a baseline of carbon fluxes throughout the global ocean to allow for changes in the future to be identified alongside spatial and temporal variability in the BCP (Boyd et al., 2019; Henson, 2014). A large research effort over many decades has worked to understand BCP export fluxes but, as highlighted by Passow and Carlson, (2012), changes in the amount of carbon that sinks out of the mixed layer, known as export flux, cannot be assumed to lead to changes in the amount of carbon that is stored below 1000 m, known as the sequestration flux.

1.3 Particle Flux

Particle flux encapsulates all manner of sinking material out of the surface ocean and is the major contributor to deep ocean carbon fluxes, often assumed to be dominated by large rare fast sinking particles (Billett et al., 1983; Suess, 1980). The IPCC definition of the long-term sequestration of carbon is 'removal from the atmosphere for over 100 years' (IPCC, 2007; Passow & Carlson, 2012). This condition is usually met after carbon penetrates below 1000 m but depending on the depth of the winter mixed layer this may vary with region (Lampitt et al., 2008b; Palevsky & Doney, 2018; Passow & Carlson, 2012; Primeau, 2005). However, a modelling study investigating carbon sequestration in the Southern Ocean found that 66 and 29 % of carbon exported to 1000 and 2000 m in the model, respectively returned to the atmosphere within 100 years, suggesting that defining flux reaching 1000 m as the sequestration flux may be overestimating carbon storage in the deep ocean (Robinson et al., 2014).

1.3.1 Sampling Methodologies

Particle fluxes are measured in the ocean using sediment traps to capture sinking material (neutrally buoyant drifting traps and tethered traps of varying designs; Bourne et al., 2019; Buesseler et al., 2000; Lampitt et al., 2008; Michaels et al., 1994; Sherman et al., 2011; Valdes and Price, 2000), particle-reactive radionuclides such as ^{234}Th and ^{210}Po (Buesseler, 1991; Buesseler et al., 2006; Villa-Alfageme et al., 2014), ^{3}H-^{3}He age and apparent oxygen utilisation (Hahm & Kim,

2008), marine snow catchers for *in situ* snapshots (Baker et al., 2017; Riley et al., 2012) and using camera systems or optical sensors deployed on gliders and Lagrangian floats, which can capture flux time-series (Bishop et al., 2016; Bourne et al., 2019; Briggs et al., 2011; Dall'Olmo & Mork, 2014; Estapa et al., 2019, 2017, 2013) or optical profilers, such as the Underwater Vision Profiler, to estimate particle properties (Stemmann et al., 2008).

These approaches are regularly used in the upper ocean but aside from sediment traps, most are unable to measure particle fluxes in the deep ocean, either due to methodological issues or sensor/equipment limitations (McDonnell et al., 2015). Moored sediment traps are the only direct method of measuring particle fluxes below 1000 m in the open ocean and will be discussed in more detail in Section 1.3.1.1 (Honjo et al., 2008; McDonnell et al., 2015). One indirect biogeochemical method that has been used to estimate the POC magnitude and global distribution at the seafloor is the benthic oxygen flux estimated from apparent oxygen utilisation measurements correlated with sedimentary organic carbon, $CaCO_3$ and accumulation rates (Jahnke, 1996).

1.3.1.1 Sediment Traps

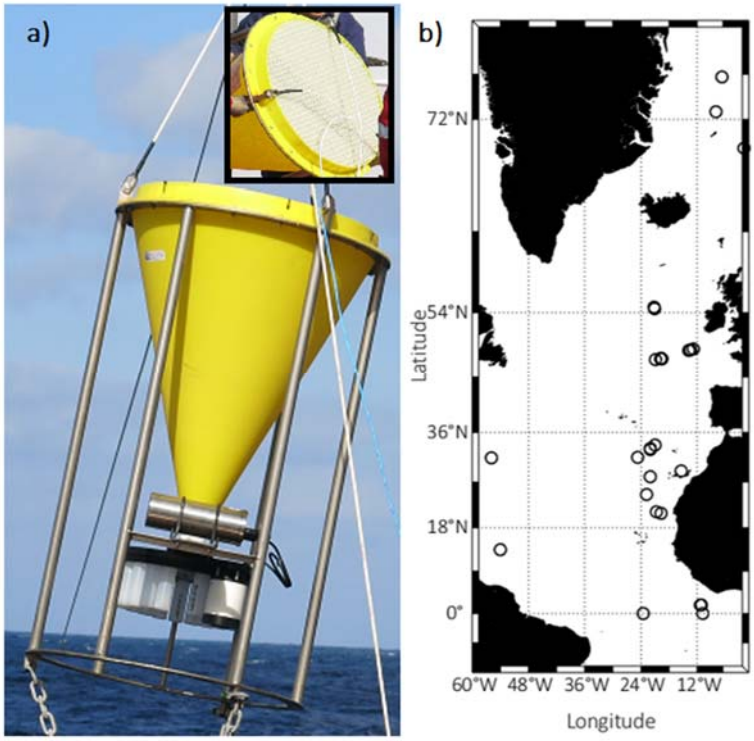

Figure 1.3 a) A 21 cup McLane sediment trap being deployed at the PAP Site. The inset shows the honeycomb baffle at the opening of the sediment traps. Photographs were taken by the author of this thesis. b) Sediment trap deployment locations in the North Atlantic replotted from Honjo et al. (2008).

Sediment traps were one of the first methods used to capture particles and remain the dominant method for collecting sinking particle flux in the deep ocean (Figure 1.3; McDonnell et al., 2015; Smetacek et al., 1978). Sediment traps provide an undisturbed, usually annual, time-series of particle fluxes, most commonly in 14 day sampling intervals. Sediment traps are moored to the seafloor and current meters and tilt meters are often deployed below the traps. Sediment traps have been deployed throughout the water column at sustained observatories for decades to attempt to collect a continuous time-series of deep ocean particle flux in a variety of locations, such as in the Northeast Atlantic at the Porcupine Abyssal Plain Site (PAP Site; Frigstad et al., 2015; Lampitt et al., 2010), in the Sargasso Sea at the Oceanic Flux Programme site and the Bermuda Atlantic Time Series site (OFP and BATS; Conte et al., 2001; Conte & Weber, 2014), at Station ALOHA near Hawaii as a part of the Hawaii Ocean Time-series programme (HOT; Karl et al., 2011; Karl & Lukas, 1996), in the North Pacific at Ocean Station P (Wong et al., 1999) and at Station M (Smith et al., 2018), in the West Antarctic Peninsula (Ducklow, 2008; Ducklow et al., 2015) and in the Fram Strait in the Arctic (Bauerfeind et al., 2009; Lalande et al., 2016). However, the spatial coverage of deep ocean sediment traps remains sparse and large swathes of the ocean remain unsampled (Figure 1.3b; Honjo et al., 2008).

1.3.1.2 Sediment Trap Methodological Issues

Biases and artefacts during sediment trap sampling are often difficult to identify and may be interpreted incorrectly as spatial or temporal variability (McDonnell et al., 2015). The two major issues plaguing sediment trap measurements are hydrodynamic bias and swimmer contamination. Hydrodynamic bias can lead to over- or undercollection of particles and the net collection of material by the sediment traps is often referred to as trapping efficiency (Baker et al., 1988; Buesseler et al., 2007; Butman, 2009; Gardner, 1980). Moored sediment traps in the deep ocean (> 1000 m) generally experience fewer issues with undercollection, whereas moored sediment traps deployed in the upper 1000 m do not provide reliable fluxes due to severe undercollection issues attributed to high current speeds and tilt (Gardner, 2000, 1980; Honjo et al., 1992). These issues in the upper ocean led to the development of neutrally buoyant Lagrangian sediment traps, which aimed to reduce hydrodynamic biases and improve the trapping efficiency (Baker et al., *in review*; Lampitt et al., 2008; Valdes & Price, 2000). Undercollection is thought to be more common, especially for slow sinking particles, and at high current speeds, generally assumed to be >12 cm s^{-1} (Baker et al., 1988), with the former likely being a minor component of deep ocean particle flux (Baker et al., 2017; Buesseler et al., 2007). Sediment traps are usually deployed with a honeycomb baffle (Figure 1.3a inset) which reduces turbulence within the collection cone and should lead to improved trapping efficiency.

Sediment traps are often contaminated with 'swimmers', which are animals that have actively swum into the sediment trap sampling bottle, and are removed either by microscopic inspection and hand-picking or by sieving, often through a 350 μm mesh (JGOFS, 1994; Lee et al., 1988). The JGOFS protocols recommend that each laboratory chooses a method and size distinction appropriate to the sample type, although screened fluxes are generally consistently higher than hand-picked fluxes (Buesseler et al., 2007; JGOFS, 1994). Sediment trap samples are usually preserved with a poison, such as mercuric chloride or sodium azide, or a fixative, usually borax-buffered formaldehyde, to prevent degradation, dissolution and to fix swimmers, which would inflate the organic carbon measurements if not removed (Hedges et al., 1993; Lee et al., 1988; Michaels et al., 1990). Sampled particle fluxes may also not accurately represent *in situ* fluxes if sediment traps are colonised, for example by Ophiuroids (brittle stars), which are common near continental margins or shallow topography, and may alter particulate composition and magnitude, via consumption and egestion, before the sinking particles enter the sampling cup (Lampitt et al., 2002). Reassuringly, deep ocean sediment traps generally have much lower swimmer contamination compared to upper ocean traps, and the use of a honeycomb baffle, for reducing turbulence, also reduces the likelihood of sediment trap sampling cups becoming blocked by large swimmers (Figure 1.3a inset; Honjo & Manganini, 1993). Other sediment trap designs were trialled, such as the 'labyrinth of doom' (Coale, 1990), which isolates swimmers from the settled fluxes using a series of funnels, to attempt to reduce swimmers, but using a preservative has remained the most commonly used methodology.

Preserving sediment trap samples also aids in preventing solubilisation of material from the particulate phase into the dissolved phase, for samples that are stored for long time periods (Antia, 2005; Bauerfeind & Bodungen, 2006; Knauer et al., 1984). Both major elements (such as C, N) and minor/trace elements (such as Zn and Mn) are lost from the particulate phase (Knauer et al., 1984). Formaldehyde is generally thought to be the superior preservative in terms of reducing dissolution, however it also precludes the measure of dissolved organic carbon in the sediment trap supernatant (Antia, 2005; Knauer et al., 1984). Zooplankton can also contribute to increased dissolved elemental concentrations in the supernatant, particularly if brine is used in the sample preservative, but is likely only to increase concentrations by ~ 2 % (Antia, 2005; Buesseler et al., 2007). The combination of the preventative measures described above are undertaken to provide the most representative record of deep ocean particle flux.

The collection efficiency of sediment traps has predominantly been quantified using radionuclide disequilibria between ^{234}Th and ^{238}U, ^{210}Pb and ^{226}Ra, and ^{230}Th and ^{231}Pa (Buesseler et al., 2007) and some studies have 'corrected' trap fluxes using this method (Guieu et al., 2005). The ^{234}Th proxy has been used to measure the collection efficiency in upper ocean sediment traps

(Buesseler, 1991; Gardner, 2000) but can be affected by non-steady state conditions and lateral advection processes, although this proxy has the advantage of not being heavily affected by swimmer contamination (Buesseler et al., 2007). ^{210}Pb has been used less widely than the ^{234}Th proxy as it can be affected by atmospheric deposition, and surface water changes in ^{210}Pb are minimal, making accurately quantifying the disequilibria difficult (Bacon et al., 1976; Buesseler et al., 2007).

^{230}Th and ^{231}Pa disequilibria has been most widely used as a proxy for deep ocean sediment traps as their half-lives are much longer, i.e. several decades for ^{230}Th compared to 24.1 days for ^{234}Th (Buesseler et al., 2007). However, ^{230}Th is scavenged similarly to ^{234}Th and can be applied as a sediment trap calibration if measured for a full seasonal cycle (Buesseler et al., 2007). This method has been applied to sediment traps throughout the global ocean in the studies by Yu et al. (2001) and Scholten et al. (2001). The main findings were that sediment traps deployed shallower than 1500 m significantly undercollect and no clear relationship between current velocity and ^{230}Th trapping efficiencies were observed. One of the biggest methodological issues is that relatively large masses of material are needed to measure accurately ^{230}Th and ^{231}Pa which means the trapping efficiency can only be easily measured in regions with sustained fluxes throughout the seasonal cycle.

1.3.2 Controls on Deep Ocean Particle Flux

The biological and physical drivers of the BCP were outlined in Section 1.2 but the drivers of deep ocean flux are discussed in further detail in this section. The major controls on particle flux to the deep ocean vary on a range of spatial and temporal scales. There is a general consensus in the oceanographic community that the three dominant controls on deep ocean particle flux are net PP in the upper ocean, community structure and ballasting by biominerals (Henson et al., 2012a; Lampitt & Antia, 1997). The rate of remineralisation, thought to be driven by temperature and oxygen concentration is also crucial, is currently the focus of the COMICS project on mesopelagic remineralisation (Henson et al., 2012a; Marsay et al., 2015; Sanders et al., 2016). In addition, the role of mesoscale eddies on deep ocean particle flux may be an important area that is currently understudied (Conte et al., 2003).

1.3.2.1 Primary Production

Several studies have observed relationships between net annual PP and organic carbon flux in the deep ocean with Lampitt and Antia, (1997) concluding that, as PP increases towards 200 g C org m^{-2} yr^{-1}, deep ocean carbon flux increases but once PP exceeds 200 g C org m^{-2} yr^{-1} there appears to be minimal effect on the magnitude of POC flux to the deep ocean. The relationship between

PP and deep ocean carbon fluxes is not always significant, especially when using satellite data to estimate PP, for example at the PAP-SO site (Lampitt et al., 2010). The relationships between flux and net PP were improved by using algorithms including seasonal variation index, which is a measure of the temporal variability of a time-series of either PP or flux, sea surface temperature (SST) and by accounting for labile and refractory fractions of sinking particles (Lutz et al., 2007).

A negative correlation between net primary production (NPP) and the export ratio (ratio of export production to NPP) has been observed in several locations (Cavan et al., 2015; Henson et al., 2015; Laws & Maiti, 2019; Maiti et al., 2013; Le Moigne et al., 2016; Stange et al., 2017) and, in a recent study, Laws and Maiti, (2019) demonstrate that the negative relationship can be explained by the time lag between production and export of organic material out of the euphotic zone. By averaging over timescales longer than the time lag between production and export it is possible to derive meaningful export ratios (Laws & Maiti, 2019). In a biogeochemical model study, the time lag between PP and export production in the North Atlantic was found to be between 20-30 days (Henson et al., 2015). A mesocosm study found lags between 2 and 15 days for the sedimentation of organic matter and demonstrated the issue with shipboard sampling compared to deep ocean flux measurements in Figure 1.4 (Stange et al., 2017), which can lead to export ratio estimates greater than one (Le Moigne et al., 2015).

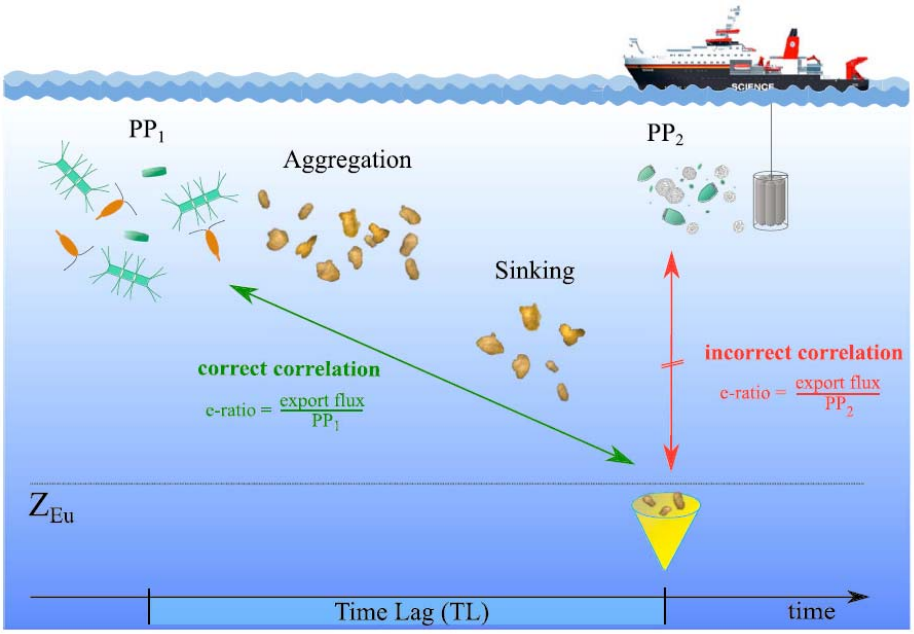

Figure 1.4 Illustration of problems relating *in situ* export efficiency without consideration of the time lag between production and sedimentation. Figure reproduced from Stange et al. (2017).

A timelag between PP and export may occur at the start of the spring bloom as phytoplankton biomass increases, whilst the zooplankton biomass growth is slower. This decoupling may be

responsible for increased export efficiency at the start of the spring bloom (Franks, 2001; Henson et al., 2015; Henson et al., 2019; Ward et al., 2014). Decoupling is an important factor in increased carbon export efficiency, and subsequent deep ocean carbon fluxes, and may occur at the start of the spring bloom, within an eddy, or in a system where PP outpaces zooplankton growth, which highlights decoupling arises over a range of spatial and temporal scales (Brix et al., 2006; Henson et al., 2019; Rii et al., 2008; Wassmànn, 1997). The magnitude of NPP sets the upper limit of possible fluxes of carbon to the deep ocean and the extent of decoupling, along with other processes, may set the efficiency for how much of the NPP reaches the deep ocean.

1.3.2.2 Community Structure

Upper ocean community structure is widely accepted to be an important driver of carbon export from the euphotic zone and the subsequent flux of carbon to the deep ocean (Agusti et al., 2015; Boyd & Newton, 1999; Buesseler, 1998; Henson et al., 2012a; Lampitt et al., 2009). Diatoms have been observed to contribute significantly to carbon export, particularly under nutrient stress, which can lead to transparent exopolymer particle (TEP) production, and the subsequent termination of a bloom (Agusti et al., 2015; Bauerfeind et al., 2009; Honjo et al., 1982; Kemp et al., 2000; Lampitt, 1985; Martin et al., 2011; Passow et al., 1993; Waniek et al., 2005b). Biogeochemical models often parameterise phytoplankton groups as diatom vs. non-diatom, which highlights their widely accepted importance in the BCP (Anderson et al., 2015; Anderson, 2005; Gehlen et al., 2006; Yool et al., 2013). High latitude diatom blooms are often succeeded by coccolithophore blooms (Holligan et al., 1993; Poulton et al., 2010), which can lead to the rapid transit of coccoliths and associated organic material to depth (Knappertsbusch & Brummer, 1995). Other planktonic organisms can contribute to the composition of deep ocean particle flux, such as radiolaria, which can lead to large carbon fluxes reaching the deep ocean, via their mini-faecal pellets (Lampitt et al., 2009) or foraminifera, which often dominate carbonate fluxes, although are unlikely to ballast POC (De La Rocha & Passow, 2007; Schiebel, 2002; Schmidt et al., 2014). Planktonic cysts have been sampled in sediment traps across the global ocean and can contribute considerably to elemental fluxes, particularly POC, BSi and Strontium (Sr; Antia et al., 1993; Belcher et al., 2018; Bernstein et al., 1987; Pospelova et al., 2018).

Zooplankton contribute to deep ocean carbon flux via fast sinking faecal pellets, which repackage phytoplankton and detrital material, and can also mediate the magnitude and lability of flux to depth, via grazing and fragmentation of the sinking POC flux (Belcher et al., 2016; Iversen & Poulsen, 2007; Mayor et al., 2014; Steinberg & Landry, 2017). The size structure of the zooplankton community may determine the export efficiency with mesozooplankton, such as krill (Belcher et al., 2019) and salps (Iversen et al., 2017), producing large fast sinking faecal pellets,

whereas microzooplankton, such as copepods, may be responsible for fragmentation of aggregates reducing the sinking rate of carbon rich particles (Belcher et al., 2016; Iversen & Poulsen, 2007; Lampitt et al., 1990; Mayor et al., 2014). Zooplankton processing in the mesopelagic zone may set the efficiency of the BCP and highlights that complex ecosystem interactions may hold the key to the controls on deep ocean carbon storage (Cavan et al., 2017).

1.3.2.3 Ballasting

Ballast minerals have been observed to be closely correlated with organic carbon fluxes in the surface ocean and in the bathypelagic zone (Armstrong et al., 2002; Francois et al., 2002; Iversen & Ploug, 2010; Klaas & Archer, 2002; Pabortsava et al., 2017; Sanders et al., 2010) but several studies have found no significant relationships between upper ocean carbon export and biominerals (Lam & Bishop, 2007; Lee et al., 2009; Riley et al., 2012; Thomalla et al., 2008). Two global studies concluded that $CaCO_3$ concentration does exhibit a relationship with deep ocean POC flux, likely by increasing the transfer efficiency through the mesopelagic zone, but concluded that upper ocean ecosystem structure is a stronger control on the fraction of export that reaches the deep ocean (Henson et al., 2012a; Lam et al., 2011). Consensus on the role of biomineral ballast on deep ocean POC flux has yet to be reached within the scientific community (Fischer & Karakaş, 2009; Francois et al., 2002; Iversen & Ploug, 2010; Klaas & Archer, 2002; Le Moigne et al., 2013; Passow, 2004; Sanders et al., 2010; Thomalla et al., 2008) and it is difficult to determine whether statistical relationships are a signal of co-occurrence during productive periods, or of a mechanistic process, relating elevated POC fluxes with greater biomineral fluxes. Ballast models are used to parameterise particle fluxes in biogeochemical models (Armstrong et al., 2002), for example in the MEDUSA global biogeochemical model (Yool et al., 2013, 2011), which will impact predictions of how the BCP may change under future climate change scenarios. The processes controlling the flux of organic carbon and associated biominerals are clearly complex, and may be hindered by the short temporal or small spatial scales of studies, with limited repeat sampling, but a mechanistic understanding is critical for our future ability to model deep ocean carbon storage.

1.3.2.4 Mesoscale Eddies

Deep ocean particle flux tends to increase as annual NPP increases (Lampitt & Antia, 1997) and PP in the upper ocean is controlled by nutrient and light availability, which is often driven by large and mesoscale physical processes (10 – 200 km), such as spring shoaling of the mixed layer and eddies, respectively (Behrenfeld & Boss, 2014; Smith et al., 1996). Mesoscale eddies can have first order effects on particles fluxes by funnelling particles to depth (Waite et al., 2016) and second order effects by replenishing upper ocean nutrients, leading to increased PP, and subsequently

increased carbon export. Model studies found eddies were responsible for 30 – 40 % of new PP in a subtropical region but the importance of eddies in Subpolar regions is not well constrained (Martin & Richards, 2001; Oschlies & Garcon, 1998). Recently formed eddies are thought to be more likely to upwell or downwell, which may stimulate PP by injecting nutrients into the surface, and may detrain phytoplankton leading to light limitation and reducing biomass, whereas mature eddies are less likely to perturb the upper ocean (Harris & Boyd, 1998; McGillicuddy, 2016; Smith et al., 1996).

The effect of eddies on particle flux was studied in the Sargasso Sea and observed that eddies of 1-2 months old stimulated PP, 3 month old eddies were associated with higher particle fluxes down to 150 m and eddies > 4 months old showed little difference but may stimulate plankton biomass (Figure 1.5; Buesseler et al., 2008; Sweeney et al., 2003). Mesoscale anticyclonic eddies were studied in the Indian Ocean and Mediterranean Sea and were found to funnel particles from the surface to 1000 m with particle concentrations up to seven times greater in the centre of the eddies compared to the flanks (Waite et al., 2016). This may increase the depth to which particles penetrate but also may become hotspots for remineralisation and zooplankton feeding (Waite et al., 2016). Knowledge of whether flux via PIPs penetrates below the mesopelagic zone, and the composition of injected and physically modified particles, is limited. The only observations of a mesoscale eddy feature impacting sediment trap fluxes in the deep ocean to date are reported in Conte et al. (2003) in the Sargasso Sea, which observed mass fluxes increasing by 2.5x and an increase in the labile bioreactive components of particulate organic matter as an eddy passed over the sampling location.

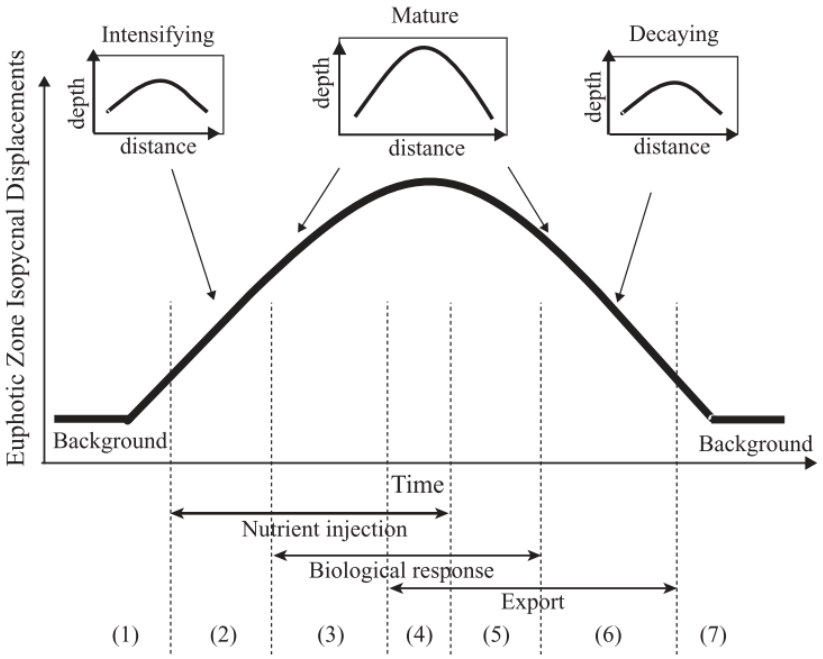

Figure 1.5 Conceptual model reproduced from Sweeney et al. (2003) of mode-water or cyclonic eddies on upper ocean biogeochemistry from studies in the Sargasso Sea. The numbers represent different stages of the eddy effects on the upper ocean biogeochemistry during an eddy life cycle.

The possibility of eddies penetrating to the ocean floor is significant for deep ocean particle flux as it may lead to enhanced current speeds, greater lateral advection and increased resuspension of sediment settled on the seafloor (Gardner et al., 2017; Klein & Lapeyre, 2009; Lampitt, 1985). This issue may be further enhanced at sampling sites, near shallow topographic features, as current speeds < 9 cm s^{-1} can cause resuspension of disaggregated particles during the passage of a mesoscale eddy in the North Atlantic (Auffret et al., 1994). If nepheloid layers are sampled in the deep ocean it may lead to samples that are more degraded (Gardner et al., 2017) but possibly larger in magnitude than if only the passively sinking flux was sampled (Lampitt et al., 2000).

1.3.3 Spatial Variability in Deep Ocean Particle Flux

Latitudinal variability in deep ocean particle flux sampled by sediment traps has been observed by several studies. The largest organic carbon fluxes occur at subpolar and temperate latitudes, however there is a strong sampling biases towards the Northern hemisphere (Honjo et al., 2008; Lampitt & Antia, 1997; Waniek et al., 2005). Smaller scale spatial variability in deep ocean carbon fluxes has only been investigated in one study to date in the Northeast Atlantic Ocean during the Joint Global Ocean Flux Study (JGOFS). Sediment traps were deployed between 3100 and 3700 m at 48 N, 19.5 W and 48 N, 21 W (i.e. a separation of ~ 100 km) for 17 months. Newton et al. (1994) concluded that there was no significant spatial variability for an annual cycle, especially for the

spring fluxes. However, the sediment trap at 19.5 W recorded a large autumn flux event, whereas the sediment trap at 21 W did not, which was attributed to either collection efficiency issues or genuine mesoscale variability (Honjo et al., 2000; Newton et al., 1994). Newton et al. (1994) called for rigorous attention to the role of mesoscale variability on particle fluxes and regional carbon budgets, but detailed studies in the deep ocean do not appear to have been undertaken and/or published.

Mesoscale spatial variability in deep ocean particle fluxes may be due to sediment traps sampling different regions of the upper ocean, which may not always be located directly above the sediment trap (Siegel & Deuser, 1997). Statistical funnels show the probability of a sampled particle originating from a location in the surface ocean, shown in Figure 1.6, with fast sinking particles having a more localised source region. Mesoscale variability in deep ocean particle fluxes may be driven by different particle source regions, advection caused by eddies and small scale physical variability, or differences in localised biological processing, which can lead to 'contamination' of time-series sites that likely will be interpreted as temporal variability (McNeil et al., 1999; Siegel & Deuser, 1997; Siegel et al., 1990). Further research is needed to determine the magnitude, drivers and regional differences of mesoscale variability in deep ocean particle fluxes and carbon sequestration.

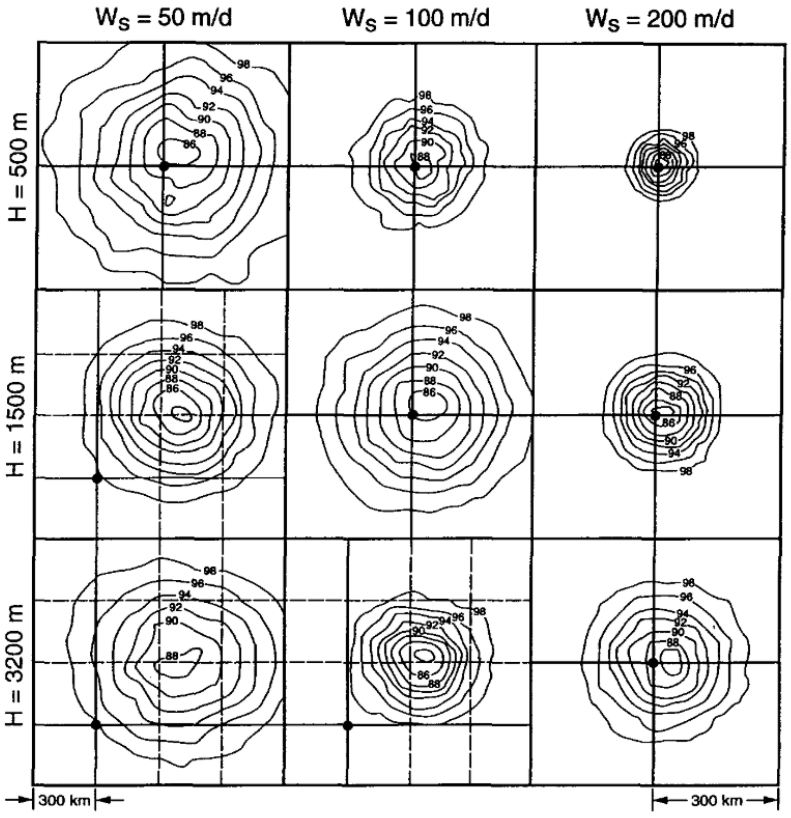

Figure 1.6 Modelled statistical funnels of sediment traps for a range of sinking speed and trap depths. Figure reproduced from Siegel and Deuser, (1997). The isolines highlight the

percentage of the particles that will have originated from within that area in the surface ocean and the black circles indicate the mooring location.

1.4 Iceland Basin

The results in this thesis focus on the Iceland Basin (IB), situated in the Subpolar North Atlantic. The IB is a dynamic region, with complex physical processes and topography, which have been outlined below.

1.4.1 Physical Characteristics

A counter-clockwise circulation has been observed in the upper ocean IB, driven by a branch of the North Atlantic Current (NAC), which feeds into the Subpolar Gyre in the Irminger Basin (Orvik & Niiler, 2002; Pollard, 2004). The proportion of the NAC current that flows into the central IB, rather than the Rockall Trough, is thought to be controlled by the North Atlantic Oscillation (NAO) index. During a low NAO phase the Subpolar Gyre contracts and more of the NAC current flows into the IB (Bower et al., 2002). The Subpolar Gyre has been observed to be declining in size and strength since the early 1990's meaning that the eastern gyre edge oscillates across the IB (Foukal & Lozier, 2017; Hátún et al., 2017). Below 1500 m the circulation is similar, with an anti-clockwise circulation in the IB which appears to be channelled by topography, with the fastest transport near the topographic features and the slowest transport in the middle of the IB (Figure 1.7; Bower et al., 2002; Yashayaev & Clarke, 2008).

The IB forms a deep (> 600 m) winter MLD due to convective cooling in the water column and strong wind forcing, which triggers the onset of deep mixing in September/ October, and shoaling of the mixed layer usually occurs in April (Gifford et al., 1995; Plueddemann et al., 1995; Yashayaev & Clarke, 2008). The winter mixed layer replenishes nutrients in the upper ocean as it shoals and the spring bloom is initiated once the mixed layer is shallower than the critical depth at which phytoplankton growth begins to exceed losses (Brody & Lozier, 2015; Gifford et al., 1995; Sverdrup, 1953).

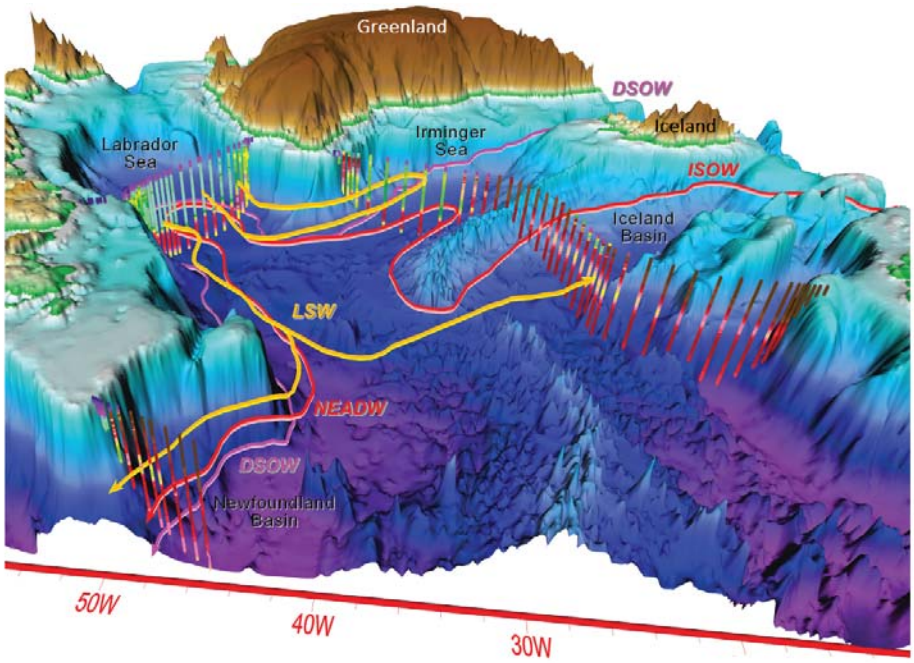

Figure 1.7 The Subpolar North Atlantic topography and intermediate and deep water masses that form the lower limb of the Atlantic meridional overturning circulation. Figure reproduced from Yashayaev and Clarke, (2008). The water mass acronyms are listed: Iceland-Scotland Overflow Water (ISOW), Denmark Strait Overflow Water (DSOW), Labrador Sea Water (LSW) and the Northeast Atlantic Deep Water (NEADW).

Cyclonic (counter-clockwise and usually upwelling) and anticyclonic (downwelling) eddies have been observed in the IB (Harris et al., 1997; Marra et al., 1995). The NAC branch described by Orvik and Niiler, (2002) was found to be heavily dominated by eddy structures with eddies travelling west towards the Irminger Basin (Harris et al., 1997). A barotropic (depth-independent mean flow) eddy, that reached the seafloor, was observed in the IB in 1991 and created a nepheloid layer which extended from 2200 m to the seafloor (2400 m) rich in labile compounds, suggesting resuspension of the previously settled spring bloom (Conte et al., 1995; Harris et al., 1997). A barotropic anticyclonic eddy in the central IB was studied in detail in June 1996, with two other similar eddies present during the sampling period, and were likely formed from a branch of the NAC, suggesting such features are likely common in the IB (Martin et al., 1998). Iceland Basin eddies range in size from 60 – 120 km, usually with a thickness of 1000 m and radial velocities up to 50 cm s^{-1} (Martin et al., 1998; Pidcock et al., 2013; Read & Pollard, 2001).

1.4.2 Biological Features

Research programmes in the 1980's and 1990's set out to investigate biological production and processes in the IB: the Biogeochemical Ocean Flux Study (BOFS) in 1989 and 1991 (Harris & Boyd, 1998; Joint et al., 1993) and the Marine Light-Mixed Layers in 1991 (Marra et al., 1995) took place

with the former complementary to JGOFS. In 2007 the Biophysical interactions in the Iceland Basin (BIB) study also took place (Poulton et al., 2010) and in 2008 the North Atlantic Bloom Experiment (NAB08) was undertaken (Briggs et al., 2011; Cetinić et al., 2015; Martin et al., 2011). These findings were summarised these findings to characterise the biological cycle in the upper ocean IB.

The timing and magnitude of the spring bloom in the subpolar North Atlantic is driven by the winter MLD, with a shallower winter MLD leading to an earlier bloom of enhanced magnitude (Henson et al., 2009). The spring bloom in the IB usually peaks during mid-late May (Chl *a* 2.5 µg L^{-1}) and is often dominated by diatoms and/ or *Phaeocystis sp.* (Gifford et al., 1995; Marra et al., 1995). Storms in spring may lead to strong mixing events, which can deepen the MLD down to 150 m, and lead to the termination of a bloom (as with *Phaeocystis* in 1991; Marra et al., 1995).

In spring 1991 in the IB, the role of zooplankton grazing was found to be minimal during the spring bloom, with copepods peaking after the spring bloom, but were only consuming 1 % of daily chlorophyll production and < 5 % of the phytoplankton standing stock (Batchelder et al., 1995; Cowles & Fessenden, 1995; Gifford et al., 1995). Nanoplankton made a significant contribution to the daily productivity prior to and after the spring bloom in 1991, with a similar observation made pre-bloom in 2012 (Daniels et al., 2015a; Gifford et al., 1995; Joint et al., 1993). Microzooplankton dominated during the declining bloom in 1991 and were found to consume 100 % of the daily chlorophyll production, which may suggest a top-down control on the bloom (Gifford et al., 1995). Conversely, during the 1989 BOFS sampling, it was unclear what limited the bloom as nitrate and silicate remained abundant with minimal grazing pressure (Joint et al., 1993). The NAB08 study found that the spring bloom in the IB in 2008 likely terminated due to silicate stress, causing TEP production and aggregation, and subsequent rapid sinking of diatom cells (Martin et al., 2011). The IB is also a seasonal HNLC region with the iron replete conditions observed in the upper ocean during summer in 2007 (Nielsdóttir et al., 2009).

The IB water column is more stable between May and August with fewer strong mixing events which, after re-stratification, were found to stimulate productivity and grazing (Marra et al., 1995). The IB in summer 1991 was found to be more biologically active in mid-summer than previously thought, with PP twice as high as expected, attributed to the cyclonic eddy the study tracked (Harris et al., 1997). During the MLML study, microzooplankton grazing during August had declined to 45 % of daily Chl *a* production (Gifford et al., 1995). The minimal grazing of PP by mesozooplankton during MLML lead to the hypothesis that they must be consuming up to 100 % of microzooplankton and/ or protist daily production to fulfil their nutritional demand (Cowles & Fessenden, 1995).

Coccolithophores are an important component of the phytoplankton community in the IB, particularly in silicate-limited waters during summer (Poulton et al., 2010). Coccolithophores produce coccoliths made of $CaCO_3$ which may detach and remain in the mixed layer (Fernandez et al., 1993). In late June in 1991 particulate inorganic carbon (PIC) concentrations were elevated and coccolithophores contributed between 40 – 90 % to phytoplankton biomass but production rates were low (Fernandez et al., 1993; Harris et al., 1997). Poulton et al. (2010) studied coccolithophores in the IB in July and August 2007 post-bloom and found they contributed to ~ 10 – 20 % of Chl *a*, phytoplankton carbon and PP, whilst small flagellates (< 5 μm) contributed > 60 % of Chl *a* (Nielsdóttir et al., 2009; Poulton et al., 2010). This may indicate a seasonal succession of phytoplankton community from diatoms to coccolithophores to flagellates. This may be attributed to the development of a seasonal HNLC regime in summer due to iron limitation, in which both diatoms and coccolithophores were found to be iron limited, and could lead to the rapid sinking of diatoms in spring (Martin et al., 2011; Nielsdóttir et al., 2009). The development of a HNLC regime may explain the termination of the bloom during 1991 when nitrate and silicate were still abundant and grazing was minimal (Joint et al., 1993).

These studies provide insight into the seasonal transitions and dynamics of phytoplankton and zooplankton populations in the IB and highlight the strong effect and importance of physical processes but how these upper ocean processes relate to the magnitude and composition of annual deep ocean particle flux in the IB is unknown.

1.5 Thesis Hypotheses and Aims

In this thesis three hypotheses will be tested:

1. The magnitude and seasonal cycle of deep ocean carbon sequestration in the Iceland Basin will be similar to the North Atlantic averages that have previously been published.
2. Mesoscale variability in deep ocean carbon fluxes will be significant for short (weekly to seasonal) timescales, but that on annual or multi-year timescales, mesoscale variability will be negligible compared to seasonal variability.
3. The first spring-time incidence of rapid shoaling in the mixed layer allows Acantharia to return to the upper ocean, from the interior ocean to the upper ocean, and changes in upper ocean conditions may be a trigger for sedimentation, such as temperature, light or chlorophyll concentration.

This thesis aims to:

1. Quantify the magnitude of deep ocean carbon sequestration and other particle flux components to the deep ocean Iceland Basin for an annual cycle for the first time. These findings will be compared to other North Atlantic and global carbon sequestration estimates and calculate the transfer efficiency of organic carbon to the deep ocean IB.
2. Utilise the unique mesoscale spatial array of the deep ocean sediment traps to explore the magnitude of spatial variability and to explore the most effective methods for identifying such variability in low spatial and temporal resolution data.
3. Identify the drivers of organic carbon flux to the deep ocean by exploring how upper ocean processes (biological, e.g. community structure and physical, e.g. mesoscale eddies) relate to the seasonal cycle and spatial variability in deep ocean particle flux.
4. Improve the current understanding on what triggers the sedimentation of Acantharian cysts to the deep ocean Iceland Basin and to provide more accurate estimates of the elemental content and sinking rates of Acantharian cysts in the Iceland Basin.

Chapter 2 Deep Ocean Carbon Storage in the Iceland Basin and the Implications of Mesoscale Spatial Variability

2.1 Introduction

It is estimated that globally the BCP exports 5 - 11 Gt C yr^{-1} into the interior ocean, with the North Atlantic Ocean contributing 1.27 Gt C yr^{-1}, or 15 %, of global export (Henson et al., 2011; Sanders et al., 2014). Particles exported from the surface ocean are rapidly remineralised during transit through the mesopelagic zone (100 – 1000 m depth) and the magnitude of organic carbon stored in sediments is thought to be < 1 % of net PP (Antia et al., 2001; Lampitt & Antia, 1997). The globally integrated POC flux to 2000 m depth has previously been estimated as 0.33 - 0.66 Gt C yr^{-1} (Henson et al., 2012a; Honjo et al., 2008; Lampitt & Antia, 1997) with an estimated 0.1 Gt C yr^{-1} reaching 2000 m depth in the Atlantic Ocean as a whole (Lampitt & Antia, 1997), and reduces to 0.04 Gt C yr^{-1} when considering 2000 m in the North Atlantic Ocean (0 - 80 N; Henson et al., 2011).

Annual POC export in the Iceland Basin (IB) has been estimated as 0.0038 - 0.0084 Gt C yr^{-1} using a satellite-based estimate and surface (< 10 m) O_2/Ar measurements respectively (Henson et al., 2012a; Quay et al., 2012). The magnitude of the POC flux to the bathypelagic IB has not been directly measured, which precludes accurate estimates of carbon sequestration in the IB and to the Subpolar North Atlantic as a whole.

The North Atlantic is likely an important region for deep ocean carbon sequestration (Takahashi et al., 2002), in particular the Subpolar North Atlantic, as it is an area of deep water formation meaning carbon may be transported via thermohaline circulation through the IB (Lozier et al., 2019), but observations remain limited to either the surface ocean or localised regions of the upper 1000 m (Briggs et al., 2011; Martin et al., 2011; Quay et al., 2012). Organic carbon that reaches the deep ocean in this region may be sequestered for a minimum of a few hundred years, as particulate or dissolved organic carbon, or may undergo remineralisation into inorganic carbon (Barange et al., 2017; DeVries et al., 2012; Fontela et al., 2016; Lampitt & Antia, 1997; Sabine, 2004). A critical factor in the efficiency of carbon storage in the Subpolar North Atlantic is deep winter mixing, as particles must sink below ~ 1500 m in the Irminger Basin to escape winter ventilation back to the atmosphere (Palevsky & Nicholson, 2018; Yashayaev & Clarke, 2008). The winter MLD in the IB is comparatively shallow compared to the Irminger Basin, usually less than 1000 m, potentially permitting less carbon to ventilate back to the upper ocean and therefore the

IB may be an efficient carbon sink compared to the Irminger Basin (Martin et al., 1998). However, the IB is likely to be a less efficient long-term carbon sink, due to a greater likelihood of carbon being ventilated back to the atmosphere during deep winter mixing in the North Atlantic as the mean maximum MLD is only 150 – 200 m (latitude 42.5 – 72.5 N; Cole et al., 2015).

Sediment traps are widely used to collect a continuous time-series of sinking particle flux in the deep ocean (McDonnell et al., 2015). Interannual variability in sampled deep ocean carbon flux of varying magnitudes has been observed in a diverse range of locations, from the Subarctic Pacific to the Subtropical Atlantic (Conte et al., 2001; Deuser, 1986; Frigstad et al., 2015; Pabortsava et al., 2017; Wong et al., 1999). Continuous time-series of deep ocean particle flux at sustained observatories are crucial to quantify the magnitude and variability of particle flux components accurately (Conte & Weber, 2014; Frigstad et al., 2015; Lampitt et al., 2010; Smith et al., 2018) and a time-series of several decades is needed to identify temporal mechanisms driving particle flux and subsequent carbon sequestration (Henson, 2014). Observatories, such as PAP, BATS and Station M, collect long-term observations but the importance of spatial variability, particularly from a mesoscale perspective, has rarely been explored. The spatial 'footprint', which is the area of the surface ocean that is represented accurately by a single sustained observatory, is dependent on the parameter of interest (Henson et al., 2016). Similarly, statistical funnels have been estimated by tracking particles reaching the deep ocean backwards in time to assess their possible source region. The resulting funnel depends on the assumed particle sinking speed, but can extend several 100's of km's from the trap location (Nodder et al., 2016; Siegel & Deuser, 1997; Siegel et al., 1990). Statistical funnels estimate the particle source region in the surface ocean but cannot assess whether the sampled particle fluxes may accurately represent a wider spatial area. Our lack of understanding of mesoscale variability therefore compromises our ability to interpret time-series of deep-ocean particle flux and hence mesoscale variability in the deep ocean is assumed to be negligible (Newton et al., 1994).

The Joint Global Ocean Flux Study (JGOFS) included the North Atlantic Bloom Experiment (NABE), in which 3 sediment traps were deployed in the deep ocean during 1989 and 1990 around 34 °N (one sediment trap) and 48 °N (two traps spaced 112 km apart; Honjo & Manganini, 1993; Newton et al., 1994). Comparisons were made between one trap array at 48 °N and the trap array at 34 °N (Honjo & Manganini, 1993) and brief comparisons were made between the two trap arrays near 48 N, which was the highest spatial resolution for deep ocean sediment trap coverage before the IB deployments. Newton et al. (1994) concluded that there was no significant mesoscale variability over the 100 km spatial scale in spring and differences in autumn fluxes were either due to issues with collection efficiency or real spatial variability in deep ocean fluxes. A mesopelagic study (POMME) that explored spatial variability in carbon export deployed four

sediment trap moorings (400 and 1000 m) in pairs in the Northeast Atlantic. The study observed an anticyclonic eddy influencing carbon export dynamics which was supported by Underwater Video Profiler data (Guidi et al., 2007; Guieu et al., 2005). The study concluded that, in eddy-dominated areas, export may be temporarily influenced down to 1000 m on scales < 100 km, which will be missed by sediment trap deployments at a singular location (Guidi et al., 2007). The magnitude of the spatial variability between the POMME sediment trap annual POC fluxes at 1000 m was 32 % which was deemed as not negligible (Guieu et al., 2005). Determining the origin of variability at sustained observatories, whether temporal or local spatial variability, is a continuing challenge, exacerbated by limited previous research into mesoscale variability in the deep ocean (Henson, 2014).

The origin of observed mesoscale variability in particle flux, whether originating from the surface ocean or arising during the transit of particles to the deep ocean, is important to consider. In the surface ocean, physical processes such as mesoscale eddies (Martin et al., 2002; Oschlies & Garcon, 1998) or frontal instabilities (Martin et al., 2001) are likely to shape the biological and biogeochemical drivers of particle flux, such as plankton community structure (d'Ovidio et al., 2010; Rodríguez et al., 2001) or the mixing of nutrients into surface waters (Woods, 1988) that may alter the magnitude and composition of flux. In the mesopelagic zone, these physical processes may lead to the subduction of particles from the mixed layer down to 1000 m, depending on the local productivity and particle size spectrum in the upper ocean (Omand et al., 2015; Stukel et al., 2017; Waite et al., 2016). Other sources of mesoscale variability in the mesopelagic and bathypelagic zones could be due to lateral advection (Siegel et al., 2008) and nepheloid layers (Gardner et al., 2018), which may alter the magnitude and composition of sampled particle flux. Biological processes, such as zooplankton community structure may alter the magnitude and composition of mesopelagic particle flux through the active transport of organic carbon to depth (Steinberg et al., 2000), or by controlling the remineralisation of particles via biotic fragmentation, with subsequent faecal pellet production (Steinberg et al., 2008). Mesoscale variability arising from biological factors in the upper ocean, such as community structure or zooplankton versus microbial remineralisation, may persist into the bathypelagic in terms of flux composition and magnitude, whereas physical drivers that shunt particles to depth are more likely to impact the magnitude rather than the composition of particle flux.

The magnitude of carbon flux to the deep ocean IB has not previously been measured. To quantify accurately the magnitude and impact of mesoscale variability in deep ocean carbon sequestration in the IB, this study utilises four sediment traps deployed below 2000 m in a mesoscale array, spaced 71 km apart. I hypothesise that for short (weekly to seasonal) timescales, mesoscale

variability in deep ocean carbon fluxes will be significant, but that on annual or multi-year timescales, mesoscale variability will be negligible compared to seasonal variability.

2.2 Methods

Four Parflux Mark 78H-21 or Parflux Mark 78H-13 sediment traps were deployed in a mesoscale array (71 km distance between traps) in the IB below 2000 m around the former Ocean Weather Station India (OWSI, 60 °N 20 °W). The traps sampled from November 2006 to July 2007 and from August 2007 to June 2008 (Table 2.1 and Figure 2.1). The water depth ranged between 2529 – 2856 m and the traps were deployed ~ 400 meters above bottom (mab), with trap depths ranging between 2101 - 2441 m. The traps deployed in 2006 were consistently deeper (mean depth 2372 m) than the 2007 deployment (mean depth 2168 m). In this thesis, the deep ocean is defined as below 2000 m and I will refer to flux below 2000 m for simplicity but potential differences due to trap deployment depths are discussed in Section 2.3.1. The sediment traps have a cone-shaped collector with an area of 0.5 m^2 and have either 21 or 13 collection cups (Table 2.1).

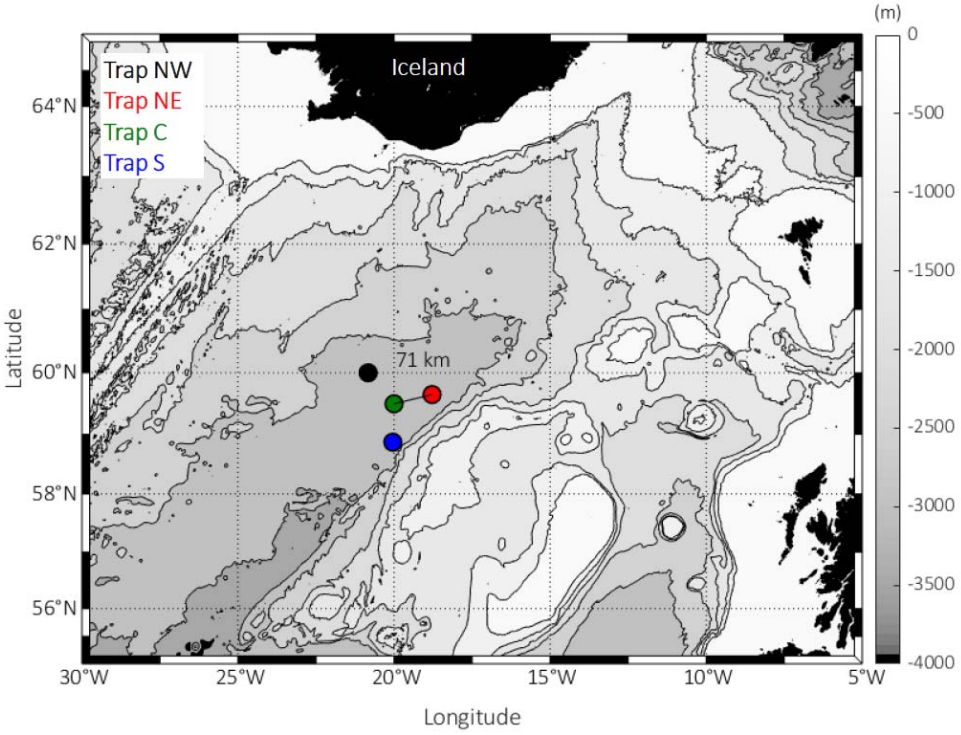

Figure 2.1 Bathymetric map of the Iceland Basin. The locations of the sediment traps deployed below 2000 m are shown and labelled in regards to their position (North West (NW), North East (NE), Centre (C) and South (S)). The colours for each trap remain consistent throughout this thesis. The black line between Trap NE and C highlights the average distance between traps of 71 km.

Four periods of flux were defined to highlight different regimes of flux collection: Period I (22nd Nov 2006 – 23rd May 2007), Period II (24th May 2007 – 29th July 2007) during which the traps had been colonised by Ophiuroids (Table 2.2), Period III (26th Aug 2007 – 18th Nov 2007), which was the beginning of deployment 2 and Period IV (19th Nov 2007 – 15th Jun 2008) in which fluxes were extremely low, and hence were not included in the analysis presented in this Chapter (detailed discussion in Section 2.3.1).

Table 2.1 Parflux sediment trap locations, deployment depth and distance from the seafloor in meters above bottom. The availability of current meter data and number of collection cups is also detailed. Cups sampled for 14 days unless specified otherwise.

* Traps began sampling on the 22nd November 2006 and finished sampling on the 29th July 2007.

** Traps began sampling on the 26th August 2007 and finished sampling on the 15th June 2008.

*** 13 cup sediment traps were deployed for periods longer than two weeks during winter to allow high resolution sampling in autumn and spring and consequently finished sampling on the 18th May 2008.

Trap	Latitude	Longitude	Depth (mab)	Current Meter Data	Collection Cups
NW (2006 – 2007) *	60° 00.063 N	20° 49.512 W	2381 m (400)	Yes	21
NE (2006 – 2007) *	59° 38.97 N	18° 46.838 W	2317 m (415)	Yes	21
C (2006 – 2007) *	59° 29.913 N	19° 59.757 W	2350 m (415)	Yes	21
S (2006 – 2007) *	58° 51.968 N	20° 24.169 W	2441 m (415)	Yes	21
NW (2007 – 2008) **	59° 59.89 N	20° 51.52 W	2194 m (410)	Not recovered	21
NE (2007 – 2008) **	59° 39.62 N	18° 50.36 W	2119 m (410)	Not recovered	21
C (2007 – 2008) **	59° 30.32 N	20° 00.78 W	2101 m (426)	Yes	13***
S (2007 – 2008) **	58° 52.14 N	20° 22.05 W	2258 m (416)	Yes	13***

Table 2.2 The number of Ophiuroids counted as swimmers (individuals per cup) and swimmer flux (individuals m^{-2} d^{-1}) in the sediment trap samples during April to July 2007 for each trap. A dash indicates that no Ophiuroids were collected. The traps were recovered in July 2007.

Date	**Trap NW**		**Trap NE**		**Trap C**		**Trap S**	
	Individuals per cup	Individuals m^{-2} d^{-1}	Individuals per cup	Individuals m^{-2} d^{-1}	Individuals per cup	Individuals m^{-2} d^{-1}	Individuals per cup	Individuals m^{-2} d^{-1}
25/04/07	1	0.14	-	-	-	-	-	-
09/05/07	-	-	2	0.29	1	0.14	1	0.14
23/05/07	21	3.0	7	1.0	14	2	10	1.43
06/06/07	27	3.86	30	4.29	6	0.86	42	6.0
20/06/07	523	74.71	164	23.43	166	23.71	157	22.43
04/07/07	618	88.29	232	33.14	105	15.0	255	36.43
18/07/07	159	22.71	226	32.29	199	28.43	196	28.0

The sediment trap moorings were deployed with an Aanderaa RCM8 current meter below the trap and sampled current speed and direction every hour (Table 2.1). For deployment 2, the current speed data for Trap NW and Trap NE were not successfully recovered and for Trap C and Trap S the minimum recorded current speed was 1.1 cm s^{-1}, which appears to be a cut off point for slower current speeds and was handled as an artefact in the dataset. To identify persistent current speed features in the hourly current speed data, daily and weekly moving means were calculated. To allow for comparable statistics between the two deployment periods, all current speeds slower than 1.1 cm s^{-1} in deployment 1 were replaced with a value of 1.1 cm s^{-1}. The strength of the relationship between the mean current speed and the percentage of current speeds > than 12 cm s^{-1} (per 14 day sampling period) with mass flux was investigated using a Spearman's rank test to evaluate the hypothesis that fast current speeds lead to reduced collection of fluxes by sediment traps.

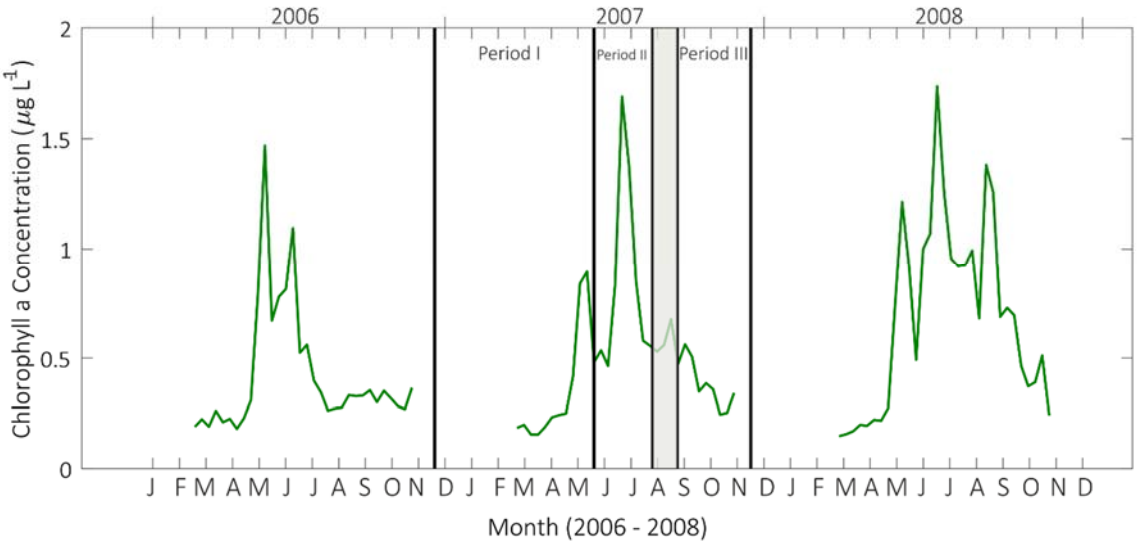

Figure 2.2 Satellite-derived chlorophyll *a* concentration (µg L^{-1}) in the Iceland Basin from 2006 to 2008. There is no data available for November to February due to the low sun angle. The particle flux time-series in the following figures have been separated into three periods and are highlighted in this figure. The grey shaded area is the period between deployments when particle flux was not sampled.

Mixed layer depth for the period of 2006 – 2008 in the IB was estimated using Argo float profiles as in Hosoda et al. (2010). Chlorophyll *a* (Chl *a*) concentration was extracted from MODIS satellite archive at 8 day, 9 km resolution (https://oceandata.sci.gsfc.nasa.gov/MODIS-Aqua/Mapped/Monthly/9km/chlor_a). The mean Chl *a* concentration for the IB, defined as extending from 58.0 °N to 61.5 °N and 16.5 °W to 28.0 °W (as defined by the General Bathymetric Chart of the Oceans, hosted by the National Geoscience Data Centre), was calculated for 2006 –

2008 (Figure 2.2). The spatial 'footprint' of upper ocean export was estimated for the four sediment trap locations and calculated as in Henson et al. (2016). The footprints are defined using 100 year sections of the historical control runs for eight Earth System Models. Pixels which have a similar mean and variability for the carbon export time-series at the chosen site, i.e. the sediment trap locations, are identified and those that are contiguous with the sediment trap locations are retained. The footprints are identified separately for each of the 8 models; only pixels which are identified in at least four of the eight models are retained to create the final footprint.

2.2.1 Sediment Trap Sample Analysis

Swimmers, defined as well-preserved animals that likely swam into the trap (Michaels et al., 1990), were removed from sediment trap samples through picking at 75x magnification under a microscope. Deployment 1 samples were picked by Corinne Pebody and deployment 2 samples were picked by the author. During Period II the sediment traps were colonised by Ophiuroids, which were removed as swimmers and counted (Table 2.2 and Figure 2.3). Samples from spring (2007 and 2008) had Acantharian cysts which were counted and separated as in Martin et al. (2010) if > 400 cysts were present in one sample. Sediment trap samples were split into 8 aliquots for analysis with mean relative standard deviation (RSD) < 5 % between split volumes.

For deployment 1 (2006 – 2007) 5 aliquots were filtered onto a cellulose nitrate filter (0.4 µm pore size), the material scraped into a pre-combusted glass jar, freeze-dried, weighed for dry weight (DW) and subsequently crushed (Martin et al., 2010). DW, POC and particulate organic nitrogen (PON) samples from deployment 1 were ran by P. Martin and reported in their thesis (Martin, 2011). For deployment 2 (2007 – 2008) this was not possible for DW and POC/PON analysis due to the very low quantities of material in 2008. Therefore for deployment 2 the DW was determined by filtering one aliquot onto pre-weighed, pre-combusted 25 or 47 mm GF/Fs (0.7 µm Fisherbrand). The filters were rinsed with borate-buffered Milli-Q (0.25 g of Sodium Tetraborate per 1 L of Milli-Q) and dried in a 40 °C oven. The filters were weighed using a Sartorius microbalance (0.001 mg precision) to determine DW, which was used to calculate mass flux using Equation 1. *A* is the collection area of the sediment traps (0.5 m^2), *d* is the sampling time in days and the 1/8th aliquot DWs were normalised to calculate total DW of the sample.

[Equation 2.1] $$Mass\ Flux\ (mg\ m^{-2}\ d^{-1}) = \frac{(DW \times 8)}{(A/d)}$$

The freeze-dried material from deployment 1 was weighed (0.6 – 5 mg) into pre-combusted silver capsules (Elemental Microanalysis, UK) and acidified with 2 mol L^{-1} HCl at 70 °C on a hotplate following the method of Nieuwenhuize et al. (1994). The silver capsules were pelleted and POC/PON was measured on a Flash 1112 Elemental Analyser (Thermo Finnigan) at Plymouth

Marine Laboratory. POC and PON were analysed in triplicates where possible with RSDs < 10 %. Blanks (acidified empty silver capsules) contributed ~ 1 ug of C which is equivalent to < 10 %, and usually ~ 1 %, to the total signal for C and N.

The DW filters for deployment 2 were used for POC/PON analysis. Filters were fumed for 24 hours in a desiccator with concentrated hydrochloric acid (37 % HCl, analysis grade) following the methodology of Hedges and Stern, (1984) to remove any calcite of biogenic or lithogenic origin.

Acantharian cyst POC/PON was measured separately. If there were > 100 cysts in a $1/8^{th}$ aliquot then replicates of > 50 cysts were analysed for deployment 2. For deployment 1, cysts were rinsed with Milli-Q as in Martin et al. (2010) and analysed for POC/PON as above. For deployment 2, the samples were rinsed once with borate-buffered Milli-Q spiked with Strontium Chloride ($SrCl_2$) to a concentration of 80 mg L^{-1} to prevent Strontium dissolution, which would affect estimates of the elemental ratios (Beers & Stewart, 1970). Cysts were then transferred into pre-weighed pre-combusted (550 °C) silver cups (Smooth Silver Capsules 5.5 x 3.5 mm or Smooth Silver Boats 4 x 11 mm, Elemental Microanalysis). The cysts were dried at 40 °C and were acidified using the dropwise addition method (Nieuwenhuize et al., 1994).

For deployment 2, POC/PON was analysed at the Stable Isotope Facility, University of Southampton on an Elementar Vario Isotope Select by the author with the assistance of Bastian Hambach and Megan Wilding. The limit of detection for the instrument was 10 µg for C and 1 µg for N and the analytical precision was ≤ 6.1 % for N and ≤ 1.7 % for C.

The 25 mm and 47 mm pre-combusted GF/F blanks, rinsed with borate-buffered Milli-Q and process blanks, had a mean blank value of 20.3 ± 9.5 µg of C and 127.3 ± 121.8 µg of C respectively; both were consistently below the detection limit for N. The mean blank C value was subtracted from all samples but N data were not corrected as blanks were below the detection limit and negligible. POC/PON fluxes were calculated similarly to Equation 1 but with C/N weight (mg) in place of *DW* and converted to moles. Flux uncertainty was assumed as 5 % to encompass splitting and weighing errors and has been propagated with analytical error (Section 2.2.1.1). Mean uncertainty for mass flux estimates for both deployments was 5.3 % and for POC flux was 7.5 %.

Filtered supernatant from the sediment trap samples in deployment 2 was saved, along with a record of the volume of supernatant in the sample bottles to allow sodium concentrations to be corrected for evaporation that may have occurred during storage or the swimmer picking process detailed further in Section 3.2.1.1. The supernatant was acidified with sub-boiled 3% HNO_3 and the solution was analysed for sodium on a Thermo X Series ICP-MS at the University of

Southampton by the author with the assistance of Dr. Matt Cooper. All deployment 1 analysis was undertaken by Patrick Martin and all deployment 2 analysis was undertaken by the author of this thesis (see Appendix F).

2.2.1.1 Uncertainty Equations

Analytical errors were propagated using standard equations throughout all calculations to estimate each measurement's uncertainty (*U*) using the standard deviation (σ). Equation 2.2 was used for to propagate errors for addition and subtraction and Equation 2.3 was used to propagate the errors associated with multiplication and division.

[Equation 2.2] $$U_{x+y} = \sqrt{\sigma_x^2 + \sigma_y^2}$$

[Equation 2.3] $$U_{x\times y} = (x \times y)\sqrt{\left(\frac{\sigma_x}{x}\right)^2 + \left(\frac{\sigma_y}{y}\right)^2}$$

2.2.2 Carbon Budget

The annual carbon fluxes to the deep ocean were calculated from end of November 2006 to the end of November 2007 (Table 2.3). The bi-monthly POC flux time-series is reported in mmol m^{-2} d^{-1} and this daily rate was interpolated into a daily time-series, which assumes that the sampled POC fluxes were at a constant rate during the sampling period. The 28 day sampling gap was filled using nearest neighbour interpolation. For deployment 2 it was clear during microscopic inspection that some samples were not well preserved, as swimmers were visibly degraded. These samples have been removed from the POC flux time-series and not included in calculations (only 1 out of 100 samples in Periods I-III were removed). Antia et al. (2001) advised calculating annual budgets over cycles of deep mixing, i.e. from winter to winter. Due to issues with sample degradation this was not possible in this study but the annual cycle used began slightly before winter and so should be fairly representative of a full mixing cycle.

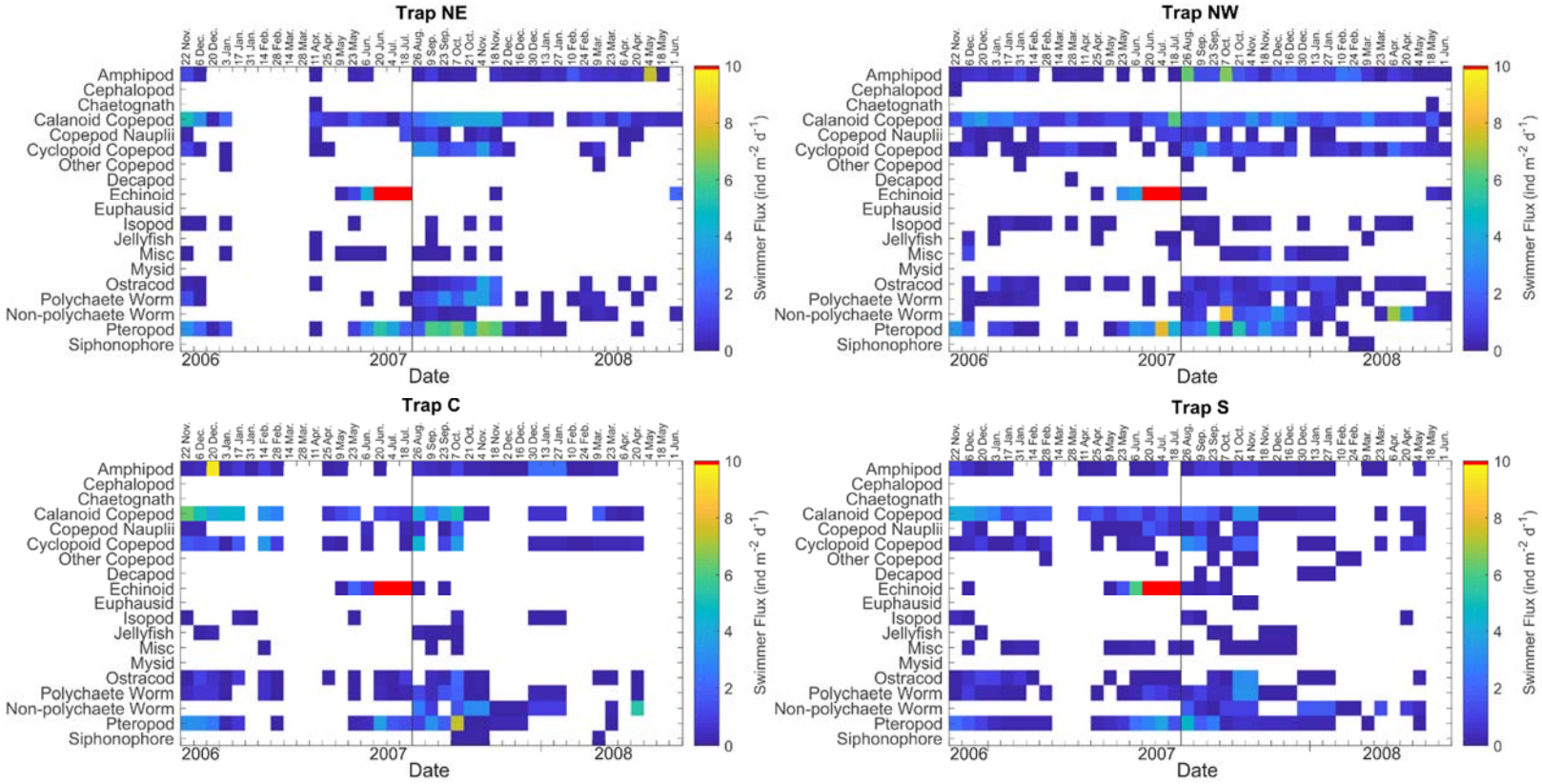

Figure 2.3 Zooplankton swimmer flux reported as individuals m^{-2} d^{-1}. The zooplankton type is shown for each 14 day sampling period. The black line indicates when the traps were recovered and redeployed meaning no samples were collected for the first 3 weeks in August 2007. In summer 2007, before the traps were recovered, there were high swimmer fluxes of echinoids (Ophiuroids) which have been reported separately in Table 2.2.

Table 2.3 Annual POC flux below 2000 m in the IB (November 2006 – November 2007) and transfer efficiency (T_{eff}) calculated using carbon export estimates from Quay et al. (2012) and Henson et al. (2012a). The propagated uncertainty is shown in brackets.

Trap	POC Flux to 2000 m (mmol C m^{-2} yr^{-1})	T_{eff} (%)	
		Quay C Export (surface ocean)	Henson C Export (100 m)
Trap NW	92.78 (± 8.00)	3.3 (± 3.5)	7.4 (± 0.7)
Trap NE	119.12 (± 7.97)	4.3 (± 4.4)	9.5 (± 0.8)
Trap C	103.60 (± 12.62)	3.7 (± 3.9)	8.3 (± 1.1)
Trap S	91.20 (± 6.69)	3.3 (± 3.4)	7.3 (± 0.6)
Mean	101.67 (± 12.28)	3.6 (± 3.8)	8.1 (± 1.1)

The transfer efficiency (T_{eff}) is the ratio of POC that sank to 2000 m depth compared to the magnitude of POC exported at 100 m (Francois et al., 2002; Henson et al., 2012a). The T_{eff} of POC to 2000 m was calculated as in Henson et al. (2012a) using POC export at 100 m (1254 ± 53 mmol m^{-2} yr^{-1}) estimated from satellite data. A second estimate was made using surface (< 10 m) carbon export (2800 ± 2700 mmol m^{-2} yr^{-1}) budgets estimated from O_2/Ar data by Quay et al. (2012) from a basin wide time-series of underway samples in the Subpolar North Atlantic.

2.2.3 Quantifying Mesoscale Spatial Variability

One of the aims of this study was to utilise the unique spatial resolution of the deep ocean sediment traps to determine whether mesoscale variability is a feature of deep ocean carbon fluxes. The POC fluxes of the four sediment trap time-series were compiled to calculate the internally standardised residual (the deviation from the mean POC flux normalised by the mean standard deviation) for each trap, the percentage deviation from the mean POC flux and the range for each sampling period as a percentage of the mean POC flux for Period I-III; these metrics were used as diagnostics to observe and quantify mesoscale variability. The mean, standard deviation, range, maximum and minimum for each diagnostic, and each trap, were calculated for the residuals and percentage deviation, and for the range of the four traps (Table 2.4). The internally standardised residuals are calculated by dividing the residuals by the standard deviation and indicate the relative variability of each trap for each sampling period (Neter et al., 1996). Standardised residuals that are greater than ±2 standard deviations from the mean are defined as outliers. In this study the standardised residuals are used to highlight periods with variability of

greater magnitude than the standard deviation of the total POC flux time-series, which we ascribe to mesoscale variability.

This study aims to identify the temporal scales (sampling period, monthly, seasonally and annually) at which mesoscale variability influences deep ocean carbon fluxes. Exploring the potential spatial variability in the data without the temporal component was not possible using the diagnostics discussed above as at least two years of data would be required to define the seasonal cycle and de-trend the time-series. To identify the presence and magnitude of possible spatial variability for the different timescales we have defined a percentage-based relative threshold limit that is not dataset specific and could be applied more widely in similar datasets to allow for identification of spatial variability.

The relative threshold was determined by multiplying the mean POC flux of all four sediment traps, at each time point, by the determined threshold. This allows the threshold to be proportional to the amount of flux collected which changes considerably during the seasonal cycle (Equation 2.4). The relative threshold is defined as 35 % based on a study on the mesoscale variability of global satellite ocean colour which found that in regions with a strong seasonal cycle, sub-monthly, small spatial scale variation (10 – 200 km) usually contributed to a third of the observed variance and specifically for the IB, small spatial scale variance ranged between 30 and 40 % of total observed variation (Doney et al., 2003). This value is an estimate of the amount of mesoscale variability in surface ocean colour and hence is an estimate of the amount of mesoscale variability we expect to originate from the surface in terms of particle flux. Greater variability is expected in the surface ocean, compared to carbon fluxes to the bathypelagic zone (Antia et al., 2001; Lampitt & Antia, 1997). For a sampling period to be identified as exceeding the expected variability the POC flux, including the full error bars, must plot beyond the 35 % relative threshold.

For each time point:

[Equation 2.4] $$Threshold\ of\ Expected\ Variability = POC\ Flux_{IBMean} \times 0.35$$

2.2.4 Beam Transmission

Beam transmission (%) data from the *RRS Discovery* cruise D321 in the Iceland Basin in October 2006, when the first sediment trap deployments were carried out, was used to investigate the presence of nepheloid layers in the Iceland Basin. Beam transmission was measured on 9 deep CTD downcasts to avoid interference from bottle fires (Briggs et al., 2011), including three of the sediment trap locations (Trap NW, C and S). The transmissometer was not calibrated on board

and so the raw beam transmission data is presented to allow for the relative difference between the mid-water and near seafloor particle loads to be compared.

2.3 Results

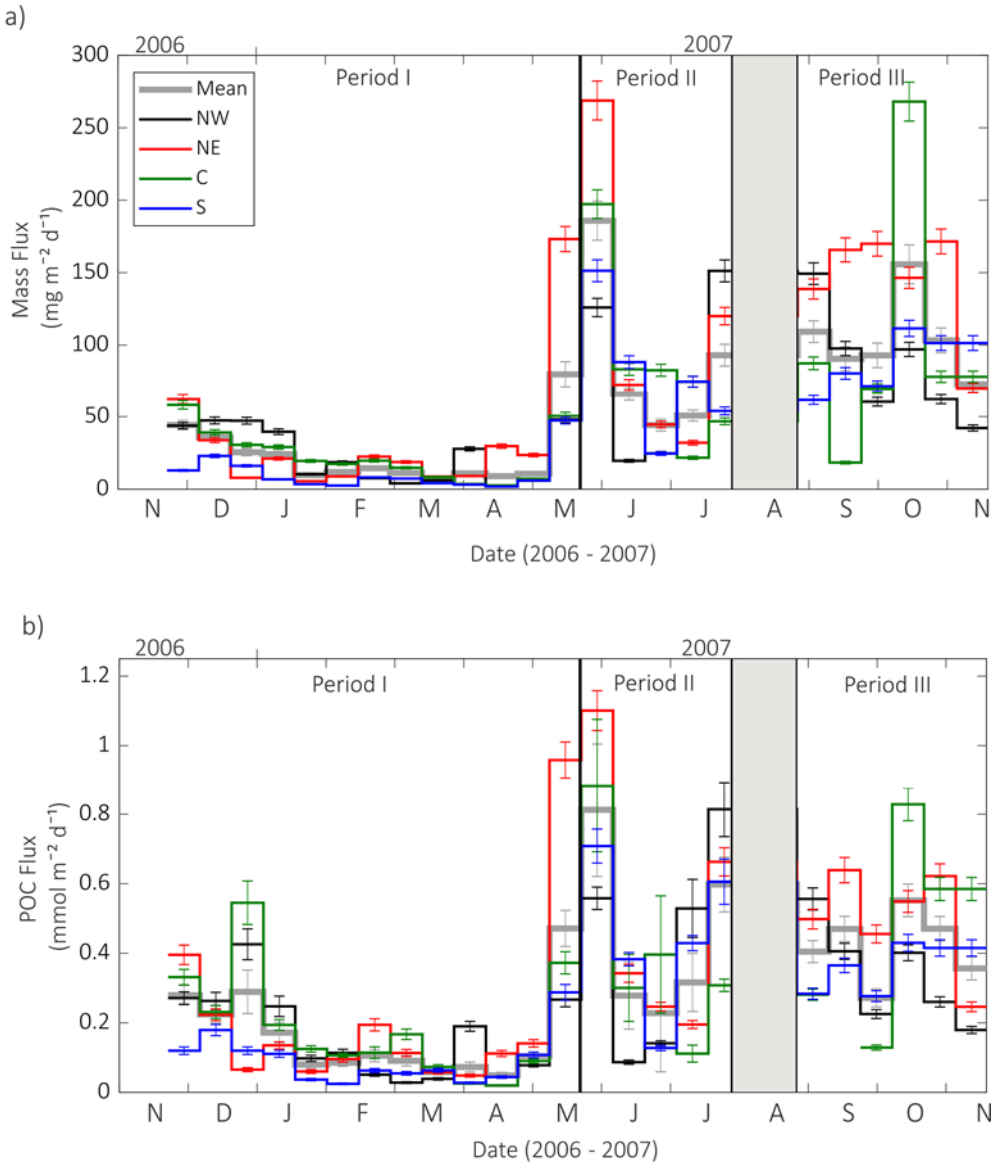

Figure 2.4 a) Mass flux and b) POC flux to the bathypelagic zone in the Iceland Basin during 2006 - 2007. Each trap is plotted by colour with errors bars reporting the propagated uncertainty. The mean flux is the thick grey line. Three flux regimes are highlighted. The sampling gap with no data collection is shaded in grey.

There is a clear seasonal cycle in surface Chl *a* concentration (Figure 2.2) and in the rate of particle flux to below 2000 m in the IB (Figure 2.4), as is expected in high latitude regions. Chl *a* concentration increases in April, and two peaks are observed in late May and mid-summer. In 2006, the Chl *a* peak in May is greater than the second peak in June, whereas for 2007 and 2008

the Chl *a* peak in June-July is greater than the initial peak in May. The Chl *a* concentration in 2007 and 2008 also remains elevated later into summer and autumn.

There is a peak in mass flux in May 2007 associated with the spring bloom, mass flux remains elevated during the summer, although fluxes are lower in June and July compared to August and September. A secondary peak in mass flux occurs during October associated with elevated chlorophyll in the autumn (Figure 2.2 and 2.4a). Mass flux then decreases steadily from autumn. These results fit well into the current understanding of deep ocean particle flux in the mid-high latitude North Atlantic (Frigstad et al., 2015; Honjo & Manganini, 1993; Waniek et al., 2005b).

2.3.1 Sediment Trap Performance

Sediment traps are the most widely used method to measure sinking particle flux in the deep ocean, however it is important to consider how well they performed during both deployments. During Period II, highlighted in Figure 2.4a, the sediment traps were colonised by Ophiuroids (Table 2.2), which may have affected the amount of material collected. Figure 2.3 highlights that the Ophiuroids were likely to have colonised the sediment traps in spring, and continued to grow on the sediment traps until they were recovered. For the deployment 2 sediment traps there was no further evidence that Ophiuroid colonisation occurred.

Mass and POC fluxes from January 2008 onwards are extremely low (Period IV, Figure 2.5 and Appendix A), even during spring which is expected to have high fluxes associated with the peak in Chl *a* concentration in Figure 2.2 (Lampitt, 1985). Examples in the literature of very low mass fluxes have been attributed to the cup opening becoming blocked (Honjo & Manganini, 1993; Wong et al., 1999), screens in the cup opening preventing collection (Conte et al., 2001) and real interannual variability possibly enhanced by low trap efficiency (Antia et al., 2001; Kuss & Kremling, 1999). Deep ocean sediment traps sometimes experience ‘deep ocean storms’ (Gardner & Sullivan, 1981), which can cause strong tilting of the trap (up to 20°; Chiswell & Nodder, 2015) and Honjo et al. (2008) highlights that data from these periods should be discarded. Unfortunately, there is no information regarding the degree of sediment trap tilt available from these sediment trap deployments and I suggest that in the future, all deep ocean sediment trap deployments should have a tilt sensor.

The sediment traps functioned correctly during Period IV, supported by high recorded fluxes of elongated Acantharian cysts in April and May in line with spring 2007 (Martin et al., 2010), suggesting that the sediment traps performed well for heavily ballasted, fast-sinking particles. However, samples from the end of November to mid-February 2008 in Traps NE, C and S contained visibly degraded swimmers (Figure 2.3) and had lower sodium concentrations

(suggesting preservative washout) compared to Trap NW, which had well preserved swimmers (Figure 2.6).

To determine whether the observations are representative of the true flux, the following indicators of trap performance were assessed: current speed, swimmer preservation and POC:PON ratios. The fluxes during Period IV are characterised by low mass, POC and PON fluxes, a lower than expected POC:PON ratio in some samples but average or elevated percentages of POC and PON of total flux (Figure 2.5).

In Period IV the percentages of POC and PON (3 – 29 % and 0.5 – 6 % respectively) to total flux are not unrealistic but there is much greater variability of the percentages between the traps. The POC:PON ratio from the beginning of the time-series to January 2008 is within the expected range, whereas from January 2008 onwards there was a shift towards lower POC:PON ratios compared to the rest of the time-series (Figure 2.5e). Low C:N ratios have been observed in upper ocean sediment traps during low flux periods dominated by fresh biogenic matter of heterotrophic origin (Hargrave et al., 1994). Hebbeln et al. (2000) observed low C:N ratios during a low flux period, hypothesised to be due to remineralisation effects, which likely act differently during a low flux period compared to during a bloom. Furthermore, the POC:PON ratio of samples in Period IV shifted towards an average value of 6 or lower, compared to ratios between 7 – 8 in Periods I-III. It should be noted that the elongated Acantharian cysts have a lower mean POC:PON ratio of 5.0 ± 1.0 compared to the mean POC:PON ratio for deployment 2, and so may contribute to the lower ratios in April and May 2008, as cysts heavily dominated the flux compared to 2007. Acantharia are heterotrophic organisms, which are often found to have lower POC:PON ratios than autotrophs (Anderson, 1992; Hargrave et al., 1994).

To further assess sediment trap performance, the current speeds during Period IV (Figure 2.7 and Figure 2.8) were compared to the previous year of current speed data (Table 2.5). The current speeds during Period IV had larger means compared to the same period the year before (Trap C 2008, mean of 13.9 (± 6.8) cm s^{-1} and Trap S 2008, mean of 12.9 (± 7.50) cm s^{-1}) and there were some instances of consistently high current speeds (> 12 cm s^{-1}), especially in January and February 2008 for Trap C and in January 2008 for Trap S (Figure 2.6 and 2.7). The mean depth of the trap deployments were shallower for deployment 2 compared to deployment 1. As the traps in deployment 2 were ~ 200 m shallower particle fluxes of a larger magnitude would be expected, instead lower fluxes were observed.

Furthermore, whilst Trap C experienced highly variable current direction in January 2008, Trap S observed an event of current speeds > 30 cm s^{-1} consistently flowing southwards (Figure 2.9), which could be indicative of a benthic storm as described by (Gardner & Sullivan, 1981). This

provides evidence that January 2008 was a highly dynamic period and not ideal conditions for sediment trap sampling but does not fully explain all traps collecting extremely low fluxes between January and June 2008, as even periods with continuously slow current speeds collected very little particle flux.

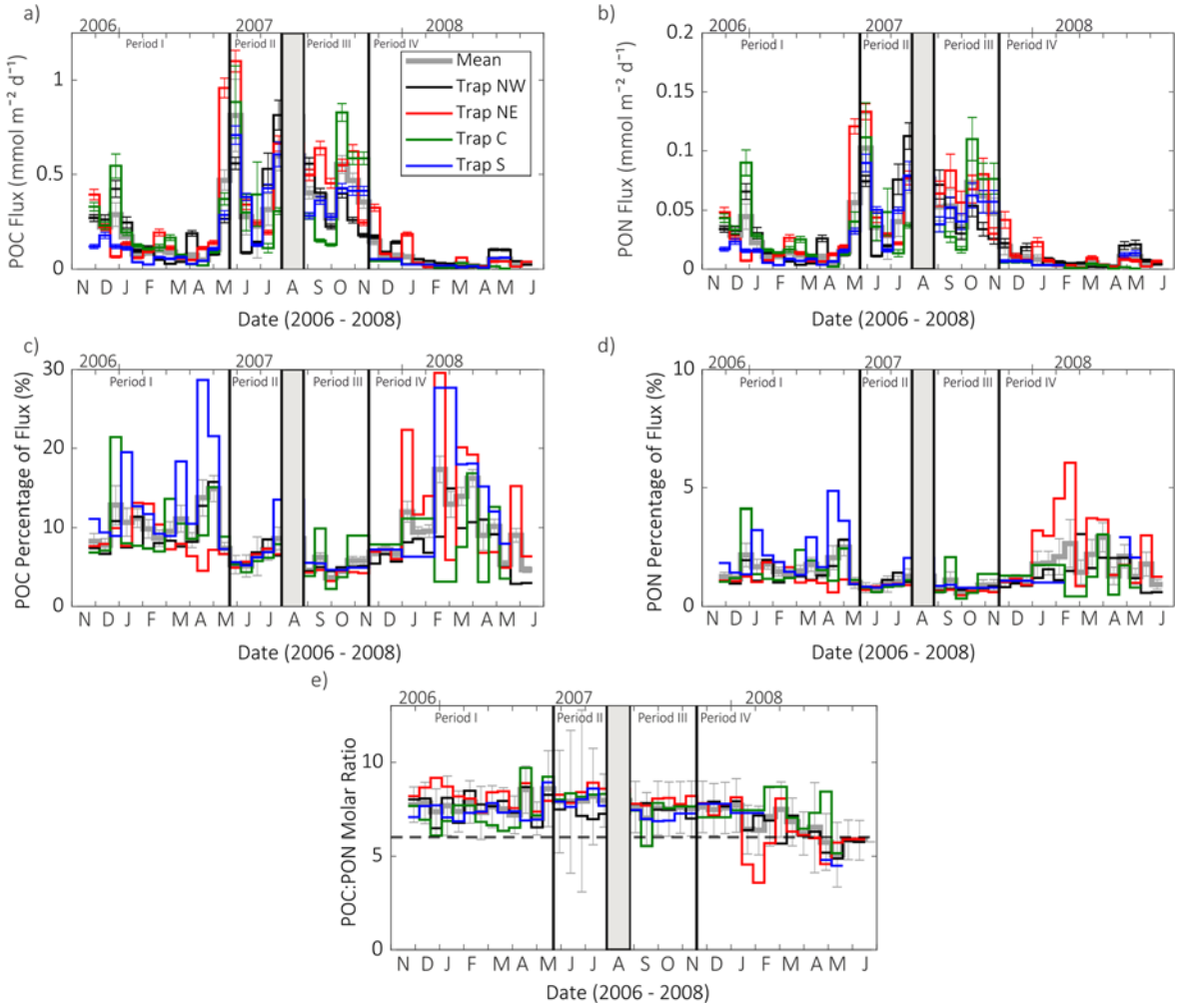

Figure 2.5 a) POC flux, b) PON flux, c) POC content of total mass flux (%), d) PON content of total mass flux (%) and e) POC:PON molar ratio below 2000 m in the Iceland Basin for 2006 – 2008. For figure e) the dashed line represents a POC:PON ratio of 6, which is usually the minimum POC:PON ratio that is expected. Acantharian cysts tend to have a lower POC:PON ratio. The ratio in April and May 2008 is expected to be below 6 as Acantharian cysts were the major contributor to flux.

To investigate whether there was a relationship between current speeds and magnitude of collected flux, a Spearman's rank test was carried out on current speed data and mass flux for all traps during both deployments. The resulting statistically significant correlation indicated an inverse relationship between current speed and mass flux (of $\rho = -0.370$ with a p value of < 0.001 (n=108), Figure 2.10). The test was also carried out for the percentage current speeds > 12 cm s^{-1} which provided a similarly significant inverse relationship ($\rho = -0.39$ with a p value of <0.001,

n=108). There were also no instances of mass fluxes > 100 mg m^{-2} d^{-1} during periods of current speeds > 15 cm s^{-1}. The presence of cysts (each trap had samples with > 1000 cysts in April/ May 2008 with a maximum of 9265 cysts in Trap NW) provides evidence that the traps were collecting very fast sinking particles (> 560 m d^{-1}; Section 4.3.1). Fast current speeds > 12 - 15 cm s^{-1} have been shown in laboratory experiments to cause sediment traps to under-collect, which would predominantly affect slower sinking particles (Baker et al., 1988; White, 1990). Therefore, it may be possible that the traps under-collected slow sinking particles, or particles were resuspended and washed out. This may suggest that during Period IV consistently faster current speeds, particularly with more incidences of current speeds greater than 12 cm s^{-1}, may have led to under-collection, or resuspension, of slower sinking particles whilst the heavily ballasted Acantharian cysts were collected efficiently by the sediment traps.

Fast current speeds could wash out preservative brine from the sample cups. This may have occurred for three traps (NE, C and S) between November 2007 and February 2008, which had visibly degraded swimmers. Furthermore, for deployment 2, traps NE, C and S had a considerably lower sodium concentration in the trap supernatant, compared to the blank preservative concentration, with most samples for Trap C and the 2008 samples from Trap S approaching seawater sodium concentrations (Figure 2.6).

In December 2008 a period of continuously high current speeds occurred, with speeds up to 36.5 cm s^{-1}, lasting for 2 - 4 weeks, which may explain the lower sodium concentrations but does not explain samples from later in 2008 that sampled low fluxes. Poorly preserved sediment trap samples are expected to be characterised by increased molar POC:PON ratios as organic nitrogen is preferentially remineralised and the POC and PON content would be low indicating a greater proportion of refractory material (Antia, 2005). However, POC makes up at least 3 % of total mass flux in all IB sediment trap samples suggesting the material is not refractory. Also, it is unlikely that the traps sampled resuspended material from benthic nepheloid layers, which usually presents as a POC content < 1 % of total flux (Gardner et al., 2017).

Samples from Period IV (late November 2007 to June 2008) have very low fluxes, with greater variability in POC/PON content and POC:PON ratio and likely under-collected sinking flux, except for Acantharian cysts, which were sampled in great numbers and were well preserved. Therefore, we have deemed the sediment trap results from Periods I,II and III reliable, whereas the results from Period IV are unusual, and hence the Period IV fluxes were not used to calculate the annual budget of carbon sequestered in the deep ocean IB or to explore the implications of mesoscale variability.

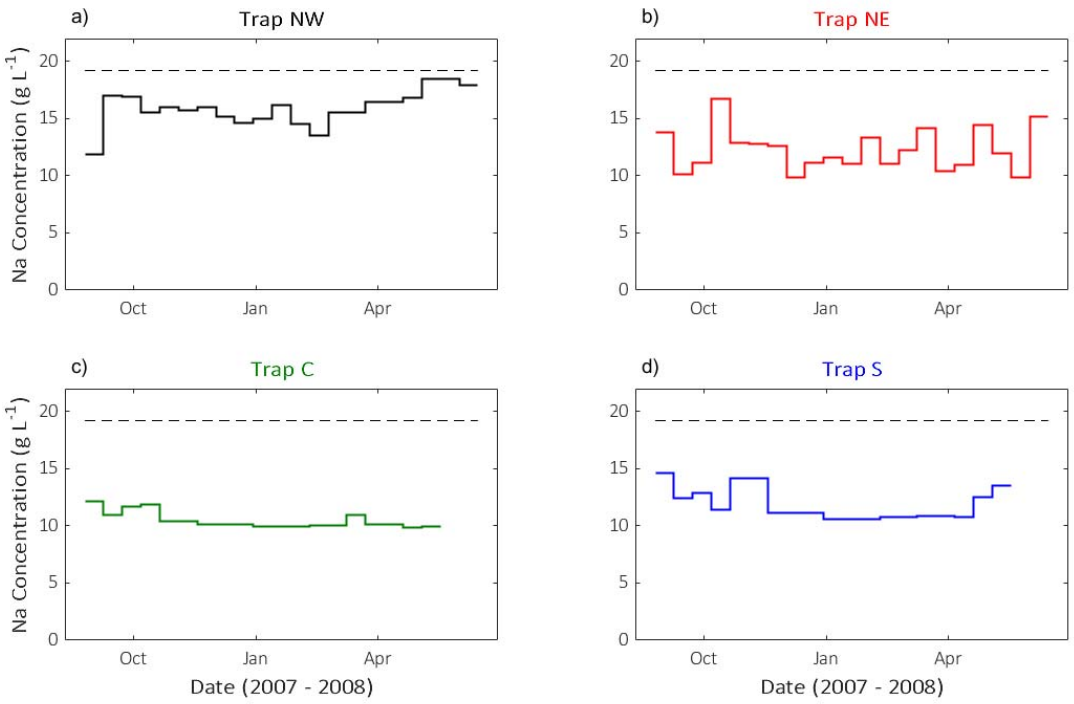

Figure 2.6 Sediment trap supernatant sodium concentration for Traps NW, NE, C and S. The dashed line represents the trap preservative blank Na concentration of 19.2 g L^{-1}. The Na concentration of seawater is usually 10.5 g L^{-1}.

Table 2.4 The mean (± standard deviation), range, maximum and minimum of the standardised residual and the percentage deviation from the mean for each individual sediment trap and the range as a percentage of the mean for the Periods I-III.

	Standardised Residual				Deviation (% of mean)				Range (% of mean)			
	Mean (± std)	Range	Max	Min	Mean (± std)	Range	Max	Min	Mean (± std)	Range	Max	Min
Trap NW	-0.19 (± 1.0)	3.8	1.7	-2.1	- 4.6 (± 53.6)	229.6	160.5	-69.1	-	-	-	-
Trap NE	0.43 (± 1.1)	5.54	3.8	-1.7	18.3 (± 46.7)	206.2	128.8	-77.4	-	-	-	-
Trap C	0.15 (± 1.1)	4.45	2.2	-2.3	8.5 (± 47.5)	153.4	88.6	- 64.8	-	-	-	-
Trap S	-0.38 (± 0.6)	2.3	0.9	-1.4	-21.8 (± 30.0)	108.8	37.7	-71.1	-	-	-	-
All	-	-	-	-	-	-	-	-	107.8 (± 45.5)	188.0	225.3	37.4

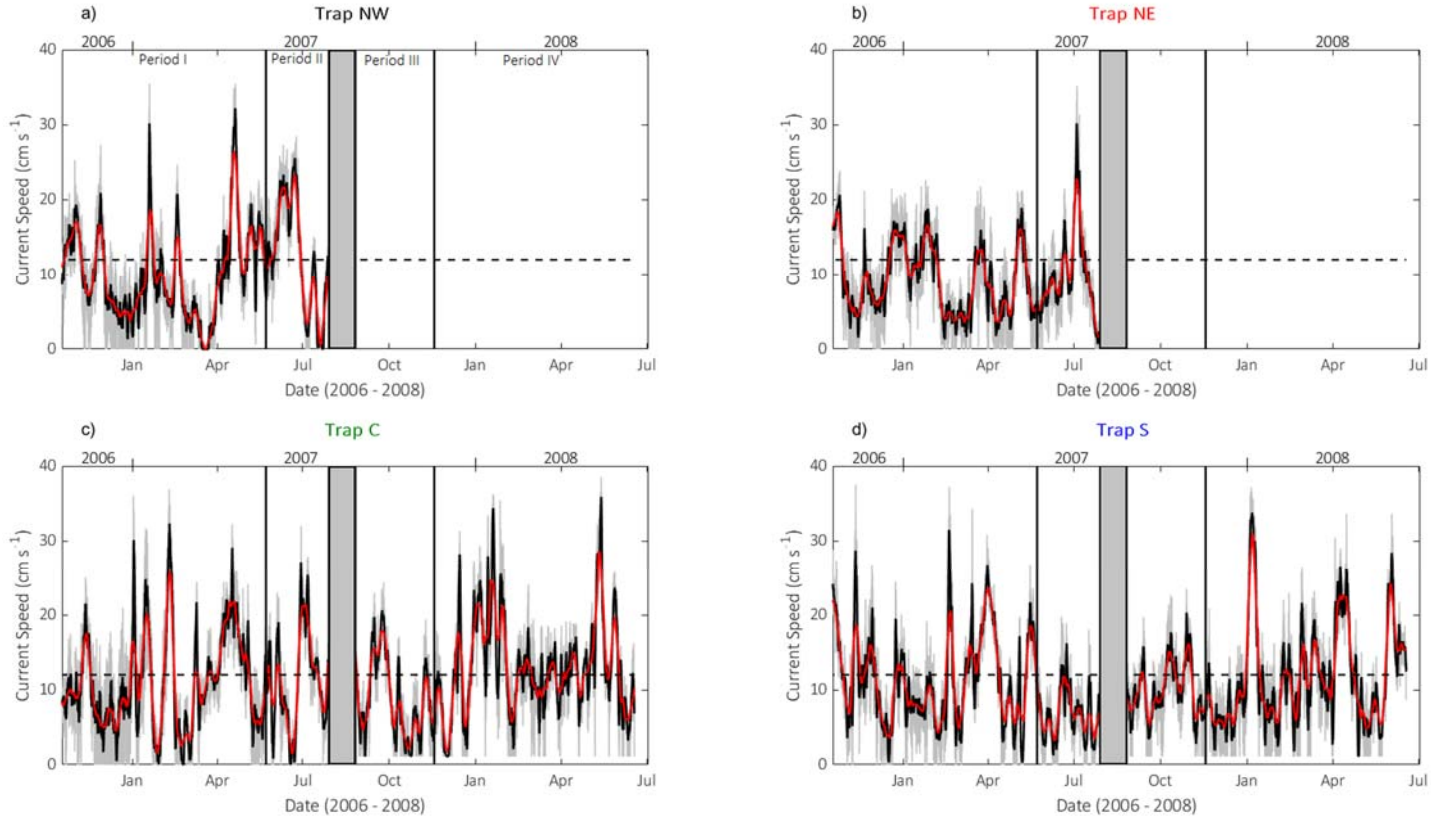

Figure 2.7 Current speed data from 2000 m at each sediment trap location - a) Trap NW, b) Trap NE, c) Trap C and d) Trap S. The data from Trap NW and Trap NE were not successfully recovered from deployment 2. The grey line is hourly data, the black line is a daily moving mean and the red line is a weekly moving mean. The black dashed horizontal line highlights current speeds of 12 cm s^{-1} above which sediment traps are often thought to under-collect (Baker et al., 1988; Gardner, 1985).

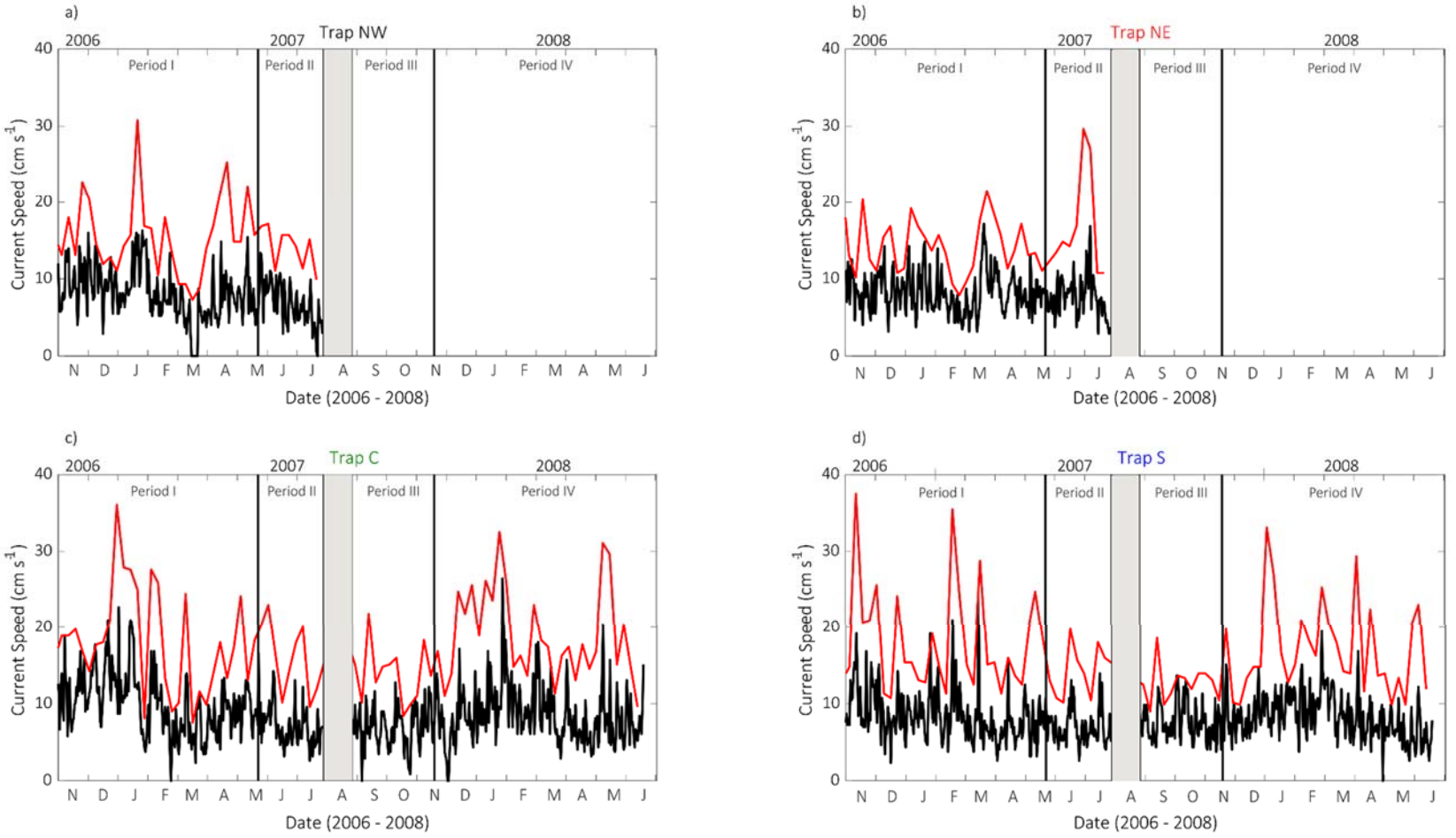

Figure 2.8 Current speed range from 2000 m at each sediment trap location - a) Trap NW, b) Trap NE, c) Trap C and d) Trap S. The data from Trap NW and Trap NE were not successfully recovered from deployment 2. The black line is the daily range and the red line is a weekly range.

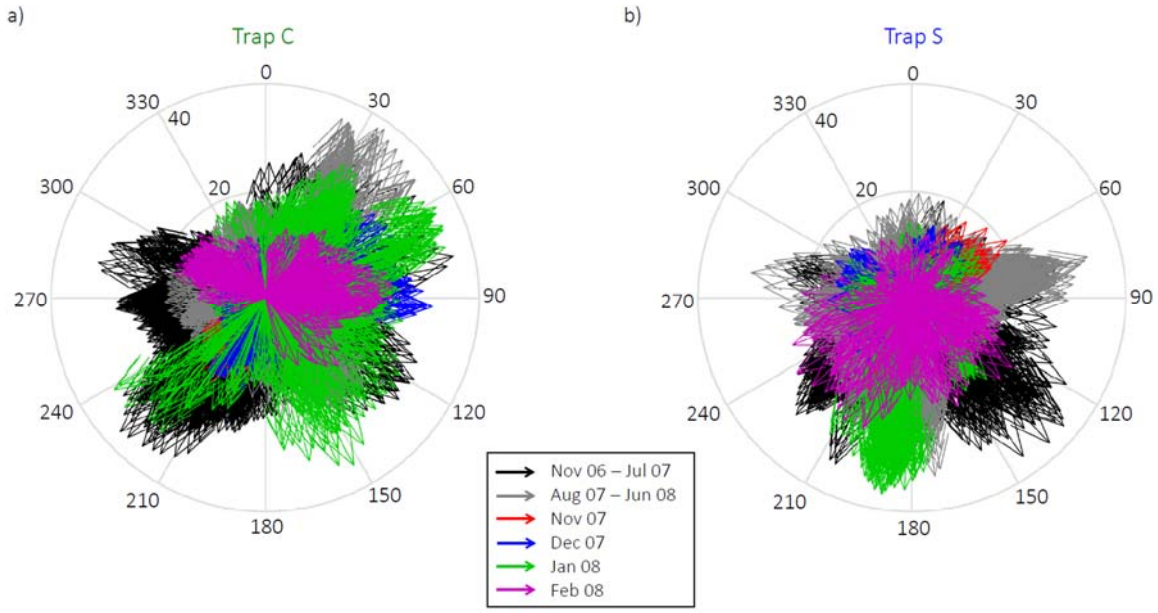

Figure 2.9 Current direction and speed (cm s^{-1}) for Trap C and Trap S from the IB. The arrows are colour coded as in the legend to highlight the strong currents and directional changes during January 2008.

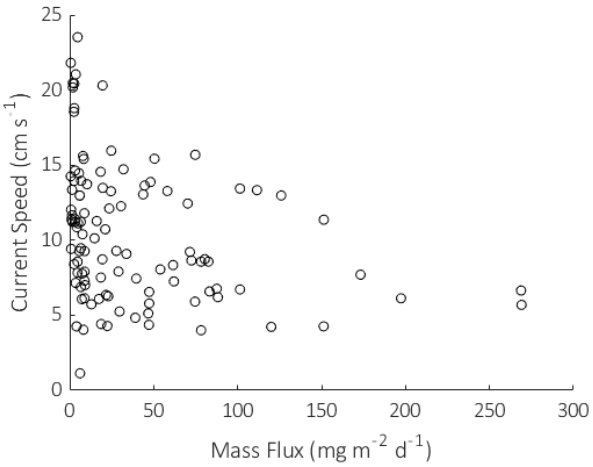

Figure 2.10 Mass flux and 14 day mean current speed for all sediment trap data from 2006 – 2008 in the Iceland Basin.

Table 2.5 A summary of current speed mean, maximum, interquartile range and percentage of the sampling time that currents were greater than 12 cm s^{-1} for each trap during the two deployments and for each period from January 1st to June 15th for 2007 and 2008 to allow for comparison. To allow the mean and maximum speeds to be comparable all speeds < 1.1 cm s^{-1} in deployment 1 have been converted to 1.1 cm s^{-1}. This may conflate the mean speeds slightly but will allow for representative comparisons between the datasets. One standard deviation is reported in the brackets.

Trap	Sampling period	Mean current speed (cm s^{-1})	Maximum current speed (cm s^{-1})	Interquartile Range	% deployment time > 12 cm s^{-1}
NW	Nov 06 – Jul 07	10.40 (± 7.03)	35.45	9.88	36.7
NE	Nov 06 – Jul 07	9.39 (± 5.37)	35.16	7.56	28.3
C	Nov 06 – Jul 07	10.98 (± 7.19)	36.91	10.17	39.3
S	Nov 06 – Jul 07	9.87 (± 6.12)	37.20	7.85	31.0
C	Aug 07 – Jun 08	11.86 (± 6.93)	38.59	8.72	45.7
S	Aug 07 – Jun 08	11.18 (± 6.54)	37.13	7.85	37.8
C	Jan 07 – Jun 07	11.62 (± 7.51)	36.91	10.46	43.0
S	Jan 07 – Jun 07	10.44 (± 6.59)	37.20	8.72	34.2
C	Jan 08 – Jun 08	13.88 (± 6.80)	38.59	7.56	57.8
S	Jan 08 – Jun 08	12.89 (± 7.50)	37.13	10.17	48.4

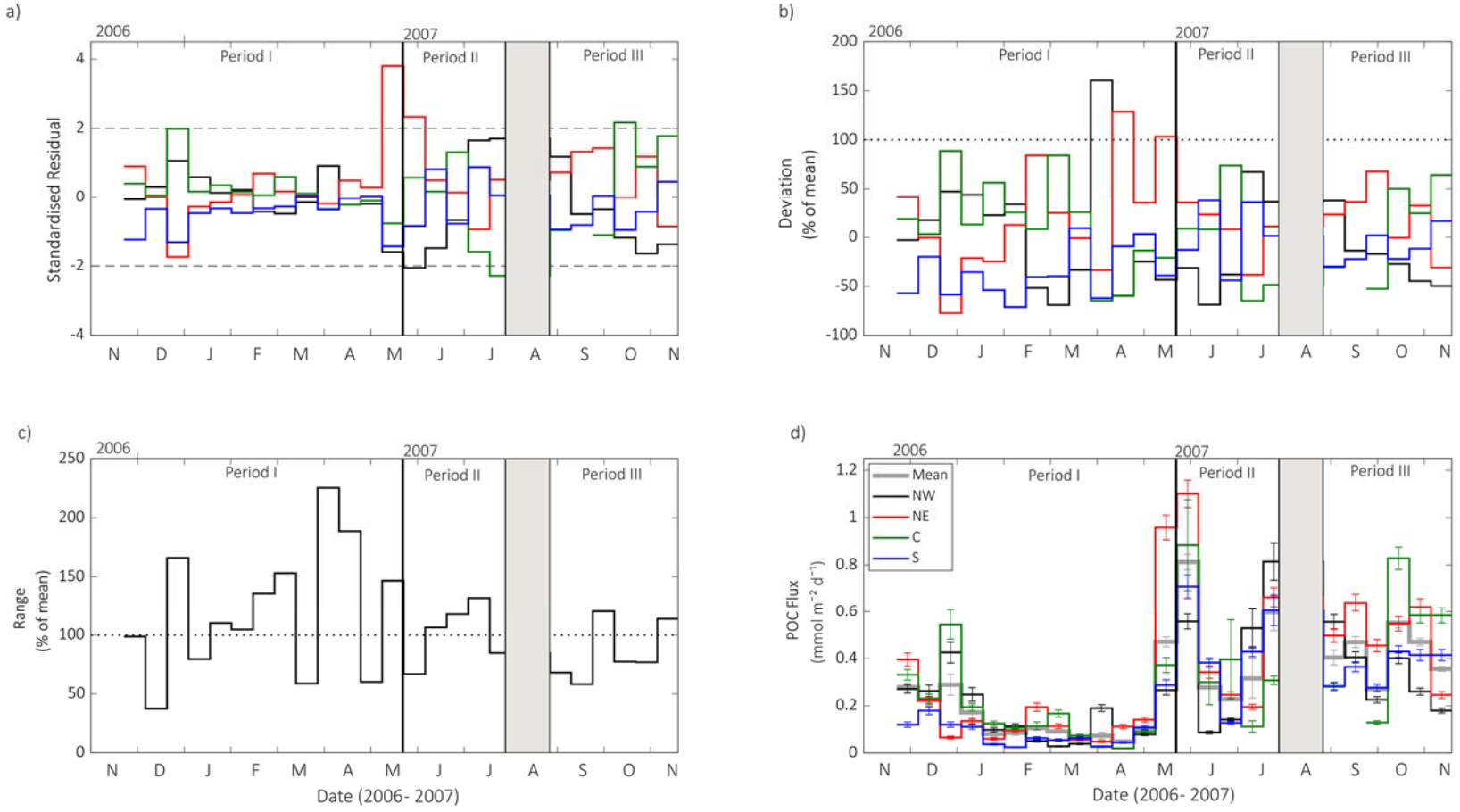

Figure 2.11 a) Standardised residuals, b) the percentage deviation of the mean, c) the range as a percentage of the mean and d) POC flux of the sediment trap dataset for Periods I-III. The dashed horizontal lines in a) highlight samples which deviate by more than two standard deviations, in b) the dashed line highlights samples which are 100 % larger than the mean POC flux and in c) the line highlights sampling periods when the range is greater than 100 % of the mean POC flux.

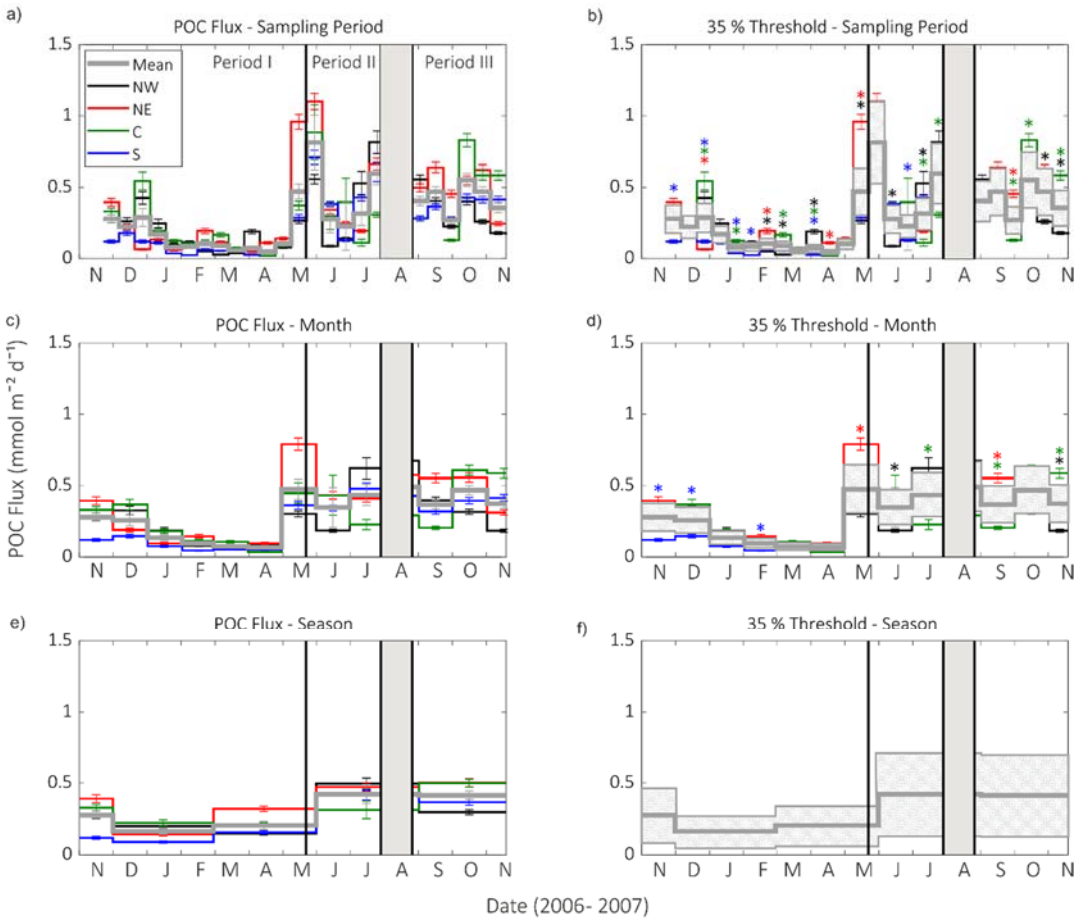

Figure 2.12 POC flux time-series (a,c,e) for all traps and the mean plotted for comparison with the relative threshold of expected spatial variability overlain in plots b), d), f). Mesoscale variability is investigated for different timescales – the sampling period (14 days) in b), monthly timescales in d) and seasonal (3 months) in f). A trap time period is considered to be exhibiting mesoscale variability if the flux and full error bars are visible outside of the threshold and have been highlighted with stars coded by the colour relating to the trap.

2.3.2 Carbon Sequestration in the Iceland Basin

The seasonal cycle of POC flux to 2000 m in the IB closely tracks the mass flux cycle (Figure 2.4). There are some instances of greater spatial variability between the traps in POC flux which is not observed in mass fluxes. The annual mean POC flux to 2000 m in the IB is 101.7 (± 12.28) mmol C m^{-2} yr^{-1}, which is 16.3 % lower than the global average of 120 (± 14.9) mmol C m^{-2} yr^{-1}, estimated by Honjo et al. (2008), and 7.8 % greater than the Atlantic Ocean average of 94.3 mmol C m^{-2} yr^{-1} in Lampitt and Antia, (1997). Variability between the traps is observed as annual POC fluxes ranged

from 91.20 to 119.12 mmol C m^{-2} yr^{-1}, with the Trap S and Trap NE having the lowest and highest flux, respectively. T_{eff} was estimated using POC export estimates of 2.8 (± 2.7) mol C m^{-2} yr^{-1} from the basin wide surface (< 10 m) ocean samples collected in the Subpolar North Atlantic (Quay et al., 2012) and 1.25 (± 0.05) mol C m^{-2} yr^{-1} from 100 m depth estimated from as in Henson et al. (2012a). The mean T_{eff} from the surface ocean was 3.6 (± 3.8) % and from 100 m was 8.1 (± 1.1) %.

2.3.3 Mesoscale Spatial Variability in the Deep Ocean Iceland Basin

Variability between the traps is apparent in Figure 2.4 for both mass and POC flux and there appears to be a general trend of less spatial variability in winter and early spring, and greater spatial variability in late spring, summer and autumn. If the percentage of POC content varies, it can lead to periods of similar mass flux but variability in POC flux, such as in late December 2006.

To assess how each traps' POC flux varies in relation to the mean POC flux, standardised residuals were calculated to highlight periods of greater variability and outliers were identified by standardised residuals greater than ±2 (Figure 2.11 and Table 2.4). The standardised residuals of the POC flux highlight that the periods that exhibit the largest mesoscale variability with values > 2 are December 2006, May 2007, August 2007 and October 2007 with the greatest variability found during the spring bloom peak in May. The mean standardised residual for Trap S was -0.38 (± 0.6), which was the lowest mean with the smallest standard deviation, whilst the mean standardised residual for Trap NE was 0.43 (± 1.1), which was the largest mean and the largest standard deviation (Table 2.4). This shows that Trap S consistently sampled lower POC fluxes with the smallest seasonally-driven differences in flux, whilst Trap NE consistently sampled greater POC fluxes and exhibited the largest seasonally-driven differences in flux (Figure 2.11). These observations are reinforced by the range, minimum and maximum of the standardised residuals in Table 2.4, with the maximum standardised residual of 3.8 during the spring bloom-associated peak in flux in Trap NE and the minimum residual of -2.3 during July 2007 for Trap C.

The standardised residuals are influenced by the magnitude of POC flux related to the seasonal cycle, with greater residuals during periods of larger fluxes. When comparing the standardised residuals with the percentage deviation of each sediment trap from the mean POC flux (Figure 2.11b), which normalises the deviation to the magnitude of flux, the variability between the traps appears more pronounced for all sampling periods. The POC flux associated with the spring bloom for Trap NW in April 2007 and for Trap NE in April and May 2007 have the greatest deviations of > 100 % greater than the mean (Figure 2.11b). The mean percentage deviation for each sediment trap follows the same trend as the standardised residuals with a mean value of -21.8 (± 30.0) %

deviation for Trap S whilst Trap NE had a mean value of 18.3 (± 46.7) % (Table 2.4). Trap NW had the largest range of percentage deviation of 230 %.

A further way to investigate the relative differences between the traps for each sampling period was to calculate the range of POC fluxes as a percentage of the mean (Figure 2.11c). The average range in POC flux between the traps for one sampling period during the time-series was 107.8 (± 45.5) % of the mean, with a minimum range of 37.4 % and a maximum range of 225.3 % (Table 2.4). Similar to the percentage deviation, the range also highlights April 2007 as the sampling period with the greatest variability, which is not detected in the standardised residuals due to the small magnitude of the POC fluxes (Figure 2.11). The other period with the second greatest range is December 2006 which is observed as a highly variable period in all plots due to Trap NW and C sampling greater POC fluxes, whilst Trap NE and Trap S sampled similar lower POC fluxes.

The variability in POC flux was also investigated for different temporal periods – the sampling period (14 days), monthly, seasonally and annually. Additionally, to investigate spatial variability using a method that is transferrable to other datasets and regions, we defined a relative threshold of expected variability originating from the surface ocean as 35 % of mean POC flux, as described in Section 2.4, which is independent for each time point. The relative threshold has been overlain on POC fluxes to highlight whether trap fluxes plot outside of the expected variability (Figure 2.12). Data points that plot beyond the thresholds (including full error bars) are considered as exhibiting mesoscale variability beyond what might be expected from surface ocean chlorophyll variability, and have been highlighted with a coloured star in the subplots b, d and f, for sample period, monthly and seasonal timescales in Figure 2.12. The figure demonstrates that, when averaging over longer time scales, the importance of mesoscale variability decreases.

Over timescales of individual sampling periods, 29 % of data points (n = 28) exhibited variability beyond the threshold, and for monthly timescales 21 % of data points (n = 10) exhibited variability greater than expected. However, no POC fluxes exceeded the threshold of expected variability on seasonal timescales. This implies that considerable spatial variability was present in deep ocean POC flux in the IB, but when evaluating the data over long temporal periods, the magnitude of the spatial variability is lessened by the temporal averaging. For Periods I-III, using the threshold of expected variability for the sampling period timescale, 29 % of instances of mesoscale variability (n = 28) were in spring, 18 % were in summer, 29 % in winter and 25 % in autumn (Figure 2.12). These findings support the hypotheses that spatial mesoscale variability is important for deep ocean POC fluxes on short temporal scales (monthly or less), whilst for longer temporal scales, there is little effect of mesoscale variability.

To support this conclusion further, the annual POC budget can also be considered. The annual percentage deviation from the mean annual POC flux was -10.3 % for Trap S, -8.8 % for Trap NW, 1.9 % for Trap C and 17.2 % for Trap NE. Therefore the traps did not deviate more than 35 % from the mean annual POC flux suggesting that, on annual timescales, mesoscale varibility in deep ocean POC flux is relatively small.

2.4 Discussion

2.4.1 Sediment Trap Performance

The sediment traps were deployed in a spatial array to investigate the influence of passing mesoscale features on deep ocean particle flux in the dynamic IB. Assessing sediment trap performance and collection efficiency has continued to be a challenge, as it is not possible to know the accurate *in situ* flux to the deep ocean (Antia et al., 1999; Scholten et al., 2001). There were periods of fast current speeds throughout the time-series (Figure 2.7), which may have affected collection efficiencies of the sediment traps but we assume that all traps have collected efficiently, excluding Period IV.

During Period II the sediment traps were colonised by Ophiuroids (Table 2.2), which are known to affect the amount of material collected. The fluxes for Period II may therefore be a lower limit of true flux, although we are unable to quantify this (Lampitt et al., 2002). The scale of the Ophiuroid colonisation compared to the study of Lampitt et al. (2002) at the PAP site was less; the most heavily colonised Trap NW, collected 1349 specimens over 95 days, compared to 1589 specimens collected over 70 days at the PAP site. The other three traps (NE, C and S) were less heavily colonised, with an average of 604 specimens collected over 81 days. Trap C was the least colonised trap, probably because it was furthest from topographic features such as the Reykjanes Ridge and the Rockall Plateau. It is possible that any mesoscale variability observed during that period may be at least partly due to Ophiuroids. The fluxes during Period II are likely to be a lower limit, but as fluxes were still of reasonable magnitude, we assume that the change to the overall carbon budget and our conclusions is minimal.

2.4.2 How Much Carbon is Sequestered in the Deep Ocean Iceland Basin?

The annual mean POC flux to 2000 m in the IB is 101.7 (± 12.3) mmol C m^{-2} yr^{-1}. This is 16.3 % lower than the global average of 120 mmol C m^{-2} yr^{-1} estimated by Honjo et al. (2008), but 7.8 % greater than the global average estimated by Lampitt and Antia, (1997) of 94.3 mmol C m^{-2} yr^{-1}. The IB estimate of annual mean POC flux to 2000 m is, however, 22 % lower than the Atlantic

Ocean average estimated by Lampitt and Antia, (1997), and 12 % lower than the North Atlantic average estimated by Henson et al. (2011) study which presented a reduced strength estimate of the BCP. The annual flux at 3000 m observed at the PAP site (11° of latitude south of OWSI) was 180 mmol C m^{-2} yr^{-1}, which is considerably larger than our observations below 2000 m in the IB (Lampitt et al., 2010). This suggests that deep ocean carbon fluxes estimated at the PAP site are not analogous to fluxes in the IB.

The T_{eff} estimates from the four traps ranged between 7.3 and 9.5 % based on calculations of export flux at 100 m (Henson et al., 2012a), and 3.3 – 4.3 % based on calculations of the export estimate by Quay et al. (2012) from the surface ocean. The T_{eff} estimated using satellite-derived carbon export at 100 m depth are expected to be greater than the T_{eff} estimates from the surface ocean samples collected in the Subpolar North Atlantic as considerable remineralisation of flux occurs in the euphotic zone. Our T_{eff} estimates based on Henson et al. (2012a) are similar to the T_{eff} estimated by Weber et al. (2016), while the lower T_{eff} estimates are more similar to those by Devries and Weber, (2017). T_{eff} has been shown to be lower at high latitudes as more labile material is exported from the surface ocean and readily remineralised (Francois et al., 2002; Henson et al., 2012a). In contrast, other studies have found the opposite trend, with greater T_{eff} at high latitudes, such as Weber et al. (2016) who found ~ 20 % of exported POC will be sequestered for > 100 years in the IB. This is the first estimate of the annual average T_{eff} to the deep ocean IB, using *in situ* carbon export data from the surface ocean and sediment trap data, with the efficiency falling in the range of 1 - 10 %, consistent with previous studies (Francois et al., 2002; Henson et al., 2012a).

The annual average T_{eff} estimate presented in this study is integrated over many different plankton community successions, which drive changes in flux magnitude and composition throughout the seasonal cycle (Henson et al., 2012a; Lampitt et al., 2009; Wilks et al., 2017), therefore there are likely to be periods where the POC flux T_{eff} is higher and periods where is it lower. An incidence of efficient transfer through the mesopelagic zone was observed during a spring diatom bloom in May 2008, in the west of the IB (61 °N 27 °W), with 25 – 43 % of POC flux at 100 m reaching 750 m (Martin et al., 2011). Unfortunately this efficient transfer coincided with the unusual Period IV sediment trap data and so we are unable to discuss whether the observed localised high T_{eff} down to 750 m impacted the POC flux at 2000 m in the IB. If episodic pulses of labile flux do penetrate below 2000 m annually it suggests that other periods of flux must have very low T_{eff} to fall within our suggested range.

The IB represents 0.6 % of the spatial extent of the North Atlantic but only contributes 0.2 (± 0.03) % of the deep ocean organic carbon flux in the North Atlantic as less than one third of the IB is

deeper than 2000 m. This budget is considered as a lower limit due to colonisation of the sediment traps during Period II, as discussed in Section 2.4.1. Due to the topography of the IB, combined with fast current speeds, sediment traps may not be the most suitable instrumentation to provide undisturbed, accurate, year-round estimates of carbon flux.

Interannual variability and the strong seasonal cycle at high latitudes are likely to affect the annual budget of carbon storage. From the dataset in this study we were unable to obtain an indication of the scale of interannual variability in particle flux in the deep ocean IB due to the flagged data for Period IV. For carbon to be sequestered in the deep ocean on timescales significant for climate change, particles must sink below the winter mixed layer depth to escape re-ventilation the following year (Palevsky & Nicholson, 2018). During the winter of 2007, Argo float profiles recorded a maximum MLD of 617 m. This is deeper than the mean North Atlantic maximum MLD, which is usually between 150 and 200 m (latitude 42.5 - 72.5 N; Cole et al., 2015). Compared to the Irminger Basin, which can experience maximum MLD > 1000 m (Pickart et al., 2002; Våge et al., 2009), sinking particles may be more likely to remain below the winter maximum MLD in the IB, but compared to the temperate North Atlantic, which has a much shallower maximum MLD, the IB is likely to be less efficient at sequestering carbon in the deep ocean on timescales significant for climate change.

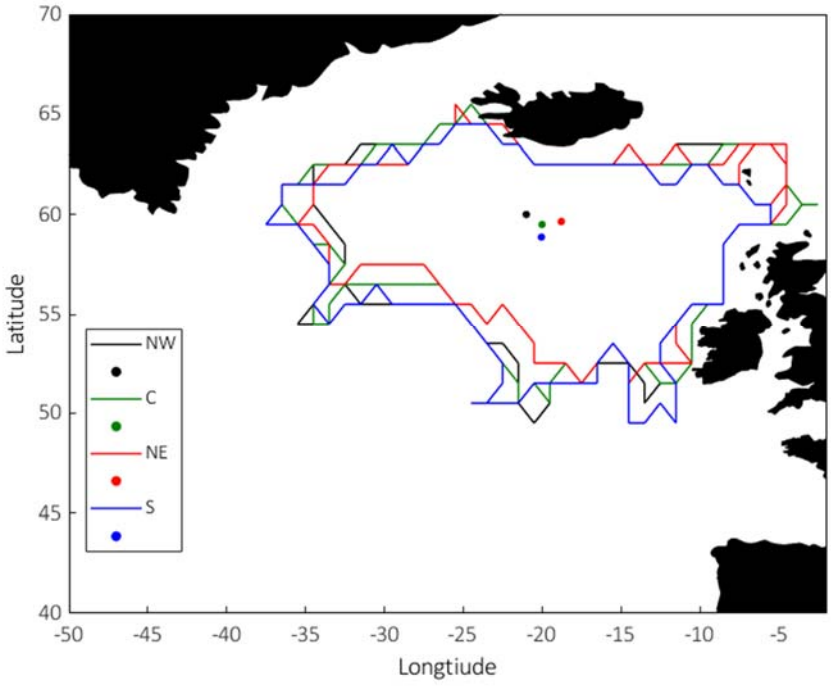

Figure 2.13 The estimated footprint of export for Trap NW (black), Trap NE (red), Trap C (green) and Trap S (blue) calculated as in Henson et al. (2016). The footprints trace around the Faroe Islands, which is an artefact due to an absence of model output, but in reality the footprints would likely include the Faroe Islands.

2.4.3 Does Spatial Mesoscale Variability Affect Deep Ocean Carbon Budgets?

2.4.3.1 Spatial Variability in Iceland Basin Upper Ocean Carbon Export

Spatial variability in deep ocean sediment traps is likely to originate from surface ocean spatial variability of biogeochemical parameters, such as primary production. The surface ocean biogeochemical properties of the IB appear to differ from the Irminger Basin Ocean Observatories Initiative and the PAP sustained observatory biogeochemical footprints in Henson et al. (2016). This suggests that the IB is a biogeochemically distinct region of the North Atlantic. The footprint for upper ocean carbon export represented by the four trap locations is shown in Figure 2.13, which, as expected, indicates that the IB is representative of the eastern Subpolar North Atlantic, but due to the complex topography of the Rockall Plateau and Reykjanes Ridge (Figure 2.1) this similarity of the footprints may not extend to the deep ocean IB. Furthermore, the four sediment trap locations have extremely similar footprints as derived from a non-mesoscale resolving model (Figure 2.13). As the biogeochemical footprints of the sediment traps derived from the model are similar, this implies that mesoscale features, which are not resolved by the model, may be responsible for the observed variability in POC flux. Alternatively, large scale processes that only impact carbon fluxes below the surface ocean may play a role, such as the mixed layer pump (Dall'Olmo et al., 2016; Giering et al., 2016; Lacour et al., 2019). The mixed layer pump transports organic particles deeper into the mesopelagic zone if there is a period of ephemeral stratification, followed by a deep mixing event, prior to sustained seasonal stratification that promotes the beginning the of the spring bloom (Dall'Olmo et al., 2016). The mixed layer pump has been found to contribute 4.58 mmol C m^{-2} d^{-1} to ocean interior in the Subpolar North Atlantic (Lacour et al., 2019), which may sustain mesopelagic organisms before the pulse of organic material associated with the spring bloom arrives.

2.4.3.2 Spatial Variability in Iceland Basin Deep Ocean Carbon Flux

This study aimed to quantify mesoscale variability in deep ocean carbon fluxes. Our finding that spatial mesoscale variability is present at 2000 m depth in the IB suggests that, due to the usually sparse measurements of sinking particle flux to the deep ocean, we cannot assume that local spatial variability is minimal (Antia et al., 2001). Spatial mesoscale variability is most likely to have originated from the surface ocean and persisted during the transit to the deep ocean, but other processes such as lateral advection (Siegel et al., 2008) or resuspended material in nepheloid layers (Gardner et al., 2018) cannot be ruled out as drivers of mesoscale variability in the deep ocean. Beam transmission data collected during the IB cruise that deployed the sediment traps in October 2006 indicates that nepheloid layers do not usually extend > 100 metres above the

seafloor, especially at the three sediment trap locations (Figure 2.14). However, it is possible that during high current speed events these nepheloid layers may extend further into the water column and affect the composition of sampled material.

Annual integrated POC fluxes to the deep ocean appear not to be greatly affected by mesoscale variability, but on timescales less than a year, spatial variability could make an important contribution to POC flux time-series. This means that POC flux time-series from an individual site may not solely represent seasonal variation, which thus complicates interpretation of seasonal and interannual variability in single trap flux time-series.

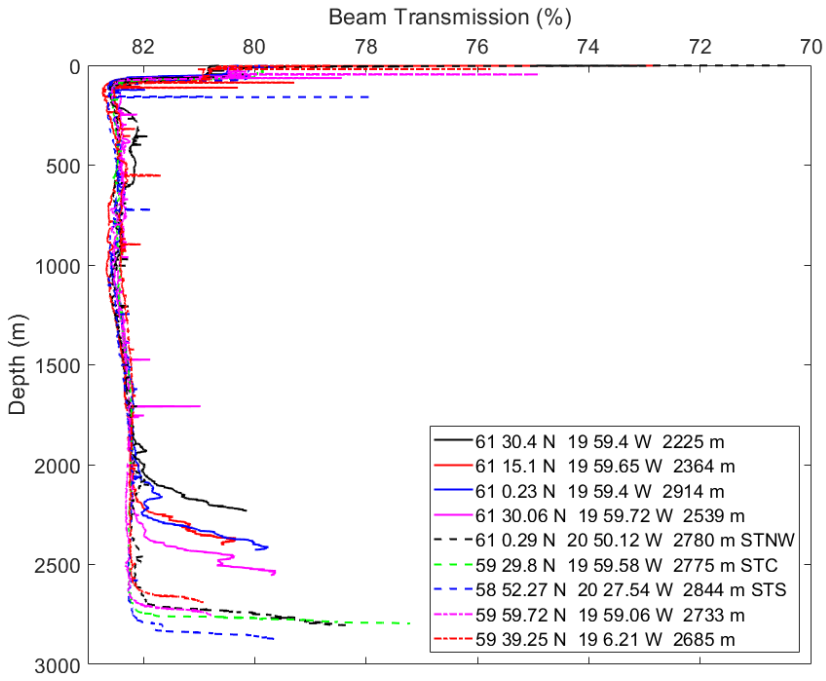

Figure 2.14 Beam transmission (%; uncalibrated) profiles in the Iceland Basin on the 16th and 17th of October 2006 to show the upward extent of nepheloid layers from the seafloor. Each profiles location is shown and the maximum water depth is shown. CTD profiles were undertaken at three of the four sediment trap locations and are indicated in the legend.

Our results highlight spring as the season with greater mesoscale variability, but mesoscale variability is observed throughout the time-series with greater variability observed transiently in all seasons. The mean range of the POC fluxes of the four sediment traps, for each sampling period as a percentage of the mean, was 108 % (Figure 2.11c), which means that the mean range is more than double the mean POC flux. Sediment trap errors are usually ~ 10 %, which means a large percentage of the variability is not accounted for. When comparing this to the relative threshold of expected variability, defined as 35 % of the mean POC flux and based on the estimated amount of mesoscale variability originating from the surface (Doney et al., 2003), it

appears that spatial variability increases as particle flux transits through the water column. However, in contrast the POMME sediment trap study found that the mesoscale variability in annual POC flux at 1000 m was 32 %, which was deemed as not negligible and suggests that spatial variability may decrease with depth when considering longer timescales (Guieu et al., 2005). Biological drivers of spatial variability in the deep ocean may be more prominent in spring and summer due to the spring bloom, whilst physical drivers of variability, particularly eddies, may be more likely to occur throughout the annual cycle and may make a greater relative contribution in autumn and winter, which will be explored in Chapter 3. Mesoscale variability becomes increasingly important for shorter averaging periods, which may have important implications for analyses of the interannual variability of short-term processes, such as spring bloom associated particle flux.

Sediment traps have a low temporal resolution, compared to other methods used for measuring carbon flux, and this study has only four sampling locations, but compared to previous deep ocean sediment trap studies, it provides the best mesoscale spatial coverage to date. To begin to observe, identify and quantify mesoscale variability using the method presented in this study, a minimum of four sediment trap locations is required to estimate the mean POC flux of the study region and to evaluate how individual trap records deviate from the mean.

Sustained ocean observatories with sediment trap arrays usually sample at one location, with sediment traps deployed at several depths, so as to quantify vertical changes in particle flux. Any spatial variability in the magnitude and composition of particle flux over short (≤ seasonal) time-scales may therefore be accidentally interpreted as interannual variation in seasonality (Henson, 2014). Such short-term spatial variability could be caused by processes such as lateral advection (Siegel et al., 2016), mesoscale eddies (Buesseler et al., 2008; Waite et al., 2016) and, extending above the seafloor, nepheloid layers (Gardner et al., 2017; McCave, 1975). Furthermore, if the amount of mesoscale variability changes with depth, driven by different processes throughout the water column (biological versus physical), the vertical flux profiles may also be impacted by such processes. A sustained time-series of several decades is likely needed to detect trends in particle flux, which means that instances of mesoscale variability altering fluxes or being interpreted as interannual variability, may make trend detection more challenging and may hinder understanding of long-term trends (Henson, 2014).

We conclude that annual budgets of carbon sequestration are not significantly impacted by mesoscale variability in the deep ocean IB. The IB compared to many ocean regions is highly dynamic with complex physical processes and topography and a strong seasonal cycle. In contrast, many sustained observatories with long-term deep ocean particle flux time-series are in locations

with less variable conditions, such as at the PAP-SO site (Lampitt et al., 2010). Sustained observatories usually record deep ocean particle flux in one location and the estimates of carbon storage are often assumed to be representative of a wide area. Over annual cycles the importance of mesoscale variability on deep ocean carbon flux appears to be less crucial but for shorter timescale studies spatial variability is important to consider as it may be mistaken for interannual variability (Henson, 2014). It is therefore reassuring that, even in the dynamic IB, mesoscale variability does not appear to play an important role in annual carbon flux estimates. However, in line with our initial hypothesis, if deep ocean carbon flux data is being investigated on shorter timescales, such as seasonally, the role of mesoscale spatial variability should be more thoroughly considered when identifying temporal signals or trends in data.

2.5 Conclusion

The magnitude of deep ocean carbon storage in the Subpolar North Atlantic has not previously been measured and particle flux studies often rely on sediment trap time-series from a single location. This study has quantified the magnitude of POC flux to below 2000 m in the IB for the first time and utilised the unique mesoscale coverage of the sediment traps to investigate whether spatial variability impacts carbon budget measurements over varying timescales from 14 days to annually. The rate of POC flux to the deep ocean Iceland Basin was found to be similar to the global ocean average estimate by Lampitt and Antia, (1997), but was 16 % lower than the most recent estimated global ocean average (Honjo et al., 2008), and 12 % lower than the North Atlantic Ocean average (Henson et al., 2011). Our estimates of T_{eff} for the IB were found to be in line with previously reported estimates for the North Atlantic.

We hypothesised that mesoscale variability will have an effect on deep ocean carbon flux but will be less important as the timescale of averaging increases. This hypothesis was supported, with mesoscale variability identified for all sampling periods, and instances of variability greater than the expected variation observed for timescales less than one month. In contrast, for timescales greater than 3 months, mesoscale variability is less important. Our results indicate that mesoscale spatial variability in deep ocean fluxes may need to be more thoroughly considered. In particular, mesoscale spatial variability at single location trap time-series from sustained observatories may be interpreted as temporal signals or interannual variability on short timescales, which may complicate long-term trend detection and interpretation. However, mesoscale variability does not appear to play an important role in annual carbon budgets and so carbon storage estimates for one-location time-series should be representative for that region.

Chapter 3 Exploring the Biological and Physical Drivers of Temporal and Spatial Variability in Deep Ocean Particle Flux in the Iceland Basin

3.1 Introduction

The seasonal cycle of material sinking from the surface ocean to the deep ocean has been studied for the past fifty years using sediment traps, with foundational studies observing a direct relationship between upper ocean primary production (PP) and deep ocean carbon flux (Deuser et al., 1981; Deuser & Ross, 1980). More recent studies of sustained time-series sediment trap records have focused on identifying the major flux components and what controls the magnitude of POC flux that reaches the bathypelagic zone (Conte & Weber, 2014; Lampitt et al., 2010; Lampitt & Antia, 1997; Smith et al., 2017). Long-term time-series of carbon sequestration are important for calculating global ocean carbon cycle budgets (Burd et al., 2010; Sabine, 2004), understanding controls on the magnitude and composition of flux to the deep ocean (Burd et al., 2010; Lampitt et al., 2010), to inform, and validate, biogeochemical models (Armstrong et al., 2002; Gehlen et al., 2006; Kwon et al., 2009; Yool et al., 2013) and predict future changes to the oceanic carbon cycle (Bopp et al., 2001; Kwon et al., 2009).

Moored deep ocean sediment traps are the main method for measuring deep ocean carbon fluxes but difficulties in linking fluxes to upper ocean processes, such as PP, have prevented a mechanistic understanding of the BCP processes in the euphotic and mesopelagic zones, which hinders understanding of fluxes that penetrate to the deep ocean (Burd et al., 2010; Frigstad et al., 2015). A direct coupling between upper ocean productivity and increased carbon fluxes below 3000 m at BATS was observed from PP shipboard measurements and mid-water sediment traps (Asper et al., 1992) whereas, in contrast, a 1 – 2 month time lag was observed at BATS between surface ocean plankton blooms measured by remote sensing and particle flux at 3000 m (Deuser et al., 1990). Rapidly sinking fluxes to the deep ocean, often driven by spring bloom-associated particle flux, are likely to originate from a localised region near to the sediment trap location whereas, during lower productivity periods, particulate fluxes may be sinking more slowly, and hence are likely to originate from further away from the trap location (Siegel & Deuser, 1997). This is one example of how the temporal, spatial and depth resolution and frequency of measurements, can lead to differing observations and explanations of key processes, which

hinders a mechanistic understanding of the functioning of the BCP (Boyd et al., 2019; Lampitt et al., 2010).

Particles that settle into deep ocean sediment traps will have undergone some degree of horizontal advection during the transit from the upper ocean to the deep ocean (Siegel et al., 2008). Deep ocean sediment trap source regions are often 100's of kilometres away from the sediment trap location but can be a localised area (Siegel et al., 2008). The magnitude of the advection will depend on the bulk particle mean sinking speed, the local velocity fields, and the depth of the trap (Siegel & Deuser, 1997). The origin of particles from the upper ocean has been predicted in a variety of studies (Abell et al., 2013; Frigstad et al., 2015; Qiu et al., 2014; Siegel et al., 2008; Siegel & Deuser, 1997; Waniek et al., 2000; Wekerle et al., 2018), based around the principle of statistical funnels (Siegel & Deuser, 1997), which may also be termed sediment catchment areas (Wekerle et al., 2018) or particle source regions (Siegel et al., 2008). The slower the sinking speed and the deeper the trap is deployed the wider the catchment areas will be (Siegel & Deuser, 1997; Waniek et al., 2000; Wekerle et al., 2018). Waniek et al. (2000) highlighted that sinking particles likely traverse at a 1° angle relative to the surface ocean due to horizontal advection of 10 – 20 m d^{-1} and average sinking speeds of 100 - 200 m d^{-1}. Predicting particle source regions has allowed studies to draw links between sea ice origin and vertical particles fluxes (Wekerle et al., 2018), and primary productivity and export in the Northeast Atlantic (Frigstad et al., 2015). Observed 'temporal' variations of deep ocean particles fluxes can be an artefact of changing sediment trap catchment areas sampling higher or lower productivity patches of the upper ocean (Deuser et al., 1988). Siegel et al. (2008) highlighted that if surface chlorophyll concentration has a similar spatial distribution to export, then using Chl *a* as a proxy for export is feasible, however, if export is controlled by the zooplankton community structure, then a more detailed knowledge of the Chl *a* concentrations of the source regions is not a useful diagnostic for understanding the spatial distribution of export. Therefore, estimating particle source regions to aid in the understanding of deep ocean fluxes may only be useful in a system that is driven by biological bottom up controls rather a system dominated by a top down control, or a system heavily influenced by physical processes such as particle injections pumps (PIP; Boyd et al., 2019).

If the relationship between upper ocean processes and deep ocean flux is characterised by direct coupling, then estimating the particle source regions will not aid in improving understanding of upper ocean processes (Alldredge & Gotschalk, 1989; Qiu et al., 2014). It is likely that direct coupling, and implied very fast sinking particles, are a transient temporal signal, likely associated with the spring bloom. It is more likely that the bulk particle sinking speeds, and hence particle source region size, vary throughout the annual cycle, as suggested by Fischer & Karakaş, (2009).

Previous work on statistical funnels and particle backtracking has focused on the Sargasso Sea, the mid-latitudes and temperature regions or in seasonally ice-covered regions (Frigstad et al., 2015; Siegel et al., 2008; Waniek et al., 2000; Wekerle et al., 2018). The importance of estimating the particle source regions in a high latitude region with a strong seasonal cycle has not previously been investigated.

Deuser et al. (1990) suggested that combining a mesoscale grid of moored sediment traps, remote sensing data and shipboard measurements, would allow for an improved understanding of spatial and temporal variability in fluxes recorded by sediment traps to understand the first order links between upper ocean PP, export, and deep ocean fluxes. In this study, I utilised the unique mesoscale array of the four sediment traps deployed in the deep ocean IB to explore in detail whether biological or physical upper ocean processes may drive mesoscale spatial variability in deep ocean particle flux. Understanding these changes may help to elucidate what drives and controls how much carbon reaches the deep ocean for long term carbon sequestration.

3.2 Methods

3.2.1 Sediment Trap Sample Analysis

The sediment trap sample collection and pre-processing was described in Chapter 2, Section 2.2. The sediment trap dry weight and POC/PON data from Chapter 2 was also used in this study but only periods I-III were used to investigate the relationship between upper ocean processes and deep ocean particle flux. The possible causes of the unusually low fluxes in Period IV were discussed in Chapter 2. The mass and POC/PON fluxes were calculated as in Chapter 2.

Sediment trap particulate material was freeze-dried by Martin, (2010) for deployment 1, to minimise the errors introduced by sample splitting and this procedure was followed for deployment 2 samples. For deployment 2, 3 of 8 aliquots were filtered onto 0.4 µm cellulose nitrate filters. The material was gently scraped into a pre-combusted (550 °C) glass vial and freeze-dried overnight. The freeze-dried material was gently crushed with a clean metal spatula to homogenise the material.

3.2.1.1 Particulate Inorganic Carbon

Calcium (Ca), Sodium (Na), Barium (Ba) and Strontium (Sr) were measured in all three fractions of the sediment trap samples from deployment 2 by the author – particulate material, filtered sediment trap supernatant and Acantharian cysts. Acantharian cysts contributed negligibly to the Ca content and so were not included in this study. The filtered sediment trap sample supernatant

was diluted 250x with 0.475 M Nitric acid (HNO_3) spiked with Indium, Rhenium and Beryllium to track instrument drift of the Inductively Coupled Plasma Mass Spectrometer (ICP/MS) during each sample run. Samples were run with multi-element standards detailed in Table B.1.1 with measured Ca and Na concentrations all within the concentration range of the standards. The samples were run on the Thermo X Series ICP-MS at the University of Southampton by the author with the assistance of Dr Matt Cooper.

The Na and Ca concentrations in the sediment trap preservative blank were 0.83 ± 0.013 mol L^{-1} and 0.010 ± 0.15 mol L^{-1} respectively. Freeze-dried particulate material was weighed out (0.5 – 8.2 mg; mean of 5.0 mg). The author carried out a detailed inter-comparison between using an Acetic acid digest (Martin et al., 2011) versus the more established method of using a 0.475 M Nitric acid (HNO_3) digest to investigate whether the different acid digests lead to varying Ca concentrations. Samples from November 2006 – July 2007 were analysed by P. Martin using a 1.0 M Acetic acid digest with the objective of targeting $CaCO_3$ of biogenic origin and to minimise the digestion of Ca from lithogenic material (Martin et al., 2011). Triplicates of deployment 2 samples were acidified separately with 10 ml of 0.475 M spiked HNO_3 (following the method of Daniels et al. 2012) and 1.0 M acetic acid (Martin et al., 2011) and left to digest overnight to allow for a comparison between the different acid digests. The digests were then filtered through a 0.45 µm syringe filter (Fisher Scientific) to remove any particulates before being diluted by 250x . Procedural blanks, sediment trap preservative blanks and reagent blanks were run alongside samples. Where possible triplicates were run for each sample. Uncertainty was estimated by propagating the analytical errors as in Section 2.2.1.1.

The digested samples in the methodology intercomparison agreed well and differences between the calculated fluxes were negligible. At higher Ca fluxes the Acetic acid digest leached slightly more Ca compared to the HNO_3 digest (Figure B.1.1). To validate comparisons between deployment 1 and deployment 2 Ca and Na data, four particulate deployment 1 samples were run, which covered a range of sample types, and agreed well for Ca flux, although the Ca percentage content from one sample from deployment 1 varied from both the Acetic acid and Nitric acid digests (Figure B.1.1).

Ca (mg) in each sample was multiplied by 2.5 ($CaCO_3$:Ca ratio) to estimate the $CaCO_3$ content per sample and $CaCO_3$ content was multiplied by 0.12 (C:$CaCO_3$ ratio) to estimate the PIC content, assuming that all digested Ca originated from PIC and was of biogenic origin.

3.2.1.2 Biogenic Silica

The particulate material and sediment trap supernatant was analysed for the biogenic silica (SiO_2; BSi) content following the method of Salter et al. (2010), which builds on the foundations of Brown et al. (2003), Mortlock & Froelich, (1989) and Strickland & Parsons, (1972). All samples were run in triplicate where possible and the analytical uncertainty was propagated throughout to determine the measurement error. Deployment 1 samples were run by Patrick Martin and deployment 2 samples were ran by the author.

Freeze-dried particulate material collected by the sediment traps was weighed out (0.9 – 8.2 mg) into the cap of a 15 ml polypropylene tube ensuring particulate material was inside the rim, otherwise the cap was discarded. The caps were screwed on and inverted. Each sample was digested in 5 ml of 0.2 M sodium hydroxide (NaOH) for 2 hours at 85 °C. Samples were cooled to room temperature and neutralised with 10.6 ml of hydrochloric acid (HCl). Samples were centrifuged at 3700 rpm for 15 minutes to ensure no particulate material entered the auto-analyser. Samples were diluted 50x with a saline solution (40 g of NaCl in 1 L of Milli-Q). Samples were capped and stored in a fridge overnight. The deployment 2 samples were shaken vigorously the next day and analysed on a QuAAtro Autoanalyzer at the National Oceanography Centre, Southampton with the assistance of Dr Ed Mawji.

The method was also adapted to measure the sediment trap supernatant to determine the extent of the biogenic silica dissolution during the 10 year storage period (Antia, 2005; Bauerfeind & Bodungen, 2006). The sediment trap supernatant was collected during filtering for mass and POC fluxes on 0.7 µm GF/F filters. Filtered sediment trap supernatant stored at 4 °C was removed from the fridge and shaken well before removing 1 ml of supernatant to a 15 ml polypropylene tube. The same methodology was followed without the centrifuging step. Supernatant samples were diluted 30x, stored in the fridge overnight and analysed as described above.

Test samples were run to determine whether digesting the supernatant altered the BSi concentration compared to undigested samples. The concentrations of the digested and undigested supernatant samples were very similar with a mean RSD of 2.65 %. The major difference between the resulting concentrations was that the digested supernatant triplicates exhibited greater variability between the triplicates. Due to the minimal differences to the concentration the supernatant samples were not digested. It should be noted that the tested supernatant concentrations are at the upper end of the concentration ranges in Figure B.2.2. Future studies are advised to undertake a more extensive comparison including a wider range of supernatant concentrations. For this study the supernatant addition made very little difference to the total BSi fluxes in Periods I-III and so the methodology testing is sufficient for this purpose.

Sediment trap supernatant was only measured from samples in which the particulate material was also measured. Many Period IV samples did not have enough freeze-dried particulate material to measure for all flux components and so BSi was not measured on very low samples in Period IV. As reported in Bauerfeind & Bodungen, (2006) the fraction of BSi in the dissolved phase increased as the sampled particulate BSi fluxes decreased, as shown in Figure 3.1. The sediment trap supernatant concentrations were corrected for any evaporation that had taken place by normalising the concentration of the recorded sample bottle volumes to 260 ml (21 sample bottle type) or 290 ml (13 sample bottle type). The mass of SiO_2 in the sample bottle was calculated, after removing the preservative blank SiO_2 concentration, and added to the BSi particulate mass before calculating total BSi fluxes.

Table 3.1 A sediment trap supernatant methodology comparison of deployment 2 samples was undertaken to determine whether digesting the supernatant was necessary. The blank-corrected supernatant concentrations are compared along with the relative standard deviation (RSD) between the triplicates. The Trap NW – 6 undigested samples had one outlier value which increased the RSD.

Sample ID	Collection Dates	Procedure	BSi Concentration (mmol L^{-1})	RSD (variability between replicates)
Trap NE - 2	09.09.07 – 22.09.2007	Digest	0.87 (± 0.012)	1.4 %
Trap S - 2	09.09.07 – 22.09.2007	Digest	0.79 (± 0.044)	5.5 %
Trap C - 4	07.10.2007 – 20.10.2007	Digest	0.76 (± 0.014)	1.8 %
Trap NW - 6	04.11.2007 – 17.11.2007	Digest	0.74 (± 0.032)	4.4 %
Trap NE - 2	09.09.07 – 22.09.2007	No digest	0.92 (± 0.009)	0.93 %
Trap S - 2	09.09.07 – 22.09.2007	No digest	0.77 (± 0.007)	0.96 %
Trap C - 4	07.10.2007 – 20.10.2007	No digest	0.77 (± 0.006)	0.81 %
Trap NW - 6	04.11.2007 – 17.11.2007	No digest	0.78 (± 0.090)	12.0 %

The samples were run with several reagent blanks, which had negligible Si concentrations and were not corrected for. The samples were run with a standard concentration range of 1 – 130 µmol L^{-1}. Some samples, particularly the intercomparison samples between deployments 1 and 2 (see Appendix B, Figure B.2.1), exceeded the calibration range due to a very high silica content. Certified reference materials (CRMs) of concentrations up to 164.9 µmol L^{-1} were producing accurate results within 1 % deviation of the certified value, which validated the high silica content

sample results that exceeded the calibration range (median concentration of above calibration samples was 160.7 µmol L^{-1}). The CRMs used for Si were Reference Material for Nutrients in Seawater (RMNS; The General Environmental Technos Co.) and had certified values between 14.2 – 164.9 µmol L^{-1} (Table 3.2).

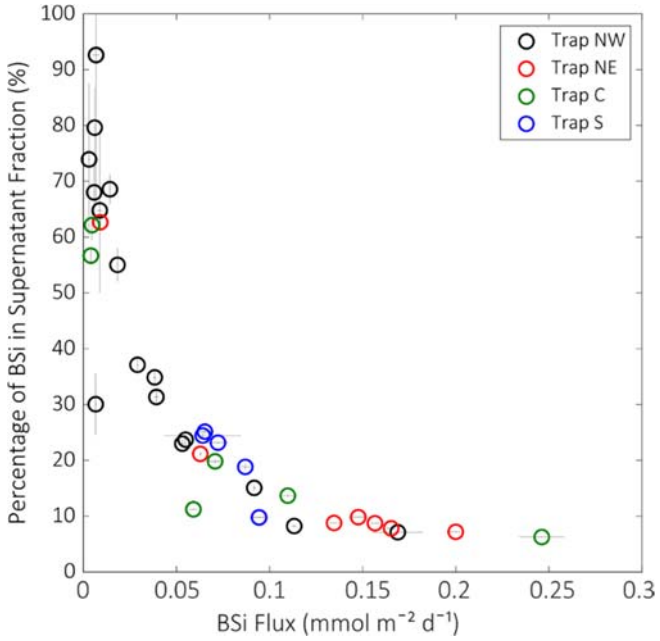

Figure 3.1 Total biogenic silica (BSi) flux and the percentage of BSi in the supernatant fraction for deployment 2 samples. The error bars show propagated analytical uncertainty. The colour of the markers indicates which sediment trap collected the sample.

Table 3.2 Certified Reference Materials used to validate the measured Si concentration. The measured and certified concentrations are represented along with the RSD and number of measurements.

CRM	Measured Si (µmol L^{-1})	Certified Value (µmol L^{-1})	RSD (%)	Number of measurements
CD	14.267	14.269	0.013	7
CJ	38.898	39.434	1.360	9
BW	61.137	61.467	0.538	4
CB	111.888	111.850	0.034	5
BZ	163.790	164.900	0.673	4

3.2.1.3 Flux Calculations

Fluxes of the measured particulate components were calculated as shown in Equations 3.1 – 3.4 and the analytical uncertainty was propagated through the calculations. The total mass of each

component was divided by the molecular mass and normalised to the sampling area (*A*) and the sampling period (*d*).

[Equation 3.1] $$POC\ Flux\ (mmol\ m^{-2}\ d^{-1}) = \frac{(Mass_{POC}/\ 12.01)}{A/d}$$

[Equation 3.2] $$PON\ Flux\ (mmol\ m^{-2}\ d^{-1}) = \frac{(Mass_{PON}/\ 14.01)}{A/d}$$

[Equation 3.3] $$CaCO_3\ Flux\ (mmol\ m^{-2}\ d^{-1}) = \frac{(Mass_{CaCO3}/\ 100.09)}{A/d}$$

[Equation 3.4] $$Particulate\ BSi\ Flux\ (mmol\ m^{-2}\ d^{-1}) = \frac{(Mass_{BSi}/\ 60.08)}{A/d}$$

The percentage contribution of each flux component was calculated by converting fluxes to mg m^{-2} d^{-1} and dividing by the total mass flux. The cumulative fluxes were summed over one annual cycle from the 22nd of November 2006 - 2007. The 28 day sampling gap during sediment trap deployments was filled using nearest neighbour interpolation. The cumulative fluxes were normalised for each trap by converting to a percentage of total annual flux for each flux component as in Lampitt and Antia, (1997). Period IV samples are included in Figure 3.5 and Table 3.4 but any samples that were clearly degraded were not included in Figure 3.3 and for $CaCO_3$ and BSi there was often not enough material (NEM) to be measured as detailed in Table 3.4.

3.2.2 Particle Source Regions

3.2.2.1 Methodology

The particle source region of sampled particulate material in sediment traps is key to understand completely the controls on particle flux (Siegel & Deuser, 1997). By predicting the particle source regions the motion of horizontal currents that affect particle sinking trajectories, and the time lag between particles sinking from the upper ocean to deep ocean sediment traps is accounted for, similar to Waniek et al. (2000). The particle backtracking modelling and current backtracking codes were written by Benoit Espinola but altered to run for the study location and temporal period and run by the author.

The particle backtracking methodology used in this study tracks particles backwards spatially and temporally from the sediment trap location and deployment depth. This means a particle originates at the sediment trap and for each day the particle is tracked backwards in time and space, which depends on the chosen average particle sinking speed and the magnitude of the current velocity components, *u* and *v* (see Equation 3.5 and 3.6). In Equation 3.5 and 3.6 the

xtrack and *ytrack* are the daily particle longitude and latitude, which creates the particles' trajectory, starting at the sediment trap location and depth and terminating at the surface ocean. For each daily timestep, the *u* and *v* components are multiplied by the number of seconds in a day (δt), converted to degrees ($dlon$ or $dlat$) and the daily displacement starting from time zero ($t = 0$) is calculated until the particle intercepts with the surface ocean. The depth of the trap and the sinking speed used determines how many timesteps the particles are backtracked for.

[Equation 3.5] $$xtrack(t-1) = lon(t) + (u(t) * \delta t)/dlon$$

[Equation 3.6] $$ytrack(t-1) = lat(t) + (v(t) * \delta t)/dlat$$

[Equation 3.7] $$depth(t-1) = depth(t) - w_{ave} \times \delta t$$

For this study the average particle sinking speed (w_{ave}) was assumed to be 100 m d^{-1}. This speed was chosen based on average sinking velocity measurements by Villa-Alfageme et al. (2016) in the IB in 2010, in which sinking velocity ranged between 60 m d^{-1} between 50 – 70 m, and increased to 110 m d^{-1} by 400 – 500 m depth. The sinking speed is also the same as the assumed speed used by Waniek et al. (2000; 2005a) for the Northeast Atlantic Ocean. During deployment 1 Trap S was deployed at 2441 m depth, which means each particle was traced backwards in time and space for 24.41 days when assuming a sinking speed of 100 m d^{-1}. An example of these particle traces for Trap S in April-June 2007 is shown in Figure 3.2. To test the sensitivity of the particle backtracking method we also used sinking speeds of 50 m d^{-1} and 200 m d^{-1} as in Waniek et al. (2000a; explored in Appendix C).

This study utilised current meter velocity from 15 m below the sediment traps and OSCAR surface current velocity to provide the *u* and *v* components used to track the particles. OSCAR surface mixed layer velocities are calculated using sea level anomalies (SLA) to estimate geostrophic velocity and ocean vector winds to estimate Ekman transport (http://www.esr.org/oscar_index.html). Current meter data was available for all traps from deployment 1 but only available from Traps C and S during deployment 2. The ocean was represented as a 2-box model with OSCAR surface currents representing 0 – 350 m and current velocity data from the current meters 15 m below the sediment traps representing 350 – 2500 m. The current velocity data was low pass filtered to remove the tidal signal, following the method of Waniek et al. (2000a; Matlab function lowpass() with a wpass of 0.01, and an example of the filtered result is shown in Appendix C.1). Monte Carlo simulations were run for sinking speeds of 50, 100 and 200 m d^{-1} for the 2-box model approach. A range of sinking speeds were used to test the sensitivity of the method to the sinking speed and to determine how much the particle source region changes depending on the sinking speed. Each daily particle track was traced 20 times and

the *u* and *v* for each time point, location and depth was allowed to vary within 1 standard deviation of the measured *u* and *v* components to determine the sensitivity of the method to the velocity field and how variability in the *u* and *v* components affect the daily particle source region location (detailed analysis in Appendix C.3).

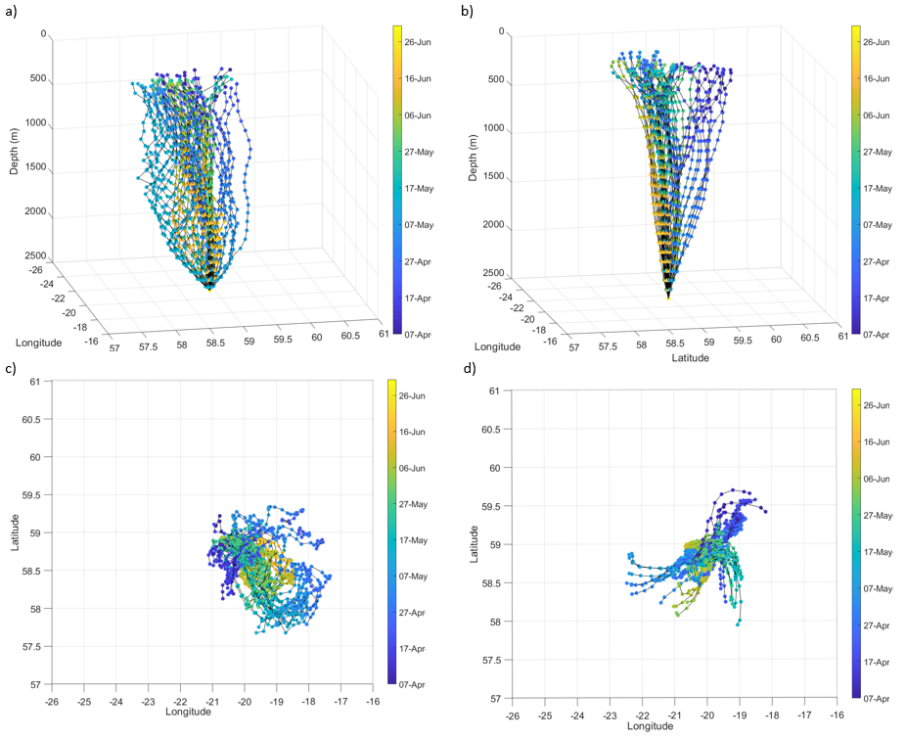

Figure 3.2 An example of the predicted particle source regions for Trap S April - June 2007 samples using a), c) OSCAR and current meter velocity and b), d) using Copernicus reanalysis model velocity to demonstrate paths of the particle trajectories. a) and b) show the daily particle tracks from the sediment trap to the surface ocean and c) and d) show the daily particle source region location at the surface ocean.

For comparison the *u* and *v* components were downloaded from the Copernicus Marine Environment Monitoring Service website (CMEMS; http://marine.copernicus.eu/services-portfolio/) and extracted from GLOBAL-REANALYSIS-PHY-001-030-DAILY. The GLORYS12V1 product is a 1/12° eddy resolving reanalysis model which uses altimetry, satellite and temperature and salinity profile data and the global forecasting CMEMS system to create a daily data product with 50 depth levels. The depth-resolved model *u* and *v* components were used in place of the 2 box model and the particle source regions were predicted for sinking speeds of 100 m d^{-1} to allow for a comparison between model and measured velocity components. An advantage of using the model data is that there is mesoscale variability in current velocities in the interior and deep ocean, whereas using current meter data provides no information on local mesoscale variability (Qiu et al., 2014; Waniek et al., 2000). However, the model current speeds are less likely to capture transient events affecting the magnitude of deep ocean current speed as demonstrated

by Figure 3.3. No Monte Carlo simulations were run for the model products due to the high computational demand of the high resolution model output files.

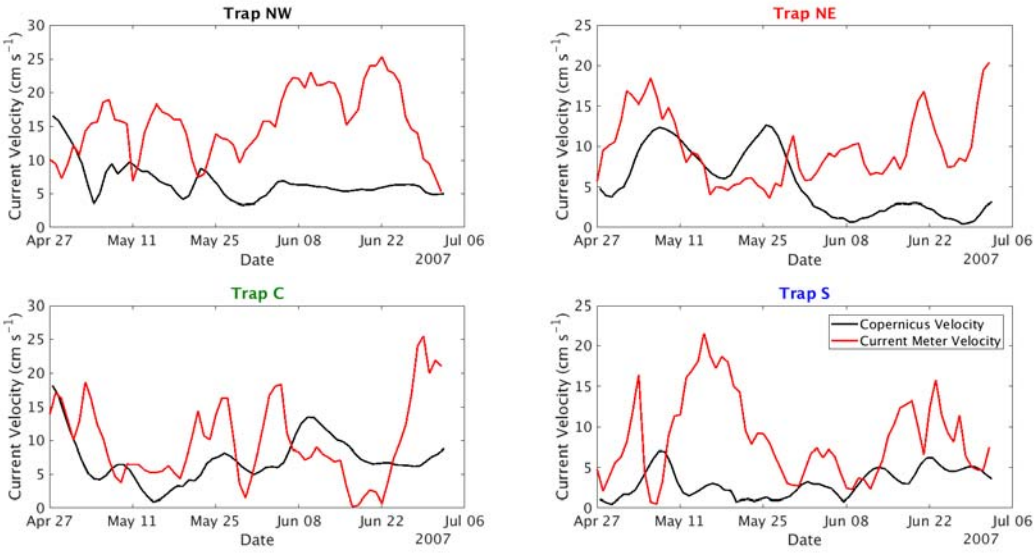

Figure 3.3 Daily average current velocity from the sediment trap locations and deployment depths between late April - June 2007 from Copernicus model velocity (black line) and current meter velocity (red line).

3.2.3 Upper Ocean Parameters

3.2.3.1 Chlorophyll *a* Concentration

Remotely-sensed monthly Chl *a* concentration data mapped at 9 km resolution was downloaded from https://oceandata.sci.gsfc.nasa.gov/MODIS-Aqua/Mapped/ to investigate the relationship between Chl *a* concentration and deep ocean particle fluxes. The Chl *a* concentration was extracted from the monthly product using the minimum and maximum extents of the predicted particle source region for each 14 day sampling period and the Chl *a* concentration was averaged over the duration of the sampling period. The Chl *a* concentration data was also extracted directly above the sediment traps for the sampling period and with a timelag equivalent to the particle backtracking method for comparison. There was no Chl *a* concentration data available between November and February due to the low sun angle at 60° N. Due to the IB having extensive cloud cover throughout the year the 8 day Chl *a* concentration satellite data product could not be used.

3.2.3.2 Continuous Plankton Recorder Data

Continuous plankton recorder (CPR) data records the presence/absence of organisms and a semi-quantitative estimate of abundance can be calculated. CPR data from the standard areas B5, B6, C5 and C6 (Figure 3.4), from 2006 to 2008 were used to explore the abundance of diatoms,

dinoflagellates, acantharia, foraminifera, radiolarians and copepods (DOI:10.7.7487/2017.80.1.1044) and coccolithophores (DOI:10.7487/2019.226.1.1223). In this study, the monthly normalised mean abundance was estimated by averaging the recorded abundances for each month and normalising to the number of tows per month. The data for the Subpolar North Atlantic was patchy and sporadic, and focused on three main areas, which I have separated into Regions 1 – 3 (Table 3.3). The CPR data was collected outside of the IB, but the samples in Region 2 and 3 do overlap with the maximum extents of the particle source regions for Trap NE, C and S.

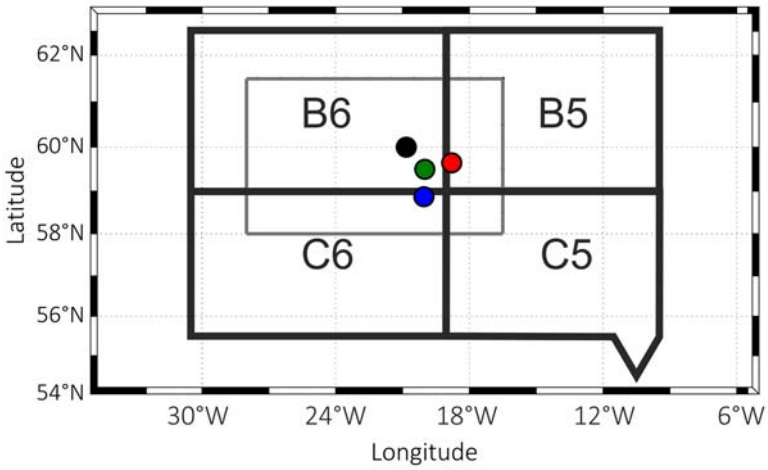

Figure 3.4 Continuous plankton recorder survey standard areas B5, B6, C5 and C6 shown in relation to the sediment trap locations. The grey box shows the outline of the Iceland Basin as defined in this thesis.

Table 3.3 The minimum and maximum latitude and longitude of the IB and the continuous plankton recorder Regions 1 - 3 defined in this study.

	Minimum Latitude	Maximum Latitude	Minimum Longitude	Maximum Longitude
Iceland Basin	58 N	61.5 N	28 W	16.5 W
Region 1	58 N	64 N	35 W	24 W
Region 2	59 N	64 N	20 W	5 W
Region 3	54 N	57 N	35 W	5 W

3.2.3.3 Sea Level Anomaly

Daily sea level anomaly (SLA; height and *u* and *v* components) data at 0.25° spatial resolution derived from satellite altimetry were downloaded from

ftp://ftp.aviso.altimetry.fr/global/delayed-time/grids/msla/. The SLA *u* and *v* components were used to calculate the eddy kinetic energy (EKE) above the traps using Equation 3.8. A time-series of the maximum EKE in a 1 degree box around the trap locations was also extracted and averaged to find the maximum EKE in each two week sampling period, for each trap.

[Equation 3.8] $$EKE\ (cm^2\ s^{-2}) = 0.5 \times (u^2 + v^2)$$

3.2.3.4 Mixed Layer Depth

Mixed layer depth could not be derived from Argo floats due to very limited spatial and temporal coverage in the IB between 2006 – 2008. Daily mixed layer depth was downloaded from Copernicus (http://marine.copernicus.eu/services-portfolio/) and extracted from GLOBAL-REANALYSIS-PHY-001-030-DAILY. The mixed layer is defined by Copernicus by a density increase relative to 10 m depth that corresponds to a temperature decrease of 0.2 °C of local surface conditions (de Boyer Montégut et al., 2004).

3.2.3.5 AVISO Mesoscale Eddy Tracking Product

The AVISO mesoscale eddy trajectory atlas (Merged version 1.0) was downloaded from (https://www.aviso.altimetry.fr/en/data/products/value-added-products/global-mesoscale-eddy-trajectory-product.html) and used to explore links between spatial variability in deep ocean particle flux and mesoscale upper ocean eddies. The eddy product is based on the work of Chelton et al. (2011) and uses the Data Unification and Altimeter Combination System (DUACS) daily delayed time gridded SLA product. Eddies are detected when reaching a diameter of 100 – 300 km and the localised minimum and maximum SLA is used to identify the characteristics of the eddy. The computed eddy characteristics are amplitude (cm), eddy type (either cyclonic or anti-cyclonic), number of days the eddy has been tracked, average geostrophic speed (cm s^{-1}), and the radius (km), estimated using the maximum of the circular averaged geostrophic speed. Each mesoscale eddy is assigned a track number and the latitude, longitude and associated time of each eddy is included in the product.

3.3 Results

3.3.1 Particle Fluxes

3.3.1.1 Temporal Variability

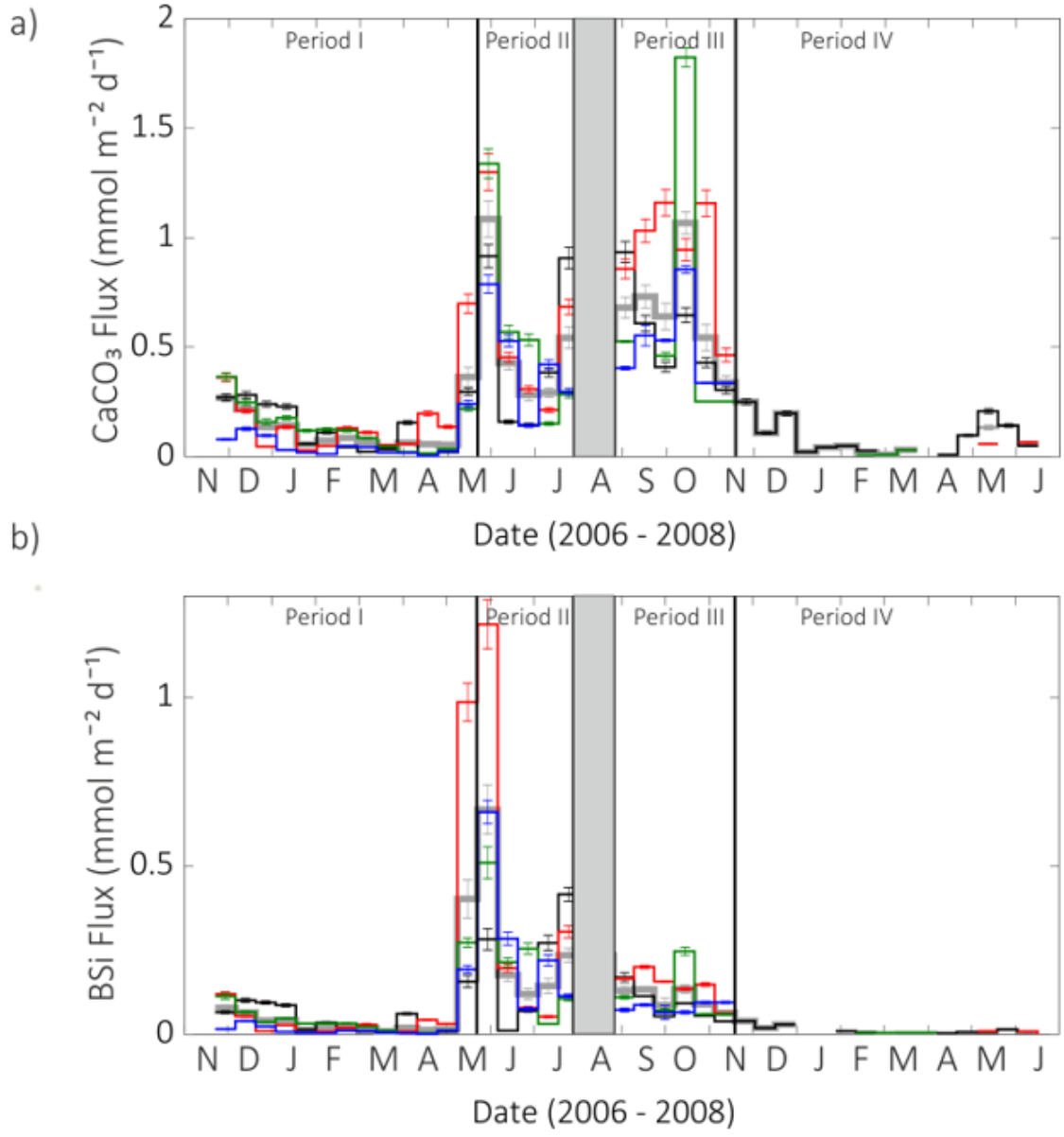

Figure 3.5 Particle fluxes to below 2000 m in the IB (2006 - 2008). a) $CaCO_3$ flux (mmol m^{-2} d^{-1}) and b) BSi flux (mmol m^{-2} d^{-1}) with degraded samples removed. The mean flux is in grey, Trap NW fluxes are in black, Trap NE fluxes in red, Trap C fluxes are in green and Trap S fluxes are in blue, which remain the same throughout this chapter. The black vertical lines represent the four flux periods outlined in Chapter 2. The greyed out period is the gap in sampling whilst the sediment traps were recovered and redeployed. The error bars show the propagated analytical uncertainty.

There is a defined seasonal cycle in the particle flux reaching the bathypelagic IB, as previously described in Chapter 2. Mass and POC fluxes are low in winter and early spring, followed by a peak in flux in May associated with the spring-bloom, fluxes are elevated during summer and increase again in autumn and early winter, with the sediment trap in the central IB reaching peak mass and POC fluxes in October (Figure 2.4). In December 2007, the fluxes decrease to smaller magnitudes which is sustained until June 2008, described as Period IV, due to these unusually low fluxes as outlined in Chapter 2. This study aims to explore the drivers of deep ocean particle flux and so focuses on the Period I-III data of well-preserved samples, as the Period IV fluxes were unusually low across all flux components, meaning drivers of these low fluxes would be challenging to determine.

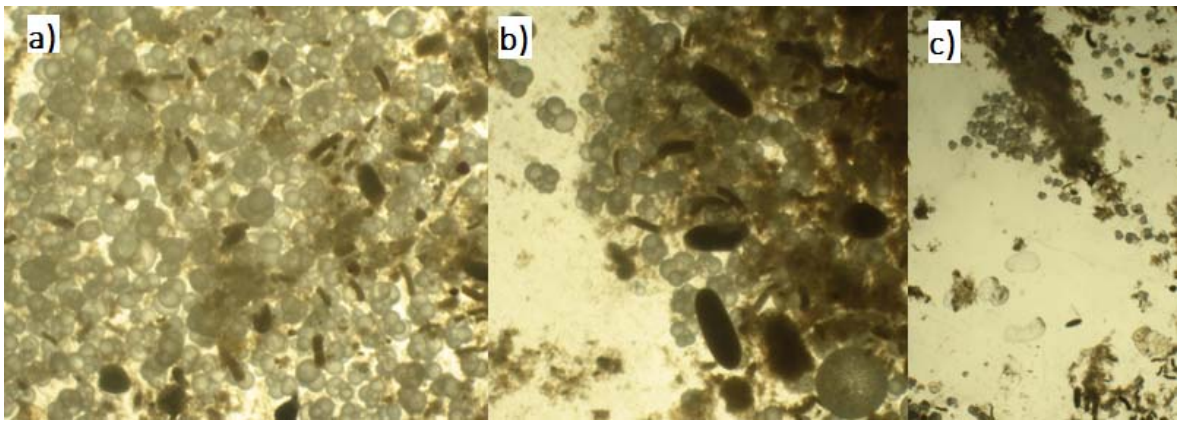

Figure 3.6 Photographs of sediment trap material from Trap S in September 2007 at 150x in a) and b) magnification to show an example of the large foraminifera tests found in the autumn samples and the fluffy brown detritus and faecal pellets on top of the tests and photograph c) is at 75x magnification and has a similar composition to b).

The $CaCO_3$ fluxes track the mass and POC flux seasonal cycle with some instances of elevated POC fluxes coinciding with increased $CaCO_3$ fluxes. $CaCO_3$ is the major component of the deep ocean IB particle flux with a mean percentage contribution of 58.5 % (range 20 - 90 %) by mass. The $CaCO_3$ flux increases with the arrival of the spring-bloom associated particle flux but the greatest sustained $CaCO_3$ fluxes were sampled in October and November 2007, particularly in Trap NE and Trap C. All samples were inspected using light microscopy during swimmer removal and the autumn 2007 samples were recorded as having many large foraminfera tests, as shown in Figure 3.6. The foraminifera tests were not observed to have organic material attached, although material may have detached during sampling or storage.

The BSi fluxes to the deep ocean IB also follow a similar seasonal cycle, with the exception that BSi makes a much greater contribution, up to 34.2 %, during the spring bloom, which coincides with the largest POC fluxes, particularly in Trap NE. The BSi fluxes steadily decrease after the spring

bloom associated peak to low fluxes in winter. Interestingly, in Period IV, there was essentially no BSi flux, whereas there was very small amounts of POC and $CaCO_3$ flux. The peak in the Trap C POC flux in November 2007 does coincide with another peak in BSi flux and $CaCO_3$ flux as previously discussed.

Table 3.4 Summary of particle fluxes and molar ratios to the deep ocean Iceland Basin between November 2006 and June 2008. Mass fluxes are reported in mg m^{-2} d^{-1} and all other fluxes are reported as mmol m^{-2} d^{-1}. Samples 1 – 18 were analysed by P. Martin and first reported in his thesis (Martin, 2011). The BSi fluxes for samples 19 – 39 is the total BSi flux, which is the sum of the supernatant and particulate fractions to account for the 10 year storage period. Some Period IV samples did not have enough material to measure every component and is noted as NEM.

* Sediment traps were recovered early and hence only sampled for 11 of the programmed 14 days.

** Bottles sampled for more than 14 days, with a maximum sampling period of 42 days.

Identified as degraded samples as discussed in Chapter 2. Italic fluxes should be treated with caution.

Sample ID	Date	Mass Flux	POC Flux	PON Flux	$CaCO_3$ Flux	BSi Flux	POC:PON	PIC:POC	BSi:POC
Trap NW - 1	22.11.2006	43.75 (±2.19)	0.27 (±0.02)	0.034 (±0.002)	0.27 (±0.014)	0.07 (±0.004)	8.01 (±0.79)	1.00 (±0.08)	0.24 (±0.02)
Trap NW - 2	06.12.2006	47.35 (±2.37)	0.26 (±0.02)	0.033 (±0.003)	0.28 (±0.015)	0.10 (±0.006)	8.06 (±1.11)	1.07 (±0.12)	0.38 (±0.04)
Trap NW - 3	20.12.2006	47.17 (±2.36)	0.43 (±0.04)	0.066 (±0.007)	0.24 (±0.014)	0.09 (±0.005)	6.47 (±0.94)	0.56 (±0.07)	0.22 (±0.03)
Trap NW - 4	03.01.2007	39.60 (±1.98)	0.25 (±0.03)	0.031 (±0.005)	0.23 (±0.012)	0.09 (±0.005)	8.09 (±1.59)	0.93 (±0.12)	0.35 (±0.05)
Trap NW - 5	17.01.2007	10.30 (±0.52)	0.10 (±0.01)	0.014 (±0.001)	0.06 (±0.003)	0.01 (±0.001)	6.76 (±0.91)	0.60 (±0.06)	0.14 (±0.01)
Trap NW - 6	31.01.2007	18.55 (±0.93)	0.11 (±0.01)	0.013 (±0.001)	0.11 (±0.006)	0.03 (±0.003)	8.48 (±1.14)	0.97 (±0.10)	0.31 (±0.04)
Trap NW - 7	14.02.2007	7.60 (±0.38)	0.05 (±0.00)	0.007 (±0.001)	0.04 (±0.002)	0.01 (±0.001)	7.74 (±1.04)	0.86 (±0.09)	0.23 (±0.03)
Trap NW - 8	28.02.2007	4.04 (±0.20)	0.03 (±0.00)	0.004 (±0.000)	0.02 (±0.001)	0.01 (±0.00)	7.65 (±1.03)	0.82 (±0.09)	0.26 (±0.03)
Trap NW - 9	14.03.2007	6.13 (±0.31)	0.04 (±0.00)	0.005 (±0.000)	0.04 (±0.002)	0.01 (±0.001)	7.93 (±0.79)	0.91 (±0.09)	0.27 (±0.03)
Trap NW - 10	28.03.2007	27.78 (±1.39)	0.19 (±0.01)	0.026 (±0.003)	0.16 (±0.008)	0.06 (±0.004)	7.31 (±0.93)	0.82 (±0.08)	0.32 (±0.03)
Trap NW - 11	11.04.2007	1.85 (±0.09)	0.02 (±0.00)	0.002 (±0.000)	0.01 (±0.001)	0.00 (±0.000)	8.68 (±1.00)	0.56 (±0.05)	0.15 (±0.01)
Trap NW - 12	25.04.2007	5.97 (±0.03)	0.08 (±0.00)	0.012 (±0.001)	0.02 (±0.001)	0.01 (±0.000)	6.51 (±0.63)	0.26 (±0.02)	0.09 (±0.01)

Sample ID	Date	Mass Flux	POC Flux	PON Flux	$CaCO_3$ Flux	BSi Flux	POC:PON	PIC:POC	BSi:POC
Trap NW - 13	09.05.2007	48.11 (±2.41)	0.27 (±0.02)	0.032 (±0.003)	0.30 (±0.016)	0.16 (±0.018)	8.26 (±0.91)	1.11 (±0.11)	0.59 (±0.08)
Trap NW - 14	23.05.2007	125.94 (±6.30)	0.56 (±0.03)	0.075 (±0.004)	0.92 (±0.053)	0.28 (±0.031)	7.47 (±0.62)	1.64 (±0.13)	0.50 (±0.06)
Trap NW - 15	06.06.2007	19.55 (±0.98)	0.09 (±0.01)	0.011 (±0.001)	0.16 (±0.008)	0.01 (±0.001)	7.84 (±0.79)	1.83 (±0.16)	0.12 (±0.01)
Trap NW - 16	20.06.2007	24.73 (±1.24)	0.14 (±0.01)	0.020 (±0.001)	0.15 (±0.007)	0.07 (±0.004)	7.13 (±0.51)	1.03 (±0.07)	0.49 (±0.04)
Trap NW - 17	04.07.2007	74.63 (±3.73)	0.53 (±0.08)	0.076 (±0.013)	0.38 (±0.019)	0.27 (±0.022)	6.96 (±1.59)	0.73 (±0.12)	0.51 (±0.09)
Trap NW – 18*	18.07.2007	151.21 (±7.56)	0.81 (±0.08)	0.112 (±0.011)	0.91 (±0.049)	0.42 (±0.021)	7.24 (±1.01)	1.11 (±0.11)	0.51 (±0.06)
Trap NW - 19	26.08.2007	149.31 (±7.47)	0.56 (±0.03)	0.072 (±0.012)	0.93 (±0.048)	0.17 (±0.014)	7.77 (±1.38)	1.68 (±0.13)	0.30 (±0.03)
Trap NW - 20	09.09.2007	97.64 (±4.89)	0.41 (±0.02)	0.052 (±0.009)	0.61 (±0.036)	0.11 (±0.001)	7.81 (±1.38)	1.50 (±0.12)	0.28 (±0.02)
Trap NW - 21	23.09.2007	60.32 (±3.02)	0.23 (±0.01)	0.030 (±0.005)	0.41 (±0.022)	0.05 (±0.002)	7.47 (±1.32)	1.82 (±0.14)	0.24 (±0.02)
Trap NW - 22	07.10.2007	97.02 (4.88)	0.40 (±0.02)	0.054 (±0.009)	0.65 (±0.034)	0.09 (±0.001)	7.47 (±1.34)	1.61 (±0.12)	0.23 (±0.01)
Trap NW - 23	21.10.2007	62.05 (±3.14)	0.26 (±0.01)	0.034 (±0.006)	0.43 (±0.022)	0.05 (±0.001)	7.68 (±1.36)	1.65 (±0.13)	0.21 (±0.01)
Trap NW - 24	04.11.2007	42.14 (±2.12)	0.18 (±0.01)	0.026 (±0.004)	0.30 (±0.017)	0.04 (±0.001)	6.99 (±1.26)	1.70 (±0.14)	0.21 (±0.01)
Trap NW - 25	18.11.2007	37.98 (±1.90)	0.17 (±0.01)	0.022 (±0.004)	0.25 (±0.013)	0.04 (±0.001)	7.81 (±1.38)	1.46 (±0.11)	0.23 (±0.01)
Trap NW - 26	02.12.2007	16.34 (±0.82)	0.09 (±0.01)	0.011 (±0.002)	0.11 (±0.006)	0.02 (±0.001)	7.89 (±1.40)	1.20 (±0.09)	0.20 (±0.01)
Trap NW - 27	16.12.2007	30.07 (±1.51)	0.14 (±0.01)	0.019 (±0.003)	0.20 (±0.010)	0.03 (±0.001)	7.63 (±1.35)	1.39 (±0.11)	0.20 (±0.01)
Trap NW - 28	30.12.2007	3.93 (±0.20)	0.03 (±0.00)	0.003 (±0.001)	0.02 (±0.001)	NEM	7.91 (±1.40)	0.79 (±0.06)	NEM
Trap NW - 29	13.01.2008	7.44 (±0.37)	0.05 (±0.00)	0.008 (±0.001)	0.04 (±0.002)	NEM	6.37 (±1.13)	0.81 (±0.06)	NEM
Trap NW - 30	27.01.2008	7.73 (±0.39)	0.04 (±0.00)	0.006 (±0.001)	0.05 (±0.002)	0.01 (±0.001)	7.15 (±1.27)	1.13 (±0.09)	0.20 (±0.03)
Trap NW - 31	10.02.2008	4.42 (±0.23)	0.03 (±0.00)	0.005 (±0.001)	0.03 (±0.001)	0.01 (±0.000)	6.88 (±1.22)	0.86 (±0.07)	0.19 (±0.02)
Trap NW - 32	24.02.2008	2.35 (±0.12)	0.03 (±0.00)	0.005 (±0.001)	NEM	NEM	5.68 (±1.01)	NEM	NEM
Trap NW - 33	09.03.2008	1.72 (±0.14)	0.01 (±0.00)	0.002 (±0.000)	NEM	NEM	7.14 (±1.26)	NEM	NEM

Sample ID	Date	Mass Flux	POC Flux	PON Flux	$CaCO_3$ Flux	BSi Flux	POC:PON	PIC:POC	BSi:POC
Trap NW - 34	23.03.2008	1.28 (±0.07)	0.01 (±0.00)	0.002 (±0.000)	NEM	NEM	6.06 (±1.07)	NEM	NEM
Trap NW - 35	06.04.2008	1.83 (±0.09)	0.02 (±0.00)	0.003 (±0.000)	0.01 (±0.000)	0.00 (±0.000)	6.28 (±1.19)	0.52 (±0.04)	0.18 (±0.03)
Trap NW - 36	20.04.2008	13.57 (±1.18)	0.10 (±0.01)	0.020 (±0.003)	0.10 (±0.005)	0.01 (±0.000)	5.19 (±0.92)	0.94 (±0.07)	0.06 (±0.01)
Trap NW - 37	04.05.2008	24.74 (±1.49)	0.10 (±0.01)	0.021 (±0.004)	0.21 (±0.011)	0.01 (±0.000)	4.88 (±0.86)	2.03 (±0.16)	0.06 (±0.00)
Trap NW - 38	18.05.2008	17.74 (±1.61)	0.04 (±0.00)	0.007 (±0.001)	0.14 (±0.007)	0.01 (±0.001)	5.82 (±1.03)	3.37 (±0.26)	0.34 (±0.02)
Trap NW - 39	01.06.2008	9.55 (±0.67)	0.02 (±0.00)	0.004 (±0.001)	0.05 (±0.003)	0.01 (±0.002)	5.77 (±1.02)	2.10 (±0.16)	0.29 (±0.08)
Trap NE - 1	22.11.2006	62.06 (±3.10)	0.40 (±0.03)	0.048 (±0.004)	0.36 (±0.018)	0.12 (±0.006)	8.19 (±0.90)	0.91 (±0.08)	0.30 (±0.03)
Trap NE - 2	06.12.2006	33.76 (±1.69)	0.22 (±0.02)	0.026 (±0.003)	0.21 (±0.010)	0.05 (±0.003)	8.65 (±1.10)	0.94 (±0.09)	0.24 (±0.02)
Trap NE - 3	20.12.2006	7.89 (±0.39)	0.07 (±0.02)	0.007 (±0.001)	0.05 (±0.002)	0.01 (±0.001)	9.17 (±1.23)	0.71 (±0.07)	0.14 (±0.01)
Trap NE - 4	03.01.2007	21.14 (±1.06)	0.14 (±0.01)	0.016 (±0.001)	0.14 (±0.007)	0.03 (±0.001)	8.70 (±1.01)	1.00 (±0.09)	0.20 (±0.02)
Trap NE - 5	17.01.2007	5.51 (±0.28)	0.06 (±0.01)	0.007 (±0.001)	0.03 (±0.001)	0.00 (±0.000)	8.17 (±1.10)	0.48 (±0.05)	0.08 (±0.01)
Trap NE - 6	31.01.2007	8.87 (±0.44)	0.10 (±0.01)	0.012 (±0.001)	0.05 (±0.003)	0.01 (±0.000)	8.06 (±1.08)	0.52 (±0.05)	0.08 (±0.01)
Trap NE - 7	14.02.2007	22.42 (±1.12)	0.19 (±0.02)	0.027 (±0.003)	0.13 (±0.007)	0.02 (±0.001)	7.32 (±0.98)	0.67 (±0.07)	0.11 (±0.01)
Trap NE - 8	28.02.2007	18.72 (±0.94)	0.11 (±0.01)	0.013 (±0.001)	0.11 (±0.006)	0.03 (±0.004)	8.39 (±1.13)	0.98 (±0.10)	0.25 (±0.04)
Trap NE - 9	14.03.2007	8.71 (±0.44)	0.06 (±0.01)	0.007 (±0.001)	0.05 (±0.003)	0.01 (±0.001)	8.45 (±1.13)	0.93 (±0.10)	0.17 (±0.02)
Trap NE - 10	28.03.2007	9.10 (±0.45)	0.05 (±0.00)	0.006 (±0.001)	0.06 (±0.003)	0.01 (±0.001)	7.54 (±1.01)	1.21 (±0.13)	0.18 (±0.02)
Trap NE - 11	11.04.2007	29.67 (±1.48)	0.11 (±0.01)	0.013 (±0.001)	0.20 (±0.010)	0.04 (±0.002)	8.88 (±1.14)	1.77 (±0.16)	0.38 (±0.04)
Trap NE - 12	25.04.2007	23.54 (±1.18)	0.14 (±0.01)	0.019 (±0.001)	0.14 (±0.007)	0.03 (±0.002)	7.36 (±0.80)	0.97 (±0.09)	0.22 (±0.02)
Trap NE - 13	09.05.2007	173.19 (±8.66)	0.96 (±0.05)	0.121 (±0.006)	0.70 (±0.044)	0.99 (±0.056)	7.94 (±0.60)	0.73 (±0.06)	1.03 (±0.08)
Trap NE - 14	23.05.2007	268.80 (±13.44)	1.10 (±0.06)	0.133 (±0.007)	1.30 (±0.083)	1.22 (±0.073)	8.27 (±0.60)	1.18 (±0.10)	1.11 (±0.09)
Trap NE - 15	06.06.2007	72.46 (±3.62)	0.34 (±0.03)	0.044 (±0.004)	0.45 (±0.023)	0.20 (±0.012)	7.82 (±0.98)	1.32 (±0.12)	0.57 (±0.06)
Trap NE - 16	20.06.2007	44.57 (±2.23)	0.25 (±0.01)	0.029 (±0.001)	0.31 (±0.016)	0.08 (±0.004)	8.40 (±0.60)	1.25 (±0.09)	0.32 (±0.02)

Sample ID	Date	Mass Flux	POC Flux	PON Flux	$CaCO_3$ Flux	BSi Flux	POC:PON	PIC:POC	BSi:POC
Trap NE - 17	04.07.2007	32.00 (±1.60)	0.20 (±0.01)	0.022 (±0.001)	0.21 (±0.011)	0.05 (±0.003)	8.91 (±0.73)	1.09 (±0.08)	0.27 (±0.02)
Trap NE - 18	18.07.2007	120.00 (±6.00)	0.66 (±0.04)	0.077 (±0.006)	0.68 (±0.034)	0.30 (±0.018)	8.59 (±0.81)	1.03 (±0.08)	0.46 (±0.04)
Trap NE - 19	26.08.2007	138.72 (±6.95)	0.50 (±0.03)	0.064 (±0.011)	0.86 (±0.045)	0.17 (±0.002)	7.78 (±1.38)	1.72 (±0.13)	0.33 (±0.02)
Trap NE - 20	09.09.2007	165.71 (±8.29)	0.64 (±0.04)	0.083 (±0.014)	1.03 (±0.053)	0.20 (±0.005)	7.68 (±1.36)	1.62 (±0.12)	0.31 (±0.02)
Trap NE - 21	23.09.2007	169.95 (±8.50)	0.46 (±0.03)	0.057 (±0.010)	1.16 (±0.060)	0.16 (±0.002)	8.06 (±1.44)	2.55 (±0.20)	0.34 (±0.02)
Trap NE - 22	07.10.2007	146.42 (±7.33)	0.55 (±0.03)	0.068 (±0.012)	0.94 (±0.051)	0.13 (±0.004)	8.09 (±1.46)	1.72 (±0.14)	0.25 (±0.02)
Trap NE - 23	21.10.2007	171.53 (±8.58)	0.62 (±0.04)	0.080 (±0.014)	1.16 (±0.060)	0.15 (±0.005)	7.76 (±1.39)	1.86 (±0.14)	0.24 (±0.02)
Trap NE - 24	04.11.2007	70.06 (±3.51)	0.25 (±0.01)	0.030 (±0.005)	0.46 (±0.030)	0.06 (±0.001)	8.20 (±1.48)	1.89 (±0.16)	0.26 (±0.01)
Trap NE – 25[#]	18.11.2007	*56.25 (±2.82)*	*0.33 (±0.02)*	*0.042 (±0.007)*	*0.39 (±0.020)*	*0.05 (±0.001)*	*7.80 (±1.38)*	*1.20 (±0.09)*	*0.15 (±0.01)*
Trap NE - 26[#]	02.12.2007	*13.48 (±0.68)*	*0.08 (±0.00)*	*0.011 (±0.002)*	*0.09 (±0.005)*	*0.02 (±0.000)*	*7.16 (±1.27)*	*1.10 (±0.08)*	*0.21 (±0.01)*
Trap NE - 27[#]	16.12.2007	*11.30 (±0.57)*	*0.06 (±0.00)*	*0.007 (±0.001)*	*0.07 (±0.004)*	*0.02 (±0.000)*	*7.76 (±1.37)*	*1.28 (±0.10)*	*0.28 (±0.02)*
Trap NE - 28[#]	30.12.2007	*9.99 (±0.51)*	*0.19 (±0.01)*	*0.023 (±0.004)*	*0.05 (±0.003)*	*0.01 (±0.000)*	*8.12 (±1.44)*	*0.27 (±0.02)*	*0.05 (±0.00)*
Trap NE - 29[#]	13.01.2008	*3.40 (±0.18)*	*0.03 (±0.00)*	*0.007 (±0.001)*	*0.01 (±0.001)*	*0.01 (±0.000)*	*4.56 (±0.81)*	*0.41 (±0.03)*	*0.22 (±0.01)*
Trap NE - 30[#]	27.01.2008	*0.91 (±0.05)*	*0.01 (±0.00)*	*0.003 (±0.000)*	*NEM*	*NEM*	*3.58 (±0.63)*	*NEM*	*NEM*
Trap NE - 31[#]	10.02.2008	*0.78 (±0.04)*	*0.02 (±0.00)*	*0.003 (±0.001)*	*NEM*	*NEM*	*5.70 (±1.01)*	*NEM*	*NEM*
Trap NE - 32	24.02.2008	2.33 (±0.12)	0.01 (±0.00)	0.001 (±0.000)	NEM	NEM	8.06 (±1.43)	NEM	NEM
Trap NE - 33	09.03.2008	3.63 (±0.19)	0.06 (±0.00)	0.010 (±0.002)	NEM	NEM	6.29 (±1.11)	NEM	NEM
Trap NE - 34	23.03.2008	1.41 (±0.15)	0.02 (±0.00)	0.004 (±0.001)	NEM	NEM	6.10 (±1.08)	NEM	NEM
Trap NE - 35	06.04.2008	2.34 (±0.12)	0.01 (±0.00)	0.002 (±0.000)	NEM	NEM	5.97 (±1.13)	NEM	NEM
Trap NE - 36	20.04.2008	7.02 (±0.59)	0.04 (±0.01)	0.009 (±0.001)	NEM	NEM	4.58 (±0.98)	NEM	NEM
Trap NE - 37	04.05.2008	9.94 (±0.50)	0.04 (±0.00)	0.007 (±0.001)	0.06 (±0.003)	0.01 (±0.000)	5.73 (±1.01)	1.43 (±0.11)	0.22 (±0.01)

Sample ID	Date	Mass Flux	POC Flux	PON Flux	$CaCO_3$ Flux	BSi Flux	POC:PON	PIC:POC	BSi:POC
Trap NE - 38[#]	18.05.2008	*1.03 (±0.05)*	*0.01 (±0.00)*	*0.002 (±0.000)*	*NEM*	*0.01 (±0.000)*	*5.90 (±1.04)*	*NEM*	*0.64 (±0.04)*
Trap NE - 39	01.06.2008	7.35 (±0.84)	0.04 (±0.00)	0.007 (±0.001)	0.07 (±0.003)	0.01 (±0.000)	5.91 (±1.05)	1.70 (±0.13)	0.21 (±0.01)
Trap C - 1	22.11.2006	58.14 (±2.91)	0.33 (±0.02)	0.043 (±0.004)	0.36 (±0.018)	0.11 (±0.009)	7.67 (±0.83)	1.10 (±0.09)	0.34 (±0.04)
Trap C - 2	06.12.2006	39.06 (±1.95)	0.23 (±0.02)	0.033 (±0.003)	0.25 (±0.012)	0.07 (±0.003)	6.92 (±0.89)	1.07 (±0.10)	0.29 (±0.03)
Trap C - 3	20.12.2006	30.54 (±1.53)	0.55 (±0.06)	0.090 (±0.011)	0.16 (±0.013)	0.04 (±0.002)	6.07 (±1.01)	0.29 (±0.04)	0.07 (±0.01)
Trap C - 4	03.01.2007	29.05 (±1.45)	0.19 (±0.02)	0.028 (±0.002)	0.18 (±0.009)	0.05 (±0.002)	6.86 (±0.72)	0.92 (±0.09)	0.24 (±0.02)
Trap C - 5	17.01.2007	19.45 (±0.97)	0.12 (±0.01)	0.016 (±0.001)	0.12 (±0.006)	0.03 (±0.002)	7.70 (±0.81)	0.96 (±0.09)	0.26 (±0.02)
Trap C - 6	31.01.2007	17.43 (±0.87)	0.11 (±0.01)	0.014 (±0.001)	0.13 (±0.007)	0.03 (±0.002)	7.69 (±0.58)	1.18 (±0.09)	0.31 (±0.02)
Trap C - 7	14.02.2007	19.65 (±0.98)	0.11 (±0.02)	0.017 (±0.002)	0.12 (±0.06)	0.03 (±0.002)	6.81 (±1.41)	1.05 (±0.16)	0.28 (±0.05)
Trap C - 8	28.02.2007	14.77 (±0.74)	0.17 (±0.02)	0.025 (±0.003)	0.09 (±0.004)	0.02 (±0.001)	6.63 (±0.89)	0.51 (±0.05)	0.13 (±0.01)
Trap C - 9	14.03.2007	8.33 (±0.42)	0.07 (±0.01)	0.012 (±0.001)	0.05 (±0.002)	0.01 (±0.001)	6.32 (±0.85)	0.64 (±0.07)	0.15 (±0.02)
Trap C - 10	28.03.2007	3.59 (±0.18)	0.03 (±0.00)	0.004 (±0.000)	0.02 (±0.001)	0.00 (±0.000)	6.50 (±0.87)	0.84 (±0.09)	0.16 (±0.02)
Trap C - 11	11.04.2007	2.63 (±0.13)	0.02 (±0.00)	0.002 (±0.000)	0.02 (±0.001)	0.00 (±0.000)	9.70 (±1.26)	0.79 (±0.07)	0.20 (±0.02)
Trap C - 12	25.04.2007	7.18 (±0.36)	0.09 (±0.01)	0.013 (±0.001)	0.04 (±0.002)	0.01 (±0.001)	7.16 (±0.77)	0.39 (±0.03)	0.13 (±0.01)
Trap C - 13	09.05.2007	50.47 (±2.52)	0.37 (±0.03)	0.040 (±0.008)	0.22 (±0.012)	0.27 (±0.013)	9.23 (±2.04)	0.59 (±0.06)	0.73 (±0.07)
Trap C - 14	23.05.2007	197.29 (±9.86)	0.88 (±0.19)	0.111 (±0.029)	1.34 (±0.068)	0.51 (±0.047)	8.00 (±2.73)	1.51 (±0.34)	0.58 (±0.14)
Trap C - 15	06.06.2007	83.26 (±4.16)	0.30 (±0.10)	0.036 (±0.012)	0.57 (±0.031)	0.21 (±0.013)	8.34 (±3.81)	1.90 (±0.62)	0.71 (±0.23)
Trap C - 16	20.06.2007	82.60 (±4.13)	0.40 (±0.17)	0.048 (±0.020)	0.53 (±0.027)	0.25 (±0.016)	8.16 (±4.84)	1.35 (±0.58)	0.64 (±0.28)
Trap C - 17	04.07.2007	21.67 (±1.08)	0.11 (±0.02)	0.013 (±0.003)	0.15 (±0.008)	0.03 (±0.002)	8.27 (±2.57)	1.36 (±0.30)	0.28 (±0.06)
Trap C - 18	18.07.2007	46.78 (±2.34)	0.31 (±0.02)	0.037 (±0.002)	0.28 (±0.017)	0.11 (±0.007)	8.30 (±0.68)	0.93 (±0.08)	0.34 (±0.03)
Trap C - 19	26.08.2007	87.39 (±4.37)	0.28 (±0.02)	0.038 (±0.006)	0.53 (±0.005)	0.11 (±0.005)	7.42 (±1.31)	1.88 (±0.11)	0.39 (±0.03)

Sample ID	Date	Mass Flux	POC Flux	PON Flux	$CaCO_3$ Flux	BSi Flux	POC:PON	PIC:POC	BSi:POC
Trap C – 20#	09.09.2007	*18.34 (±0.92)*	*0.15 (±0.01)*	*0.027 (±0.005)*	*0.10 (±0.002)*	*NEM*	*5.54 (±0.98)*	*0.65 (±0.04)*	*0.18 (±0.01)*
Trap C - 21	23.09.2007	69.70 (±3.51)	0.13 (±0.01)	0.016 (±0.003)	0.46 (±0.015)	0.07 (±0.005)	7.82 (±1.38)	3.58 (±0.24)	0.55 (±0.05)
Trap C - 22	07.10.2007	268.05 (±13.43)	0.83 (±0.05)	0.110 (±0.018)	1.82 (±0.043)	0.25 (±0.012)	7.54 (±1.33)	2.20 (±0.14)	0.30 (±0.02)
Trap C – 23**	21.10.2007	78.08 (±3.91)	0.58 (±0.03)	0.077 (±0.013)	0.25 (±0.002)	0.06 (±0.003)	7.63 (±1.35)	0.43 (±0.02)	0.10 (±0.01)
Trap C - 24#**	18.11.2007	*6.55 (±0.33)*	*0.04 (±0.00)*	*0.006 (±0.001)*	*0.01 (±0.000)*	*0.01 (±0.000)*	*7.06 (±1.25)*	*0.32 (±0.02)*	*0.17 (±0.01)*
Trap C – 25#**	30.12.2007	*2.68 (±0.15)*	*0.02 (±0.00)*	*0.003 (±0.001)*	*0.00 (±0.000)*	*0.00 (±0.000)*	*7.43 (±1.32)*	*0.17 (±0.01)*	*0.15 (±0.01)*
Trap C – 26**	10.02.2008	3.10 (±0.16)	0.01 (±0.00)	0.001 (±0.000)	0.01 (±0.000)	0.00 (±0.000)	8.69 (±1.54)	1.17 (±0.07)	0.50 (±0.03)
Trap C - 27	09.03.2008	5.00 (±0.25)	0.03 (±0.00)	0.004 (±0.001)	0.03 (±0.000)	0.00 (±0.000)	7.03 (±1.24)	0.99 (±0.06)	0.15 (±0.01)
Trap C - 28	23.03.2008	1.51 (±0.08)	0.02 (±0.00)	0.003 (±0.001)	NEM	NEM	6.44 (±1.14)	NEM	NEM
Trap C - 29#	06.04.2008	*1.40 (±0.07)*	*0.00 (±0.00)*	*0.000 (±0.000)*	*NEM*	*NEM*	*7.29 (±2.40)*	*NEM*	*NEM*
Trap C – 30	20.04.2008	1.37 (±0.07)	0.01 (±0.00)	0.002 (±0.000)	NEM	NEM	8.43 (±1.50)	NEM	NEM
Trap C - 31	04.05.2008	0.93 (±0.06)	0.00 (±0.00)	0.001 (±0.000)	NEM	NEM	5.16 (±1.71)	NEM	NEM
Trap S - 1	22.11.2006	12.94 (±0.65)	0.12 (±0.01)	0.017 (±0.002)	0.08 (±0.004)	0.02 (±0.001)	7.06 (±0.95)	0.66 (±0.07)	0.13 (±0.01)
Trap S - 2	06.12.2006	22.90 (±1.15)	0.18 (±0.02)	0.023 (±0.002)	0.13 (±0.007)	0.04 (±0.002)	7.66 (±1.03)	0.71 (±0.08)	0.22 (±0.02)
Trap S - 3	20.12.2006	16.09 (±0.80)	0.12 (±0.01)	0.016 (±0.002)	0.10 (±0.005)	0.02 (±0.001)	7.70 (±1.03)	0.81 (±0.08)	0.19 (±0.02)
Trap S - 4	03.01.2007	6.81 (±0.34)	0.11 (±0.01)	0.016 (±0.002)	0.03 (±0.002)	0.01 (±0.000)	7.05 (±0.95)	0.28 (±0.03)	0.06 (±0.01)
Trap S - 5	17.01.2007	3.50 (±0.17)	0.04 (±0.00)	0.005 (±0.001)	0.02 (±0.001)	0.00 (±0.000)	6.84 (±0.92)	0.51 (±0.05)	0.12 (±0.01)
Trap S - 6	31.01.2007	2.51 (±0.13)	0.02 (±0.00)	0.003 (±0.000)	0.01 (±0.001)	0.00 (±0.000)	7.29 (±0.98)	0.49 (±0.05)	0.13 (±0.01)
Trap S - 7	14.02.2007	8.16 (±0.41)	0.06 (±0.01)	0.009 (±0.001)	0.05 (±0.003)	0.01 (±0.001)	7.35 (±0.99)	0.78 (±0.08)	0.17 (±0.02)
Trap S - 8	28.02.2007	7.34 (±0.37)	0.05 (±0.00)	0.007 (±0.001)	0.04 (±0.002)	0.01 (±0.001)	7.82 (±1.05)	0.80 (±0.08)	0.18 (±0.02)
Trap S - 9	14.03.2007	4.16 (±0.21)	0.06 (±0.01)	0.009 (±0.001)	0.02 (±0.001)	0.00 (±0.000)	7.31 (±0.98)	0.29 (±0.03)	0.08 (±0.01)
Trap S - 10	28.03.2007	3.15 (±0.16)	0.03 (±0.00)	0.004 (±0.000)	0.02 (±0.001)	0.00 (±0.000)	7.38 (±0.99)	0.65 (±0.07)	0.13 (±0.01)

Sample ID	Date	Mass Flux	POC Flux	PON Flux	$CaCO_3$ Flux	BSi Flux	POC:PON	PIC:POC	BSi:POC
Trap S - 11	11.04.2007	1.85 (±0.09)	0.04 (±0.00)	0.006 (±0.001)	0.00 (±0.000)	0.00 (±0.000)	6.88 (±0.90)	0.08 (±0.01)	0.02 (±0.00)
Trap S - 12	25.04.2007	5.99 (±0.30)	0.11 (±0.01)	0.016 (±0.002)	0.02 (±0.001)	0.01 (±0.001)	6.94 (±0.88)	0.23 (±0.02)	0.10 (±0.01)
Trap S - 13	09.05.2007	47.36 (±2.37)	0.29 (±0.02)	0.032 (±0.003)	0.24 (±0.017)	0.19 (±0.012)	8.92 (±1.00)	0.84 (±0.09)	0.67 (±0.07)
Trap S - 14	23.05.2007	151.31 (±7.57)	0.71 (±0.05)	0.090 (±0.007)	0.79 (±0.041)	0.66 (±0.034)	7.90 (±0.86)	1.11 (±0.10)	0.93 (±0.08)
Trap S - 15	06.06.2007	88.23 (±4.41)	0.38 (±0.02)	0.050 (±0.003)	0.53 (±0.027)	0.28 (±0.019)	7.61 (±0.56)	1.38 (±0.10)	0.74 (±0.06)
Trap S - 16	20.06.2007	24.57 (±1.23)	0.13 (±0.01)	0.016 (±0.001)	0.14 (±0.007)	0.07 (±0.005)	8.02 (±0.87)	1.11 (±0.09)	0.59 (±0.05)
Trap S - 17	04.07.2007	74.74 (±3.74)	0.43 (±0.02)	0.050 (±0.003)	0.42 (±0.021)	0.22 (±0.016)	8.60 (±0.61)	0.98 (±0.07)	0.51 (±0.05)
Trap S - 18	18.07.2007	53.94 (±2.70)	0.61 (±0.07)	0.079 (±0.012)	0.30 (±0.015)	0.11 (±0.006)	7.67 (±1.42)	0.49 (±0.06)	0.19 (±0.02)
Trap S - 19	26.08.2007	61.55 (±3.08)	0.28 (±0.02)	0.038 (±0.006)	0.40 (±0.008)	0.07 (±0.005)	7.44 (±1.32)	1.43 (±0.09)	0.25 (±0.02)
Trap S - 20	09.09.2007	80.43 (±4.02)	0.37 (±0.02)	0.052 (±0.009)	0.55 (±0.047)	0.09 (±0.004)	6.96 (±1.23)	1.52 (±0.16)	0.24 (±0.02)
Trap S - 21	23.09.2007	71.56 (±3.58)	0.28 (±0.02)	0.040 (±0.007)	0.53 (±0.006)	0.06 (±0.021)	6.85 (±1.21)	1.92 (±0.11)	0.23 (±0.08)
Trap S - 22	07.10.2007	111.52 (±5.58)	0.43 (±0.02)	0.063 (±0.011)	0.86 (±0.017)	0.07 (±0.005)	6.88 (±1.22)	1.99 (±0.12)	0.15 (±0.01)
Trap S – 23**	21.10.2007	101.40 (±5.07)	0.42 (±0.02)	0.057 (±0.010)	0.34 (±0.003)	0.09 (±0.003)	7.26 (±1.29)	0.81 (±0.05)	0.23 (±0.02)
Trap S - 24#**	18.11.2007	*8.83 (±0.48)*	*NEM*	*NEM*	*NEM*	*0.01 (±0.000)*	*7.78 (±1.38)*	*0.32 (±0.02)*	*0.21 (±0.01)*
Trap S - 25#**	30.12.2007	*4.67 (±0.31)*	*NEM*	*NEM*	*NEM*	*0.01 (±0.000)*	*7.29 (±1.29)*	*0.34 (±0.02)*	*0.54 (±0.04)*
Trap S - 26#**	10.02.2008	*0.81 (±0.04)*	*NEM*	*NEM*	*NEM*	*NEM*	*NEM*	*NEM*	*NEM*
Trap S - 27#	09.03.2008	*0.63 (±0.06)*	*NEM*	*NEM*	*NEM*	*NEM*	*NEM*	*NEM*	*NEM*
Trap S - 28#	23.03.2008	*1.06 (±0.05)*	*NEM*	*NEM*	*NEM*	*NEM*	*NEM*	*NEM*	*NEM*
Trap S - 29	06.04.2008	0.63 (±0.07)	NEM	NEM	NEM	NEM	NEM	NEM	NEM
Trap S - 30	20.04.2008	5.76 (±0.39)	0.06 (±0.00)	0.012 (±0.002)	NEM	NEM	4.80 (±0.85)	NEM	NEM
Trap S - 31	04.05.2008	9.19 (±0.46)	0.06 (±0.00)	0.014 (±0.002)	NEM	NEM	4.49 (±0.79)	NEM	NEM

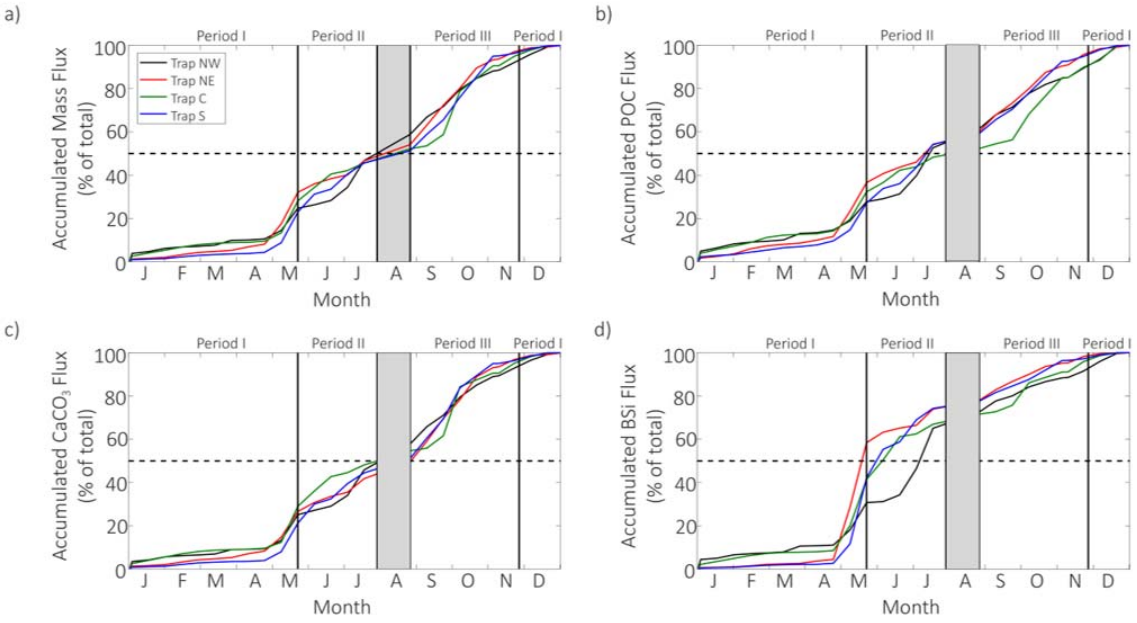

Figure 3.7 Cumulative sum of flux during an annual cycle (22nd Nov 2006 – 2007) as a percentage of the total flux for a) Mass, b) POC, c) $CaCO_3$ and d) BSi. Flux periods I-III are highlighted by the black vertical lines. The dashed black line highlights when 50 % of the annual fluxes have accumulated. The fluxes during the 28 day gap in sampling (grey box) between periods II and III was filled using nearest neighbour interpolation.

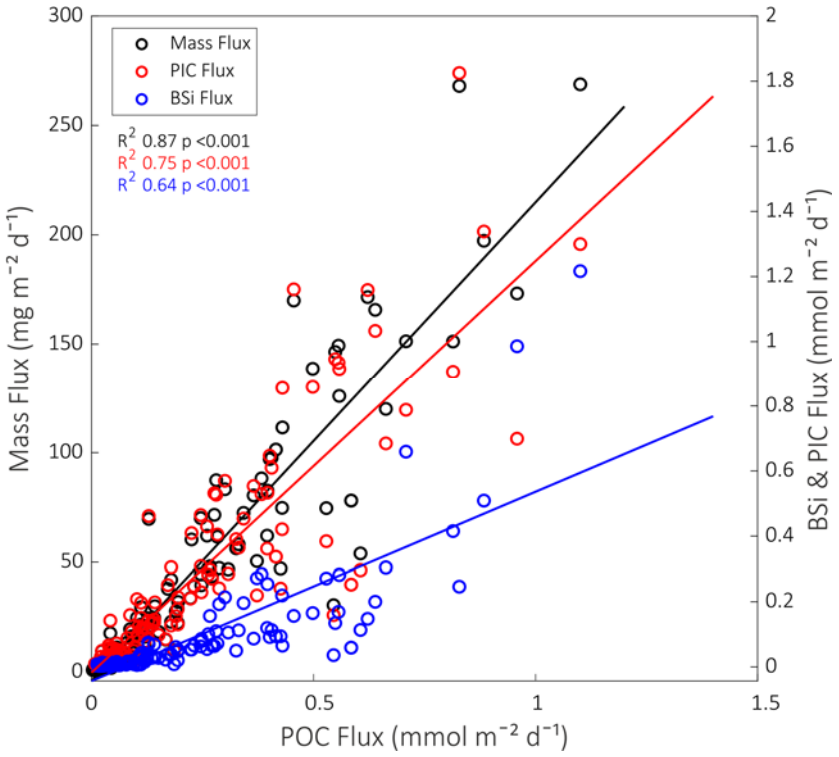

Figure 3.8 POC flux plotted against mass flux (black; left axis), PIC flux (red; right axis) and BSi flux (blue; right axis). All flux components have a strong statistically significant linear relationship with POC flux.

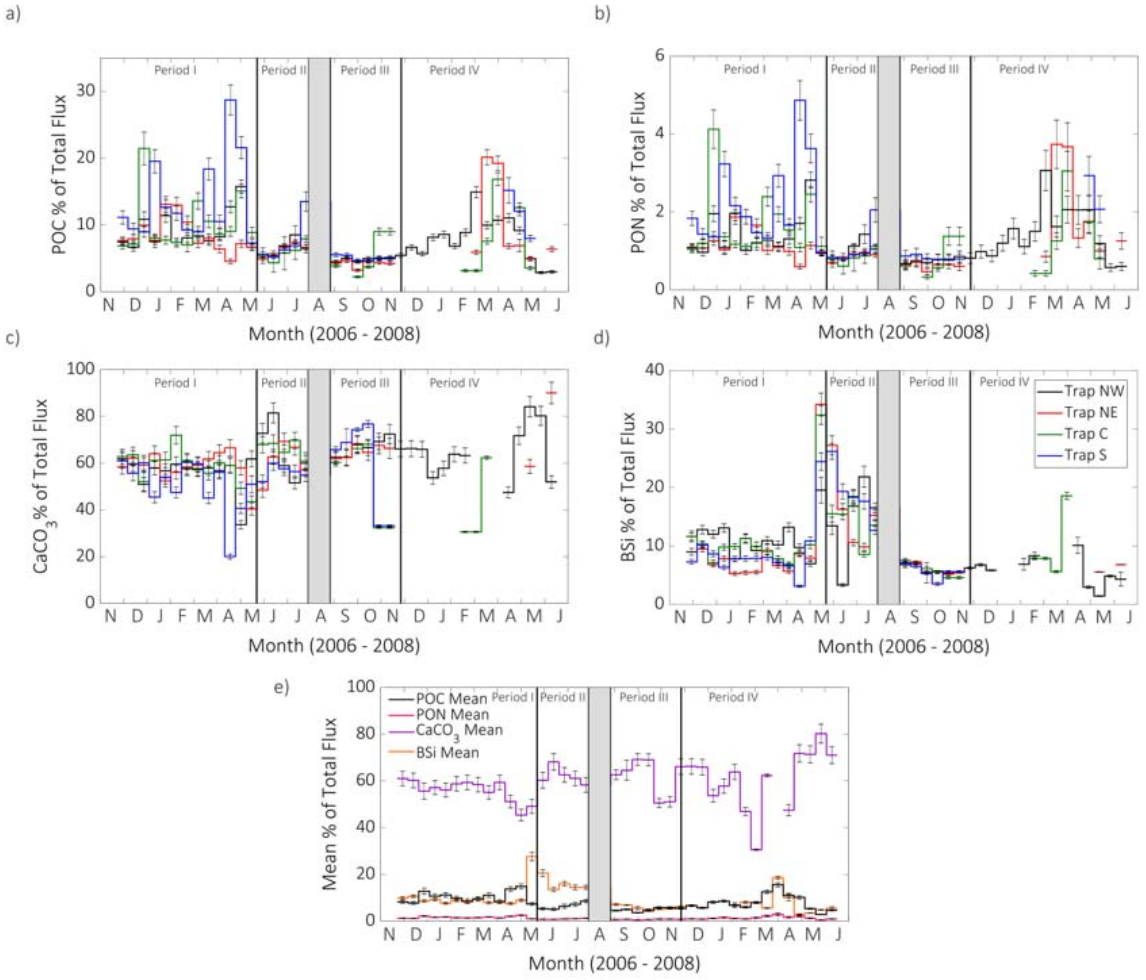

Figure 3.9 Percentage composition of the dominant particle flux components. a) POC flux percentage, b) PON flux percentage, c) $CaCO_3$ flux percentage, d) BSi flux percentage and e) mean percentage of total flux of the four sediment traps for POC, PON, $CaCO_3$ and BSi. The percentage of the mass of each components is calculated by dividing by the total mass flux. The errorbars in d) show the standard deviation between the percentage values. The black vertical lines indicate the four different flux periods and the grey shading represents the period during the two deployments. Note the different y axes. Errorbars are the propagated analytical uncertainty.

The cumulative fluxes during one annual cycle between 22nd November 2006 - 2007 show that the most rapid accumulation occurs during the spring-bloom associated flux sinking into the trap in May, particularly for BSi flux (Figure 3.7). Fluxes continue to accumulate steadily through summer with another increase in the rate of accumulation in September and October across all components, although the rate of BSi accumulation is lower. This is supported by the strength of the linear relationships between POC flux and the biomineral fluxes in Figure 3.8. Mass and PIC fluxes had strong significant linear relationships with POC flux, whilst BSi flux has a moderate significant linear relationship. For Traps NE and S, less than 10 % of the mass, $CaCO_3$ and BSi flux is

collected between the end of November in 2006 until May 2007 and less than 20 % for Traps NW and C. A similar pattern is seen for POC flux, with less than 20 % of the flux accumulated between November 2006 and April 2007 for Traps NE and S, and less than 30 % during the same time period for Traps NW and C.

The percentage contribution of POC to total flux usually falls within 6 - 10 % and temporal variability in the contribution of POC is evident from Figure 3.9. In winter and spring POC tends to make a greater contribution to total flux with a mean of 10.1 % and fluxes ranging between 5 - 29 %, but as shown by the accumulation rates in Figure 3.7, as fluxes are low the relative contribution to the annual POC flux is small. There appears to be greater spatial variability between the traps in winter and spring, with some traps deviating with greater POC contributions of > 10 %, particularly Trap S. The percentage contribution of POC flux in late spring, summer and autumn, when mass fluxes were higher, was lower with a mean percentage contribution of 5.6 %, and a range of 5 – 14 %. There was very little spatial variability in the flux elemental composition between the traps, suggesting that the composition of the material collected was very similar across the IB. The percentage contribution of PON total flux exhibits the same temporal pattern and magnitude of spatial variability as the POC percentage contribution to total mass flux.

The $CaCO_3$ percentage contribution to total flux (Figure 3.9c) does not exhibit large temporal variability. In winter and spring $CaCO_3$ makes a mean contribution of 55.9 %, with a range of 20 - 73 % to the total mass flux. Trap S appears to have instances of lower $CaCO_3$ percentage contribution, with one extreme value of only 20 % in mid-April 2007. Generally, the $CaCO_3$ contribution is lower in the pre-spring bloom particle flux when the percentage contribution of BSi increases (Figure 3.9d). In summer and autumn the percentage contribution of $CaCO_3$ is slightly higher in some traps, with a mean contribution of 61.6 % and a range of 32 – 81 %. In October and November 2007 Traps C and S had a sample with very low $CaCO_3$ percentage compared to the other traps, 32 % compared to 68 % (Appendix A). This may be indicative of poorly preserved samples as the buffered formaldehyde may have been washed out of the sample cup and the $CaCO_3$ would have dissolved in the undersaturated deep ocean water, as can be seen in some of the traps in Period IV in which there was not enough particulate material to measure each component.

The percentage contribution of BSi to total flux follows an inverse temporal cycle to the $CaCO_3$ percentage contribution, with generally low contributions throughout most of the annual cycle and much higher contributions during the spring-bloom associated particle flux and summer. In winter and early spring the BSi contributed 3 - 13 % of total flux, with a mean contribution of 8.6 %, whereas for spring-bloom associated particle flux the BSi contributed 13 - 34 % of total flux,

with a mean contribution of 24.1 %. The BSi contribution decreases throughout summer to low levels in autumn with a mean contribution of 5.8 %. Spatial variability between the traps was greatest during late spring and summer and lowest during autumn for the BSi percentage contribution.

The mean percentage composition of each of the components was calculated for the time-series. This highlights that the POC content of the flux increases preceding the spring bloom associated flux and that the spring bloom associated flux is higher in BSi content and has a lower $CaCO_3$ content.

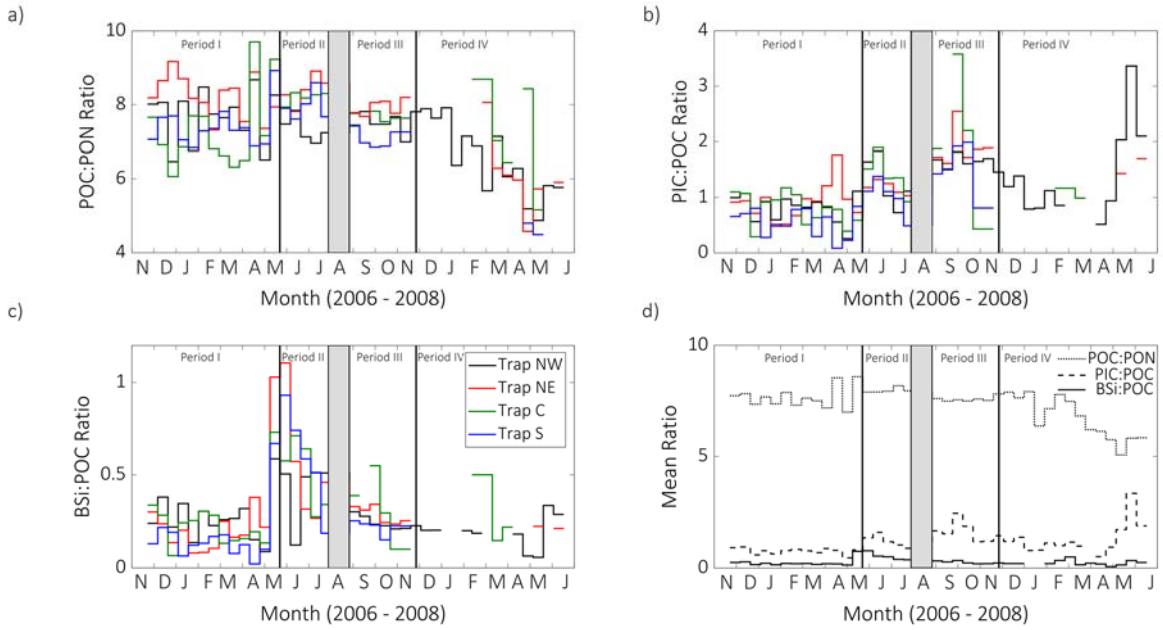

Figure 3.10 Molar ratios of particle flux components. a) POC:PON molar ratio, b) PIC:POC molar ratio, c) BSi:POC ratio and d) mean molar ratios of the four sediment traps. The black vertical lines indicate the four flux periods and the grey shaded area highlights the sampling gap between deployments as described in Chapter 2.

The observed changes in flux composition are also evident in the PIC:POC and BSi:POC ratios with the former being highest in the autumn and the latter being highest in the late spring and summer. The POC:PON ratio exhibits spatial variability but is fairly constant for Periods I-III, ranging between 6 – 9.5, whereas for Period IV the ratio decreases steadily towards a low of ~ 4.5, as discussed further in Chapter 2, Section 2.3.1.

3.3.2 Particle Source Regions

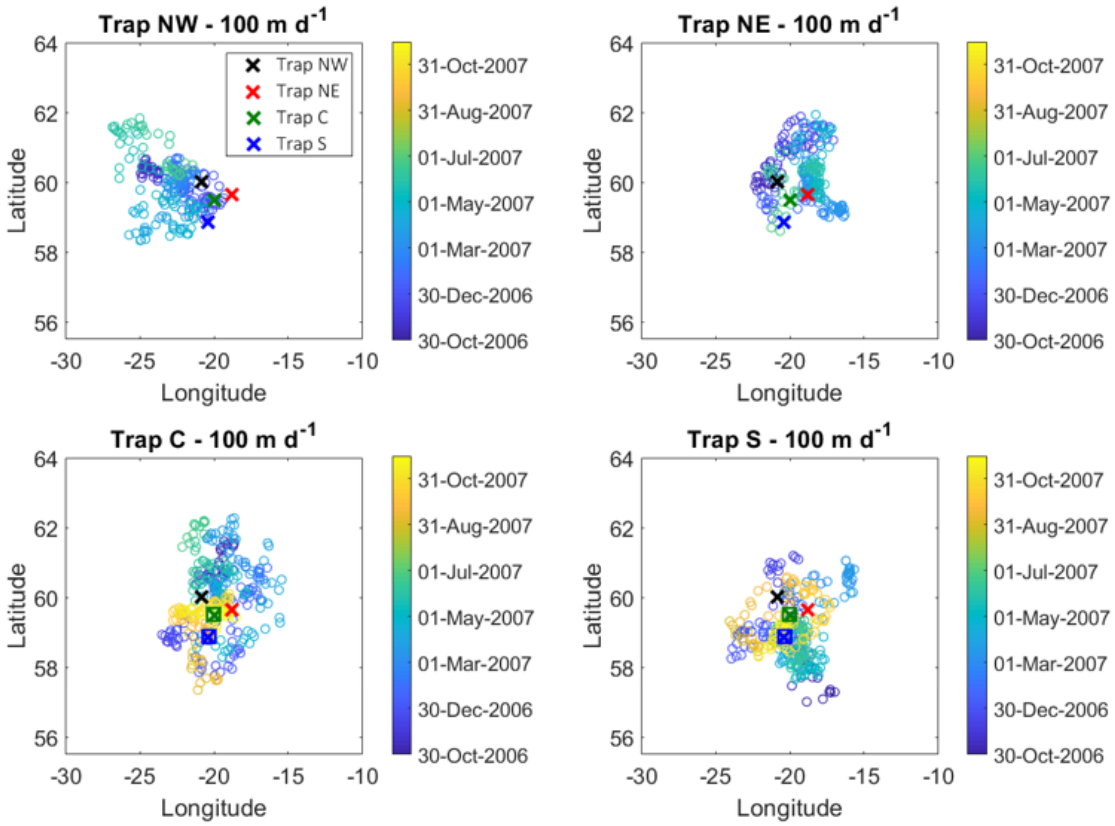

Figure 3.11 Predicted particle source regions for Trap a) NW, b) NE, c) C and d) S assuming that the bulk particle sinking speed was 100 m d^{-1}. The particle source regions were predicted using current meter velocity collected 15 m below the sediment traps and OSCAR surface current velocity. The colour bar indicates the timing of when each individual particle reached the surface ocean. The sediment trap locations are highlighted by the coloured crosses and the squares indicate that for Trap C and Trap S the particle source regions were also predicted for deployment 2.

To explore and understand the mesoscale variability in sediment trap fluxes in the IB I have estimated where the particle source regions for each trap likely would have originated for each day of the sampling time-series. Two differing approaches were used to backtrack the particles; using current meter velocity and OSCAR surface current velocity (Figure 3.11 and 3.12) and using Copernicus physical reanalysis model output (Figure 3.12). The advantages of using the model output is greater depth resolution and no constraints due to deployment periods or data gaps, such as at the beginning of the sampling period when backtracking is not possible without prior current meter data. However, the model output likely underestimates the currents in the deep ocean, particularly short temporal and small localised events (Figure 3.3), which leads to more localised particle source regions (Figure 3.12).

Method Validation

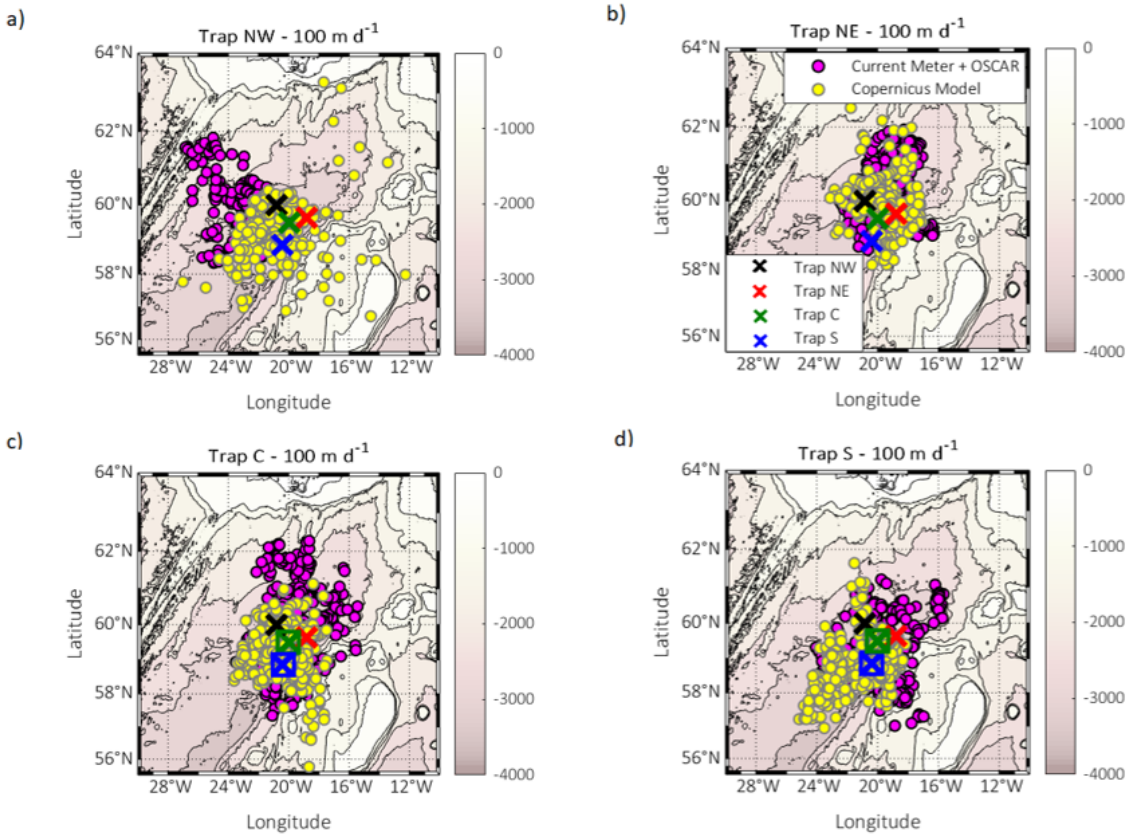

Figure 3.12 Particle source regions of the deep ocean Iceland Basin for Periods I-III comparing the current velocity data termed 'Current Meter + OSCAR' and the physical reanalysis model output termed 'Copernicus Model'. a) Trap NW, b) Trap NE, c) Trap C and d) Trap S source regions with the traps highlighted by the coloured crosses. Only deployment 1 was compared for Traps NW and NE as the current meter data was not successfully recovered from deployment 2. The bathymetry of the Subpolar North Atlantic is shown by the contours and depth is shown by the colour bar.

Validating the predicted particle source regions is challenging as the origin of individual particles, and mean origin of all the particles in a deep ocean sediment trap sample is not known. The two approaches of using current meter and OSCAR data and Copernicus model output are compared in Figure 3.12 and Figure C.2.1. The particle source regions for the sediment traps are mostly located in the central IB and the mean particle source regions for the different approaches, and the different traps, all fall mostly within the IB, except for Trap NW and Trap NE particle source region predicted using current meter and OSCAR velocities. The Trap NE and Trap S source regions, in Figure 3.12, have similar spatial extents regardless of the approach, whereas the Trap NW source regions have a more North-westerly extent when predicted using current meter and OSCAR data and has a more South-easterly extent when using model data. Trap C particle source

regions extend Northwards more frequently when using the current meter and OSCAR velocity data compared to the model source regions. The mean distance between the sediment trap locations and mean particle source locations was 69.8 km (43 - 114 km) for current meter and OSCAR velocities and 53.3 km (27 - 92 km) for the model velocities (Figure C.3.1). This is also demonstrated by the example particle traces in Figure 3.2. The mean particle source regions extend to a similar radius (~ 100 km) from the sediment trap locations as in previous studies for a bulk sinking speed of 100 m d^{-1} and trap depths between 2000 and 2500 m (Siegel & Deuser, 1997; Waniek et al., 2000).

The effects of small changes (random error between +/-1 standard deviation) in the *u* and *v* velocity components from the current meter and OSCAR product, throughout the water column were assessed using 20 Monte Carlo simulations. This is shown in Figure C.3.1 and highlights that the particle source regions become slightly wider in extent with slower sinking speeds but the difference in the particle source regions between the 20 simulations is minimal and does not affect the interpretation of the results in this thesis.

3.3.3 Linking Upper Ocean Processes with Deep Ocean Particle Flux

3.3.3.1 Biological Drivers

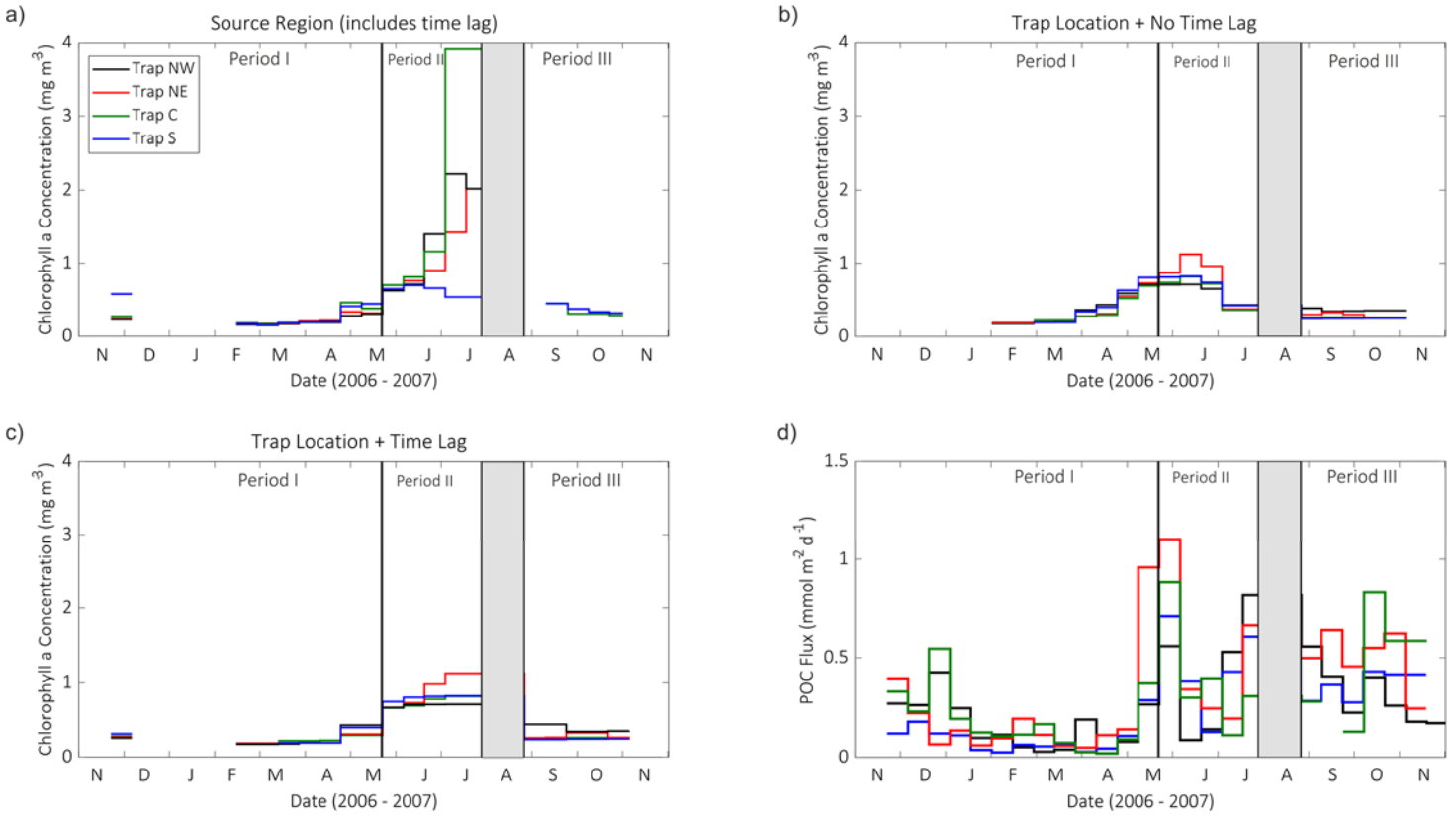

Figure 3.13 Satellite chlorophyll *a* concentration extracted using a) particle source regions b) trap locations (without time lag), and c) trap locations (with time lag) for the four sediment traps and d) POC flux. The three flux periods are highlighted and the sampling gap during sediment traps deployments is in grey.

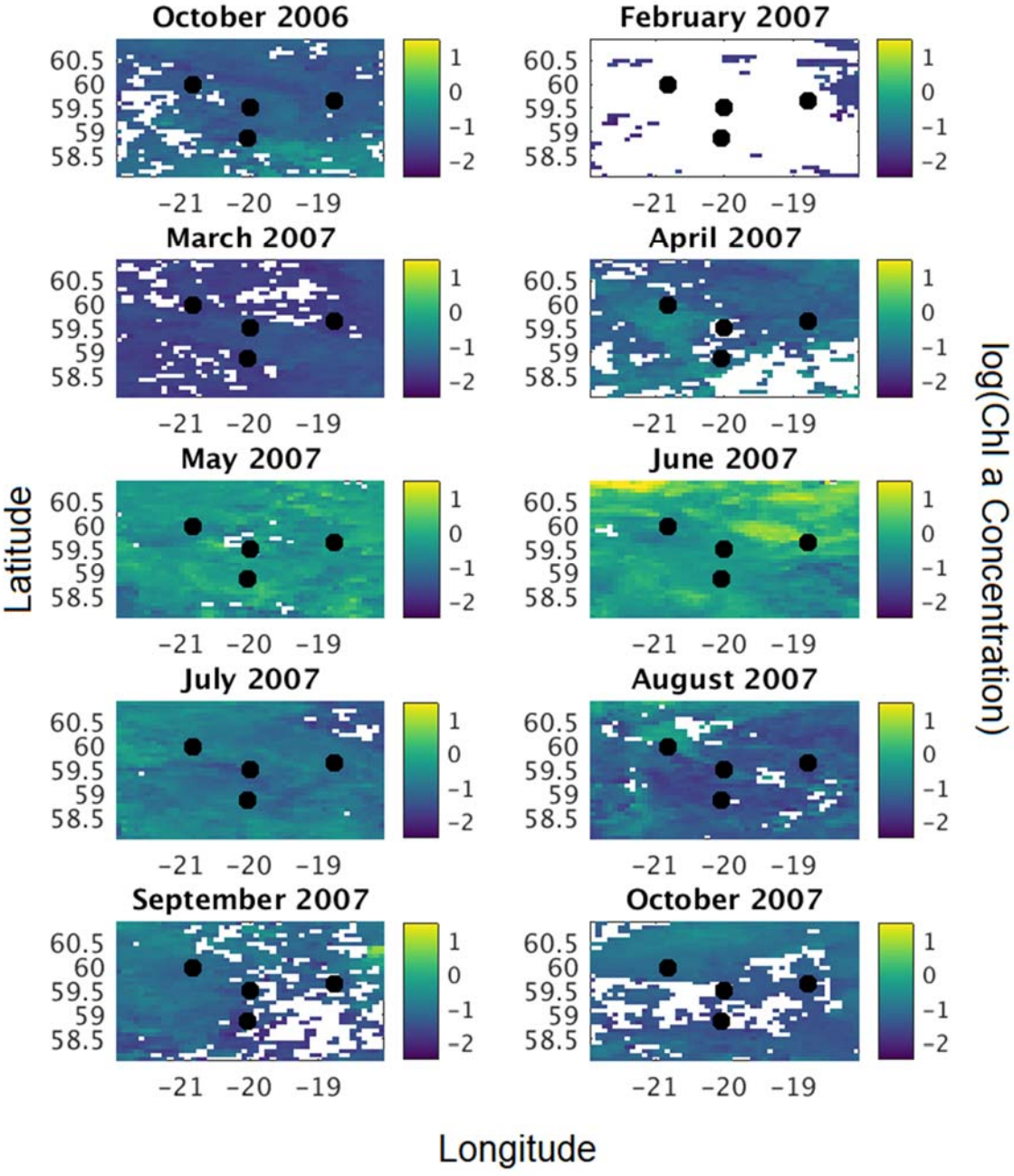

Figure 3.14 Remotely sensed monthly chlorophyll *a* concentration (mg m^{-3}) in the Iceland Basin between October 2006 - 2007. Note the log scale. The black circles refer to the sediment trap locations. White indicates where cloud cover has obscured data collection.

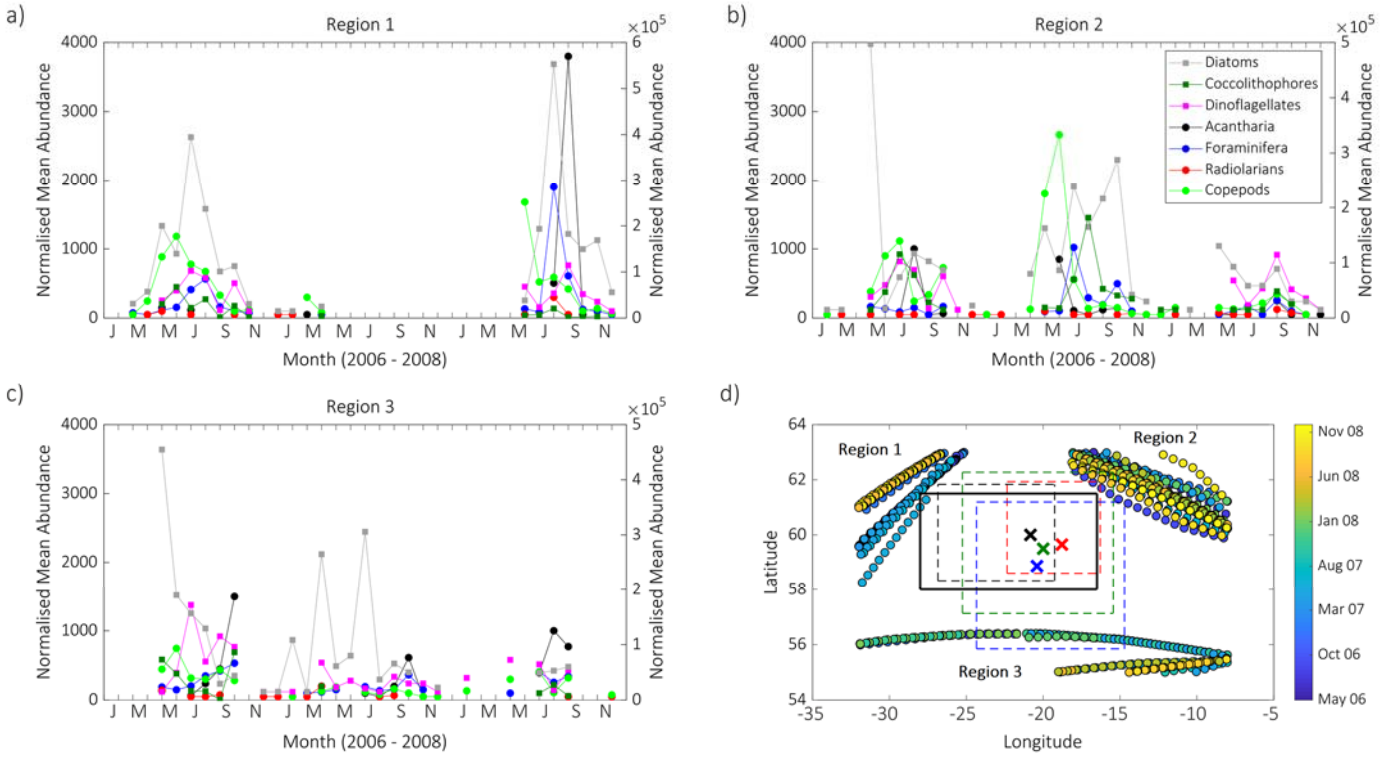

Figure 3.15 Continuous Plankton Recorder (CPR) mean abundance normalised to the number of tows averaged for the areas encompassing the Iceland Basin (B5, B6, C5 and C6). The CPR data originated from three areas within the four standards areas which we have labelled as a) Region 1, b) Region 2 and c) Region 3. The three regions are highlighted in the map in d). For panels a) to c) the normalised mean abundance is shown for different plankton groups – diatoms (grey), coccolithophores (dark green), dinoflagellates (pink), acantharia (black), foraminifera (blue), non-acantharian radiolarians (red) and copepods (green). The square markers (diatoms, coccolithophores and dinoflagellates) indicate that the data is plotted on the right axes, whilst all other groups plot against the left axes. Panel d) shows the location and timing (colour bar) of the CPR data (Table 3.3). The thick black box indicates the area defined as the IB. The four dashed boxes show the minimum and maximum extents of the particle source regions for each trap (estimated used current meter and OSCAR velocity) and the crosses show the locations of the trap – Trap NW (black), Trap NE (red), Trap C (green) and Trap S (blue).

The Chl *a* concentration extracted at the sediment trap location showed a similar seasonal cycle and magnitude for the four traps, with concentrations beginning to increase in April, peaking in June and decreasing from July back down to ambient concentrations (Figure 3.13 and Figure 3.14). Trap NE had the highest Chl *a* concentrations up to 1 mg m^{-3} which peaks after the largest Trap NE POC flux. The time lag and trap location Chl *a* concentration is similar in magnitude but the time lag concentration aligns with the source region Chl *a* concentration. However, the sampling period Chl *a* concentration tracks the POC flux increase much more closely, which may be an indication of rapid sinking of the particulate material to the deep ocean. This may suggest that, during spring, a time lag between upper ocean processes and deep ocean particle flux is not necessary to improve our mechanistic understanding of processes in high latitude regions with a strong seasonal cycle, especially when the particle sinking time lag is less than the sediment trap sampling period (Figure 3.13).

The Chl *a* concentration extracted using the minimum and maximum extent of the predicted particle source regions for each sampling period shows similar patterns to the Chl *a* concentration at the sediment trap location for winter and early spring, but the predicted particle source region concentrations are much greater in June through to August for Traps NW, NE and C, whereas Trap S concentrations remain similar to the above trap concentration throughout. Trap C particle source region Chl *a* concentration peaks to 3.9 mg m^{-3} in June, with the associated particle flux reaching the sediment trap in July.

The CPR data indicates that in 2007 diatoms in Regions 2 and 3 generally increase throughout spring and summer and in Region 2 until October when the peak in abundance is reached. BSi fluxes in the traps peaked during the spring bloom and steadily decreased towards winter suggesting that peak abundance in the surface does not necessarily correlate with deep ocean BSi fluxes, unless diatom abundances in the central IB are not well represented by Region 2 CPR data. In Region 2 copepods increased in abundance following the spring bloom and then return to low levels in summer. In Region 2, coccolithophores and foraminifera peak in summer which aligns well with increases in $CaCO_3$ flux (Figure 3.5).

3.3.3.2 Physical Drivers

The IB is a physically dynamic region. According to SLA and EKE maps the most dynamic periods during the sediment trap deployments were December 2007, January 2007, September – October 2007 and December 2007 – January 2008 (Figure 3.16 – 3.18). The central IB has eddy features developing, traversing and dissipating continuously throughout the sampling period. Eddies with the largest radii tended to be anticyclonic eddies, which traversed over the entire IB, whereas

cyclonic eddies tended to be present towards the east of the basin, except for one strong eddy feature in September-October 2007.

The upper ocean data presented in this results section will be used to explore five case studies with instances of notable mesoscale variability to further understand how biological and physical processes affect deep ocean carbon sequestration in the Iceland Basin.

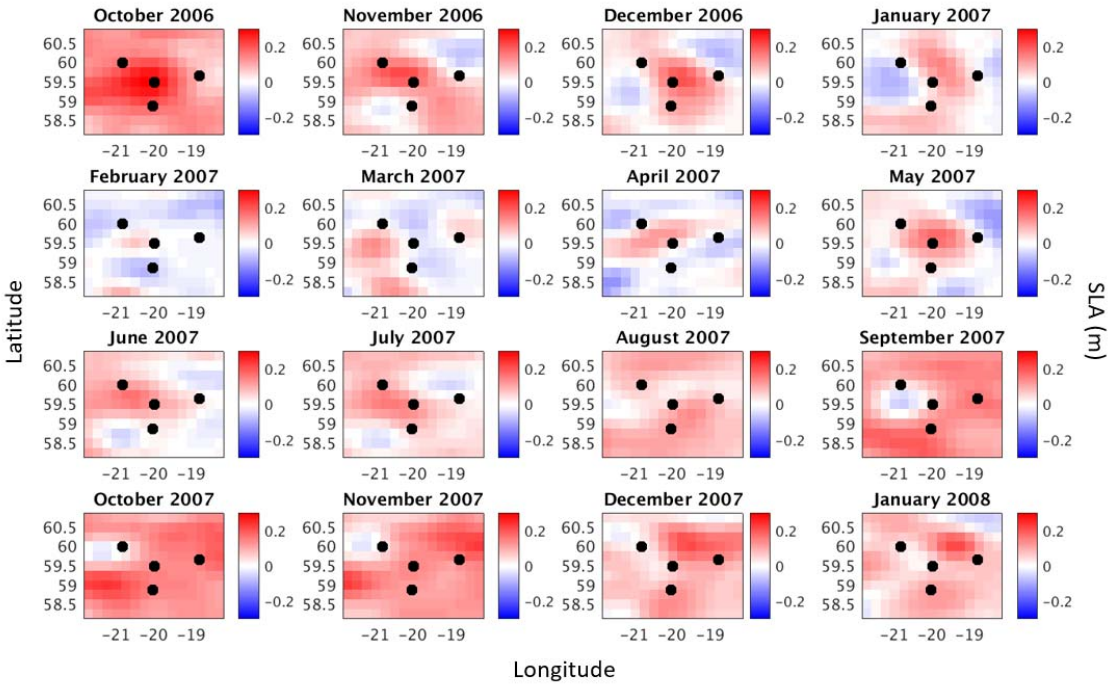

Figure 3.16 Mean monthly sea level anomaly from October 2006 to January 2008 for the area surrounding the sediment traps (black dots).

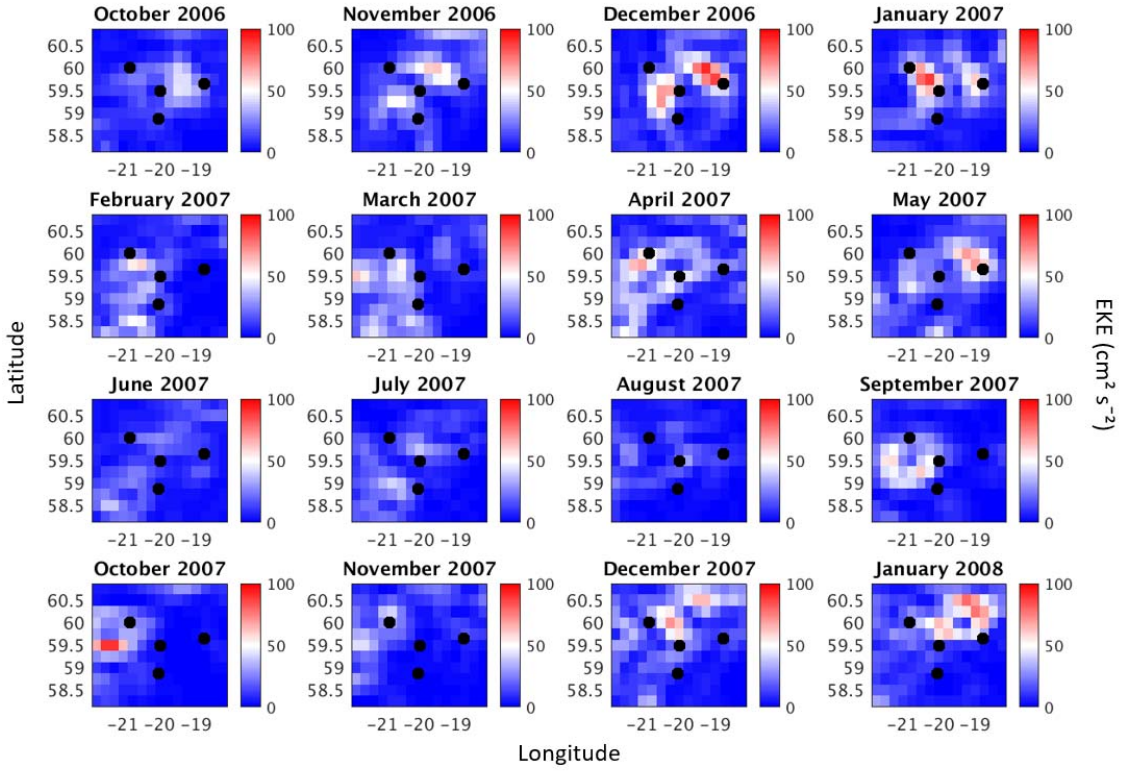

Figure 3.17 Eddy Kinetic Energy (EKE) calculated from *u* and *v* SLA components for October 2006 - January 2008 in the Iceland Basin. The black circles highlight the sediment trap locations.

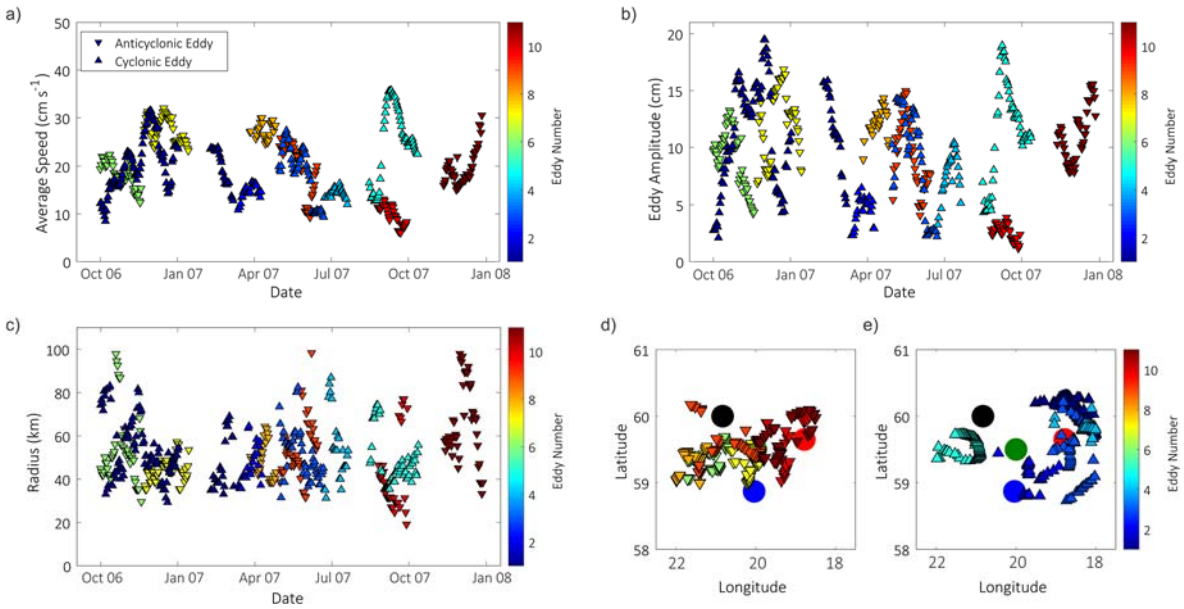

Figure 3.18 Mesoscale eddies in the Iceland Basin during trap sampling. a) Average traversing speed of the eddy (colour bar highlights each individual eddy with the colours remaining consistent throughout the panels), b) eddy amplitude (cm), c) eddy radius (km), d) map of the anticyclonic eddies and e) map of the cyclonic eddies. In all panels the downward-facing arrows indicate anticyclonic eddies and the upward-

facing arrows indicate cyclonic eddies. In d) and e) the sediment trap locations are marked by the coloured circles.

3.4 Discussion

3.4.1 Seasonal Cycle of Particle Flux

The seasonal cycle of particle flux to the deep ocean IB exhibits a succession of flux composition that is expected for high latitude regions. Winter fluxes are low and spring bloom-associated fluxes are likely diatom driven, in keeping with previous observations (Martin et al., 2011). Summer fluxes remain elevated and a second peak in fluxes is observed in autumn before returning to low winter levels. $CaCO_3$ is the major component throughout the time-series, whereas BSi fluxes are important during spring as also found in deep ocean sediment trap observations from 54 N, 21 W (Waniek et al., 2005b). The period of the largest accumulation for the four sediment traps was during spring, and for mass, POC and $CaCO_3$ fluxes steadily accumulated from spring to winter. 50 % of the annual flux was collected between 145 and 185 Julian days for BSi fluxes and between 200 – 220 days for mass, POC and $CaCO_3$ fluxes, much later than the mean of 90 days at the PAP site (Lampitt & Antia, 1997) but were in line with deep ocean fluxes at 54 N, 21 W, suggesting that observed differences, between the IB and the PAP Site are latitudinally driven (Waniek et al., 2005b). The mesoscale spatial differences in the sediment trap accumulation rates are negligible compared to the latitudinal differences shown by Lampitt and Antia, (1997).

3.4.1.1 Drivers of Spring Fluxes to the Deep Ocean

The role of ballasting in driving particle fluxes has been studied heavily for the past few decades (Armstrong et al., 2002; Ittekkot, 1993; Klaas & Archer, 2002; Lam & Bishop, 2007; Sanders et al., 2010) but with confounding results. In the IB $CaCO_3$ is a major component throughout the time-series and tracks the seasonal cycle of mass and POC fluxes. This makes it difficult to determine whether the $CaCO_3$ is ballasting the particulate material that settles into the deep ocean sediment trap samples, i.e. a causal relationship, or if the organisms associated with the sinking $CaCO_3$ are sinking independently from the organic material, i.e. a non-causal relationship. The linear relationship between POC and $CaCO_3$ fluxes was strong and significant in the deep ocean IB (Figure 3.8) but is not definitive evidence for a mechanistic relationship (Francois et al., 2002; Ragueneau et al., 2006).

A global analysis by Francois et al. (2002) found that export is transferred to the deep ocean more efficiently in $CaCO_3$ dominated regions, compared to BSi dominated regions on annual timescales

but, as Ragueneau et al. (2006) highlights, averaging global and annual data can result in a loss of important spatial and temporal context. Thomalla et al. (2008) highlighted that decoupling of calcite and BSi from POC flux, due to remineralisation of POC, leads to the increase in biomineral to organic carbon ratio with depth but does not indicate a mechanistic relationship.

From visual inspection of the autumn deployment 2 samples, a large proportion of the flux was made up of empty foraminifera tests, particularly in autumn, which are unlikely to act as ballast for organic material according to roller tank experiments (Schiebel, 2002; Schmidt et al., 2014), and observations by Fischer & Karakaş, (2009), in which foraminifera tests were not associated with large organic sinking particles. Size-fractionated $CaCO_3$ measurements could be undertaken to separate out the foraminifera $CaCO_3$ from the coccolithophore $CaCO_3$ to test whether this changes the interpretation of $CaCO_3$ ballasting relationships. It is possible that there is a causal relationship between coccolithophore $CaCO_3$ and POC flux magnitude, which is masked by foraminifera $CaCO_3$ dominating deep ocean $CaCO_3$ flux.

BSi fluxes may exhibit a mechanistic effect on POC fluxes, with the large spring bloom-associated POC fluxes occurring at the same time as peak BSi fluxes. The statistically significant positive linear relationship (R^2 0.64) between POC and BSi found here is weaker due to BSi fluxes only increasing in magnitude during spring. Diatoms are known to dominate the North Atlantic spring bloom after re-stratification of the upper ocean (Daniels et al., 2015; Henson et al., 2009; Savidge et al., 1992) and the termination of the bloom often leads to rapid export of marine snow, which has been sampled in deep ocean sediment traps and has been observed to settle to the seafloor (Honjo et al., 1982; Lampitt, 1985). A decoupling between PP and upper ocean remineralisation, by bacterial and zooplankton communities, during the initial spring bloom has been considered as the rationale for efficient export at the beginning of the spring bloom, whereas later in the seasonal cycle, even when primary productivity is very high, deep ocean fluxes are not as great as the spring bloom associated peak in flux (Briggs et al., 2011; Buesseler et al., 1998; Henson et al., 2019; Lam et al., 2011). Decoupling would explain why elevated BSi fluxes are not always associated with highly efficient export of POC to the deep ocean, except at the beginning of the spring bloom.

Previous observations of decoupling and the role of BSi fit with the findings in this study of BSi likely being a driver of POC fluxes to the deep ocean and supports the drifting sediment trap measurements between 150 and 750 m during May 2008 to the North West of the IB (61 N, 26.5 W; Martin et al., 2011). The May 2008 Lagrangian study tracked a distinct patch of elevated chlorophyll concentration. Glider Chl *a* data indicated that the bloom started on April 19th 2008. A peak in diatom abundance between the 8th and 11th of May was observed with an *in situ* Chl *a*

concentration peak of almost 4 mg m^{-3}, whereas satellite Chl *a* concentration peaked at 2 mg m^{-3} (Briggs et al., 2011; Martin et al., 2011). Molar POC:PON ratios from the drifting sediment traps in 2008 ranged between 4.4 and 6.7 (Martin et al., 2011), whilst deep ocean sediment trap material in spring 2007, assuming a similar bloom and flux event occurs every spring, had POC:PON ratios between ~ 8 – 9, indicating some degree of degradation during sinking. The POC percentage contribution to mass flux ranged between 8 – 13 % in the mesopelagic zone in 2008 (Martin et al., 2011), and 8 – 9 % during the peak deep ocean POC flux in May 2007 in this study. These findings support the hypothesis of the rapid transit of material to the deep ocean bypassing remineralisation in the mesopelagic zone. The mesopelagic zone rain ratio (PIC:POC) measured in the upper ocean in 2008 was < 0.13 but in the deep ocean spring 2007 sediment trap samples POC:PON ratios were always greater than 0.13 and usually up to 1 which highlights the lability of the POC, the recalcitrant nature of $CaCO_3$, and the chemical decoupling between the biomineral and organic material as discussed by Thomalla et al. (2008). TEP fluxes were high from the 14th to the 18th of May and coincided with the highest molar BSi:POC ratios (Martin et al., 2011).

The May 2008 Lagrangian study estimated mesopelagic sinking rates between 73 and 100 m d^{-1} (Briggs et al., 2011; Martin et al., 2011), whereas the results in this study suggested very rapid sinking (within the 14 day sampling period i.e. faster than 180 m d^{-1}) during spring with upper ocean Chl *a* concentrations following a similar pattern to deep ocean POC flux when no time lag is used (Figure 3.12). However, this may be an artefact of the peak in Chl *a* concentration occurring below 10 m depth in the water column, as shown by glider data from May 2008 in Briggs et al. (2011). Extracting satellite chlorophyll data from the particle source region and using a time lag based on a mean sinking speed of 100 m d^{-1} did not improve statistical relationships between upper ocean biological processes and deep ocean particle flux, either due to missing the early Chl *a* concentration peak, using monthly Chl *a* data or due to a mean sinking speed of 100 m d^{-1} during the spring bloom underestimating the true sinking rate of particles (Fischer & Karakaş, 2009). Differences between using shipboard upper ocean biological measurements and remote sensing data, in relation to deep ocean particle flux, has been observed before in the Sargasso Sea, with *in situ* measurements concluding that a rapid transit of particles to depth occurred whilst a remote sensing study observed a 1-2 month time lag, although the studies did not overlap in time (Asper et al., 1992; Deuser et al., 1990). Interestingly, Waniek et al. (2005b) observed rapid transit of particles to the deep ocean sediment traps, with chlorophyll concentrations and fluxes peaking within the same month, in the subtropical and temperature regions in the Atlantic Ocean but not at 54 °N 21 °W.

The mean particle sinking rate is likely to change throughout the seasonal cycle coinciding with changes in community structure and particle transformations (Fischer & Karakaş, 2009). Without

in situ measurements, the true timing and magnitude of the peak in Chl *a* concentration associated with the spring bloom is difficult to discern. Particle source regions may not improve our understanding of the links between upper ocean biological processes and deep ocean particle flux without greater depth resolution measurements around the sampling site.

The cause of the termination of the bloom in the May 2008 Lagrangian study was thought to be silica limitation, in line with previous studies (Martin et al., 2011). If the IB experiences silica limitation annually it is surprising that there was elevated BSi fluxes penetrating below 2000 m throughout summer in 2007 in this study, unless the BSi was sinking slowly and undergoing dissolution at a slow rate (Giering et al., 2017). A study in the IB during late summer in 2007 concluded that the upper ocean becomes iron limited, impacting diatoms and coccolithophores, and is a seasonal HNLC region. This may suggest that iron stress was also a driving factor behind the termination of the diatom bloom (Nielsdóttir et al., 2009). It is unfortunate that the unusually low Period IV deep ocean sediment trap fluxes occurred during spring 2008 as particle export through the mesopelagic seems to have been very efficient (T_{eff} 25 – 43 %; Martin et al., 2011). If the data had been reliable, I could have ground-truthed further the idea that efficient transport through the mesopelagic leads to large deep ocean POC fluxes (Lampitt, 1985), as well as providing information on the composition of flux reaching the deep ocean.

3.4.2 Investigating Mesoscale Variability in Deep Ocean POC Flux

In Chapter 2 I utilised different statistical methods to extract instances of mesoscale variability in the deep ocean POC flux time-series in the IB. To investigate the drivers of spatial variability in the deep ocean I have identified the 5 periods of the greatest mesoscale spatial variability to explore as case studies and outlined them in Table 3.5.

Table 3.5 A summary of five case studies with the greatest observed mesoscale spatial variability during one sampling period of the deep ocean POC fluxes. For each case study the sampling period, the deviating trap, the mode of variability and the statistical indicators of mesoscale variability identified in Chapter 2 are detailed.

	Sampling Period	Traps	Variability	Variability Indicators	Eddy Influenced
Case 1	20th Dec 2006 – 3rd Jan 2007	Trap NW Trap C	Two trap fluxes elevated	Standardised residual, standard deviation, range, 35 % threshold	Yes

Case 2	28th Mar 2007 – 11th Apr 2007	Trap NW	One trap flux elevated	Standard deviation, range, 35 % threshold	Yes
Case 3	12th Apr 2007 – 25th Apr 2007	Trap NE	One trap flux elevated	Standard deviation, range, 35 % threshold	No
Case 4	9th May 2007 – 23rd May 2007	Trap NE	One trap flux > twice as large as other fluxes	Standardised residual, standard deviation, 35 % threshold	Yes
Case 5	7th Oct 2007 – 21st Oct 2007	Trap C	One trap flux elevated	Standardised residual, 35 % threshold	Yes

3.4.2.1 Case Study 1

Case study 1 took place between the 20th December 2006 and the 3rd of January 2007 and was characterised by two sediment traps sampling elevated POC fluxes, whilst the other two sediment traps sampled lower fluxes that agree well with the other winter samples. The elevated POC fluxes in Traps NW and C were not found for the other particle flux components, i.e. mass, $CaCO_3$ and BSi flux. The POC and PON percentage contributions to total flux increased during this period, the relative contribution doubling for Trap C compared to the previous and later samples, but the $CaCO_3$ and BSi percentage contribution to total flux changed very little, with a slight increase in the BSi percentage for Trap NW. The POC:PON ratio was much lower for Trap NW and C during this event, decreasing from 8 - 7 to 6 - 6.5 suggesting the material reaching the sediment traps was likely fresher and had not undergone significant remineralisation. Unfortunately there is no Chl *a* concentration data available during this time due to the low sun angle in winter and there were also limited CPR samples. During December and January very low abundances of radiolarians, copepods, diatoms and dinoflagellates were found in the three defined CPR regions.

There was an anticyclonic eddy (yellow triangles in Figure 3.18) with a peak SLA of > 0.2 m over Trap C in late December 2006, with a peak average speed of > 30 cm s^{-1}, and a radius of up to 60 km. The highest EKE observed in December and January of up 100 cm^2 s^{-2} was associated with the eddy observed over Trap C, as shown in Figure 3.16. Trap NW is in between high and low SLA regions, whilst Trap C is below the highest SLA during December 2006 (Figure 3.16). It seems likely that the increased particle fluxes in Traps NW and C were possibly driven by the mesoscale eddy funnelling particles to depth as indicated by fresher, more organic carbon rich material reaching

the deep ocean, with little changes to the biomineral content and small increases in mass flux. This proposed funnelling of particles is likely to have greater BSi content due to lower BSi dissolution rates below the euphotic zone (Van Cappellen et al., 2002) meaning less time for dissolution to occur in the undersaturated surface waters. Transient winter diatom blooms in the North Atlantic Subpolar gyre may be common and are likely driven by mixed-layer eddies which seed the euphotic zone and the following blooms may contribute to winter carbon export (Lacour et al., 2017).

Previous studies have found instances were eddies have increased particle flux within the mesopelagic zone (Buesseler et al., 2008; Guidi et al., 2008; Guieu et al., 2005). A mode-water eddy in the Sargasso Sea was found to have increased diatom biomass in its centre leading to increased BSi fluxes (Buesseler et al., 2008) and a further study of nine eddy events in the Sargasso Sea found that 1-2 month old eddies led to a large biological response, eddies ~ 3 months old had a large biological response and high thorium fluxes and eddies older than 3-4 months showed no clear response (Sweeney et al., 2003). In the POMME experiment, mesopelagic sediment trap material under the influence of an anticyclonic eddy was found to be enriched in $CaCO_3$ and have a lower lithogenic and BSi content with the highest POC export observed in summer rather than spring (Guieu et al., 2005), suggesting the combination of eddy properties and upper ocean community structure may affect how eddies alter particle fluxes.

The mesoscale eddy observed over the sediment traps during this case study was first detected by the AVISO eddy tracking algorithm in mid-November and was sustained until early January, suggesting the eddy was 1-2 months old when the increases in deep ocean particle flux were observed. The particle fluxes arrived earlier in the eddies 'life cycle' than would be expected based on the work of Sweeney et al. (2003) who showed that as eddies mature their associated productivity and export characteristics change. However, the body of previous research on eddies and the effect on particle flux has focused on the tropical, subtropical and temperate regions, often in the mesopelagic zone, meaning it is challenging to extrapolate their findings to the deep ocean high latitude regions with a strong seasonal cycle (Buesseler et al., 2008; Conte et al., 2003; Honjo et al., 1999; Sweeney et al., 2003).

3.4.2.2 Case Study 2

Case study 2 is characterised by increased mass, POC, $CaCO_3$ and BSi fluxes from 28th March to 11th April 2007 in Trap NW, whilst other sediment trap fluxes remained low. During this sampling period, Trap NW percentage contributions of different flux components did not change, except for a small increase in the percentage of BSi flux. During April the Chl *a* concentration above the trap location begins to increase with similar timing to previous pre-bloom observations in the

Eastern IB in April 2012 (Daniels et al., 2015; Giering et al., 2016). In Region 2 CPR data, high abundances of diatoms and copepods were observed during this period and Region 3 also had high diatom abundances and a small peak in dinoflagellate abundance. The predicted particle source region for Trap NW is not well represented by the CPR spatial coverage. A weak cyclonic eddy was present in the IB during March and early April 2007 traversing near Trap C and S, whilst a fast moving anticyclonic eddy was observed in April 2007 south of Trap NW. The largest EKE in April 2007 was located at the fringes of the eddy south of Trap NW, which experienced increased fluxes at this time.

Daniels et al. (2015) observed high diatom abundance in the Eastern IB in mid-late April in 2012, dominated by *Chaetoceros* and later *Psuedo-nitzschia*, which were detrained out of the surface waters during increased mixing. The pre-bloom period in the IB is thought to be characterised by net growth and detrainment due to the upper ocean instabilities, similar to the changes in MLD observed in our study in early April 2007 (Figure 3.19; Daniels et al., 2015; Giering et al., 2016). Dall'Olmo et al. (2016) reported that the seasonal mixed layer pump can input between 23 to > 100 % of the carbon supplied by fast sinking particles into the mesopelagic zone in high latitude regions, which may in turn supply the deep ocean with increased particle flux. A transient shoaling and subsequent deepening of the MLD occurs in early April above all the traps in the IB (Figure 3.19). Trap NW had increased EKEs south of the trap, which aligns with the general particle source region for Trap NW between March – May 2007 (Figure 3.11), and increased current speeds up to a daily average of 30 cm s^{-1} were recorded during this sampling period by the current meter below the sediment trap (Figure 2.7). The drivers of this increased POC flux in Trap NW are likely to be linked to the annual proliferation of diatoms at the start of the spring bloom (Daniels et al., 2015), supported by an increase in the BSi percentage contribution to total flux and the anticyclonic downwelling eddy driving high EKEs for the Trap NW particle source region, which may have led to the subduction of diatoms to the deep ocean.

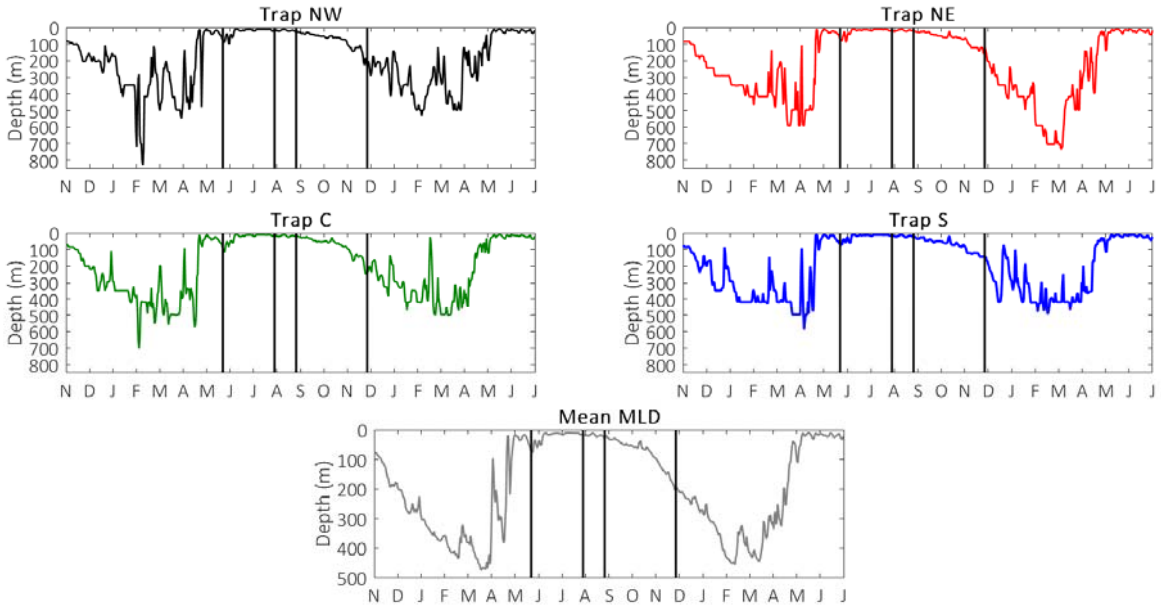

Figure 3.19 Mixed Layer Depth at each sediment trap location. a) Trap NW, b) Trap NE, c) Trap C, d) Trap S and e) Iceland Basin mean extracted from the Copernicus physical reanalysis model.

3.4.2.3 Case Study 3

Case study 3 shows increased mass, POC and $CaCO_3$ fluxes in Trap NE between the 12th - 25th of April 2007. Interestingly, Trap NE fluxes were associated with a lower POC and PON content and an elevated $CaCO_3$ content, whilst BSi content remained similar to previous and later fluxes. The POC:PON, PIC:POC and BSi:POC ratios were higher, similar to the other traps during that sampling period for the POC:PON ratio. This suggests that although greater mass fluxes were sampled by the sediment traps the sinking material in the IB was generally more degraded, including the elevated fluxes in Trap NE.

Chl *a* concentrations were approaching 0.6 mg m^{-3} in April over Trap NE. The CPR data is the same as for Case study 2 with high diatom abundances and elevated dinoflagellate abundances. The cyclonic eddy observed near Trap NE throughout mid-late April 2007 (Figure 3.18) was ~ 2 months old, which according to Sweeney et al. (2003), may be the beginning of when eddies become efficient exporters of particulate material. In case study 2 the strong upper ocean eddy activity appeared to influence the faster current speeds recorded in the deep ocean but for this study no clear related signal was observed. The higher POC:PON ratio may suggest that sinking material is undergoing greater remineralisation compared to case study 2 as the spring bloom is more established and, similar to case study 2, eddy activity in the upper ocean may have influenced the deep ocean particle flux, in terms of magnitude but not composition. Case study 2 and 3 highlight that only tenuous links can be drawn between upper ocean physical processes and deep ocean

particle fluxes and, as suggested by Boyd et al. (2019), a high resolution 4D sampling strategy is needed to quantify the contribution of PIPs, such as eddy subduction.

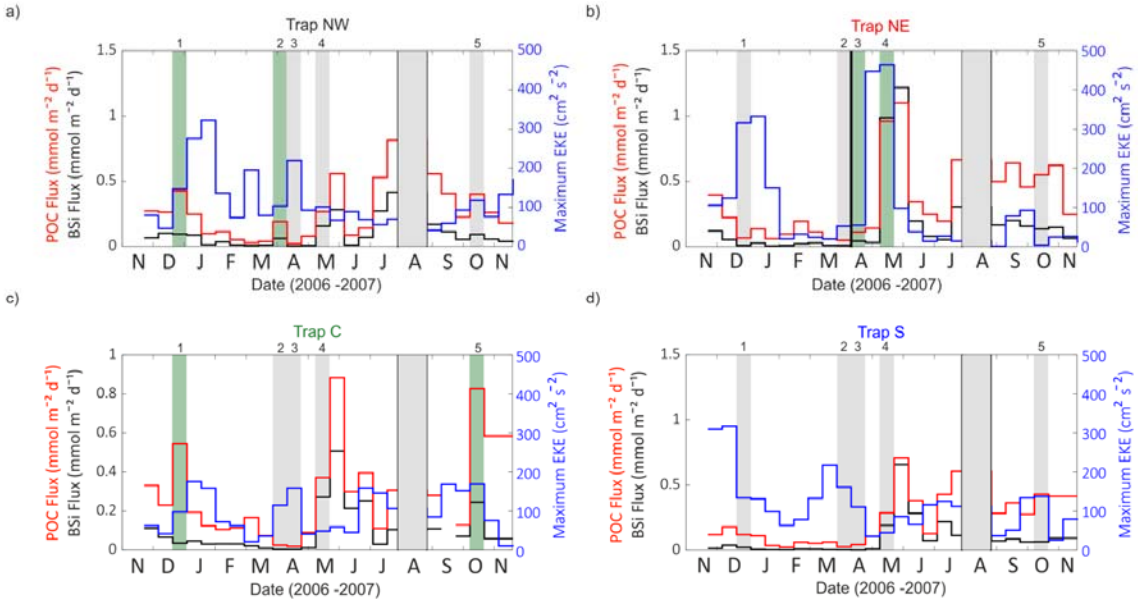

Figure 3.20 POC (red) and BSi (black) fluxes plotted against the maximum EKE (blue) of a 1 degree box around each trap location. a) Trap NW, b) Trap NE, c) Trap C and d) Trap S. The five case studies are labelled 1-5 and highlighted by a grey background, or the deviating traps were highlighted with a light green background. The grey box overlain on top of the data indicates the period when the sediment traps were recovered and redeployed.

3.4.2.4 Case Study 4

During case study 4 (9th – 23rd May 2007) Trap NE mass, POC, $CaCO_3$ and BSi fluxes were twice as large as the other three trap fluxes but all traps were elevated as the spring bloom-associated flux was sampled by the sediment traps. The POC content is the lowest of the four traps, but with very little spatial variability. The Trap NE $CaCO_3$ content is also the lowest and the BSi content is the highest of the four sediment traps. It is worth noting that the BSi content is elevated for all four traps during this period ranging between 22 - 34 % of the total flux. The POC:PON ratio of the Trap NE fluxes is the lowest of the four traps (7.94 compared to 8.26 – 9.23) for that sampling period suggesting the Trap NE particulate material was fresher. The BSi:POC ratio for Trap NE was very high ~ 1, and considerably higher than the other traps, whereas the PIC:POC ratio is similar to the other three traps. The Chl *a* concentration was increasing in May both at the trap location and in the particle source region. The Trap NE particle source region extent was closest to Region 2, in which May CPR data showed increased diatom abundances compared to April and a large relative

jump in copepod abundances. A cyclonic eddy was present over Trap NE during May and June 2007 with a radius of up to > 60 km (Figure 3.18).

The elevated POC fluxes in this case study appear to be driven by the increased BSi:POC ratio, likely driven by diatoms as observed in the deep mesopelagic in May 2008 by Martin et al. (2011), and supported by other previous work in the deep ocean North Atlantic (Waniek et al., 2005b). One interesting feature of this case study is that the magnitude of fluxes in Trap NE were much greater but the percentage composition was very similar to the other traps, suggesting that either the upper ocean composition of export or subsequent remineralisation were spatially homogenous during this time in the IB. The greater magnitude in all fluxes in Trap NE compared to the other traps may be due to the high EKEs observed over Trap NE in May 2007 compared to the other three sediment traps as demonstrated by Figure 3.20.

3.4.2.5 Case Study 5

Case study 5 is focused on the elevated Trap C fluxes between the 7th and the 21st of October 2007. The Trap C mass, POC, $CaCO_3$ and BSi fluxes are elevated compared to the other trap fluxes during that sampling period. The POC, PON, $CaCO_3$ and BSi percentage contributions to total flux, and the ratios, are very similar to the other three traps, and to samples prior to and after the case study sampling period. The PIC:POC ratios between late-September to November are elevated for all traps, likely due to the substantial contribution of foraminifera tests in the sediment trap samples (Figure 3.6). Chl *a* concentration was low in October and had returned to pre-spring bloom levels. CPR samples from Region 2 observed the highest diatom abundances in October for all of 2007 as well as an increase in foraminifera. Region 3 CPR data also showed smaller increases in diatom, acantharia, foraminifera, dinoflagellate and copepod abundances. It is noteworthy that instances of elevated diatom abundances do not always relate to increased fluxes, except in spring likely due to a decoupling between phytoplankton and zooplankton biomass (Buesseler, 1998), as previously discussed in Section 3.4.2, although it is possible that the Region 2 and 3 CPR data was not an accurate representation of the central IB.

Visual inspection of the all the samples during this period noted large brown very dense particulate material and some gelatinous material but neither were easily identifiable. Increased BSi fluxes could also be indicative of increased radiolarian or phaeodarian contributions to particle flux, which has been found to make considerable contributions to interior and deep ocean particle flux in other oceanic regions (Ikenoue et al., 2019; Lampitt et al., 2009).

Preceding the sampling period there was a cyclonic eddy North West of Trap C traversing at speeds up to 35 cm s^{-1}, with eddy amplitudes approaching 20 cm and a radius up to 70 km. The

eddy was tracked by the AVISO eddy tracking product from mid-August to early October 2007 (Figure 3.18) and the October 2007 map of SLA indicates that it was a dynamic period in the upper ocean. There was a very high EKE to the west of Trap C (Figure 3.17), which aligns with the predicted particle source regions in Figure 3.11 for Trap C in October 2007.

In summer, and likely autumn, the IB is a seasonal HNLC area due to silicate and iron limitation (Martin et al., 2011; Nielsdóttir et al., 2009). The large anticyclonic eddy in the IB in October 2007 may have replenished the upper ocean with nutrients from deeper waters (Martin & Richards, 2001) terminating the seasonal HNLC conditions (Lacour et al., 2017; Nielsdóttir et al., 2009). This may have stimulated diatom production, if the silicate and iron limitation were remedied, which may have contributed to increased flux to the deep ocean as a second order effect of the mesoscale eddy.

3.5 Conclusion

This study has confirmed that diatoms drive the spring bloom and associated particle flux in the IB, with the spring bloom associated flux being a key period of carbon sequestration in the deep ocean. Determining the drivers of mesoscale variability in deep ocean POC flux relies on knowledge of mean sinking speed, particle origin and flux composition, which means oversimplified assumptions and lack of spatial data can hinder our understanding. This study highlights that community structure is important in spring but that increased fluxes in autumn and winter are more likely to be as a first-order result of mesoscale eddies, due to the injection of particles to the interior ocean, or possibility as a second-order result of nutrient replenishment and subsequent export. The injection of particles to the deep ocean seems to rely on the combination of strong EKE near to the trap location, and/or particle source region, increased diatom abundance and BSi fluxes to depth. Elevated EKEs may have increased seabed advection, which could be posed as influencing the observed mesoscale spatial variability, but the increased fluxes were often fresher rather than more refractory (Gardner et al., 2017). This study may have observed evidence of the injection of particles to depth which seem to be associated with the eddy flanks, rather than the highest EKEs, which means identifying such relationships quantitatively is challenging. For case studies 1, 2 and 3 the high EKEs associated with the anticyclonic eddies appear after the increased POC fluxes whereas for case studies 4 and 5 elevated EKEs are observed during the period of increased POC fluxes but there are not enough observations in this study to draw conclusions confidently. For all of the five case studies of mesoscale variability between the sediment traps increases in BSi flux were observed, similar to observations in Conte et al. (2003), which seem to coincide with increased diatom abundance in CPR data, but it is possible that the increased BSi fluxes could also be driven by radiolaria or

phaeodaria. In summary, the traditional 1D approach to measure BCP processes is insufficient to further our understanding of the biological and physical processes driving deep ocean particles fluxes and a 4D sampling approach, that moves away from empirical relationships, and instead work towards a mechanistic understanding of sinking flux, is overdue (Boyd et al., 2019; Burd et al., 2010).

Chapter 4 Acantharian Cysts in the Iceland Basin: the Role of Celestite and the Potential Triggers of Rapid Sedimentation to the Deep Ocean

4.1 Introduction

The contribution Acantharian cysts make to deep ocean carbon sequestration was quantified in the previous decade, with observed POC fluxes up to 0.43 mmol m^{-2} d^{-1}, as a result of opportunistic sampling of cysts in sediment traps (Belcher et al., 2018). Acantharia are micro-zooplankton protists, of the radiolarian subphylum and are found ubiquitously throughout the global ocean (Antia et al., 1993; Bernstein et al., 1987; Biard et al., 2016; Michaels, 1988; Michaels, 1991; Spindler & Beyer, 1990). Acantharia are the only marine organism with a skeleton made from celestite ($SrSO_4$), the densest known biomineral (Bernstein et al., 1987; Odum, 1951). The reproductive mechanism of some Acantharia clades is via the formation of celestite-coated cysts, which sink rapidly to the interior ocean (Decelle et al., 2013). The reproductive cycle of Acantharia is not well understood but the sedimentation of cysts to the deep ocean has been shown to contribute to deep ocean carbon flux and may affect the oceanic Strontium (Sr) cycle (Belcher et al., 2018; Bernstein et al., 1987; Martin et al., 2010).

Acantharia are heterotrophic, feeding on bacteria, small plankton and zooplankton (Caron & Swanberg, 1990; Swanberg & Caron, 1991), and some species host photosymbionts (Decelle et al., 2012; Schewiakoff, 1926). Acantharia have been sampled throughout the upper ocean, with photosymbiont-hosting Acantharia inhabiting the sunlit surface layers (usually < 50 m; Michaels, 1988), whilst non-symbiont cyst-forming Acantharia tend to reside deeper in the water column (Antia et al., 1993; Bernstein et al., 1987; Schewiakoff, 1926).

Acantharian cysts have been opportunistically sampled in sediment traps in the bathypelagic zone (> 1000 m; Michaels, 1991; Michaels et al., 1995), allowing the contribution of Acantharian cysts to the biological carbon pump to be quantified. Acantharian cysts were found to contribute up to 26 % of particulate organic carbon (POC) flux during a bloom in the Southern Ocean (Belcher et al., 2018) and 48 % of pre-bloom POC flux in the IB (Martin et al., 2010). Large fluxes of Acantharian cysts have been sampled in the upper ocean in locations such as the Greenland Sea (fluxes up to 33 000 ind. m^{-2} d^{-1}; Antia et al. 1993) and the Sargasso Sea (fluxes up to 12 676 ind. m^{-2} d^{-1}; Michaels et al. 1995). In

previous studies most Acantharian cysts had undergone complete dissolution by 1000 m (Antia et al., 1993; Bernstein et al., 1987), with very few cysts sampled below that depth prior to the study by Martin et al. (2010).

Acantharian cysts sink rapidly out of the upper ocean and undergo excystment, which is the release of gametes, known as swarmers, at depth through pores, or through the celestite shell, due to dissolution (Antia et al., 1993; Bernstein et al., 1999; Decelle et al., 2013). Swarmers likely form juveniles at depth which ascend to the upper ocean, but the timing and mechanism driving ascension is unclear, due to difficulties with sampling and culturing of these protists (Beers & Stewart, 1970; Decelle et al., 2013; Decelle & Not, 2015; Schewiakoff, 1926).

The sedimentation of cysts sinking to the bathypelagic ocean in high latitude regions is thought to be a regular annual event (Antia et al., 1993; Belcher et al., 2018; Martin et al., 2011). It has been hypothesised that in high latitude regions the heterotrophic Acantharia undergo encystment, and rapid sedimentation coincident with the spring bloom, to utilise the flux of organic matter to the seafloor for the juveniles to feed on (Belcher et al., 2018; Decelle et al., 2013; Martin et al., 2010; Spindler & Beyer, 1990). The mechanisms by which the juveniles survive for an entire annual cycle, ascend from > 1500 m depth to the upper ocean and the exact trigger/ timing for encystment remain unknown (Belcher et al., 2018).

Acantharia are important to the global oceanic Sr budget as they are the only marine organisms that incorporates Sr as a major component (Bernstein et al., 1987). The oceanic Strontium cycle is of interest as Strontium isotopes can be used as a chronostratigraphic tool and as an indicator of continental weathering (Capo & Depaolo, 1990). Sr/Ca ratios in microfossils are also used to reconstruct Cenozoic Sr/Ca ratios (Graham et al., 1982) and as a palaeotemperature indicator (Beck et al., 1992; Stoll & Schrag, 1998; de Villiers, 1999). Sr is undersaturated in seawater, leading to the rapid dissolution of celestite, which precludes preservation in seafloor sediments and samples (Antia et al., 1993; Beers & Stewart, 1970; Schewiakoff, 1902). The influence of Acantharia on dissolved Sr concentrations and Sr/Cl ratios has been observed globally, with celestite production, and subsequent shallow dissolution of Acantharia, driving an upper ocean vertical Sr gradient that increases with depth (Bernstein et al., 1987; De Deckker, 2004; de Villiers, 1999). Acantharian skeletons can also co-precipitate Barium (Ba), forming $BaSO_4$, as well as other trace elements, which may similarly affect the oceanic Barium and trace element cycles (Bernstein et al., 1992; Brass, 1980).

This study presents the second year of a two year time-series of Acantharian cyst flux to the deep ocean IB, which builds on the initial findings of Martin et al. (2010). Sampled particle fluxes were very low during peak Acantharian cyst flux, and cyst fluxes were very large in two of the sediment trap samples. This study presents improved estimates of POC:Sr ratios, and '*in situ*' sinking rates, as the cysts were less likely to have undergone significant dissolution compared to previously sampled cysts. We utilise these findings to estimate the relative contribution of cysts to annual Sr flux to the deep ocean, and discuss the implications of cyst POC flux to the deep ocean. This study also aims to improve the understanding of the preferred environmental conditions of cyst-forming Acantharia, discusses possible drivers of sedimentation, and advantages of encystment using data from this study and from the literature. I hypothesise that the first spring-time incidence of rapid shoaling in the mixed layer allows Acantharia, from the interior ocean to the upper ocean, and changes in upper ocean conditions may be a trigger for sedimentation, such as temperature, light or chlorophyll concentration. The role of celestite and rapid sedimentation as a successful reproductive strategy is discussed.

4.2 Methods

4.2.1 Sample Analysis

4.2.1.1 Sample Preparation

The sediment trap samples from deployment 1 were analysed by Patrick Martin in Martin et al. (2010). The sediment trap samples from deployment 2 were picked, processed and analysed by the author. Acantharian cysts were observed in spring in IB sediment trap samples in 2007 and 2008. Sediment trap metadata is outlined in Chapter 2, Section 2.2. Acantharian cysts were counted and separated if > 400 cysts were present in one sample as in Martin et al. (2010). Acantharian cysts were analysed for POC, particulate organic nitrogen (PON), Sr and Ba content. The Ba content of the cyst samples were extremely low and were below the calibration range and hence were not included in the study.

4.2.1.2 POC/PON Analysis

For deployment 1, cysts were rinsed with Milli-Q as in Martin et al. (2010) and analysed for POC/PON. The silver capsules were pelleted and POC/PON was measured on a Flash 1112 Elemental Analyser (Thermo Finnigan) based at Plymouth Marine Laboratory. POC and PON were analysed in

triplicates where possible with RSDs < 10 %. Blanks (acidified empty silver capsules) contributed < 10 %, and usually ~ 1 %, to the total signal for C and N.

For sediment trap samples with > 100 cysts in a 1/8th aliquot, replicate analysis of a minimum of 50 cysts was carried out for POC/PON analysis of cysts collected during deployment 2. For deployment 2, the samples were rinsed once with borate-buffered Milli-Q spiked with Strontium chloride to a concentration of 0.91 mmol L^{-1} to prevent Sr dissolution altering estimates of the true percentage of C and N in the cysts (Beers & Stewart, 1970; Brass, 1980). Cysts were then transferred into pre-weighed pre-combusted (550 °C) silver cups (Smooth Silver Capsules 5.5 x 3.5 mm or Smooth Silver Boats 4 x 11 mm, Elemental Microanalysis). The cysts were dried at 40 °C and were acidified using the dropwise addition method (Nieuwenhuize et al., 1994). For deployment 2, the C/N samples were measured by the author with the assistance of Bastian Hambach and Megan Wilding in running the Elementar instrument at the SEAPORT stable isotope laboratory at the University of Southampton. The limit of detection for the instrument was 10 µg for C and 1 µg for N and the analytical precision was ≤ 6.1 % for N and ≤ 1.7 % for C.

4.2.1.3 Strontium Analysis

Sr was measured in all three fractions of the sediment trap samples – cysts, particulate material and supernatant for the cysts collected during deployment 2. The deployment 2 Sr was measured in the filtered supernatant captured during filtration. This differs slightly from deployment 1 samples analysed by Martin et al. (2010), where the supernatant was subsampled before microscopic inspection, whereas we sampled post-inspection to account for any Sr dissolution caused during microscopic inspection and to ensure that there was no particulate material in the supernatant. There was no particulate Sr data available for deployment 1. The dissolved Sr was not corrected due to NaCl addition to the trap preservative but the blank sediment trap preservative Sr concentration (86.82 µmol L^{-1}) was subtracted from supernatant Sr concentrations from deployment 1 samples. For deployment 1 the supernatant was diluted 250x with 3 % HNO_3 spiked with In, Re and Be (referred to as spiked HNO_3) to track instrument drift of the Thermo X Series ICP-MS (University of Southampton) as per Martin et al. (2010).

The dissolved Sr supernatant concentration of deployment 2 samples were corrected for evaporation that had occurred over the 10 year storage period and during sample preparation. The volume of supernatant in the trap bottles was measured prior to splitting and normalised to 265 mls for collection bottles used on 21-bottle sediment traps (Trap NW and NE), and 290 mls for collection bottles used on 13-bottle sediment traps (Trap C and Trap S). Generally the corrected dissolved Sr

concentrations (76 % of samples were corrected) were altered minimally with a mean percentage difference in concentration of 18.0 ± 12.0 % which equated to a mean concentration difference for Sr of 46.3 ± 100.1 µmol L^{-1}. The large standard deviation of Sr for the mean percentage difference is likely due to the elevated concentrations in the sediment trap supernatant of samples with Acantharian cysts present. The evaporation correction is validated by the Sr concentrations being brought in line with the trap blank preservative concentrations. Pre-correction, the Sr concentrations on average were 23.0 ± 26.4 % different from the trap preservative mean of 89.32 ± 0.96 µmol L^{-1}, whereas post-correction the Sr concentrations were only 5.7 ± 4.1 % different from the preservative concentrations which fall within the estimated uncertainty of the preservative blank values.

The Acantharian cysts were counted out into clean (10 % HCl and 10 % HNO_3 overnight acid baths) 2 ml Eppendorfs and as much supernatant as possible was removed via pipette (< 50 µl remaining in Eppendorf). The cysts were dried overnight in a 40 °C oven. Cysts were acidified with 1 ml of 3 % spiked HNO_3 and left to digest overnight before being diluted 250x. Freeze-dried particulate material was weighed out (0.5 – 8.2 mg) and acidified with 10 ml of 1 M Acetic acid and left to digest overnight following the method in Martin et al. (2010). The digest was then filtered through a 0.45 µm syringe filter (Fisherbrand™) to remove any particulates before being diluted 100x with spiked HNO_3. Procedural blanks, sediment trap preservative blanks and spiked HNO_3 blanks were analysed alongside samples. Where possible 3 replicates were analysed for each sample. Deployment 2 particulate material and Acantharian cysts were analysed for Strontium, Calcium and Barium by the author with assistance from Dr Matt Cooper at the University of Southampton in operating the Thermo X Series ICP MS. To calculate the total Sr flux, all fractions of Sr were analysed from the sediment trap sample cups. Sr concentrations and Sr flux analytical errors were propagated to estimate the uncertainty. For particulate concentrations and fluxes, errors were propagated with 5 % uncertainty to account for processing, splitting and weighing errors

4.2.2 Flux Calculations

POC and Sr fluxes were calculated as in Equation 4.1 and 4.2, respectively. In Equation 4.1 and 4.2, *A* is the collection area of the sediment traps (0.5 m^2), *d* is the sampling time in days. The POC per cyst ($Cyst_{POC}$; mg) and Sr per cyst ($Cyst_{Sr}$; mg) was multiplied by the total number of cysts (N_{Cyst}) and divided by the molecular mass (mr).

[Equation 4.1] $$POC\ Flux\ (mmol\ m^{-2}\ d^{-1}) = (Cyst_{POC} * N_{Cyst}/\ mr)/A/d$$

[Equation 4.2] $$Sr\ Flux\ (mmol\ m^{-2}\ d^{-1}) = (Cyst_{Sr} * N_{Cyst}/\ mr)/A/d$$

Analytical errors were propagated using standard uncertainty equations (Section 2.2.1.1) and mass flux erros were assumed to be 5 % to account for splitting and weighing errors.

The mean integrated cyst flux per annual event was calculated by averaging the sediment trap cyst flux per event (ind. m^{-2}) and scaling up to the size of the IB (250 670 km^2; 61.5 °N to 58 °N and 16.5 °W to 28 °W).

4.2.3 Strontium Budget

The annual Sr fluxes to the deep ocean were calculated from end of November 2006 to the end of November 2007 for each sediment trap. The bi-monthly time-series of total Sr flux (supernatant, particulate and cyst) and total Sr flux minus the cyst Sr contribution was interpolated into a daily time-series and sampling gaps were filled using nearest neighbour interpolation as in Chapter 2. There was no particulate Sr data available for deployment 1. To estimate the predicted Sr particulate flux for deployment 1 we have used known Sr:Ca ratios for particulate material (de Villiers, 1999), with further details and validation in Appendix D.

The percentage contribution of Acantharian cyst Sr to the total annual Sr budget was calculated relative to the November 2006 – November 2007 budget, even for the cysts sampled in 2008, due to the unusually low particulate fluxes from January 2008 (Period IV outlined in Chapter 2).

4.2.4 Sinking Rates

Cysts were separated from the samples that contained well-preserved cysts (Trap NW, 27th Apr – 10th May, n=20 and 11th May – 24th May, n=100), and were photographed and sized for length and width using ImageJ. These well-preserved cysts, referred to as model cysts from hereon in, were taken from the sample cups with the highest number of cysts as these cysts are likely to have undergone minimal celestite dissolution. Therefore, the measured sinking rates in this study are likely to be closer to *in situ* sinking rates measured for this cyst type. Cyst sinking rates were measured by sinking cysts individually in a measuring cylinder (diameter 6 cm) filled with filtered 4000 m North Atlantic seawater maintained at 6 °C. The cyst sinking time (n = 104) was recorded over a distance of 13.3 cm, after the cyst had initially sunk 15 cm, and was used to estimate the sinking rate in m d^{-1}, similarly to Martin et al. (2010).

4.2.5 Acantharian Cyst Source Regions

The sinking tracks and predicted surface ocean location of the Acantharian cysts were estimated using particle backtracking and model output (see Section 3.2.2). The particle backtracking modelling and current backtracking codes were written by Benoit Espinola, altered for this study and run by the author. The source regions were determined for the mean measured sinking rate of the Acantharian cysts (760 m d^{-1}) and +/- one standard deviation (560 m d^{-1} and 960 m d^{-1}) using the Copernicus physical reanalysis model *u* and *v* components as there was no current meter data available in 2008 for Traps NW and NE. The effect of sinking speed on the source region is minimal and is explored in more detail in Appendix C.2. The difference in the particle source regions using current meter and OSCAR surface ocean velocities, as in Chapter 3 (Section 3.2.2), compared to the model output is explored in Appendix C.2. Generally, the particle source regions using the model output are more localised to the sediment trap location but show broadly similar locations.

Using the predicted particle source region should allow for a more precise comparison between cyst fluxes and upper ocean parameters, such as sea surface temperature (SST), Chl *a* concentration, photosynthetically active radiation (PAR) and mixed layer depth (MLD) by accounting for the timelag from the upper to the deep ocean and the effect of current velocity on the sinking cysts. This analysis aims to further our understanding of the triggers of Acantharian cyst sedimentation events.

Monthly Chl *a*, 8 day Chl *a*, 8 day SST and 8 day PAR 9 km mapped products were downloaded from https://oceandata.sci.gsfc.nasa.gov/MODIS-Aqua/Mapped/ to investigate the influence of chlorophyll concentration, temperature and light on the cyst sedimentation event timing. Mixed layer depth could not be derived from Argo floats due to very limited spatial and temporal coverage in the IB between 2006 – 2008. Daily mixed layer depth was downloaded from Copernicus (http://marine.copernicus.eu/services-portfolio/) and extracted from GLOBAL-REANALYSIS-PHY-001-030-DAILY. The GLORYS12V1 product is a 1/12° eddy resolving reanalysis model which uses altimetry, satellite and temperature and salinity profile data and the global forecasting CMEMS system to create a daily data product with 50 depth levels. The mixed layer is defined by a density increase relative to 10 m depth, which corresponds to a temperature decrease of 0.2 °C, in local surface conditions. The mean IB (61.5 °N to 58 °N and 16.5 °W to 28 °W) SST, Chl *a* (8 day and monthly 9 km resolution), PAR and MLD was extracted and averaged for 2007 and 2008 to allow comparison between localised particle source region conditions. Monthly chlorophyll was used for particle source region time-series due to heavy cloud cover in the 8 day Chl *a* product.

4.2.6 Acantharia Biomass

Continuous Plankton Recorder (CPR) data records the presence/absence of Acantharia and allows a semi-quantitative estimate of Acantharian biomass to be calculated (Richardson et al., 2006). CPR data from the standards areas B5, B6, C5 and C6, from 2006 to 2008 were used to explore Acantharian abundance. The Continuous Plankton Recorder data was supplied by David Johns and has a DOI:10.7487/2017.80.1.1044. The data from the Subpolar North Atlantic was patchy and sporadic with a clear bias towards summer and autumn sampling as shown in Figure 3.14. The mean normalised abundance of Acantharia was calculated by summing the abundances per month and normalising to the number of tows per month.

4.3 Results

4.3.1 Acantharian Cyst Characteristics

Acantharian cysts were collected in spring sediment trap samples from below 2000 m in the IB in 2007 and 2008 supporting the hypothesis that a spring flux of Acantharian cysts to the bathypelagic is an annual event (Martin et al., 2010; Figure 4.1). The elongated cysts observed in 2007 and 2008 had the same morphology and belong to the order Holacanthida (Decelle et al., 2013). The sediment trap samples in spring 2008 predominantly consisted of Acantharian cysts with little other particulate flux material (see Chapter 2, Section 2.3). Very low fluxes of particulate matter, combined with the extremely high flux of cysts (Table 4.1), allowed the characteristics of Acantharian cysts to be more precisely measured. Cysts were easily separated from low volumes of particulate material and the celestite coating was less likely to have undergone serious dissolution (Figure 4.1c).

The model cysts collected in Trap NW during early-mid May 2008 ranged in length from 490 – 1050 µm, with a mean of 764 (± 106) µm, and ranged in width from 89 – 240 µm with a mean of 175 (± 34) µm (n = 120; Table 4.1). The sinking rates of the model cysts (n = 104) ranged between 191 – 1208 m d^{-1}, with a mean of 760 (± 204) m d^{-1}. The size and sinking rate measurements of the cysts from spring 2008 are comparable to measurements of cysts sampled in spring 2007 in Martin et al. (2010). The mean sinking rate of the model cysts was faster than the 2007 cyst measurements in Martin et al. (2010; 490 m d^{-1}). This was expected due to the model cysts retaining more of the celestite coating, which acts as efficient ballasting material.

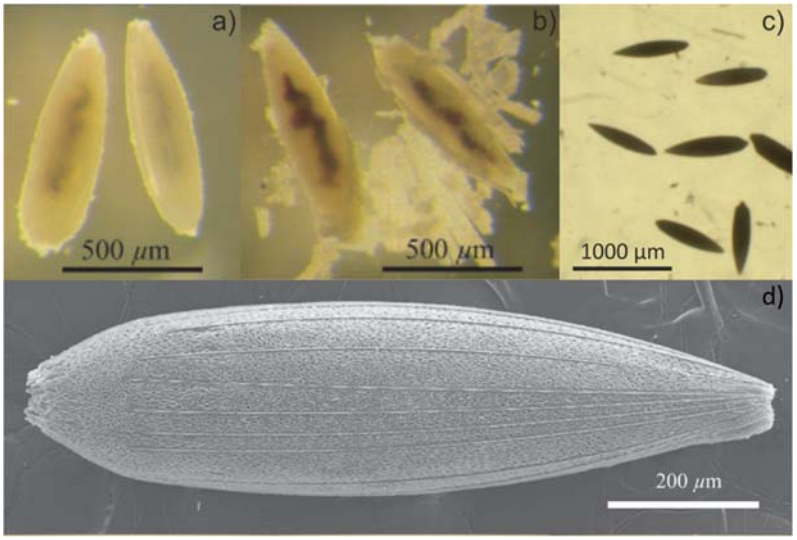

Figure 4.1 Acantharian cysts sampled in the deep ocean Iceland Basin. a) Cysts sampled in 2007 with celestite coating intact, b) cysts sampled in 2007 with the celestite coating shattered and c) shows the 'model' cysts from 2008 with a well-preserved opaque celestite coating. d) Scanning electron micrograph of an elongated Acantharia cyst sampled during deployment 1. The spicules of the Acantharian appear to have folded over to form the basic celestite structure. Figures a), b) and d) are reproduced from Martin et al. (2010).

Table 4.1 A summary of the length, width and sinking rate of Acantharian cysts sampled in the Iceland Basin in spring 2007 (Martin et al., 2010) and spring 2008.

		Length (μm)	Width (μm)	Sinking Rate (m d^{-1})
Spring 2007 Martin et al. (2010)	Range	600 – 1000	100 – 300	-
	Mean (± stdev)	-	-	490 (± 150)
	Number of cysts	n = 29	n = 29	n = 29
Spring 2008 This study	Range	490 – 1050	89 – 240	191 - 1208
	Mean (± stdev)	764 (± 106)	175 (± 34)	760 (± 204)
	Number of cysts	n = 120	n = 120	n = 104

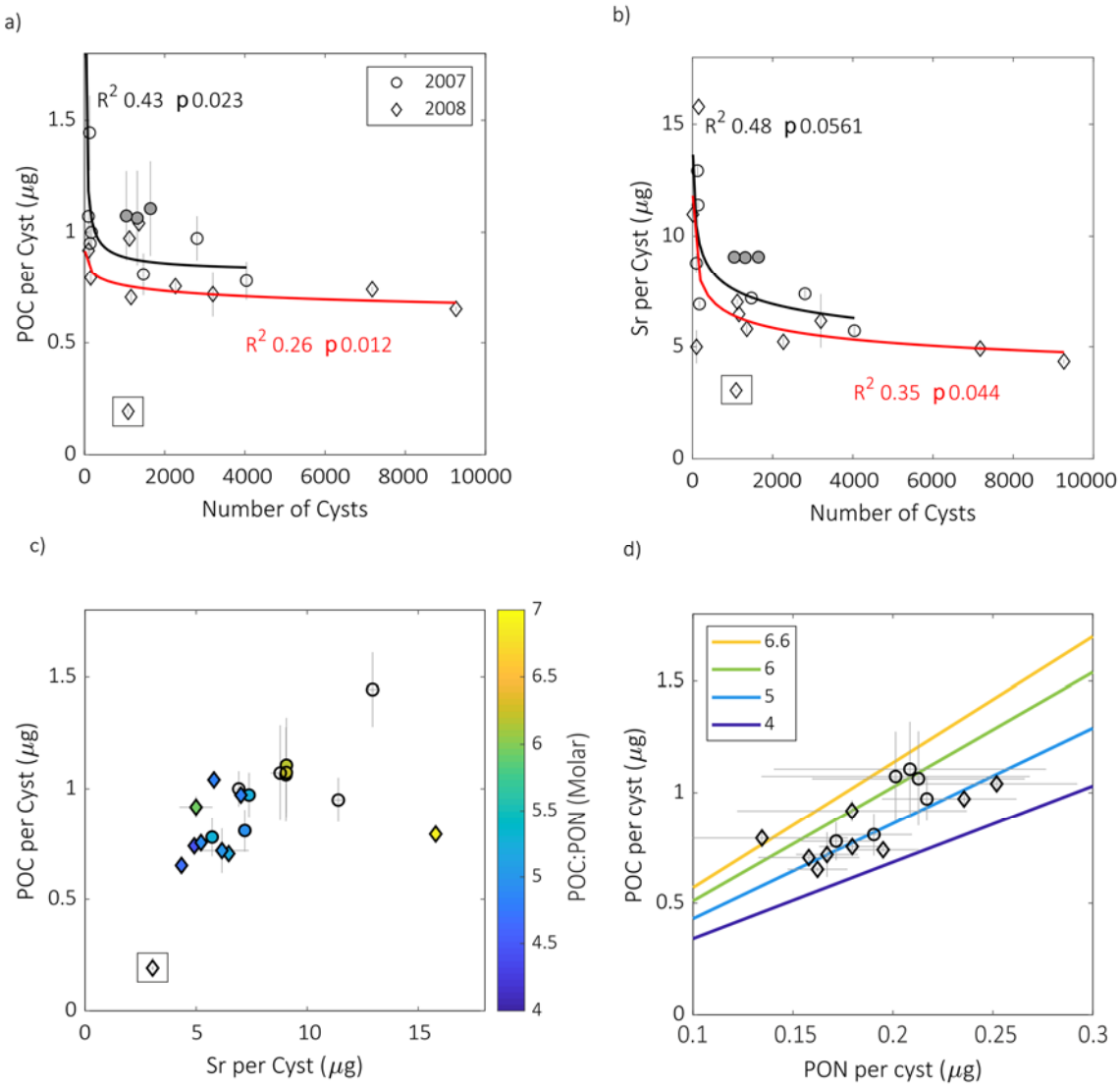

Figure 4.2 a) POC content (µg) per cyst and b) Sr content (µg) per cyst and the number of cysts sampled, c) POC content (µg) per cyst and Sr content (µg) per cyst and d) POC and PON content (µg) per cyst with the colour bar showing POC:PON molar ratio. The black circles highlight the 2007 data and the black diamonds highlight the 2008 data. The data point highlighted by a black box in a), b) and c) was below the carbon calibration range and so is likely an underestimate and was not included in the non-linear model for estimating the regression coefficients. The grey-filled samples in a) and b) were calculated from the average of the 2007 data and so were not included in the non-linear model for estimating the regression coefficients to avoid biasing the model. The R^2 and *p* value for the power relationships is detailed. Grey errorbars show propagated uncertainty. In d) the coloured lines relate to the POC:PON molar ratios.

The POC, PON and Sr content per cyst can be used as a conversion factor when only cyst POC or Sr is measured such as in Belcher et al. (2018) and Decelle et al. (2013). The POC, PON and Sr content per

cyst is presented in Table 4.2, along with the values from the model cysts, which are likely to provide a closer to *in situ* elemental content. The mean POC content per cyst was 0.85 (± 0.23) µg whilst the model cysts had a lower POC content per cyst of 0.65 (± 0.02) µg. PON content per cyst follows a similar trend but with smaller differences with a mean PON per cyst of 0.19 (± 0.03) and the best-preserved cyst PON content of 0.16 (± 0.03) µg. These differences also affect the POC:PON molar ratio, with a mean ratio of 5.26 (± 0.85) and a ratio of 4.69 (± 0.21) for the model cysts which implies that the organic material in the model cysts are richer in PON compared to cysts that have undergone some degree of dissolution.

Table 4.2 The mean cyst and model cyst estimates for the POC per cyst, PON per cyst, POC:PON molar ratio, Sr per cyst and POC:Sr molar ratio for both 2007 and 2008 cysts (Martin et al., 2010). n indicates the number of samples averaged to estimate the mean. The model cysts were found in Trap NW in mid-May 2008. The weights and ratios are reported with propagated analytical uncertainty.

	POC per cyst (µg)	PON per cyst (µg)	POC:PON (molar)	Sr per cyst (µg)	POC:Sr (molar)
Mean (± stdev)	0.85 (± 0.23)	0.19 (± 0.03)	5.26 (± 0.85)	7.46 (± 2.92)	0.90 (± 0.26)
n	20	15	15	21	20
Model cysts (± uncertainty)	0.65 (± 0.02)	0.16 (± 0.03)	4.69 (± 0.21)	4.34 (± 0.10)	1.10 (± 0.05)

The POC and Sr content per cyst exhibits a weak power relationship with the number of cysts present in a sample (Figure 4.2a and 4.2b), demonstrating better preservation of cysts when large amounts are sampled. The relationship is similar for cysts sampled in spring 2007 and 2008 but cysts sampled in 2008 have slightly lower amounts of POC and Sr per cyst. Sr content per cyst is greater for samples with lower cyst numbers, which is an overestimate compared to the model Sr cyst content, due to Sr dissolution leading to cysts being indistinguishable from other particulate material. The number of cysts that had undergone complete dissolution of their celestite shell until they are unidentifiable will be affected by the rate at which cysts settled into the sediment trap sampling cup, the rate of dissolution of the celestite, and the number of cysts in total that settled into the sampling cup. The effect of celestite dissolution is demonstrated by the cysts from the mid-May cups in 2007 (grey filled data points in Figure 4.2a and b) that could not be separated from the fluffy particle flux. The cyst and POC flux for mid-May samples were calculated from an average of the Sr flux and cyst flux from the measured samples (Martin et al., 2010). By using model cyst

content in Table 4.2 it appears the cyst number flux was underestimated by ~ 50 % and the cyst POC flux was underestimated by ~ 20 %.

The highest cyst numbers were sampled in late April – early May 2008 in Trap NW, with 7176 and 9265 cysts collected, respectively. These high cyst fluxes led to the greatest dissolved Sr concentrations in the sample supernatant of 850 ± 10 µmol L^{-1} and 830 ± 5 µmol L^{-1}, which is approaching Sr saturation in seawater (910 µmol L^{-1}; Beers, 1970). The dissolved Sr acts as a buffer, meaning the majority of the cysts were easily identified and separated, with an estimated 510 – 660 cysts per day sinking into the sediment trap.

4.3.2 Acantharian Cyst Fluxes

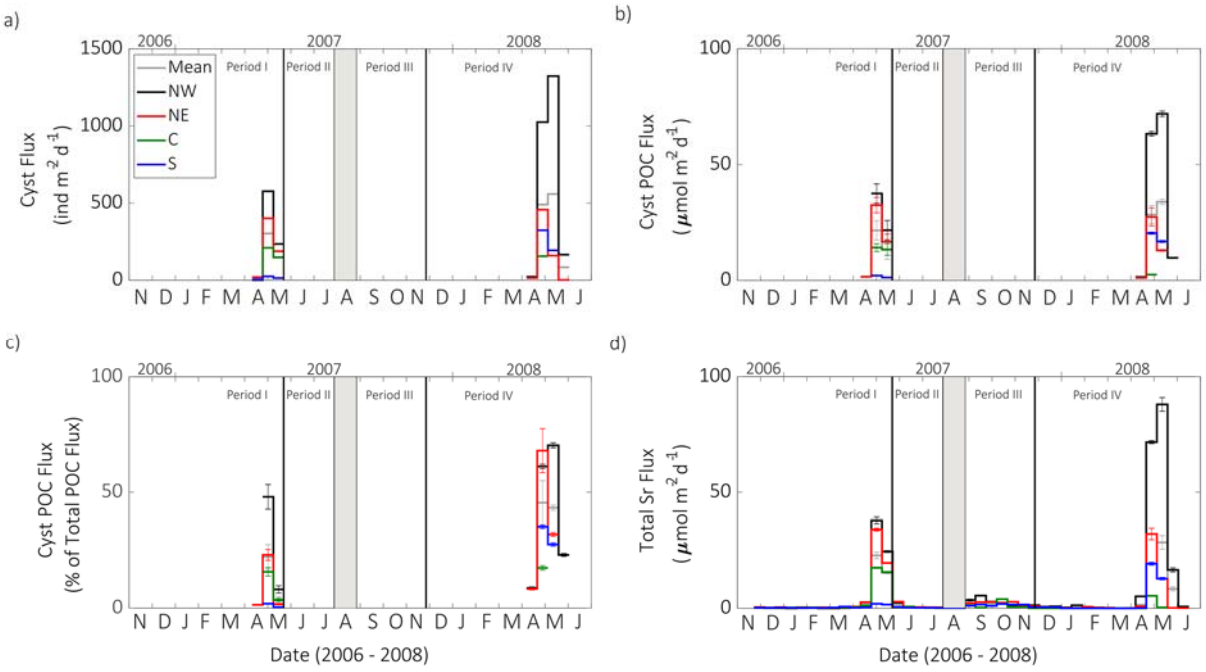

Figure 4.3 a) Cyst flux (individuals m^{-2} d^{-1}) for spring 2007 and spring 2008 for Traps NW, NE, C and S, b) cyst POC flux (µmol m^{-2} d^{-1}), c) cyst POC flux as a percentage of total POC flux and d) total Sr flux (µmol m^{-2} d^{-1}). The error bars show propagated uncertainty. The black vertical lines highlight the four flux Periods I-IV as outlined in Chapter 2.

The timing of Acantharian cysts settling into sediment trap samples below 2000 m in the IB was very similar for both 2007 and 2008 with a small flux occurring in mid-April. The major sedimentation event of the cysts into the traps occurs in late-April until mid-May (Figure 4.3). The spring flux of Acantharia cysts to the bathypelagic IB appears to be an annual, regular and basin-wide phenomena.

Table 4.3 Summary of Acantharian cyst fluxes from 2007, reported by Martin et al. (2010), and 2008, reported in this study. Total Sr flux is the sum of supernatant and cyst fluxes for 2007 samples and is the sum of the supernatant, particulate and cyst fractions for 2008 samples. The propagated analytical uncertainty is in brackets. Some samples were very small and were either below detection limit (BDL) or below calibration range (BCR).

Trap ID	Timing	Date	Cyst Flux (ind m^{-2} d^{-1})	Total Sr Flux (µmol m^{-2} d^{-1})	Cyst Sr Flux (µmol m^{-2} d^{-1})	POC Cyst Flux (µmol m^{-2} d^{-1})	PON Cyst Flux (µmol m^{-2} d^{-1})
2007 (Martin et al., 2010)							
NW	mid-Apr	18/04/2007	18	2.66 (± 0.05)	-	2.17 (± 0.25)	BDL
	early-May	02/05/2007	577	37.66 (± 1.60)	15.29 (± 1.37)	37.50 (± 4.17)	7.07 (± 0.71)
	mid-May	16/05/2007	235	24.31 (± 0.57)	5.02 (± 0.34)	21.67 (± 4.17)	3.50 (± 1.14)
NE	mid-Apr	18/04/2007	20	2.60 (± 0.05)	-	1.58 (± 0.17)	BDL
	early-May	02/05/2007	401	33.78 (± 0.91)	8.33 (± 0.57)	32.50 (± 3.33)	6.21 (± 0.64)
	mid-May	16/05/2007	188	19.40 (± 0.34)	2.28 (± 0.11)	16.67 (± 3.33)	2.86 (± 0.71)
C	mid-Apr	18/04/2007	0	-	-	-	-
	early-May	02/05/2007	210	17.23 (± 0.23)	0.80 (± 0.23)	14.17 (± 1.67)	2.86 (± 0.29)
	mid-May	16/05/2007	149	15.41 (± 0.23)	0.68 (± 0.23)	13.33 (± 2.50)	2.14 (± 0.71)
S	mid-Apr	18/04/2007	2	-	-	-	-
	early-May	02/05/2007	25	1.97 (± 0.05)	-	2.08 (± 0.17)	BDL

	mid-May	16/05/2007	14	1.40 (± 0.07)	0.03 (± 0.01)	1.25 (± 0.25)	BDL
2008 (this study)							
NW	mid-Apr	13/04/2008	22	5.17 (± 0.089)	0.001 (1.3×10^{-5})	BCR	BCR
	late-Apr	27/04/2008	1025	71.65 (± 0.66)	28.82 (± 0.27)	63.62 (± 0.99)	14.29 (± 1.32)
	mid-May	11/05/2008	1324	87.98 (± 2.94)	37.64 (± 0.21)	71.92 (± 1.12)	15.34 (± 1.42)
	late-May	25/05/2008	166	16.63 (± 0.88)	0.01 ($\pm 7.95 \times 10^{-4}$)	9.75 (± 0.26)	1.87 (± 0.30)
NE	mid-Apr	13/04/2008	14	0.82 (± 0.12)	0.001 ($\pm 1.12 \times 10^{-5}$)	BCR	BCR
	late-Apr	27/04/2008	457	32.16 (± 6.30)	8.63 (± 0.90)	27.40 (± 3.84)	5.46 (± 0.51)
	mid-May	11/05/2008	160	12.81 (± 0.21)	0.04 (± 0.01)	12.96 (± 0.35)	2.69 (± 0.30)
	late-May	25/05/2008	2	0.20 (± 0.04)	-	-	-
C	late-Apr	27/04/2008	156	5.40 (± 0.09)	0.01 ($\pm 9.3 \times 10^{-5}$)	BCR	BDL
S	late-Apr	27/04/2008	324	19.31 (± 0.69)	0.21 (± 0.03)	20.39 (± 0.47)	4.16 (± 0.38)
	mid-May	11/05/2008	194	12.84 (± 0.52)	0.01 (± 0.002)	16.81 (± 0.45)	3.49 (± 0.56)

The cyst flux, reported as individuals m^{-2} d^{-1}, were similar in 2007 and 2008 for Trap NE and Trap C, whereas Trap S fluxes were greater in 2008. Trap NW cyst fluxes were more than twice the previous year's greatest flux (577 ind m^{-2} d^{-1}) with the largest cyst flux of 1324 ind m^{-2} d^{-1}. This is the highest recorded flux of cysts below 2000 m, and second highest below 1000 m, surpassed only by fluxes observed in the Scotia Sea by Belcher et al. (2018; 1500 m, 2706 ind m^{-2} d^{-1}; discussed further in Section 4.4.1.2). The total number of individuals that settled into each trap during the sedimentation event was estimated by calculating the cumulative sum of the daily fluxes for the number of days cysts were sampled (Table 4.4), with the lowest in Trap S (2007) with 572 ind. m^{-2} and the greatest number of estimated cysts during a sedimentation event was 35 514 ind. m^{-2} in Trap NW in 2008. The mean integrated flux of cysts per event was used to estimate the mean number of cysts fluxing to the deep ocean IB, by multiplying by the Iceland Basin area, which for spring 2007 was 1.6 x 10^{15} individuals and in spring 2008 was 3.4 x 10^{15} individuals, more than double the number for 2007. This may overestimate the number of cysts fluxing to the deep ocean IB if the distribution of the cysts is heterogeneous but provides an idea of the scale of the annual sedimentation event in the IB.

Table 4.4 Cysts per sedimentation event (ind m^{-2}) and the mean cyst flux per event integrated to estimate the IB total number of individuals. The sedimentation event in 2007 lasted for 42 days and the sedimentation event in 2008 lasted for 56 days, but in both cases the majority of the cysts settled into the traps within a 28 day window.

	Cysts (ind m^{-2})	
	2007	2008
Trap NW	11 620	35 514
Trap NE	8 526	8 868
Trap C	5 026	2 178
Trap S	574	7 250
Trap Mean	6 437	13 453
IB Total (ind.)	1.6 x 10^{15}	3.4 x 10^{15}

The cyst POC flux closely tracks the number of cysts (Figure 4.3a and 4.3b), with greater numbers of cysts leading to larger POC fluxes. The greatest cyst POC flux was observed during the large sedimentation event in 2008 in Trap NW with a flux of ~ 70 µmol m^{-2} d^{-1} which contributed 70.3 % of the total POC flux collected in the mid-May Trap NW sample. This is the largest recorded percentage contribution of cyst POC to POC flux in the deep ocean to date (discussed further in

Section 4.4.1.3) but is due to the extremely low fluxes sampled during the spring bloom in 2008. This is further shown by all cyst POC fluxes in 2008 contributing a minimum of 8 % to the total POC flux, whilst in 2007 during spring-bloom related particle flux, cyst POC flux contributed a maximum of 10 % of the total POC flux. On annual timescales, the POC flux contribution by the cysts is negligible with < 1 % of the annual POC flux originating from the Acantharian cysts in the IB.

Similarly to the POC flux, the total Sr flux (Figure 4.3d) tracks the cyst flux. Sr is slightly elevated during samples with greater particle flux (i.e. August – December 2007; Figure 4.3d) but the magnitude of this is negligible compared to the amount of Sr reaching the deep ocean via the sedimentation of the Acantharian cysts.

4.3.3 Strontium Fractionation in Sediment Trap Samples

The Sr originating from Acantharian celestite is predominantly in the dissolved fraction of the sediment trap sample supernatant, except during periods of exceptionally high cyst flux (Figure 4.4). During high fluxes a larger proportion of the Sr is found in the cysts (up to 43 %) and a smaller amount is found in the particulate fraction (up to 9.5 %), likely due to breakage of the celestite shell, which can shatter easily if it is preserved well, as shown in Figure 4.1b. Measuring the dissolved fraction when cyst fluxes are of low-moderate magnitude is an effective way to estimate their contribution, but for large cyst fluxes the Sr fluxes will underestimate the magnitude of the cyst flux.

4.3.4 Annual Strontium Budget

The annual Sr budget for the trap locations in the IB was estimated using particulate Ca flux converted to Sr flux using literature Sr:Ca ratios (Appendix D), from November 2006 – November 2007, with and without the cyst contribution, to investigate and highlight the role of Acantharian cysts in the Sr cycle in the Subpolar North Atlantic. A greater Sr cyst flux in the Northern sector of the IB was observed, with the fluxes from Trap NW consistently greater than the other trap fluxes. The estimated Sr fluxes in 2007 without cysts ranged between 0.28 to 0.46 mmol m^{-2} yr^{-1}, whilst total Sr fluxes including cysts, ranged from 0.34 to 1.36 mmol m^{-2} yr^{-1}. The Acantharian cysts therefore contributed up to 70 % of the annual particulate Sr flux in the IB in 2007 during a 42 day sedimentation event. The 2008 cyst flux contribution was compared relative to the annual Sr budget for 2007 and was found to have greater Sr fluxes up to 2.50 ± 0.06 mmol m^{-2} yr^{-1} (see Section 4.24), which contributed more than the largest annual Sr flux in 2007, with a relative contribution to the 2007 Sr fluxes up to 184 % in a 56 day sedimentation event.

4.3.5 Upper Ocean Environmental Conditions

The timing of the start of the Acantharian cyst sedimentation event to the deep ocean was very similar for both 2007 and 2008 for all traps. The first incidence of cysts and elevated Sr levels were sampled in early-mid April and the first sample with considerable cyst flux was mid-late April. The trigger for encystment and sedimentation of Acantharian cysts is not well understood and is hypothesised to be linked to increasing chlorophyll concentrations to allow swarmers to feed on the spring bloom associated particle flux in the deep ocean (Decelle et al., 2013; Martin et al., 2010).

I hypothesise that the first incidence of rapid shoaling in the mixed layer in spring allows Acantharia to return to the upper ocean but they will likely remain below the shallower MLD. Furthermore, I hypothesise that upper ocean environmental conditions, such as temperature, light or chlorophyll concentration, are a trigger for sedimentation. To explore these hypotheses the particle source regions of the Acantharian cysts were estimated based on the local current velocities. The predicted particle source regions for Acantharian cysts sinking at a mean rate of 760 m d^{-1} are shown in Figure 4.5 for each trap for 2007 and 2008. The particle source regions are similar for both years due to the fast sinking rate but there are some observed differences driven by local interannual variability. The source regions were also predicted using +/- 1 standard deviation of the mean measured sinking rates, and confirms that the faster the sinking rate, the smaller and more representative the particle source region is, and closer to the sediment trap location (Appendix C). These particle source regions were then used to extract upper ocean properties as shown in Figure 4.6.

The Chl *a* concentration in the source regions in 2007 is generally low throughout April and early-mid May (< 0.5 mg m^{-3}) for Trap NW and NE, whilst Trap C and Trap S had elevated Chl *a* concentrations in May (up to 0.75 mg m^{-3}; Figure 4.6). In 2008, Chl *a* concentrations were also low in April, but were elevated for Trap NW, C and S source regions, with concentrations up to 1.3 mg m^{-3}. The Chl *a* concentrations may be underestimates as monthly output was used to compensate for heavy cloud cover in the IB during spring. There does not appear to be any relationship in terms of magnitude or timing between cyst fluxes and Chl *a* concentration as, for example, Trap NW 2008 had the highest cyst fluxes and the highest Chl *a* concentration, whilst Trap C 2008 had the second highest Chl *a* concentration but the lowest cyst fluxes of all the recorded sedimentation events in 2007 and 2008.

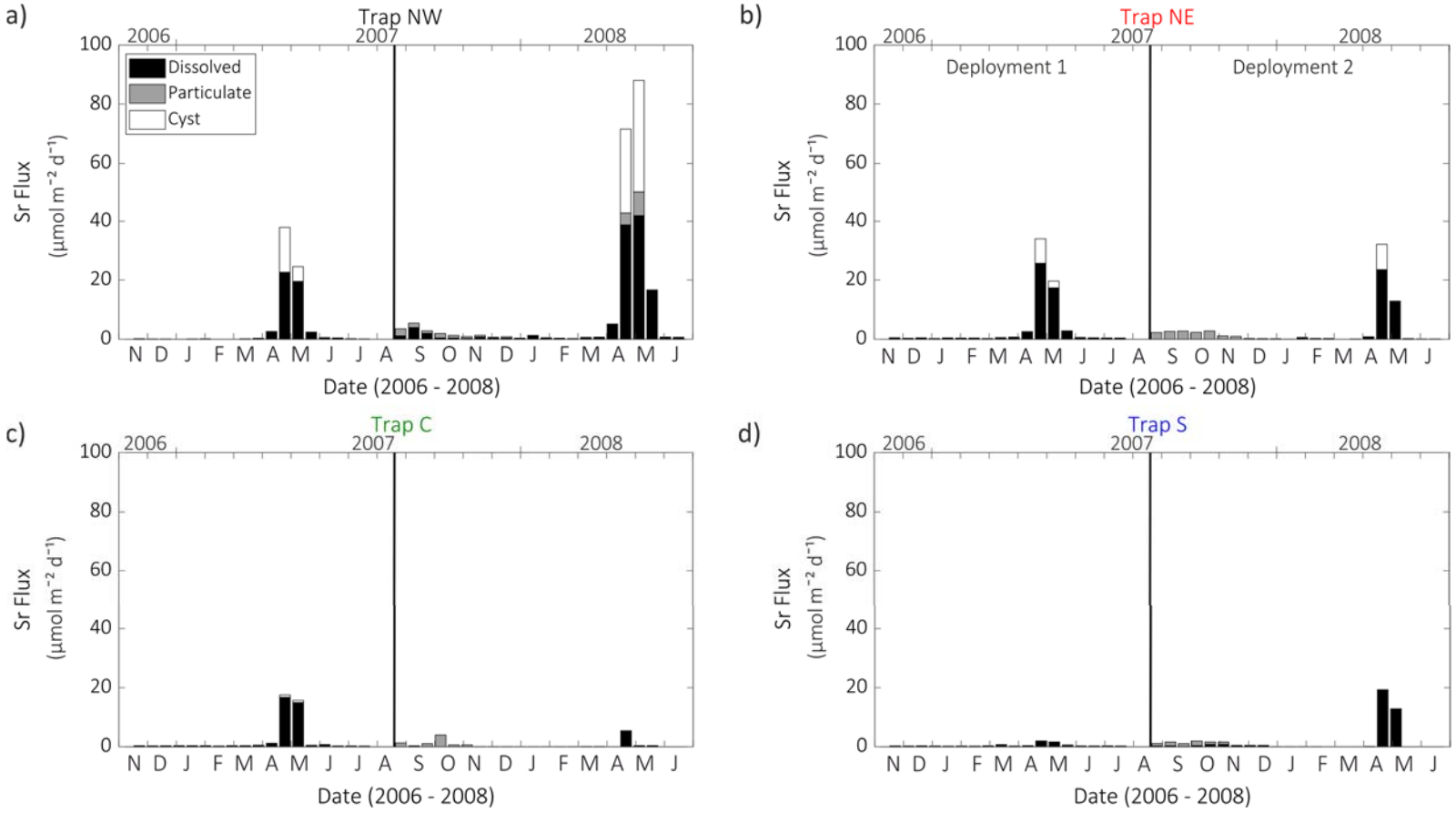

Figure 4.4 Sr total fluxes (µmol m^{-2} d^{-1}) below 2000 m in the Iceland Basin in 2007 and 2008 for the four sediment traps a) NW, b) NE, c) C and d) S. The fractions in which the Sr is found is shown by the stacked bars, with dissolved Sr shown by the black bar, particulate Sr in grey and cyst-associated Sr in white. Deployment 1 and deployment 2 are separated by the thick black line. No particulate Sr data were available from deployment 1.

Table 4.5 Annual and daily mean Sr fluxes, with and without cysts for 2007 for below 2000 m in the IB for each sediment trap. The 2008 cyst flux was compared to the 2007 Sr budget without cysts due to the unusually low fluxes sampled in period IV as discussed in previous chapters. The percentage contribution the cysts made to the Sr flux is reported for 2007 and 2008. The propagated analytical uncertainty is in brackets.

	2007					2008		
	Without cyst flux		With cyst flux					Relative to D1 Sr budget
	Sr Flux (mmol m^{-2} yr^{-1})	Mean Sr Flux (µmol m^{-2} d^{-1})	Sr Flux (mmol m^{-2} yr^{-1})	Mean Sr Flux (µmol m^{-2} d^{-1})	Cyst Sr as a % of Sr budget	Cyst Sr Flux (mmol m^{-2} yr^{-1})	Mean Cyst Sr Flux (µmol m^{-2} d^{-1})	Cyst Sr as a % of Sr budget
Trap NW	0.41 (0.02)	1.12 (0.06)	1.36 (0.05)	3.72 (0.14)	69.7 (13.5)	2.50 (0.06)	6.84 (0.18)	184.1 (9.9)
Trap NE	0.46 (0.02)	1.26 (0.06)	1.29 (0.03)	3.53 (0.09)	64.3 (10.6)	0.64 (0.04)	1.75 (0.11)	49.5 (3.4)
Trap C	0.32 (0.01)	0.89 (0.03)	0.81 (0.02)	2.23 (0.06)	60.2 (9.7)	0.08 (0.003)	0.22 (0.007)	9.9 (0.3)
Trap S	0.28 (0.02)	0.76 (0.07)	0.34 (0.03)	0.94 (0.07)	18.7 (6.2)	0.45 (0.02)	1.22 (0.05)	130.7 (8.2)

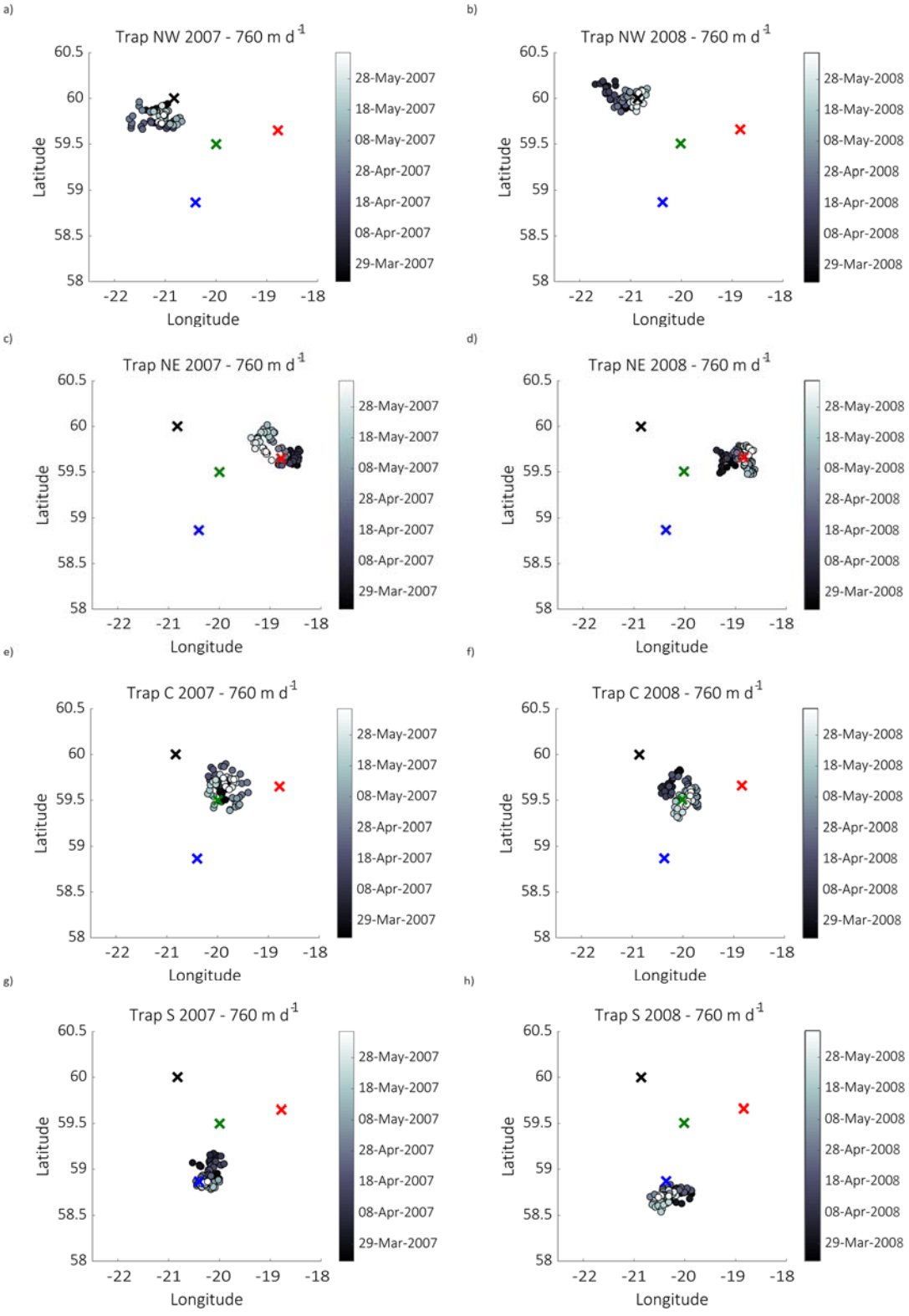

Figure 4.5 Acantharian cyst upper ocean source regions estimated using the mean measured sinking velocity of 760 m d^{-1}. The crosses represent the sediment trap locations: Trap NW is black, Trap NE is red, Trap C is green and Trap S is blue. Panels a), c), e) and g) are the source regions for the 2007 sedimentation event and panels b), d), f) and h) are the source regions for the 2008 sedimentation event. The marker colours represent the timing that the cysts reached the sediment traps during the sedimentation event.

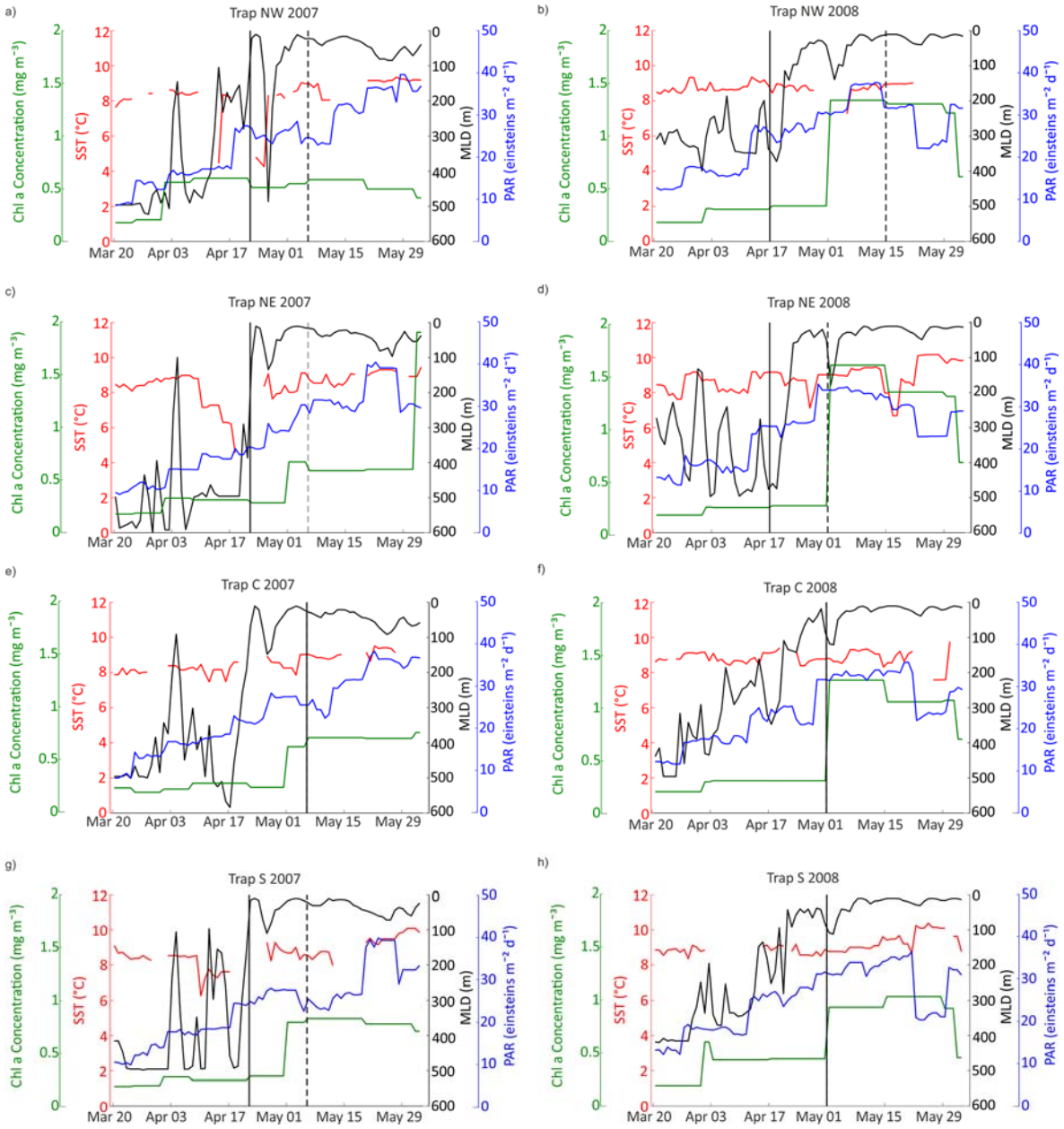

Figure 4.6 Upper ocean environmental data for the Acantharian cyst estimated source regions. Each panel shows satellite-derived chlorophyll *a* concentration (green), PAR (blue) and SST (red) and MLD (black). The panels highlight the sedimentation events for 2007 for a) Trap NW, c) Trap NE, e) Trap C and g) Trap S and for 2008 for b) Trap NW, d) Trap NE, f) Trap C and h) Trap S. Each panel highlights the date the cysts would have left the upper ocean (assuming a sinking speed of 760 m d^{-1}) to generate the first occurrence of Acantharian cysts in a sediment trap sample (solid black vertical line) and the date that the peak abundance of cysts would have sank out of the upper ocean (dashed black vertical line). For panels where there is only one line the first occurrence and peak in cyst flux coincide. This method assumes that the mid-point of the two week sediment trap sampling period is the most representative date and assumes that all the cysts would have taken 3 days to reach the deep ocean (760 m d^{-1} mean sinking rate is equivalent to 2.63 days to 2000 m).

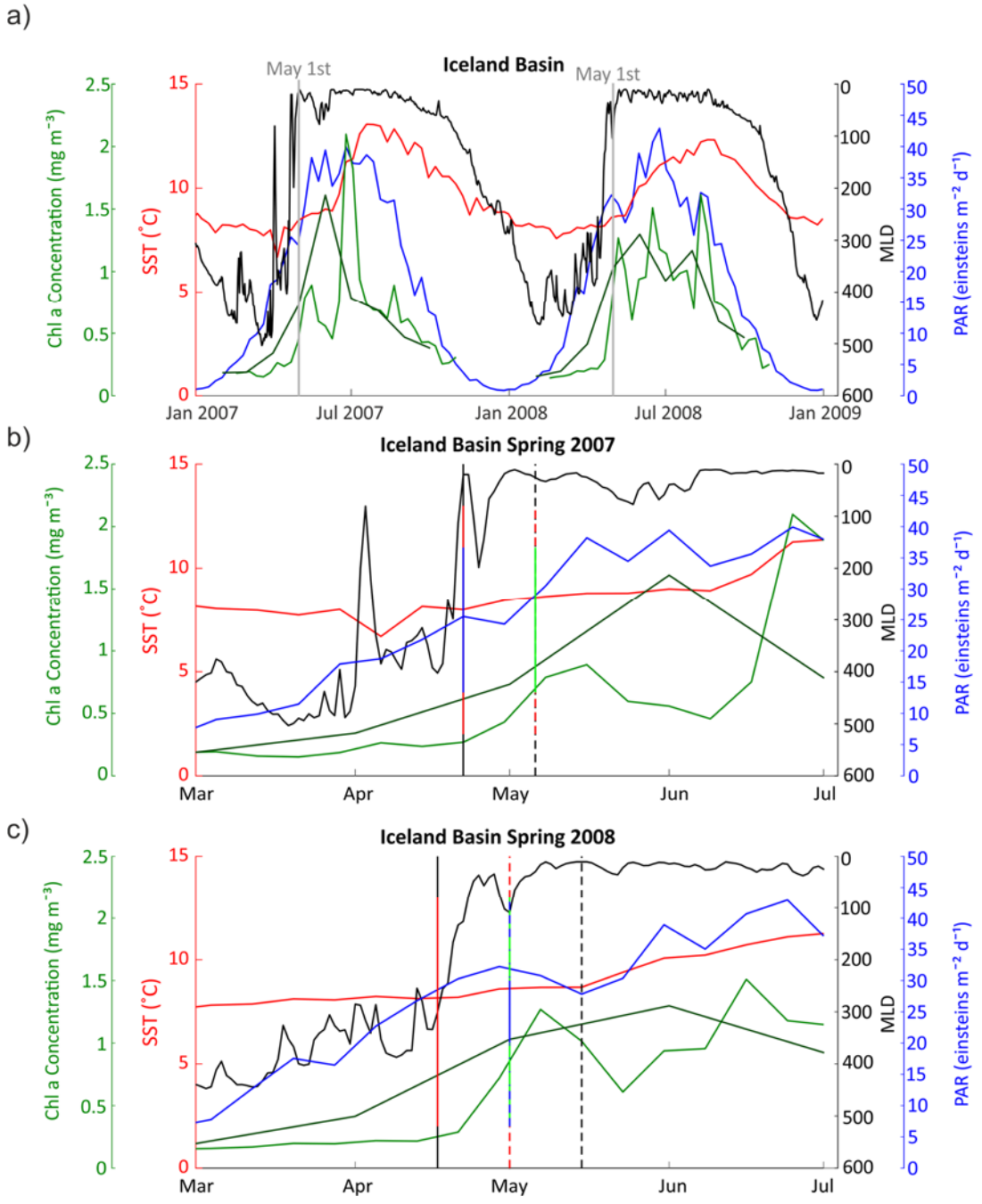

Figure 4.7 Upper ocean conditions in the Iceland Basin for 2007 and 2008. a) Mean chlorophyll *a* (8 day light green, monthly dark green), SST (red), MLD (black) and PAR (blue) in the IB for 2007 and 2008. The grey line highlights May 1st which often coincided with the peak cyst flux. b) and c) show the same parameters as a) but zoomed in for spring 2007 and spring 2008 during the Acantharian sedimentation events. The vertical lines in b) and c) highlight the date that the first incidence of cysts would have sank out of the upper ocean (solid line) and the date that the peak sampled cyst flux would have sank out of the upper ocean (dashed line). The colours of the lines relate to the sediment traps (Trap NW – red, Trap NE – black, Trap C – green, Trap S – blue).

The SST of the particle source regions generally ranged between 8 – 9 °C, with transient mixing events temporarily decreasing the temperature to 6 – 8 °C (Figure 4.6). There does not appear to be any relationship between cyst flux magnitude and timing of the sedimentation event with SST. Cyst-forming Acantharia are thought to inhabit mesopelagic waters and so may be affected by temperature changes deeper in the water column.

Throughout April and May in both years PAR steadily increases from ~ 10 - 15 Einsteins m^{-2} d^{-1} to > 30 Einsteins m^{-2} d^{-1}. One interesting feature in all panels in Figure 4.6 is that PAR has a step change in early May, in both years, where the increasing trend pauses and either plateaus for up to two weeks, or decreases slightly, before starting to increase steadily. This step change coincides, in every instance, with the timing that the peak cyst flux sank out of the upper ocean, which suggests that light levels could be a potential trigger for sedimentation. This possibility is discussed further in Section 4.4.4.

The IB experiences deep winter mixed layers down to 600 m. Re-stratification of the water column in spring usually begins in late March, with several shoaling and deepening transient events until a final shoaling event in May. April is a dynamic period in the IB and it is possible that these mixing events also play a role in repopulating the upper ocean with Acantharia and in triggering the cyst sedimentation events, but due to the high variability it is difficult to find a causal relationship to upper ocean conditions. Interestingly, for Traps NW and NE in both years, and Trap S in 2007, the first cyst occurrence (solid black line in Figure 4.6) coincides, or is just before, the rapid shoaling event from 300 – 600 m to a mixed layer of ~ 100 m. The role of the mixed layer as a trigger for encystment is discussed further in Section 4.4.4.

4.3.6 Acantharia Spatial Distribution

The Acantharian cyst fluxes exhibit interannual spatial variability which may aid in our understanding of what drives sedimentation and their reproductive strategy. During the 2007 sedimentation event, Trap C collected a small cyst flux but very few cysts were sampled in 2008, whilst Trap S had the opposite pattern. For Trap C there is very little difference in the predicted source regions in 2007 and 2008, whereas for Trap S in 2007, the source region was predominantly above the sediment trap, between Trap C and S, whilst in 2008, the cysts originated from south of Trap S (Figure 4.5). The topography south of Trap S becomes increasingly shallow which may support my hypothesis that the Acantharia cysts originate from ‘shallower’ (~ 1000 m) waters but drift with the currents into the open ocean IB where they encyst and sink to the deep ocean.

Trap NE sampled very similar cyst fluxes for both years whereas Trap NW in 2008 sampled much larger fluxes. The particle source regions were fairly localised near the sediment trap locations due to the very fast sinking speeds of the Acantharian cysts (Appendix C.4). The estimated cyst particle source region during spring for Trap NW using current meter data and OSCAR surface velocity components had a bigger spatial range compared to Trap NE in 2007, extending as far as 22 W. Trap NW and Trap NE sampled cysts from opposite sides of the Iceland Basin in spring 2007 and hence it is possible that the larger fluxes sampled by Trap NW are driven by greater Acantharian biomass in the Northwest IB.

4.3.7 Acantharia Abundance

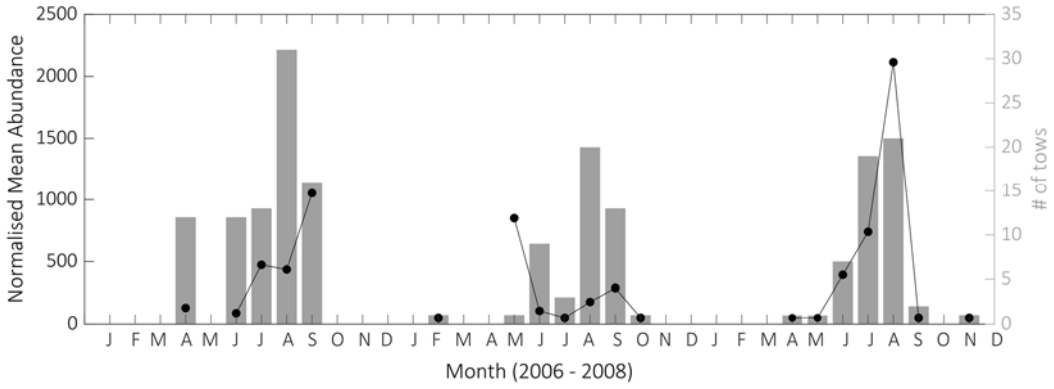

Figure 4.8 Mean monthly Acantharia abundance normalised to the number of CPR tows per month for 2006 – 2008 in the Iceland Basin. The black line and markers are the normalised mean abundance and the grey bars indicate the number of tows in area B5, B6, C5 and C6.

The timing of the sedimentation event, starting in mid-April, leads to the expectation that Acantharian abundance would be elevated in April and May. However, the normalised Acantharian abundance from CPR data in Figure 4.8 records elevated abundances in summer and autumn in 2006 and 2007, whereas in May 2007 a single tow recorded elevated Acantharia normalised mean abundance of ~ 900 individuals per tow and a small increase in abundance in late autumn and summer.

Acantharia are thought to reside between 0 – 300 m, with symbiont-hosting Acantharia thought to reside in the surface layers, whilst non-symbiont, cyst-forming Acantharia can reside deeper in the water column. This aligns with no clear signal of elevated Acantharian abundances in spring from CPR which only samples the surface ocean (Figure 4.8). The spatial and temporal coverage of the CPR data in the IB were very low during 2006 – 2008 with a bias towards summer and autumn.

4.4 Discussion

4.4.1 Acantharian Cyst Sedimentation Events

4.4.1.1 Cyst Morphology

This study builds on the previous findings of Martin et al. (2010) and confirms that the sedimentation of Acantharian cysts down to the bathypelagic IB is a regular annual event. The sedimentation begins in mid-April, just prior to the spring bloom, and is sustained until late May. The Acantharian cysts sampled in 2007 and 2008 have the same morphology, originating from the Order Holacanthida (Decelle et al., 2013). The sampled cysts were of a similar size for both years (Table 4.1), which is considerably larger than the sizes of cysts sampled in previous studies in other locations (Antia et al., 1993; Belcher et al., 2018; Spindler & Beyer, 1990). Elongated cysts, from the order Holacanthida, have been sampled in the Southern Ocean, the South China Sea and the Indian Ocean suggesting they are not exclusive to high latitude regions (Belcher et al., 2018; Decelle et al., 2013; Spindler & Beyer, 1990).

The cysts sampled in this study appear to have been formed by the Acantharian spicules folding in one direction, to form the basis of the celestite structure around the organic material, as shown by the SEM image in Figure 4.1d reproduced from Martin et al. (2010). Some Acantharia eject their spicules during encystment, whereas these elongated cysts appear to utilise their spicules, which may be less energetically expensive, and the shape and amount of celestite would allow the cyst to sink rapidly.

The cysts sampled in 2008 had a faster measured sinking speed of 760 m d^{-1} compared to 490 m d^{-1} in 2007 (Table 4.1). The Acantharian cyst sinking rates measured in this study are faster than previous measurements, likely due to the larger cysts which may contain more celestite ballast. In the Greenland Sea, the measured mean cyst sinking rate was 238 m d^{-1}, whilst the estimated sinking rate from integrated cyst flux losses between 100 and 300 m, was 100 - 150 m d^{-1} (Antia et al., 1993). At 500 m depth in the Greenland Sea nearly all the cysts had disappeared which suggests a two day sinking and/or dissolution timescale (Antia et al., 1993). The difference between the measured and estimated sinking rates suggest that other processes must be contributing to cyst loss with depth, such as grazing or advection, but excystment or dissolution were thought to be more likely (Antia et al., 1993). The fast sinking rates measured in this study suggest Acantharian cysts have a 2 - 3 day sinking time before reaching the deep ocean, similar to the Greenland Sea cysts, which highlights that there must be a reproductive advantage to sinking rapidly out of the surface ocean, which will be discussed more in Section 4.4.5.

The sinking rate of the cysts is faster than most measurements of marine snow and phytodetritus estimates, and falls within the range of measured sinking rates of large faecal pellets from chaetognaths, pteropods and salps (Turner, 2002; range 27 - 2700 m d^{-1}). Single plankton cells are closer in size to the cysts, but the sinking rates are often much slower (e.g. diatoms < 50 m d^{-1} (Eppley et al., 1967), foraminifera up to 583 m d^{-1} (Takahashi & Be, 1984), radiolarians up to 416 m d^{-1} (Takahashi & Honjo, 1983)). The streamlined shape and celestite incorporation indicate that the cysts are designed to sink rapidly from the surface ocean to the seafloor. Further exploration into the advantages of rapid sinking at the start of the spring bloom as a reproductive strategy is detailed in Section 4.4.4.

4.4.1.2 Acantharian Cyst Strontium Content and Flux

Acantharian cysts of the same morphology were also observed by Martin et al. (2011) in May 2008 in the Western IB, over the Rekyjanes Ridge. The study sampled cysts using PELAGRA Lagrangian sediment traps deployed between 160 - 730 m from early- to mid-May, with measured Sr fluxes up to 553 µmol m^{-2} d^{-1}. An estimation of the number of cysts fluxing to the deep ocean based on the Sr fluxes, and the Sr content per cyst (Table 4.2), predicts cyst fluxes between 153 – 11 156 ind. m^{-2} d^{-1}. The highest sampled cyst flux in the deep ocean IB was 1324 ind. m^{-2} d^{-1}, which suggests that either the cyst fluxes over the Rekyjanes Ridge are much greater than in the IB or that the majority of cysts are grazed or undergo dissolution between 760 and 2000 m, either before or during excystment.

The deep ocean cyst fluxes from this study and estimated upper ocean cyst fluxes from Martin et al. (2011) are in line with previous studies that sampled cysts in the upper ocean (< 1000 m). For example, in the Greenland Sea, Antia et al. (1993) sampled fluxes ranging between 349 – 33 000 ind. m^{-2} d^{-1}, and in the Sargasso Sea Michaels et al. (1995) sampled fluxes at 150 m of 12 676 ind. m^{-2} d^{-1} and Bernstein et al. (1992) sampled lower fluxes at 400 m of 1420 ind. m^{-2} d^{-1}. However, in the deep ocean (> 1500 m), in the Greenland Sea, Antia et al. (1993) sampled fluxes at 2200 m of only 15 ind. m^{-2} d^{-1}, and in the Sargasso Sea, Bernstein et al. (1992) sampled fluxes at 1500 m of 8 ind. m^{-2} d^{-1}. The observed cyst fluxes below 2000 m in the IB are the second largest recorded in the bathypelagic with Belcher et al. (2018) observing cyst fluxes up to 2706 ind. m^{-2} d^{-1} at 1500 m in the Scotia Sea in December 2012. This highlights that the cyst fluxes sampled in Martin et al. (2010), this study and in Belcher et al. (2018) are large in magnitude compared to previous studies in the deep ocean.

4.4.1.3 Acantharian Cyst POC Fluxes

Recent studies on the contribution of Acantharian cysts to deep ocean POC flux have highlighted that the magnitude and spatial and temporal coverage of these events is unknown. The largest POC flux in this study of 0.072 mmol m^{-2} d^{-1} was observed in early May 2008 in the NW trap which contributed 70 % to the total POC flux in the sample, due to the unusually low fluxes at that time. In May 2007 cysts contributed up to 48 % of POC flux in pre-bloom sediment trap samples, with a POC flux of 0.0375 mmol m^{-2} d^{-1} (Martin et al., 2010). Acantharian cysts sampled in the deep ocean by Belcher et al. (2018) were much smaller than the cysts in this study. They exported more POC to depth, with fluxes up to 0.43 mmol m^{-2} d^{-1}, which was 26 % of the total POC flux. Previous studies of Acantharian cysts in the upper ocean generally find cysts contribute < 5 % to total POC flux, except at 100 m in the Greenland Sea in which cysts contributed 32 % of total POC flux (Antia et al., 1993; Bernstein et al., 1992; Michaels et al., 1995). Belcher et al. (2018) estimated a POC content of 1.9 µg of POC per cyst based on conversion factors (Antia et al., 1993; 0.33 µg of POC per cyst and a C:volume conversion factor of 0.048 pg C μm^{-3}) versus 0.65 µg of POC per model cyst in this study (Table 4.2).

Acantharian cysts have a POC:PON ratio lower than the Redfield ratio of 6.6, likely due to them being heterotrophic (Anderson, 1992; Hargrave et al., 1994). Cysts that have undergone greater dissolution (indicated by lower cyst numbers and elevated Sr content per cyst; Figure 4.2a and c) appear to have a slightly higher POC and PON content per cyst. This is counterintuitive as cysts that have experienced dissolution may have leached organic material from the cyst into the surrounding supernatant, and would be predicted to have a lower POC content per cyst.

Cysts were rinsed to remove any attached particulate material, however cysts that have undergone celestite dissolution are visibly much stickier, with greater amounts of material attached, compared to the model cysts. The deployment 1 cysts were rinsed 3x with deionised water by Martin et al. (2010), whilst for deployment 2, I rinsed the cysts once with a $SrCl_2$ buffered deionised water, to prevent celestite dissolution changing the elemental content of the cysts and there was very little other particulate material in the deployment 2 samples. If the rinses were unsuccessful in removing all the non-cyst particulate material for the dissolved cysts this may explain the higher POC content per cyst, and the greater POC:PON ratio, whilst the model cysts, with very little attached material, may be more representative of *in situ* cyst elemental composition. The model cysts appear to have undergone very little degradation during their fast transit from the surface ocean to the deep ocean, which may support the idea that they are viable cysts.

4.4.1.4 Strontium Flux

Acantharian cysts dominate the annual particulate Sr budget in the IB even though the cyst sedimentation event lasts for < 2 months. The non-cyst particulate Sr flux contributes a small amount to the annual total, as Sr is only a trace element in non-Acantharian plankton (Martin & Knauer, 1973). The Sr fluxes in this study have a range of 0.001 – 37.64 µmol m^{-2} d^{-1}. Sediment trap Sr fluxes (dissolved Sr only) were measured by Decelle et al. (2013) in the subtropical North and South Atlantic and in the Scotia Sea with fluxes ranging between 0.3 – 14 µmol m^{-2} d^{-1}. The Sr fluxes in the IB are more than twice as large as the Decelle et al. (2013) Sr fluxes, highlighting the important role of Acantharia cysts in the high latitude Sr budget, which will be discussed further in Section 4.4.3.

4.4.2 Spatial and Depth Distribution

4.4.2.1 Acantharia Spatial Distribution

The location where Acantharia ascend to the upper ocean will be different to the predicted source region of the sinking Acantharia cysts as the Acantharia will have drifted with the currents in the upper ocean and knowledge of where they ascend from is crucial to furthering our understanding of the reproductive strategy of the cysts.

The seminal paper on 'Die Acantharia' by Schewiakoff, (1926) highlighted the important role of currents in the diffusion of Acantharia and has been supported by several studies summarised by Bottazzi, (1978). However, the role of currents has rarely been discussed in the context of Acantharian cyst sedimentation and the evolutionary advantage of this strategy. Reid, (1978) studied dinoflagellate cysts in the upper ocean and seafloor sediments of the North Atlantic and similarly hypothesised that the cysts' sediment distribution may be beyond the centres of production, implying movement by either currents, or sediment transport. Similarities between dinoflagellate cyst distributions and current patterns in the North Atlantic were also noted by Harland, (1983). This may support the hypothesis that Acantharia utilise the currents to increase their spatial distribution but that the cysts are designed to sink over shallower topography, rather than to the deep ocean but due to strong currents and complex topography in the IB, overshoot areas of shallower topography, such as near the Rekyjanes ridge.

Previous studies that have sampled Acantharian cysts in the deep ocean are all relatively near to shallow topographic features in which the water depth rapidly decreases, such as at station P2 in the Scotia Sea (Belcher et al., 2018), in the Greenland Sea (Antia et al., 1993) and at BATS (Bernstein et al., 1992). This could support the hypothesis that the cysts evolutionary strategy is

to sink to water depths < 1500 m, to allow for shorter vertical transit to the upper ocean, but a fraction of the population drift with currents into a more open ocean setting before sedimentation. This hypothesis is supported by the Acantharian cyst fluxes up to 11 156 ind. m^2 d^{-1} found at 730 m by Martin et al. (2011) in early May 2008 in water depths of ~ 1400m, and near to the crest of the Rekyjanes Ridge, which has water depths as shallow as 700 m. This hypothesis is further supported by Antia et al. (1993) who suggested that cysts sinking in a coastal environment allowed repopulation to occur when conditions were more favourable but that this was unlikely to occur in the open ocean. Antia et al. (1993) suggested that if swarmers are released into the winter mixed layer they could be mixed to the surface on an annual basis. Acantharia may reside shallower in the water column after the shoaling of the deep winter mixed layer in the Subpolar North Atlantic, when the upper ocean is more physically stable, and this may explain the regular timing of the cyst sedimentation event after the shoaling of the MLD in the IB.

4.4.2.2 Acantharia Depth Distribution

The depth distribution of Acantharia is different for symbiont-hosting and cyst-forming Acantharia as the latter do not require light to acquire energy (Decelle & Not, 2015). The depth distribution of Acantharia is also likely to change on short timescales, i.e. daily to seasonal cycles (Bottazzi & Andreoli, 1982), with Schewiakoff, (1926) observing that Acantharia live in the surface layers during summer when the upper ocean is calm and sunny (Michaels, 1988) but descend to 100 - 200 m during winter, and that Acantharia are particularly sensitive to wave motion and changes in specific gravity.

The cysts in this study are of the order Holocanthida, which are thought to be a more primitive type of Acantharia compared to symbiont-hosting Acantharia, with fewer myonemes to control buoyancy regulation (Febvre & Febvre-Chevalier, 2001; Schewiakoff, 1926) and hence are often found below 400 m (Bottazzi, 1978). Previous literature found no cysts in the upper 50 m in a site near Antarctica with most cysts found between 150 and 300 m (Spindler & Beyer, 1990). Cyst observations from the East Greenland Sea found cysts at 100 and 300 m, with larger cysts (> 200 µm) dominating at depth (Antia et al., 1993). Adult Acantharia of the order Holacanthida and Chaunacanthida have been sampled thousands of meters deep in the water column with lipid reserves and food vacuoles (Antia et al., 1993; Bernstein et al., 1987; Schewiakoff, 1926). Acantharian gametes from cyst-forming clades have been sampled via 18S RNA data throughout the mesopelagic and bathypelagic Atlantic Ocean (Decelle et al., 2013 and references within) and juveniles have been sampled at high abundances between 500 and 900 m depth (Bottazzi & Andreoli, 1982). These studies suggest that juvenile Acantharia may develop from gametes in the lower mesopelagic and then ascend to undergo their annual reproductive cycle.

4.4.3 Carbon Sequestration or Strontium Shunt?

Research into Acantharia in the past decade has been revived due to their potential for contributing significantly to deep ocean carbon storage via the rapid sinking of their cysts in high latitude regions (Belcher et al., 2018; Decelle et al., 2013; Martin et al., 2010). One important consideration for whether this rapid flux of cysts contribute to deep ocean carbon storage, on climate-relevant timescales, is the viability of the sinking cysts. If the cysts collected in the deep ocean sediment traps are viable then within one annual cycle it is possible that the majority of the cyst organic carbon that reached the deep ocean will ascend as Acantharian gametes or juveniles. However, if the viable cysts have sunk too deep to repopulate the upper ocean successfully, as suggested in Section 4.4.2, the cyst driven POC flux may contribute to long term carbon storage. If the cysts are viable then cysts found in sediment trap samples should be handled similar to how larvae are handled in sediment trap samples, i.e. removed as a 'swimmer' and not included in the deep ocean carbon budget as it will lead to an inflated POC flux (Buesseler et al., 2007).

The process and depth of excystment is still not well understood. The amount of organic carbon released, via swarmers, into the surrounding waters and what percentage of swarmers, and associated carbon, will be unsuccessful in reproducing and hence will not ascend to the upper ocean is unknown (Antia et al., 1993). Furthermore, if juvenile Acantharia feed to form lipid stores and food vacuoles in the deep ocean (Schewiakoff, 1926), and later ascend they may be driving a net loss of carbon in the deep ocean. The ascending Acantharia would therefore only temporarily shunt POC to the deep ocean via cysts but on timescales of less than one year.

The influence of the sedimentation of Acantharian cysts on deep ocean POC flux might be temporary but the cysts can contribute up to 70 % of the annual particulate Sr flux to the deep ocean in a < 2 month period. The Sr fluxes measured during peak cyst flux in Trap NW in 2008 are the largest recorded Acantharian cyst Sr fluxes in the deep ocean and it was double the greatest Sr flux in Trap NW in 2007 and more than five times larger than the Sr fluxes in Decelle et al. (2013) from the Scotia Sea at 2000 m. The celestite coating of the cysts will dissolve in the deep ocean. The deep ocean is enriched by ~ 2 % in Sr compared to the upper ocean (Bernstein et al., 1987; de Villiers, 1999) and has lower water temperatures, which may slow the rate of dissolution, although the effect of increased pressure may counteract the concentration and temperature differences but there is limited knowledge of biogenic celestite kinetics (Rushdi et al., 2000). These conditions may be beneficial to the cysts' reproductive cycle and is discussed further in Section 4.4.5.

Celestite-coated cysts fluxing to the deep ocean rapidly shunt Sr to depth compared to mean oceanic residence time for Sr of 2 – 5 million years (de Villiers, 1999). Surface ocean Sr

concentration tends to be higher (by 1.5 %) at high latitudes and a Sr concentration profile at 60 °N 20 °W, had a minimum Sr concentration at 100 m and a maximum Sr concentration at 1700 m, with concentrations between 1330 and 2500 m elevated in Sr compared to the upper ocean de Villiers, (1999). This profile minima coincides with the depth supposedly inhabited by Acantharia in the upper ocean and the maxima coincides with the dissolution of cyst celestite at depth. Modelled Sr fluxes to the deep ocean were estimated using vertical Sr profiles for the Pacific Ocean and ranged between 0.05 to 6 mmol m^{-2} yr^{-1} (de Villiers, 1999), which is in line with sediment trap fluxes at 400 m (0.012 to 6 mmol m^{-2} yr^{-1}) and 900 m (0.06 to 0.74 mmol m^{-2} yr^{-1}) in the Pacific Ocean (Bernstein et al., 1987). I calculated the measured particulate, and particulate plus cyst, Sr fluxes as annual fluxes for comparison. Annual fluxes of particulate Sr in the IB ranged between 0.28 – 0.46 mmol m^{-2} yr^{-1} and annual fluxes of particulate and cyst fluxes ranged between 0.08 – 2.50 mmol m^{-2} yr^{-1}. The greatest cyst flux below 2000 m in the IB is comparable to 400 m sediment trap fluxes, whilst the particulate material fluxes sit within the expected values. The flux of Sr out of the upper ocean by Acantharian skeletons was predicted by Brass (1980), using three independent methods, as between 3 – 12 µmol m^{-2} d^{-1}. The total Sr fluxes during the cyst sedimentation events ranged between 0.2 – 88 µmol m^{-2} d^{-1} further highlighting the impressive magnitude of the Sr flux by the cyst sedimentation events.

Particulate Sr fluxes are usually driven by $CaCO_3$ fluxes as Sr is incorporated during $CaCO_3$ biomineralisation (de Villiers, 1999). Calcite has a much lower Sr content (1.5 µmol/mmol) compared to aragonite (8.6 µmol/mmol) but both of the Sr fluxes associated with $CaCO_3$ are small, even when $CaCO_3$ dominates the particulate fraction, compared to the Sr fluxes driven by the Acantharian cyst sedimentation. This Sr shunt to the deep ocean may have important consequences for the global Sr cycle and palaeotemperature Sr/Ca proxies that aim to reconstruct SST, particularly for Quaternary reconstructions with smaller changes in Sr/Ca ratios (Bernstein et al., 1987; de Villiers, 1999).

4.4.4 Encystment and Sedimentation Timing

The regular timing and annual sedimentation of Acantharian cysts in the IB implies that there is an evolutionary advantage to sinking rapidly to the deep ocean. The triggers for Acantharian encystment and subsequent sedimentation are not well understood due to sampling often occurring opportunistically and an inability to culture Acantharia for laboratory studies (Decelle & Not, 2015). From the first study on the deep ocean sedimentation event in the IB, Martin et al. (2010) hypothesised that the encystment and sedimentation timing coincides with the spring bloom so that the swarmers can feed on the spring bloom associated flux post-excystment. A similar cycle was observed in marine ciliate cysts with the peak fluxes coinciding with peak Chl *a*

concentration (Reid, 1987). For freshwater ciliates, the peak abundance of cells occurred during peak Chl *a* concentration, whilst the percentage of encystment had a negative linear relationship with Chl *a* concentration (multiple regression analysis, r=-0.77; Muller & Wunsch, 1999). The cyst flux from the 2007 - 2008 IB dataset and Chl *a* concentration in the surface ocean do not appear to have any relationship with the timing of the cyst sedimentation in Figure 4.6. This is supported by the observations of Belcher et al. (2018) with the greatest cyst fluxes during a year of anomalously low Chl *a* concentration. This may be due, in this study, to the use of monthly Chl *a* concentration satellite products, due to extensive cloud cover, which makes it difficult to explore these results in greater temporal resolution.

I hypothesised that the unstable water column in late March and April may play a role in repopulating the upper ocean with Acantharia; as the mixed layer shoals Acantharia may move to reside shallower in the water column but likely remain below the MLD. The Acantharia may then feed in the upper ocean before encystment and subsequent sedimentation being triggered by environmental factors. It is challenging to discern the trigger for encystment as there is no previous research on the timescale for Acantharia to complete encystment. For Traps NW and NE, which had large cyst fluxes in both years, the timing of the first cysts sinking out of the upper ocean coincides with the rapid shoaling event to an MLD of < 100 m. The physical processes driving the shoaling of the MLD could trigger the sedimentation, in a similar way observed by Michaels, (1988), in which Acantharia changed their buoyancy and sank to the bottom of a laboratory chamber when experiencing a physical disturbance, such as gentle stirring.

The timing of the first cysts leaving the upper ocean coincided with a plateau or decrease in PAR levels during early May. This could imply that light levels are a trigger for sedimentation, however cyst-forming Acantharia are generally thought to reside below 50 m, where changes in the light levels would be minimal (Decelle et al., 2013).

Acantharia in high latitude regions appear to have an annual temporal cycle in regions with high seasonality, with annual cyst sedimentation events sometimes preceding spring phytoplankton blooms (Bottazzi, 1978; Martin et al., 2010). However, for particularly cold high latitude regions, such as the Greenland Sea, the Scotia Sea and the Weddell Sea, the cyst sedimentation events appear to occur in summer (Antia et al., 1993; Belcher et al., 2018; Spindler & Beyer, 1990). In the Scotia Sea and the Greenland Sea the cysts sediment after the spring bloom associated chlorophyll peak, and after the peak POC flux, which may suggest different mechanisms triggering cyst sedimentation events. Furthermore, Belcher et al. (2018) suggested that because the high cyst flux in the Scotia Sea coincided with atypically low chlorophyll concentration, that the

heterotrophic Acantharia outcompeted other plankton as they could feed on bacteria and zooplankton.

4.4.5 Cyst-forming Acantharia Reproductive Cycle

The rapid sedimentation to the deep ocean of Acantharian cysts during the spring bloom was proposed by Martin et al. (2010) as advantageous to escape predation and to feed on the spring bloom associated particle flux. This hypothesis did not describe the possible mechanism by which juvenile Acantharia would ascend ~ 2500 m to repopulate the upper ocean in early spring within an annual cycle. Swarmers are < 5 µm in size (Decelle et al., 2013) and Acantharia shed their myonemes, which control buoyance regulation, during encystment (Febvre & Febvre-Chevalier, 2001) which makes it very unlikely that the swarmers ascend. However, juvenile or adult Acantharia, with myonemes for buoyancy control, may be able to rise through the water column but the fraction of the population that rises > 2000 m and reaches a hospitable upper ocean environment is unknown. Several previous studies on Acantharian cysts have found that cysts often do not reach the seafloor, with Antia et al. (1993) observing maximum cyst dissolution between 500 and 1000 m, which has also been observed in previous studies in varying locations (Bernstein et al., 1987; Spindler & Beyer, 1990).

The celestite cyst shell surrounding the swarmers may act as protection from predation, but I hypothesise it could also act as a timer, with the celestite dissolving at a slower rate in the cold, slightly Sr enriched, although still undersaturated, deep ocean. The celestite shell would eventually rupture releasing the swarmers at depth but the timing/delay mechanism cannot be predicted as the rate of the dissolution of biogenic celestite in the deep ocean is unknown. Bernstein et al. (1987) suggested that Acantharian cysts appear to have a much greater Sr concentration, and a smaller surface area than Acantharia skeletons, i.e. they may dissolve more slowly, which may support the idea of the cyst coating acting as a timer (Bernstein et al., 1987; Bishop et al., 1977). Furthermore, Antia et al. (1993) suggested for cysts sinking into the mesopelagic zone that dissolution may primarily occur subsequent to excystment and death. The celestite shell acting as a unique timing mechanism, as well as possible protection from predation, may provide an explanation for the ecological benefit of the energetically expensive process of incorporating celestite, which readily dissolves in seawater, as a major component of Acantharian cysts (Decelle & Not, 2015). Cyst-forming Acantharia are thought to be more primitive than the symbiont-hosting Acantharia (Schewiakoff, 1926), which may explain why symbiont-hosting Acantharia have a celestite skeleton even though, since hosting photosymbionts, they no longer undergo encystment.

Whilst the proposed strategy of Acantharian swarmers being released at the seafloor to feed off the spring bloom seems logical, previous studies of Acantharia have shown they are 'generalist' feeders, taking advantage of what is around them (Amaral-Zettler et al., 1997; Decelle & Not, 2015). Feeding studies found they mostly ate tintinnids, copepods, larvae, bacteria and a small amount of phytoplankton (diatoms and dinoflagellates; Amaral-Zettler et al., 1997; Bernstein et al., 1999; Decelle & Not, 2015; Swanberg & Caron, 1991). I cannot confidently conclude what the reproductive advantage of rapid sinking is for the Acantharian cysts in the IB, but I suggest that cysts that sink to shallower seafloors are more likely to repopulate the upper ocean within an annual cycle.

4.5 Conclusion

In this study I have confirmed the hypothesis that there is a regular annual sedimentation of Acantharian cysts to the deep ocean IB in spring. The high flux of cysts sampled in spring 2008 allowed improved estimates of *'in situ'* sinking rate, POC cyst content and Sr cyst content. The streamlined morphology, incorporation of celestite into the cysts and the fast sinking rates highlight the cysts purpose is to sink rapidly out of the surface ocean. I hypothesise that the benefit of a celestite coating may be to act as a timer as the celestite dissolves at the seafloor, delaying the release of swarmers and the reproductive process and aiding the Acantharia in repopulating the upper ocean during the next spring.

In this study, I aimed to explore the potential triggers of cyst sedimentation to attempt to better understand the reproductive advantage of sinking rapidly in spring. I found no clear trends with the timing of cysts leaving the upper ocean and changes in chlorophyll concentration, light or sea surface temperature. However, the timing of the rapid shoaling of the mixed layer depth coincided well, especially for the high cyst fluxes, with the first incidence of cysts sampled in the sediment traps. This rapid shoaling of the MLD occurred at the same time in both years, as did the start of the cyst sedimentation so further exploration would be needed to see if the timing co-varies or if this is an artefact of a small number of data points to draw conclusions from.

The reproductive cycle of Acantharia is not well understood. In this study I suggest that cysts that sink to shallower depths are more likely to repopulate the upper ocean in the following year. The IB cysts may have originated from Acantharia that have drifted with the upper ocean currents beyond the ideal locations for cyst sedimentation. This may mean that by sinking to a shallower seafloor the cyst swarmers may form Acantharia at depth, which then may ascend with the shoaling of the winter mixed layer and may regulate the annual timing of the cyst sedimentation event beginning in April.

Acantharian cysts have been reported to contribute significantly to deep ocean POC flux. In this study, cysts contributed up to 70 % of POC flux, but this is likely an artefact of the extremely low particle fluxes sampled in 2008. In 2007 Acantharian cysts contributed up to 48 % of the total POC flux prior to the spring bloom fluxes. If the Acantharian cysts are considered to be viable, I suggest that they should be treated as swimmers and removed from sediment trap samples, similarly to larvae. Viable cysts may lead to the formation of Acantharia, which will ascend to the upper ocean within an annual cycle, meaning minimal POC sequestration in the deep ocean, unless the cysts in the deep ocean IB are unable to return to the upper ocean. The annual particulate Strontium flux to the deep ocean is usually driven by fluxes of $CaCO_3$, which incorporates Sr, but in this study I found that the annual particulate Sr flux is dominated by the Acantharian cyst sedimentation event and this study has reported the largest cyst Strontium flux to the deep ocean to date. The Acantharian cyst Strontium shunt may have important consequences for the global Strontium cycle and Sr/Ca palaeoceanographic proxies, which are based on the assumption that Sr has a long residence time of 2-5 million years.

Chapter 5 Synthesis

5.1 Summary

In this thesis I aimed to further our understanding of the magnitude and drivers of deep ocean carbon sequestration by utilising the unique mesoscale spatial array of the four sediment traps deployed below 2000 m in the Iceland Basin between November 2006 and June 2008.

5.1.1 Key Finding in the Area of Carbon Sequestration

In Chapter 2, the mean annual POC flux to below 2000 m in the Iceland Basin was found to be similar to previous global and regional estimates (within +/- 16 %) with a similar transfer efficiency between 100 m and 2000 m as other North Atlantic estimates (Henson et al., 2011; Honjo et al., 2008; Lampitt & Antia, 1997). This suggests the Subpolar North Atlantic annual average carbon flux is similar to the mid-latitude North Atlantic. However, I demonstrated in Chapter 3 that 50 % of the annual flux arrived later in the annual cycle (summer) in the IB when compared to mid-latitude sediment trap results from the North Atlantic (early spring; Lampitt & Antia, 1997). This may suggest that, at higher latitudes, the spring bloom associated flux is not the only flux event that contributes significantly during an annual cycle and in different regions of the North Atlantic the timing and drivers of deep ocean carbon sequestration may vary.

5.1.2 Key Finding in the Area of Mesoscale Spatial Variability

Spatial variability in interior ocean carbon fluxes has rarely been studied (Guidi et al., 2008; Guieu et al., 2005) and mesoscale spatial variability below 2000 m has been explored in only one instance by Newton et al. (1994) in the North Atlantic centred around 48 °N and 20 °W between 3000 - 3700 m depth. The Newton et al. (1994) deep ocean carbon flux dataset originates from the JGOFS programme, in which one time-series from the Netherlands remains unpublished (Figure 5.1), and indicates that there are instances of mesoscale variability in summer and autumn in the Northeast Atlantic. The findings from Newton et al. (1994) suggest that, during spring, the sediment traps were unaffected by spatial variability on scales of 100 km, whereas during autumn a large POC flux event sampled by Newton et al. (1994) at 19.5 W was not observed by Honjo and Manganini, (1993) at 21 W for the same sampling period. Newton et al. (1994) concluded that the ‘missing’ autumn flux at 21 W was either due to issues with collection efficiency or genuine mesoscale variability in the deep ocean and called for more rigorous attention to mesoscale

variability in particle fluxes. The mesoscale variability in the JGOFS POC fluxes was much greater in magnitude than the instances of mesoscale variability presented in this thesis. The Netherlands JGOFS flux data varies greatly on short temporal timescales, which is usually missed by the 14 day sampling period of deep ocean sediment traps. Since the JGOFS programme few studies have researched the problem of the mesoscale variability of particle flux, particularly in the interior and deep ocean, meaning that many deep ocean flux studies often assume mesoscale variability to be negligible (Boyd & Newton, 1999). The gap in knowledge surrounding mesoscale variability in deep ocean particle flux was a motivator for this thesis and I have shown that mesoscale variability is not negligible on less than seasonal timescales.

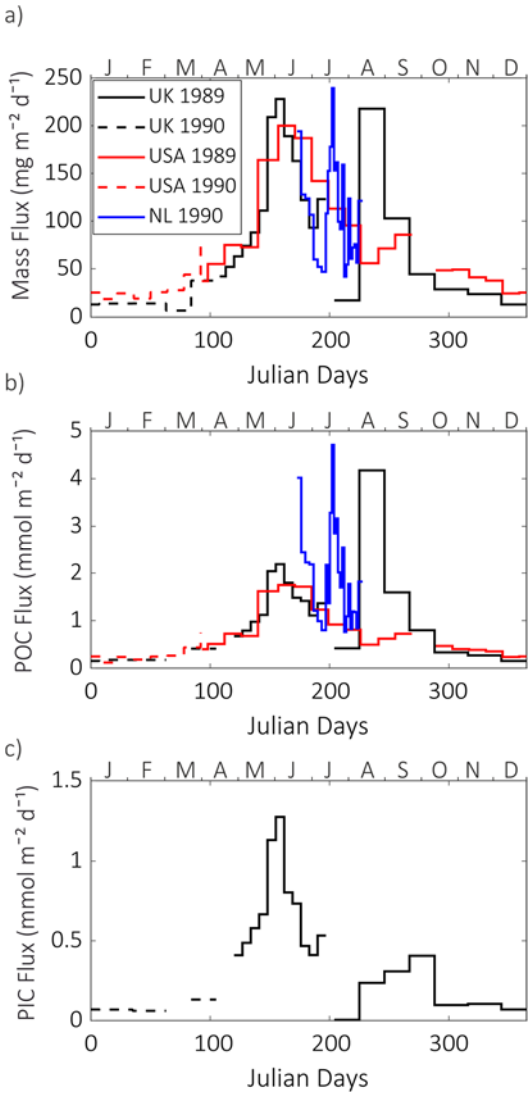

Figure 5.1 Mass flux, b) POC flux and c) PIC flux from three sediment traps deployed between 3000 and 3700 m depth around 48 °N and 20 °W in the North Atlantic Ocean in 1989 - 1990. The sediment traps were deployed as part of the JGOFS programme. The UK traps were deployed at 47.8 °N and 19.5 °W at 3100 m (Newton et al., 1994), the USA sediment traps were deployed at 48 °N and 21 °W at 3700 m between 1989 – 1990 (Honjo & Manganini, 1993), and the Netherlands sediment traps were deployed at 47

°N and 20 °W in 1990. The deep ocean fluxes from the latter have not previously been published.

Previously, the POMME study had four sediment trap moorings at 1000 m in the Northeast Atlantic deployed in a mesoscale array, which found that the variability of annual POC flux was 32 %, which was deemed to be significant (Guieu et al., 2005). The observed variability in POC flux between traps found by the POMME study is very similar to the 35 % threshold I defined to identify mesoscale variability in Chapter 2, based on the mesoscale variability in the upper ocean Iceland Basin of satellite ocean colour in Doney et al. (2003). There appears to be scientific consensus amongst these studies that spatial variability of one third of the total magnitude of fluxes for a mesoscale area (10 – 200 km) cannot be overlooked.

In Chapter 2 I concluded that mesoscale spatial variability in deep ocean carbon fluxes may be important, particularly on shorter than seasonal timescales, and may affect the interpretation of data at single location sediment traps at sustained observatories as a time-series i.e. ignoring spatial variability. The case studies of mesoscale variability explored in Chapter 3 found that increased POC fluxes coincided with increased BSi fluxes, likely diatom driven in spring, and often coincided with mesoscale eddies traversing nearby or over the sediment trap locations. An underwater vision profiler, used during the POMME study in the Northeast Atlantic to measure sinking aggregates in the upper 1000 m, concluded that in areas of increased eddy activity, fluxes may be temporarily influenced down to 1000 m on scales < 100 km (Guidi et al., 2007). The findings in this study and previous studies suggest that when interpreting transient signals from single sediment trap datasets, the presence of mesoscale eddies near to the trap location should be considered in detail, as in Conte et al. (2003) for the BATS deep ocean sediment trap fluxes. If sediment trap data is interpreted as a time-series, POC fluxes may be underestimated if there is eddy activity surrounding the sediment trap that hasn't influenced the sampled particle flux. Conversely, the POC flux may be an overestimate if there is low eddy activity around the wider trap location, but the sampled particle flux is influenced by a localised feature. That statement assumes that eddies always lead to increased POC fluxes in the deep ocean, which is in line with our findings from Chapter 3, but should be extrapolated to different temporal or regional settings with caution.

The quantitative importance of transient mesoscale events to deep ocean POC flux was calculated for each of these five case studies by combining the results from Chapter 2 and 3 (Table 5.1). The smallest contribution of the additional POC flux (i.e. case study POC flux – baseline POC flux) in a 14 day sampling period to the annual POC flux was 0.99 % and the largest contribution was 7.6 % during the spring bloom associated flux. The total contribution of mesoscale variability in deep

ocean POC flux for one annual cycle was 7.4 % for Trap NW, 8.6 % for Trap NE and 11.1 % for Trap C. Interestingly, none of the five instances of the greatest mesoscale variability were observed in Trap S fluxes and Trap S also had the lowest annual POC flux of the four sediment traps. Single location observations at sustained observatories may under or overestimate annual carbon budgets for a localised region by up to 11 % depending on whether mesoscale events are sampled or not. These findings support the idea that some instances of observed 'interannual' variability may be an artefact of localised mesoscale variability.

Table 5.1 The contribution of the mesoscale variability case studies to the annual POC fluxes for each sediment trap. The POC flux baseline was calculated by averaging the POC fluxes from the sediment traps that did not exhibit increased fluxes.

Case Study	Sediment Trap	POC Flux Baseline (mmol m^{-2} d^{-1})	Case Study POC Flux (mmol m^{-2} d^{-1})	Annual POC Flux (mmol m^{-2})	Contribution to Annual POC Flux (%)
1	NW	0.09	0.43	92.8	5.0
1	C	0.09	0.54	103.6	6.1
2	NW	0.03	0.19	92.8	2.4
3	NE	0.03	0.11	119.1	0.99
4	NE	0.31	0.96	119.1	7.6
5	C	0.46	0.83	103.6	5.0

5.1.3 Key Finding in the Area of Biological Drivers of POC Flux

The importance of community structure in terms of the biomineral content and planktonic composition of deep ocean particle flux has been demonstrated in this thesis. In Chapter 3, the link between increased BSi fluxes and increased POC fluxes were observed at several time periods throughout the annual cycle, both during the spring bloom and during periods of greater mesoscale variability, and is likely due to a greater contribution of diatoms to total flux. The role of decoupling between primary production, carbon export and upper ocean remineralisation has been explored in Chapter 3. Decoupling is known to occur during the early spring bloom, due to a temporal offset between PP and remineralisation, and decoupling may occur within a mesoscale eddy, due to a spatial decoupling occurring as particles are funnelled to depth and hence bypass the most active remineralisation zone in the upper mesopelagic, leading to the efficient sequestration of carbon in the deep ocean (Buesseler, 1998; Henson et al., 2019; Omand et al.,

2015; Waite et al., 2016). Therefore, the role of decoupling may be a critical factor in explaining the increased efficiency of POC fluxes to depth and may occur on a variety of spatial scales. Decoupling could explain why elevated BSi fluxes are not always associated with increased efficiency of POC export, except during periods of decoupling prior to the peak spring bloom and within an eddy. The process and importance of spatial decoupling is an area that needs more attention as it is not currently parameterised by biogeochemical models and hence they may underestimate export flux and particle flux to the deep ocean during periods of decoupling (Henson et al., 2019).

The annual sedimentation of Acantharian cysts prior to and during the spring bloom in the Iceland Basin further supports the importance of community structure as a driver of particle flux composition. My results show that deep ocean particle fluxes can be dominated by a monospecific planktonic component. The Acantharian cyst sedimentation events in the IB do not carry large magnitudes of POC to the deep ocean on timescales relevant to the climate system but the celestite-ballasted cysts will contribute considerably to the mass flux. If the majority of sampled Acantharian cysts are thought to be viable the cyst POC should not be included in deep ocean POC fluxes and carbon budgets but should instead be treated as larval stages and removed from the trap samples (Buesseler et al., 2007). The Acantharian cyst sedimentation event did transport large amounts of Sr to the deep ocean which may have important implications for Sr/Ca ratios used as a palaeotemperature proxy (de Villiers, 1999) and Sr should be considered as a non-conservative element (Bernstein et al., 1992). Ultimately, the observed fluxes of Acantharian cysts highlight the importance in understanding what components of the plankton community are found in sediment trap samples. Chapter 4 demonstrates how our understanding of these fluxes can change considerably by undertaking visual microscopy of samples as the Acantharian cysts in the IB were identified by P. Martin due to their unusual shape and relatively large size for a planktonic cyst.

5.2 Reflecting on Results

In this thesis I demonstrate the importance of considering biological and physical mechanisms in a mesoscale spatial context whereas most studies can only report on a singular sediment trap location. This is essential to develop an improved understanding of deep ocean carbon sequestration.

Previous research by Siegel and Deuser, (1997) estimated the statistical funnel above deep ocean sediment traps, which highlighted that understanding the temporal and spatial characteristics of the current flows above deep ocean traps is key to interpreting the variability in sampled fluxes.

Deuser et al. (1990) also suggested combining a mesoscale grid of moored sediment traps in the deep ocean, along with remote sensing and shipboard measurements, to allow for improved understanding of spatial and temporal variability in fluxes and could allow links with upper ocean processes to be made. The results in this thesis are the first step towards quantifying and understanding the drivers of mesoscale variability in deep ocean sediment trap fluxes. If increased biological data from remote sensing and depth resolved shipboard measurements were available, as suggested by Deuser et al. (1990), a more developed understanding of the links between upper ocean export and mesoscale variability in deep ocean particle fluxes would likely have been achieved, particularly in terms of whether the variability originates from the upper ocean or arises during the transit of particles to the deep ocean.

The original aim of this study, and the rationale for the unique mesoscale spatial array of the sediment traps in the deep ocean, was to provide an undisturbed time-series of deep ocean particle flux in the IB. For example, if a mesoscale eddy (usually of the order of 100 km) did pass over one or more of the sediment traps, due to the spatial array, a minimum of two sediment traps would be affected, with the other two sediment traps collecting efficiently. This implicitly assumed that sediment traps would undercollect particulate material if a mesoscale eddy passed over them. In this thesis I have shown that mesoscale eddies passing over trap locations led to increased POC fluxes under some circumstances. Conversely, a strong eddy feature from late December 2007 to January 2008 may have led to the issues with the unusually low fluxes in 2008, but this appeared to have affected every sediment trap to some extent, so the exact cause remains unclear.

An unfortunate aspect of the study was the 2008 sediment trap samples that exhibited signs of degradation and sampled unusually low fluxes. The NAB08 Lagrangian study of upper ocean export within a diatom bloom in May 2008 in the West of the Iceland Basin carried out detailed measurements on carbon export and mesopelagic flux using drifting sediment traps, ^{234}Th radionuclide measurements and backscatter measurements from gliders (Briggs et al., 2011; Martin et al., 2011). Examining the NAB08 results alongside the deep ocean particle fluxes in the IB would have been a unique opportunity to better understand the dynamics between primary production, carbon export and remineralisation of organic carbon fluxes down to 750 m with the fraction of flux that eventually reached the deep ocean (Briggs et al., 2011; Martin et al., 2011). The T_{eff} during the May 2008 upper ocean study was found to be very high down to 750 m (24 – 43 %) and it would have been a highly informative observation to determine if the localised high T_{eff} impacted the POC flux below 2000 m in the IB (Martin et al., 2011).

The unusually low fluxes during Period IV (December 2007 to June 2008) highlight that, in the IB, sediment traps may not be the most suitable instrumentation to provide undisturbed, accurate, year-round estimates of carbon flux due to fast current speeds in the IB, which may lead to undercollection of sinking material (Baker et al., 1988; Buesseler et al., 2007). There are very few other methods for measuring particle flux signals in the deep ocean and no other methods for capturing and analysing the biological components and chemical composition of particle flux in the deep ocean. In Section 5.3.1 I outline possible sampling regimes to overcome some of these issues and suggest an alternate location for repeating such an experiment.

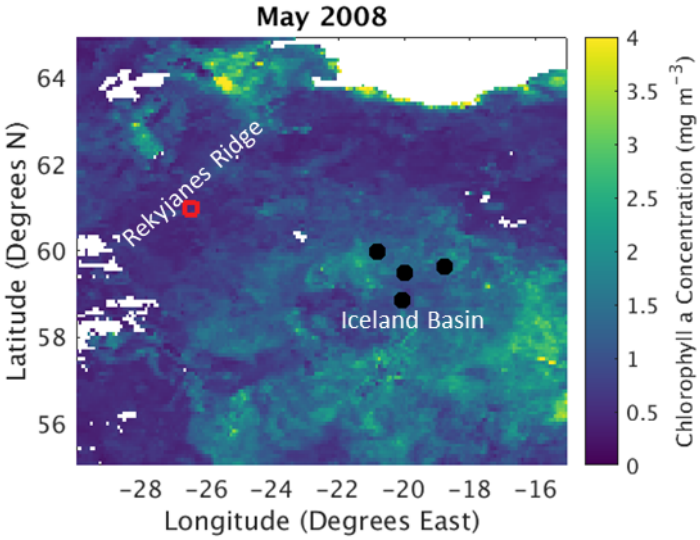

Figure 5.2 Monthly chlorophyll *a* concentration for May 2008 in the Subpolar North Atlantic. The black circles show the locations of the deep ocean sediment traps in the central Iceland Basin and the red square indicates the location of the May 2008 study by Martin et al. (2011) over the Rekyjanes Ridge. White pixels indicate cloud cover.

If the deep ocean particle fluxes in Period IV (December 2007 – June 2008) had been reliable, I could of have tested the hypothesis that efficient transport through the mesopelagic, as observed by Martin et al. (2011) in the Western Iceland Basin, would penetrate to the deep ocean leading to elevated deep ocean POC fluxes (Lampitt, 1985). The comparison would have improved understanding of the composition of flux reaching the deep ocean and how the composition of flux is altered by remineralisation between the euphotic zone and the mesopelagic zone. If this comparison had been possible the interpretation would have relied on the assumption that particle flux in the Western Iceland Basin over the Rekyjanes ridge was comparable to the central Iceland Basin. This may not have been justifiable as the Chl *a* concentration over the Rekyjanes ridge in May 2008 is generally lower than in the central Iceland Basin (Figure 5.2) although the sampling in the Western IB was carried out within a diatom bloom.

5.3 Recommendations for Future Studies

5.3.1 Investigating Mesoscale Spatial Variability

The Iceland Basin was a challenging region to attempt to link upper ocean processes with deep ocean particle flux for several reasons:

1. the complex topography and strong current velocity events in the deep water column
2. limited satellite chlorophyll *a* data due to the low angle of the sun in winter and high cloud coverage throughout much of the year
3. limited CPR data, particularly for the years sampled by the sediment traps

The methods employed in this thesis of identifying periods of mesoscale variability and using particle source regions to explore links between the upper ocean biological and physical processes could be utilised at other time-series sites to investigate further the main drivers of deep ocean carbon flux and subsequent carbon sequestration, even if there were not multiple sediment traps deployed.

The sediment traps in this study were deployed in a unique mesoscale spatial array whilst sediment trap deployments at sustained observatories are usually in a singular location. Identifying mesoscale spatial variability at sustained observatories is not possible using the methods in this study without a spatial array of sediment trap fluxes to average and compare. However, I propose that long-term time-series sediment trap data could be interpolated into a daily time-series (to account for variable timing of sampling periods in different years) and averaged to create a multi-year climatology of POC flux. The threshold method, used in Chapter 2, to identify transient changes in deep ocean POC flux by highlighting deviations of individual trap POC fluxes of > 35 % of the mean POC flux, could be used to identify interannual deviations to explore whether the variability is driven by mesoscale variability in the upper ocean or genuine interannual variability. This method would assume that there was no trend in the baseline of particle flux over the years used to calculate the mean climatology. Such a study could be carried out at sustained observatories such as the PAP Site, which also has a wide range of upper ocean data, including from sensors moored at 30 m, and generally lower current speeds in the deep ocean (usually < 10 cm s^{-1}; Lampitt et al., 2001), and would allow a better understanding of the processes in the euphotic zone related to deep ocean POC fluxes.

Sediment traps are the most widely used device to measure deep ocean particle fluxes, but as discussed in Section 5.2, issues with collection efficiency, and limited temporal and spatial resolution, can hinder the scientific community's ability to develop a mechanistic understanding

of what controls deep ocean particle flux. Optical devices have recently grown in popularity for measuring particle properties, such as fluorescence and backscatter, in the upper 1000 m in the ocean and can provide high resolution 3D and 4D coverage on scales not previously possible from shipboard or sustained observatories (Dickey et al., 2006). However, many optical devices have a limited maximum depth range, often between 600 – 1000 m, and hence are not suitable for sampling in the deep ocean. The WETLABS ECO-BB-RTD backscatter sensor has a depth rating down to 6000 m but rarely appears to have been used to measure backscatter in the deep ocean. Backscatter is now routinely used to carry out analysis of particle 'spikes' to estimate POC concentration and bulk sinking rates to estimate carbon flux (Briggs et al., 2011).

Backscatter has also been used in the deep ocean, with the instruments often termed nephelometers, to quantify seawater turbidity throughout the water column (Eittreim et al., 1976). Nephelometer studies have found that turbidity is closely linked to the biogenic rain of particles (Eittreim et al., 1976) and have been used to quantify deep ocean turbidity increases caused by benthic storms in the Northwest Atlantic (Gardner et al., 2017) and to explore how global nepheloid layers relate to upper ocean dynamics (Gardner et al., 2018). However, these studies can only provide information on the concentration of particulate matter and hence cannot provide information on particle properties or the biological and chemical content of particulate matter.

One possible interesting avenue for advancing the technology of deep ocean sediment trap studies would be to deploy a backscatter sensor above a deep ocean sediment trap to collect information on the relationship between particle spikes and POC flux in the deep ocean from the sediment trap samples. A spatial array of backscatter sensors could be deployed around a sediment trap location to further study the mesoscale spatial variability throughout an annual cycle in the deep ocean particle flux. Backscatter sensors have been used on Bio Argo floats down to 2000 m, but only results down to 1000 m have currently been published (Bellacicco et al., 2019; Mignot et al., 2018), and at an OOI mooring using a wire walker down to ~ 4000 m but this data has not yet been published. Autonomous underwater vehicles and gliders that can dive to 6000 m have been deployed but the signal to noise ratio becomes problematic at low particle concentrations, however they may still be useful during periods of elevated fluxes. An array of wirewalkers with backscatter sensors could also be deployed in a spatial array around a sustained observatory sediment trap mooring to increase the spatial, temporal and vertical resolution even further. Furthermore, using sensor technology in the deep ocean will increase the temporal resolution of particle flux measurements up to several orders of magnitude depending on the length of deployment and the sampling rate. The resolution of deep ocean sediment trap data, along with the lack of information in the 1000's of meters between the euphotic zone and the

deep ocean, and the limited spatial coverage, is a major factor hindering the progress of further understanding what controls flux to the deep ocean and how it varies globally.

5.3.2 Improving Particle Source Region Estimations

For future studies attempting to predict sediment trap particle source regions using *in situ* data I would suggest having an array of current meters deployed in a mesoscale array around the sediment trap, and if feasible, at several depths throughout the water column. One of the issues with using the singular locations of the current meter data from the sediment traps and the simplistic 2 box model, is that it implicitly assumes that there is no mesoscale spatial variability in deep ocean currents. There is a high possibility of mesoscale variability in deep ocean current characteristics as suggested by observed links between upper ocean eddy kinetic energy and deep ocean benthic storms (Gardner et al., 2017). Another way to improve the estimates of sediment trap particle source regions may be to use *in situ* upper ocean current velocities rather than the OSCAR derived current velocities between 0 – 350 m.

On reflection a more representative method of estimating sediment trap particle source regions may be to use a varying sinking speed, rather than a fixed sinking speed of 100 m d^{-1}, as in this thesis. For example, this study and previous studies have observed a rapid transit of particle flux to the deep ocean in spring, suggesting a 20 – 30 day time lag does not correctly represent spring particle flux (Asper et al., 1992; Deuser et al., 1990; Waniek et al., 2005b). However, assigning varying magnitudes of bulk sinking speeds during an annual cycle is challenging at present due to limited knowledge of how sinking speeds change with depth, time and particle flux composition (Villa-Alfageme et al., 2016).

5.4 Future Work

5.4.1 Ballasting: Silica versus Calcite?

In Chapter 3 the role of biomineral ballasting as a driver of POC flux to the deep ocean was explored. Increased BSi flux is correlated with the spring bloom related peak in POC flux and increased POC fluxes in the mesoscale spatial variability case studies coinciding with increased abundances of diatoms in the CPR data. The relationship between deep ocean POC flux and the $CaCO_3$ flux is strong and statistically significant but as to whether $CaCO_3$ is a driver of POC flux remains uncertain as there are no instances were $CaCO_3$ alone coincides with elevated POC fluxes. One possible area for future work would be to measure the size fractionated $CaCO_3$ in an attempt to separate the foraminiferal $CaCO_3$ from the coccolithophore $CaCO_3$ throughout the annual cycle

and the community structure controlling the $CaCO_3$ fluxes could be confirmed via scanning electron microscopy. From visual inspection, as discussed in Chapter 3, foraminifera tests appeared to have very little organic material associated with them whilst the coccolithophores were too small to identify using light microscopy. Different regions of the ocean are often classified as either a silica ocean or a calcite ocean but this is likely an oversimplification (Honjo et al., 2008). A more in-depth understanding of the origin of the $CaCO_3$ material reaching the deep ocean may aid in understanding the role of ballasting and possible shifts in biomineral importance throughout the annual cycle.

5.4.2 Acantharia Reproductive Strategy

Advancing understanding of the annual reproductive cycles of Acantharia is hindered by the lack of experimental work as Acantharia have never been successfully cultured (Decelle & Not, 2015). Furthermore, Acantharian cysts that sink to the deep ocean cannot be sampled in sufficient quantities without preservation in sediment trap samples, which would affect the properties of the cysts. An improved understanding of the dissolution kinetics of biogenic celestite under differing temperature and pressure conditions may aid in our understanding of the length of time that a cyst would remain intact in the deep ocean and whether the cyst organic coating protects them from rapid dissolution (Bernstein et al., 1992; Dove & Czank, 1995). In Chapter 4 I hypothesised that Acantharian cysts reproductive strategy was to sink to water depths < 1500 m to allow juveniles to ascend to the surface within one annual cycle. Tracking surface currents back in time for several months from the estimated Acantharian cyst upper ocean source regions may allow for determination of where the cysts likely ascended from. This may help inform where the majority of cysts sedimented, and if sedimentation occurs in shallower water depths, such as over the Rekyjanes ridge, or whether they likely remained within, and ascended from, the open ocean Iceland Basin. This will aid in confirming or rejecting the hypothesis I proposed in Chapter 4 that the cyst-forming Acantharian reproductive strategy is more successful if cysts sink to a shallower seafloor (< 2500 m) than in the central Iceland Basin.

5.5 Closing Statement

In this thesis I have reported on an annual cycle of deep ocean particle fluxes in the Iceland Basin. Utilising the unique mesoscale spatial array of the deployed sediment traps allowed for mesoscale variability in deep ocean fluxes to be identified, quantified and the drivers of the variability to be explored. Whilst this study has been a step forward in the scientific community's understanding of mesoscale spatial variability deep ocean particles fluxes, this area of research will only be significantly advanced with 4D sampling, which would have greater spatial, depth and temporal

resolution (Boyd et al., 2019). High spatial and temporal resolution datasets to target key processes specifically will hopefully provide information on whether processes, such as mesoscale eddies, need to be parameterised in global biogeochemical models. The interaction of mesoscale variability with ocean biogeochemistry and sinking particles may be necessary to represent fluxes of carbon to the deep ocean accurately. Alternatively, on larger geographical scales processes driving mesoscale variability may be negligible to global carbon sequestration in the deep ocean.

Appendix A Particle Flux Time Series

Particle fluxes and composition below 2000 m in the IB including the degraded samples (Table 3.4). In the results chapters the samples that were clearly degraded, mainly indicated by very degraded swimmers, were removed from the interpretation as they do not represent accurately the particle fluxes to the deep ocean Iceland Basin.

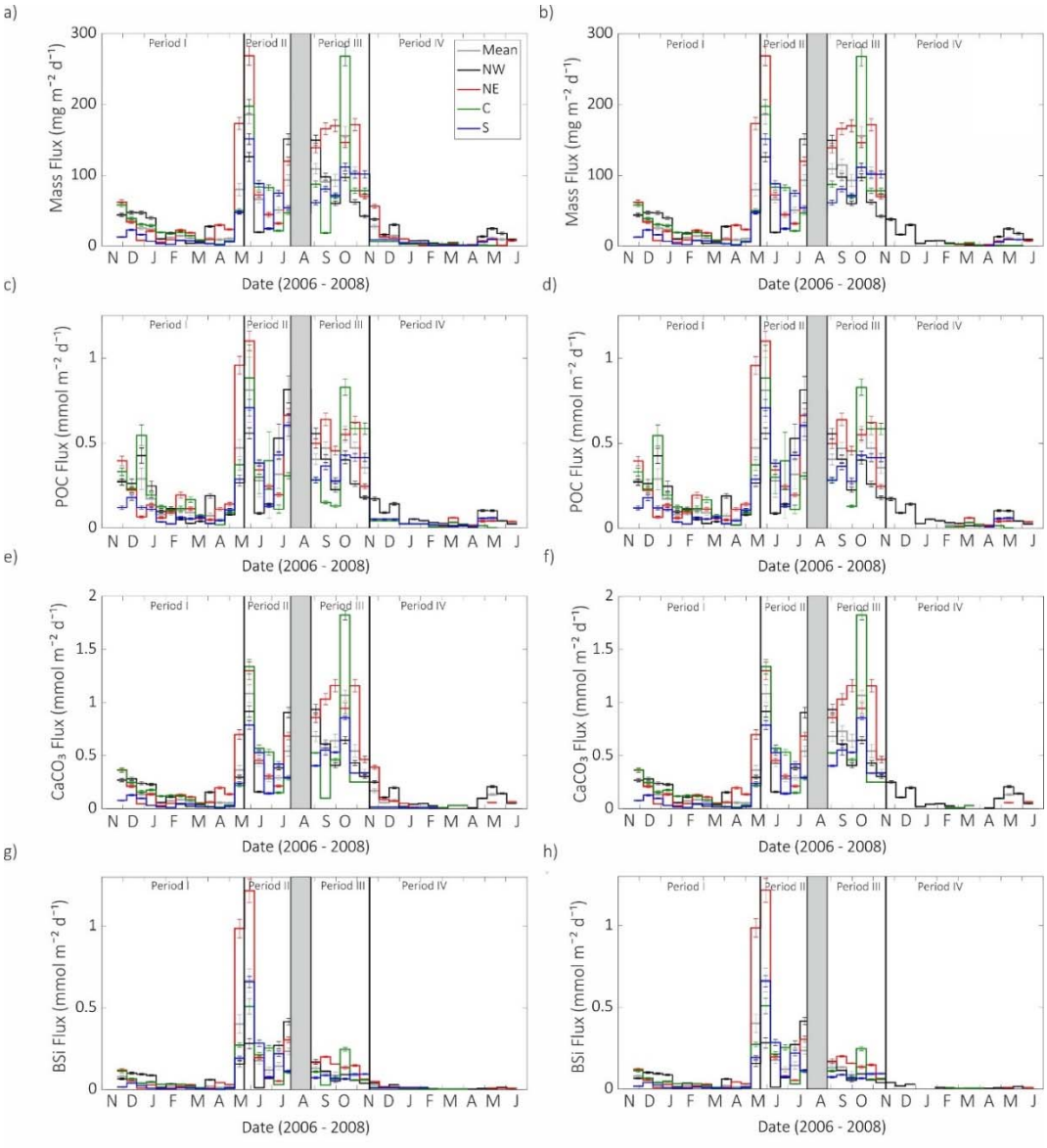

Figure A.1.1 Particle fluxes to below 2000 m in the IB (2006 - 2008). a) Mass flux (mg m^{-2} d^{-1}), b) mass flux (mg m^{-2} d^{-1}) with degraded samples removed, c) POC flux (mmol m^{-2} d^{-1}), d) POC flux (mmol m^{-2} d^{-1}) with degraded samples removed, e) $CaCO_3$ flux (mmol m^{-2} d^{-1}), f) $CaCO_3$ flux (mmol m^{-2} d^{-1}) with degraded samples removed, g) BSi flux (mmol m^{-2} d^{-1}), h) BSi flux (mmol m^{-2} d^{-1}) with degraded samples removed. The mean flux is in grey, Trap NW fluxes are in black, Trap NE fluxes in red, Trap C fluxes are in green and Trap S fluxes are in blue. The black vertical lines represent

the four flux periods outlined in Chapter 2. The greyed out period is the gap in sampling whilst the sediment traps were recovered and redeployed. The error bars show the propagated analytical uncertainty.

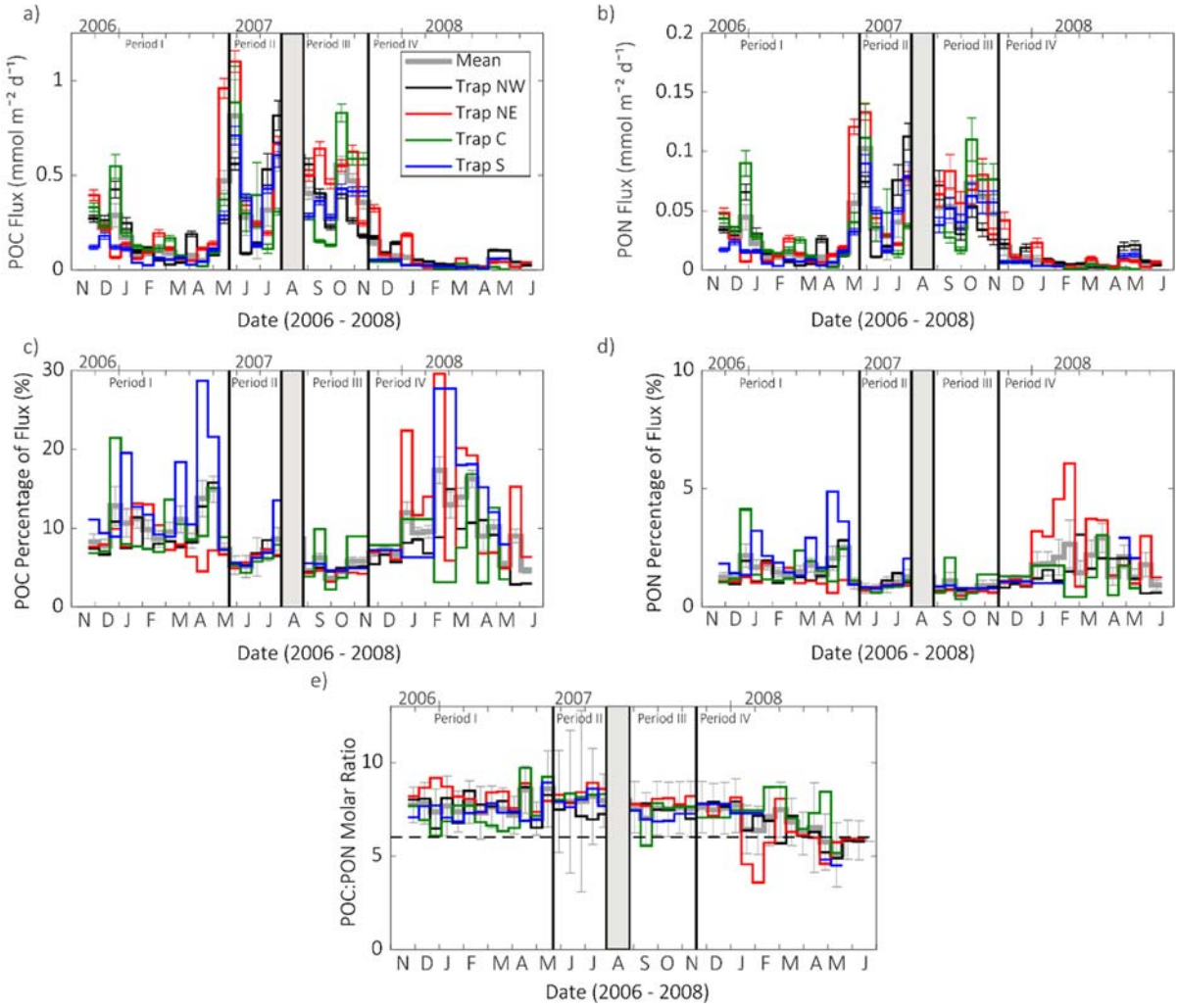

Figure A.2.1 a) POC flux, b) PON Flux, c) POC content of total flux (%), d) PON content of total flux (%) and e) POC:PON Molar Ratio below 2000 m in the IB for 2006 – 2008. For figure e) the dashed line represents a POC:PON ratio of 6, which is usually the minimum POC:PON ratio that is expected. Acantharian cysts tend to have a lower POC:PON ratio. The ratio in April and May 2008 is expected to be below 6 as cysts were the major contributor to flux.

Appendix B Biomineral Analysis

B.1 Calcite and Celestite Methodology

Table B.1.1 Multi-element standard concentration ranges for Na, Ca, Sr and Ba. The mean (± standard deviation) of the measured concentrations for the three fractions are presented. Underlined values indicate that the measurements have been utilised and data presented.

Element	Minimum Concentration (ppm)	Maximum Concentration (ppm)	Mean measured concentration (ppm)		
			Supernatant	Particulates	Cysts
Na	0.5	200	64.0 (± 21.2)	0.11 (± 0.36)	1.54 (± 1.59)
Ca	0.5	200	2.14 (± 0.54)	5.05 (± 1.58)	0.78 (± 1.07)
Sr	0.01	2	0.06 (± 0.09)	0.03 (± 0.04)	0.39 (± 0.59)
Ba	0.001	0.2	0.0002 (± 0.00009)	0.02 (± 0.01)	0.0009 (± 0.0009)

Table B.1.2 Intercomparison samples used to validate particle flux analysis in this study with the first deployment samples analysed by P. Martin.

Sample ID	Sampling Period	Type	Comparison Parameters
Trap NW (42) - 1	22.11.2006 – 05.12.2006	Late autumn	BSi
Trap NW (42) - 10	28.03.2007 – 10.04.2007	Pre-bloom	Ca/Sr, BSi
Trap C (43) - 6	31.01.2007 – 13.02.2007	Late winter	Ca/Sr, BSi
Trap C (43) - 10	28.03.2007 – 10.04.2007	Pre-bloom	BSi
Trap C (43) - 18	18.07.2007 – 29.07.2007	Late summer	BSi
Trap NE (44) - 14	23.05.2007 – 05.06.2007	Bloom	Ca/Sr, BSi
Trap NE (44) - 15	06.06.2007 – 19.06.2007	Post-bloom	BSi
Trap S (45) - 2	06.12.2006 – 19.12.2006	Early winter	Ca/Sr, BSi
Trap S (45) - 14	23.05.2007 – 05.06.2007	Bloom	BSi

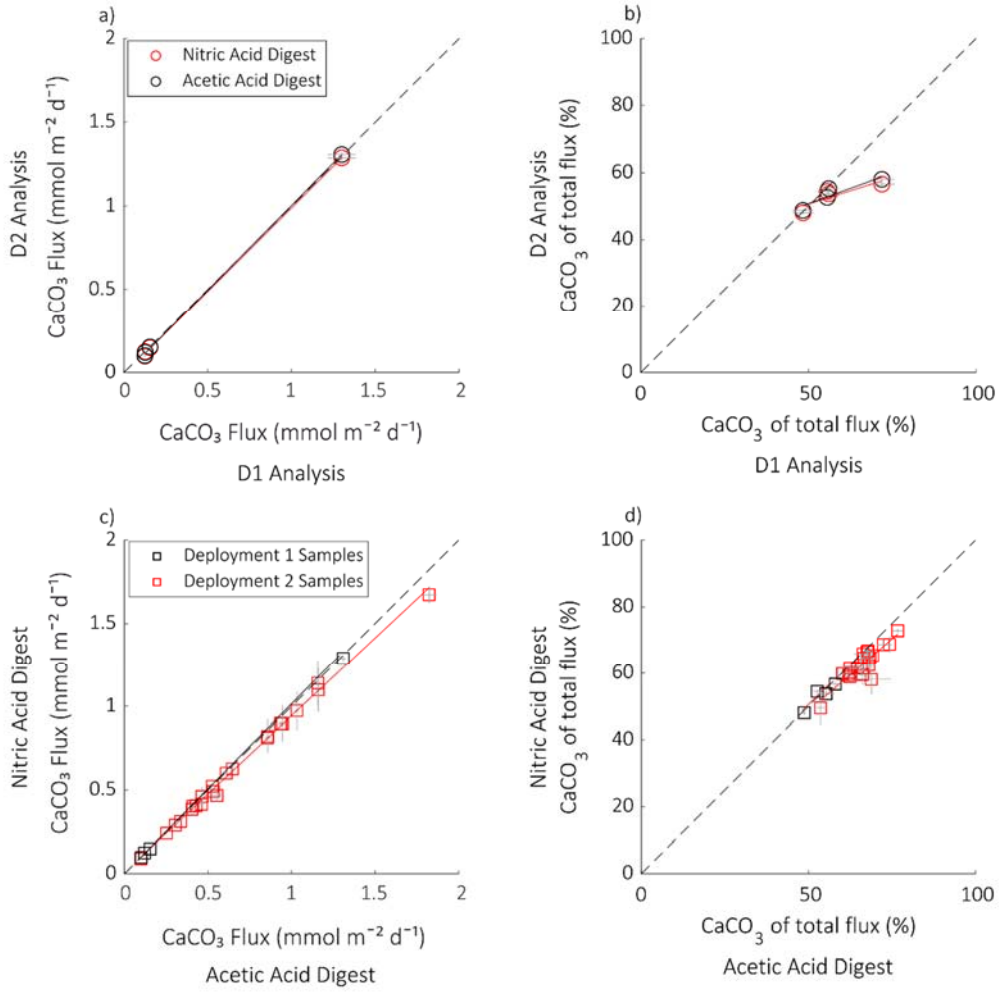

Figure B.1.1 Comparison of digest procedures for Calcium. a) $CaCO_3$ flux from the deployment 1 samples and analysis (which used an Acetic acid digest) compared with analysis of deployment 1 samples using a Nitric acid digest and an Acetic acid digest. b) $CaCO_3$ flux as a percentage of total mass flux for the deployment 1 samples, similar to a). c) $CaCO_3$ flux estimates when using a Nitric acid versus an Acetic acid digest for the re-analysed deployment 1 samples and for the deployment 2 samples. d) $CaCO_3$ flux as a percentage of total mass flux for the deployment 1 and 2 samples, similarly to c). The dashed black line represents the 1:1 line. The error bars show the propagated analytical uncertainty.

Figure B.1.1 suggests that there is very little difference between using a 0.4 M Nitric acid or a 1 M Acetic acid digest to measure Calcium. The Acetic acid digests, although originally picked as a weaker digest to minimise the amount of Ca released from lithogenic sources, rather than biogenic sources, appears to liberate slightly greater Ca than the Nitric acid digests. This small discrepancy makes very little difference to the $CaCO_3$ flux estimates. $CaCO_3$ as a percentage of total flux is not statistically significant due to one of the four values deviating from the 1:1 line but

all other deployment 1 comparisons have good agreement. All other statistical tests show good agreement between the Acetic acid and Nitric acid digests. The Acetic acid digest appears to liberate slightly more Calcium compared to the Nitric digests. The $CaCO_3$ percentage of total flux comparison for the deployment 2 samples, which was a more extensive comparison (n=22), was statistically significant with an R^2 value of 0.768 (Table B.1.3).

Table B.1.3 Linear model statistics for intercomparison samples for $CaCO_3$ analysis for both the Nitric acid and Acetic acid digests and for BSi analysis. The comparison was carried out between fluxes and percentage of total flux.

Parameter (digest type)	R^2 (*p* value)	Number of samples
$CaCO_3$ flux (Nitric acid; deployment 1 samples)	**1.0 (< 0.001)**	4
$CaCO_3$ content (% of total flux; Nitric acid deployment 1 samples)	0.6 (0.143)	4
$CaCO_3$ flux (Acetic acid; deployment 1 samples)	**1.0 (< 0.001)**	4
$CaCO_3$ content (% of total flux; Acetic acid; deployment 1 samples)	0.75 (0.087)	4
$CaCO_3$ flux (Nitric vs Acetic acid – deployment 2 analysis; deployment 1 samples)	**1.0 (< 0.001)**	4
$CaCO_3$ content (% of total flux; Nitric vs Acetic acid – deployment 2 analysis, deployment 1 samples)	0.77 (0.0811)	4
$CaCO_3$ Flux (Nitric vs Acetic acid – deployment 2 samples)	**0.996 (< 0.001)**	22
$CaCO_3$ content (% of total flux; Nitric vs Acetic acid – deployment 2 samples)	**0.768 (< 0.001)**	22
BSi Flux (Sodium Hydroxide)	**0.997 (< 0.001)**	9
BSi content (% of total flux)	**0.973 (< 0.001)**	9

B.2 Biogenic Silica Methodology

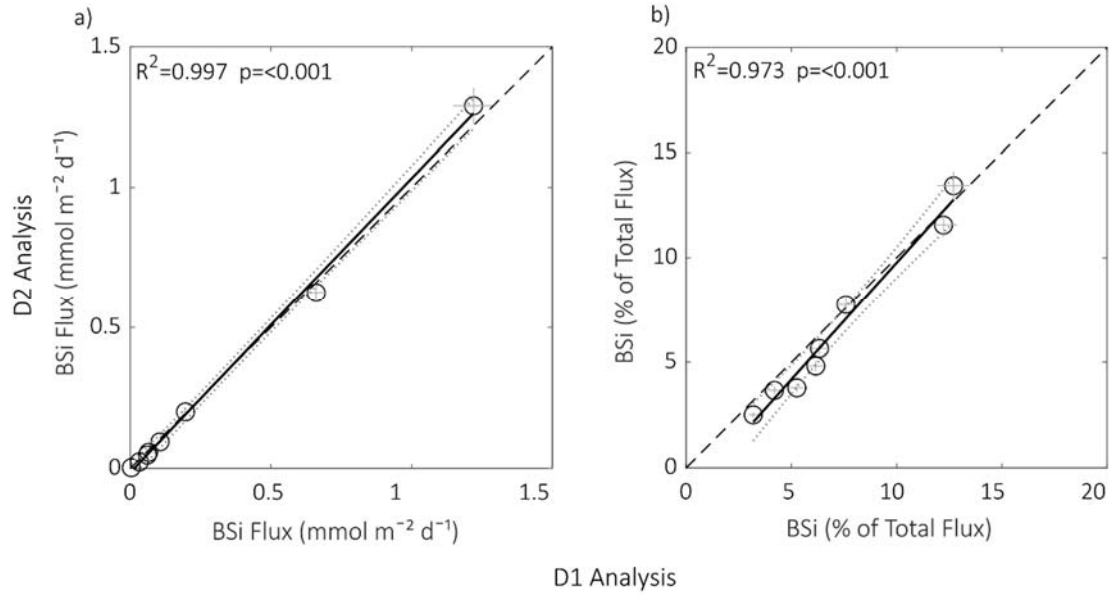

Figure B.2.1 Comparison of sediment trap samples analysed during deployment 1 (D1) with analysis of deployment 2 (D2) samples. a) Comparison of BSi flux (mmol m^{-2} d^{-1}) and b) comparison of BSi as a percentage (%) of total mass flux. The R^2 and *p* value of the very strong statistically significant relationships are shown. The dashed black line is the 1:1 line and the dotted grey lines are the 95 % confidence intervals. The grey error bars show the propagated uncertainty.

Sediment trap samples from deployment 1 were re-run during deployment 2 analyses to validate and compare the analysis. A range of samples were chosen to cover a range of flux types, as detailed in Table B.1.2, including the highest BSi flux samples from the time-series. The methodology used was very similar and results, which included any sediment weighing errors, compared excellently. The BSi fluxes plotted very close to the 1:1 line and had a positive strong statistically significant linear relationship (R^2 0.997, *p* value < 0.001). The relationship between the two sets of analyses for BSi as a percentage fraction of the total mass flux exhibited slightly more variation around the 1:1 line but still had a positive strong statistically significant relationship (R^2 0.973, *p* value < 0.001). This validates that the methods were consistent and that the time-series values should not be affected by differences arising from methodology.

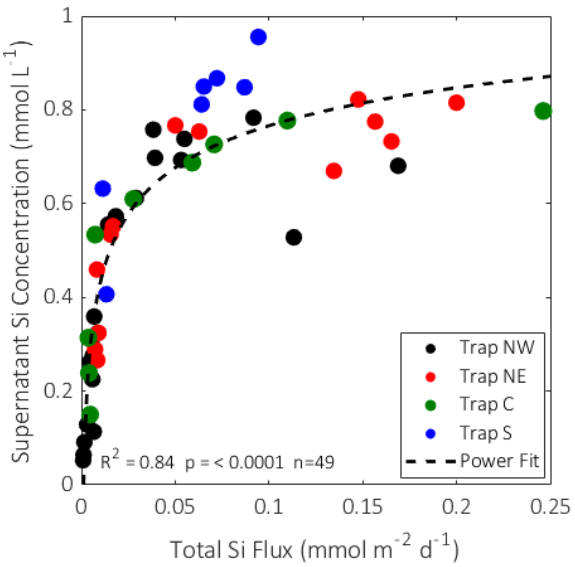

Figure B.2.2 Total (particulate + supernatant) BSi flux (mmol m^{-2} d^{-1}) compared with the supernatant BSi concentration (mmol L^{-1}). A strong significant positive power relationship was observed with an R^2 of 0.84 and a *p* value of <0.0001. The relationship indicates that BSi will dissolve up to excess concentrations of 0.96 mmol L^{-1} greater than blank sediment trap preservative (mean concentration of 0.0152 ± 0.0249 mmol L^{-1}, n=9).

The sediment trap filtered supernatant BSi concentration increases with the total BSi flux until a plateau at ~ 0.8 mmol L^{-1}. The supernatant BSi concentrations were corrected for the preservative blank, which is made with deep ocean seawater and had a mean BSi concentration of 0.015 mmol L^{-1}. This falls in line with the BSi saturation state in seawater, which at low temperatures ranges between 1 – 1.2 mmol L^{-1} (Bauerfeind & Bodungen, 2006). The BSi supernatant concentrations were corrected for evaporation as described in Section 3.2.1.2 and the largest uncorrected supernatant concentrations fell within 1 – 1.2 mmol L^{-1}.

Appendix C Particle Source Regions

C.1 Current Meter Velocity Processing

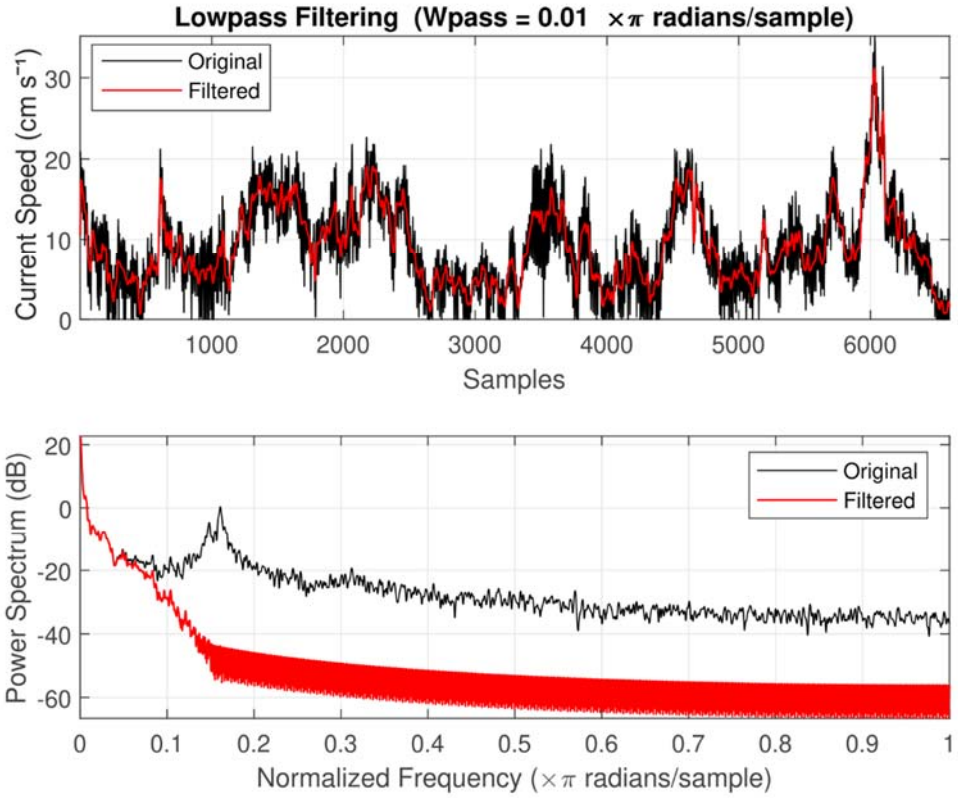

Figure C.1.1 An example of the lowpass filtered current speed data from the Trap C current meter deployed below the sediment trap. The lowpass() function in MATLAB was used with a *wpass* of 0.01. The lowpass filter smooths the current speed timeseries, removing hourly and tidal variability, as described by Waniek et al. (2000).

C.2 Data versus Model Comparison

The particle source region methodology was discussed in detail in Chapter 3, Section 3.2.2.

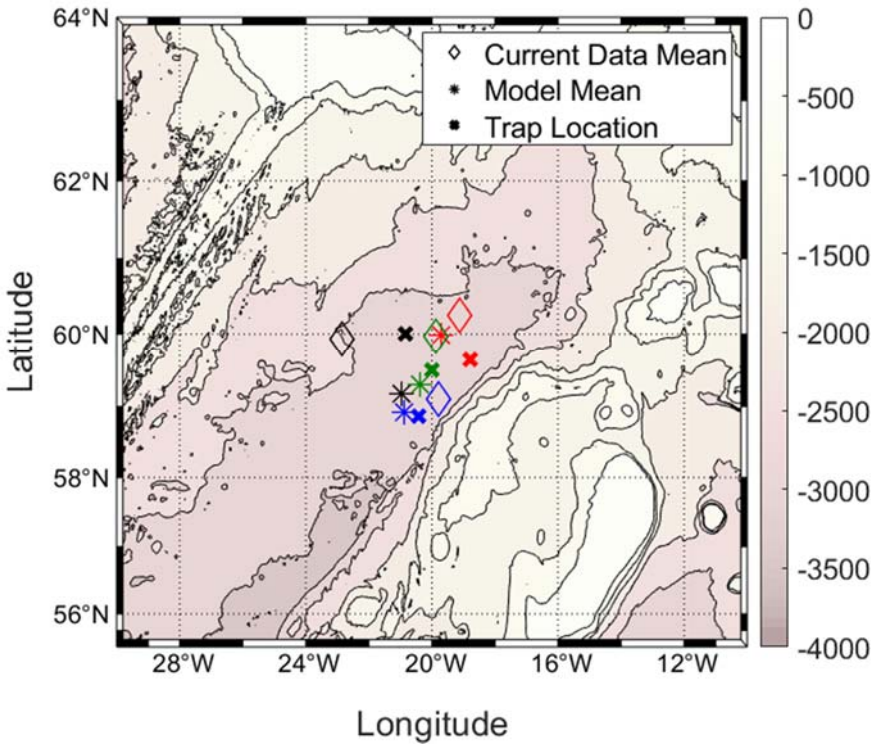

Figure C.2.1 The mean predicted particle source region for each sediment trap using current meter and OSCAR velocity (diamonds) and Copernicus model velocity (star). The crosses indicate the sediment trap locations. The particle source regions were predicted for deployment 1 and 2 for Trap C and Trap S but only deployment 1 for Trap NW and Trap NE as the deployment 2 current meter data were not successfully recovered.

C.3 Monte Carlo Simulations

Monte Carlo simulations were run to test whether errors in *u* and *v* current meter velocity components would cause the predicted particle source regions to show variability. The *u* and *v* components were allowed to vary randomly within +/- one standard deviation. Figure C.3.1 highlights that, as expected, the slower the assumed sinking speed the wider the predicted particle source regions extend. The particle source regions appear to have very similar shapes in Figure C.3.1, suggesting that errors in the *u* and *v* components would not affect the interpretation of the results in this thesis. The mean particle source regions for each sediment trap and sinking speed are detailed in Table C.3.1, with the RSDs shown in brackets. The RSDs between the 20 Monte Carlo simulations are all less than 1 % further suggesting that the errors in *u* and *v* will be negligible to the interpretation of the results in this thesis.

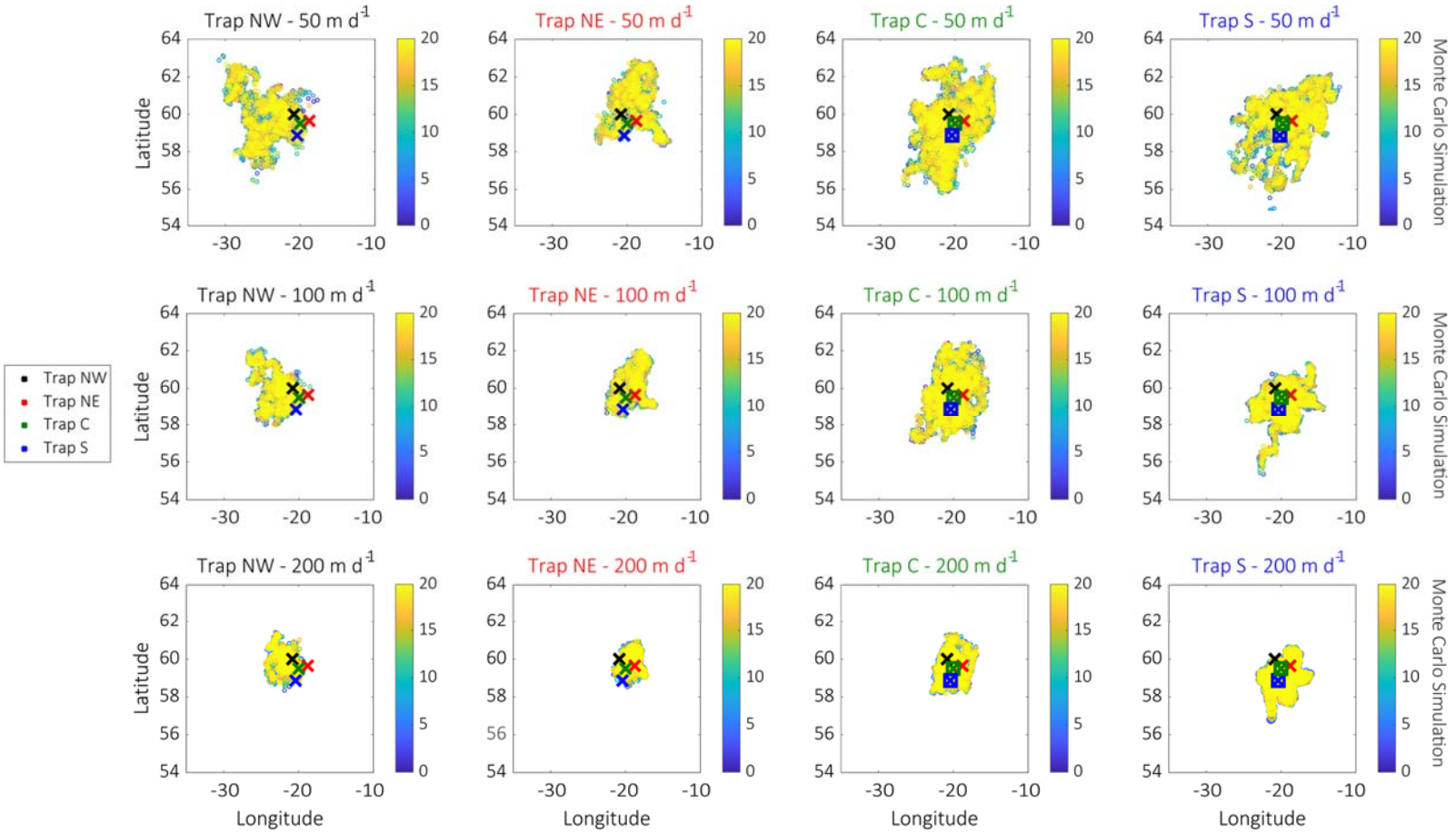

Figure C.3.1 Predicted particle source regions for each sediment trap using mean sinking speeds of 50 m d^{-1}, 100 m d^{-1} and 200 m d^{-1}. 20 Monte Carlo simulations (shown by the colour bar) were run to explore the errors introduced by +/- 1 standard deviation on the *u* and *v* components of the current meter velocity and OSCAR current velocity.

Table C.3.1 Mean latitude and longitude of each Monte Carlo simulation (+/- one standard deviation) for each sediment trap particle source region with assumed mean sinking speeds of 50 m d^{-1}, 100 m d^{-1} and 200 m d^{-1}. The RSD of the mean latitude and longitude of the 20 Monte Carlo simulations is shown in brackets.

Trap	Mean Latitude	Mean Longitude	Mean Latitude	Mean Longitude	Mean Latitude	Mean Longitude
	50 m d^{-1}		100 m d^{-1}		200 m d^{-1}	
Trap NW	59.8979 (0.078)	-24.4461 (0.32)	59.94878 (0.046)	-22.8442 (0.17)	60.03003 (0.017)	-21.8919 (0.12)
Trap NE	60.45659 (0.08)	-18.6148 (0.45)	60.11732 (0.032)	-18.7680 (0.19)	59.87425 (0.024)	-18.8352 (0.094)
Trap C	59.36339 (0.047)	-20.5896 (0.24)	59.64926 (0.015)	-20.2729 (0.15)	59.57977 (0.01)	-20.1306 (0.063)
Trap S	59.51092 (0.05)	-18.7991 (0.21)	59.10916 (0.023)	-19.6653 (0.13)	59.0013 (0.0087)	-20.0179 (0.063)

C.4 Acantharian Cyst Source Regions

The Acantharia cyst source regions in the upper ocean were estimated using the particle backtracking code described in Chapter 3.2.2 using the measured mean cyst sinking speed of 760 m d^{-1}. The mean measured sinking speed uncertainty was quantified by the standard deviation which was +/- 200 m d^{-1}. To explore the sensitivity of the source regions to different sinking speeds I ran the particle backtracking code for sinking speeds of 560 and 960 m d^{-1}. The estimated source regions are shown in Figure C.4.1 and Figure C.4.3. As expected, the faster the sinking speed the more localised the source region and the smaller the mean distance is from the sediment trap location. The differing source regions make little difference to the conclusions regarding the timing and triggers of the Acantharian cyst sedimentation event, as evidenced by Figure C.4.2 and Figure C.4.4.

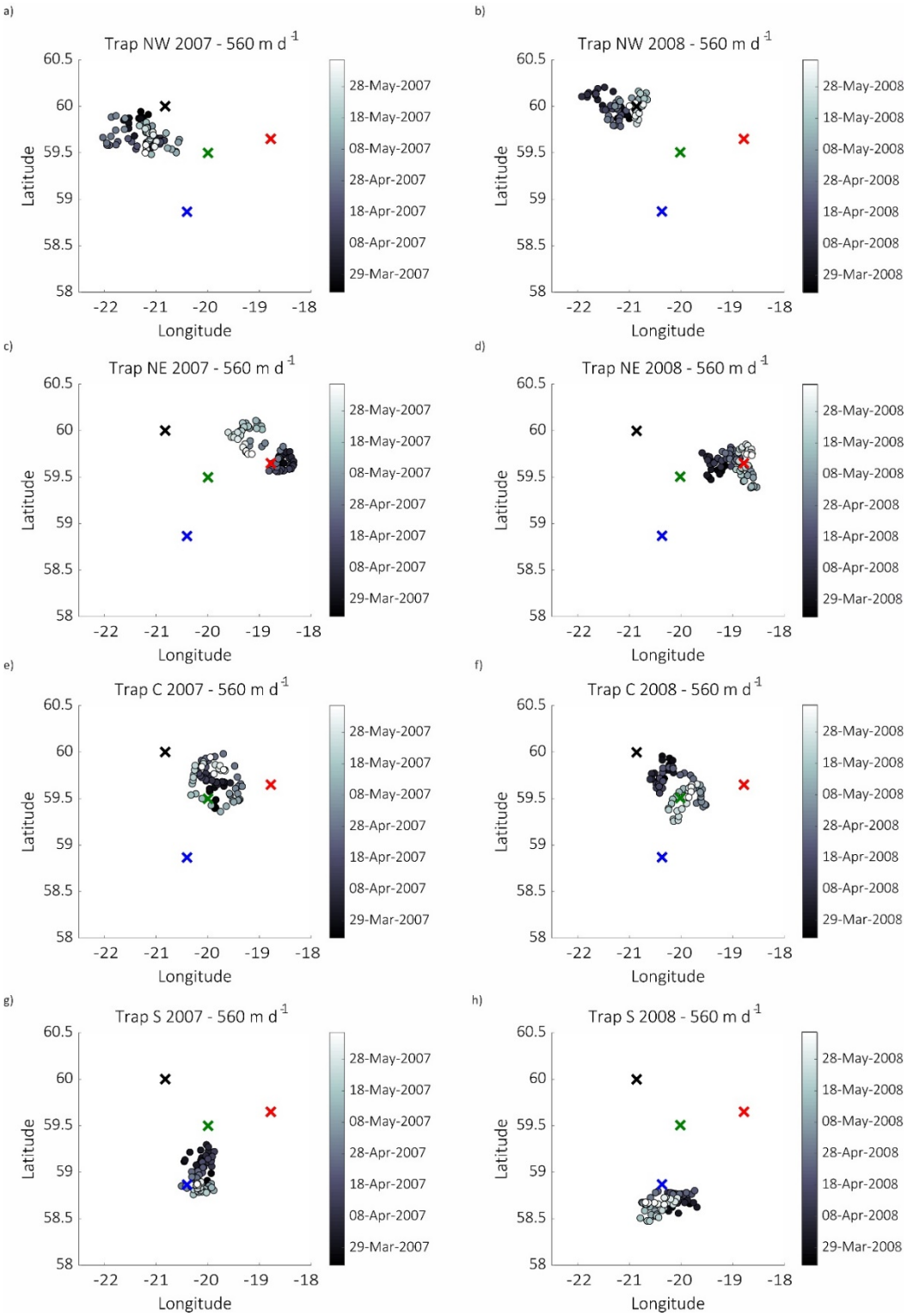

Figure C.4.1 Acantharian cyst source regions estimated using the lower uncertainty estimate of the measured sinking velocity of 560 m d^{-1}. The crosses represent the sediment trap locations: black is Trap NW, red is Trap NE, green is Trap C and blue is Trap S. Panels a), c), e) and g) are the source regions for the 2007 sedimentation event and panels b), d), f) and h) are the source regions for the 2008 sedimentation event. The marker colours represent the timing that the cysts reached the sediment traps during the sedimentation event.

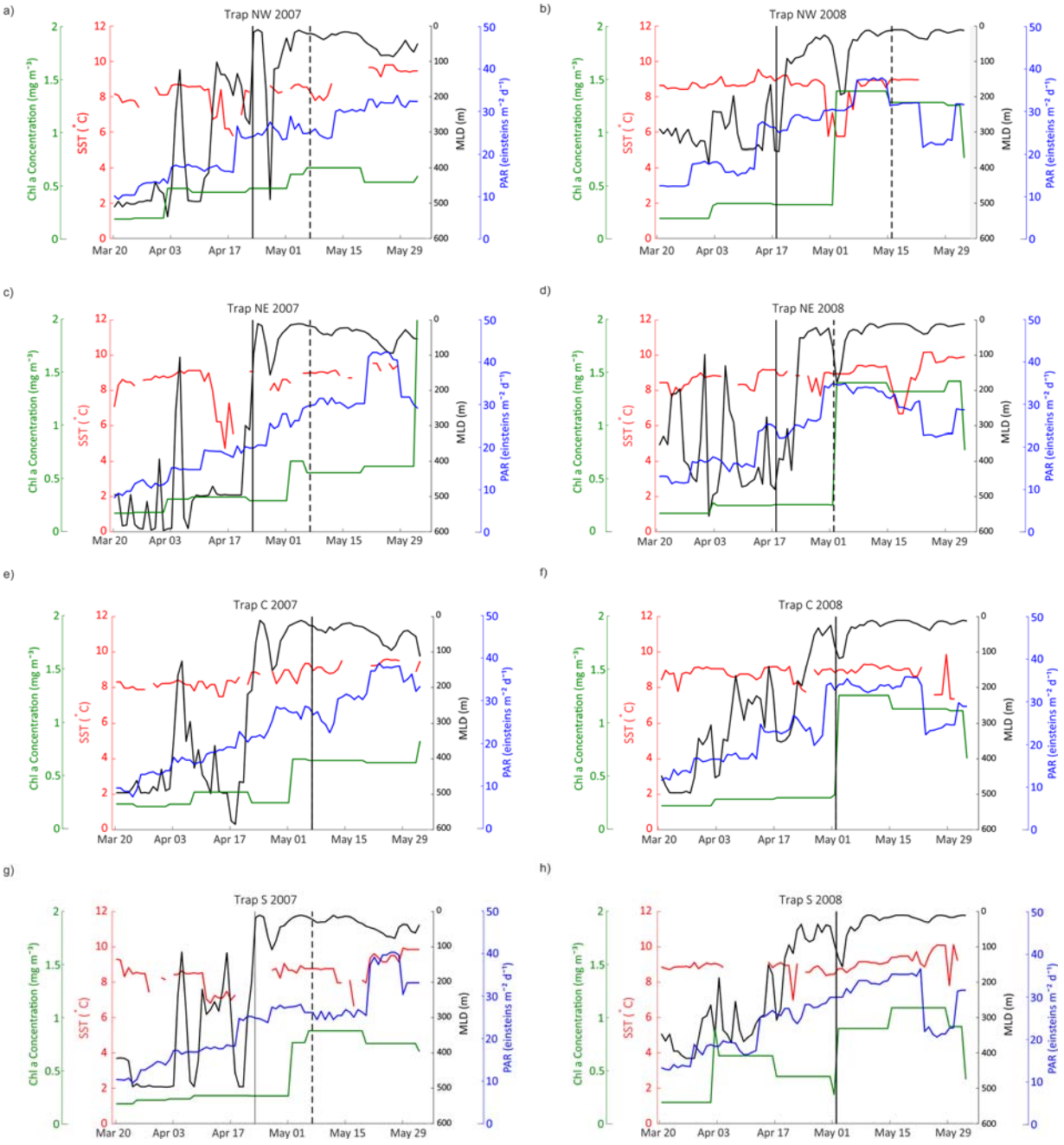

Figure C.4.2 Upper ocean environmental data for the Acantharian cyst predicted source regions using a sinking speed of 560 m d^{-1}. Each panel shows satellite-derived Chl *a* concentration, PAR and SST and physical reanalysis model derivation of MLD. The panels highlight the sedimentation events for 2007 for a) Trap NW, c) Trap NE, e) Trap C and g) Trap S and for 2008 for b) Trap NW, d) Trap NE, f) Trap C and h) Trap S. Each panel highlights the upper ocean date of the first occurrence of Acantharian cysts in a sediment trap sample with a solid black vertical line and the date that the peak abundance of cysts would have been in the upper ocean by a dashed black vertical line. For panels where there is only one line the first occurrence and peak in cyst flux coincide. This method assumes that the mid-point of the two week sediment trap sampling period is the most representative date and assumes that all the cysts would have taken 4 days to reach the deep ocean (560 m d^{-1} sinking rate is equivalent to 3.57 days to 2000 m).

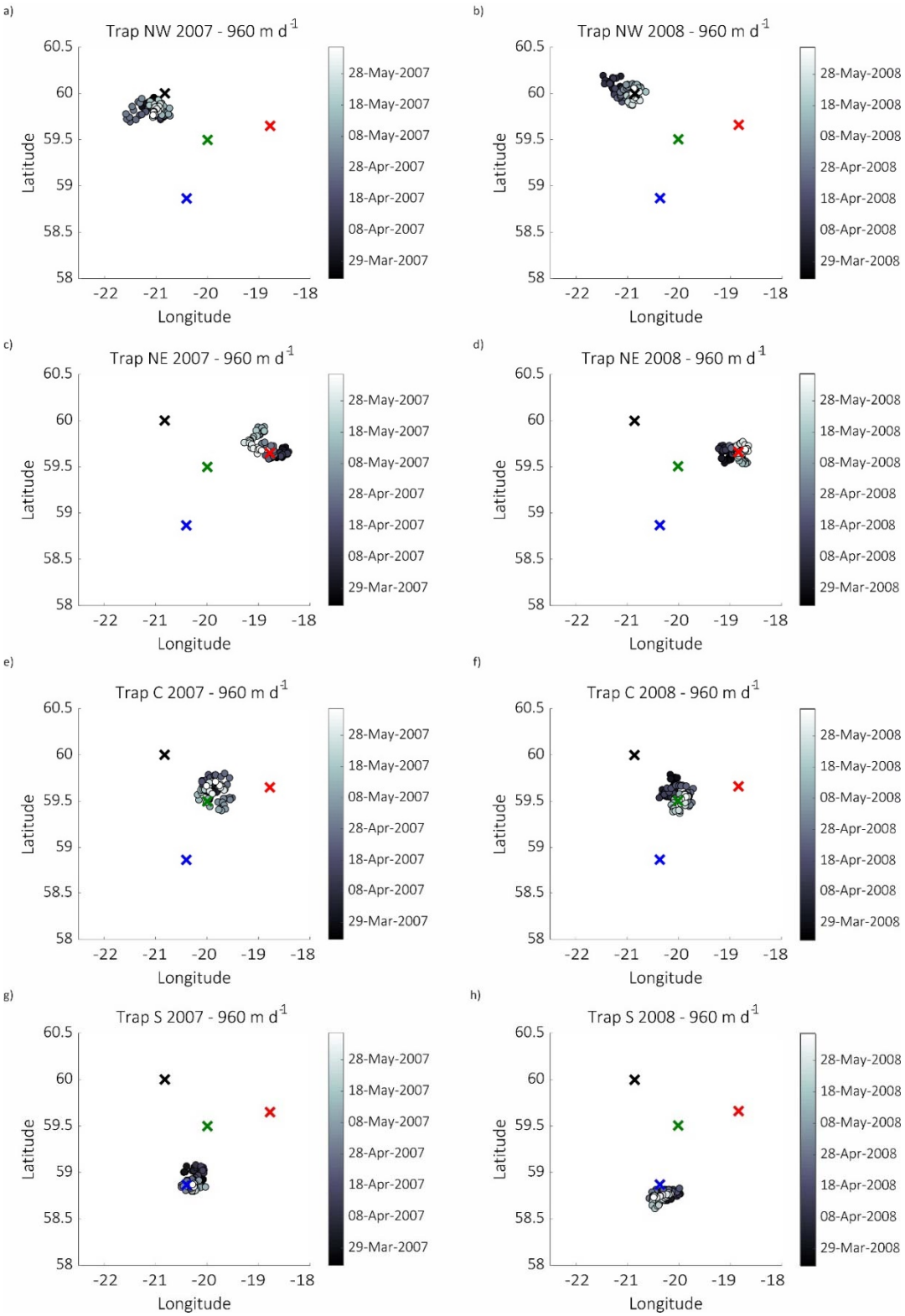

Figure C.4.3 Acantharian cyst source regions estimated using the higher uncertainty estimate of the measured sinking velocity of 960 m d^{-1}. The crosses represent the sediment trap locations: black is Trap NW, red is Trap NE, green is Trap C and blue is Trap S. Panels a), c), e) and g) are the source regions for the 2007 sedimentation event and panels b), d), f) and h) are the source regions for the 2008 sedimentation event. The marker colours represent the timing that the cysts reached the sediment traps during the sedimentation event.

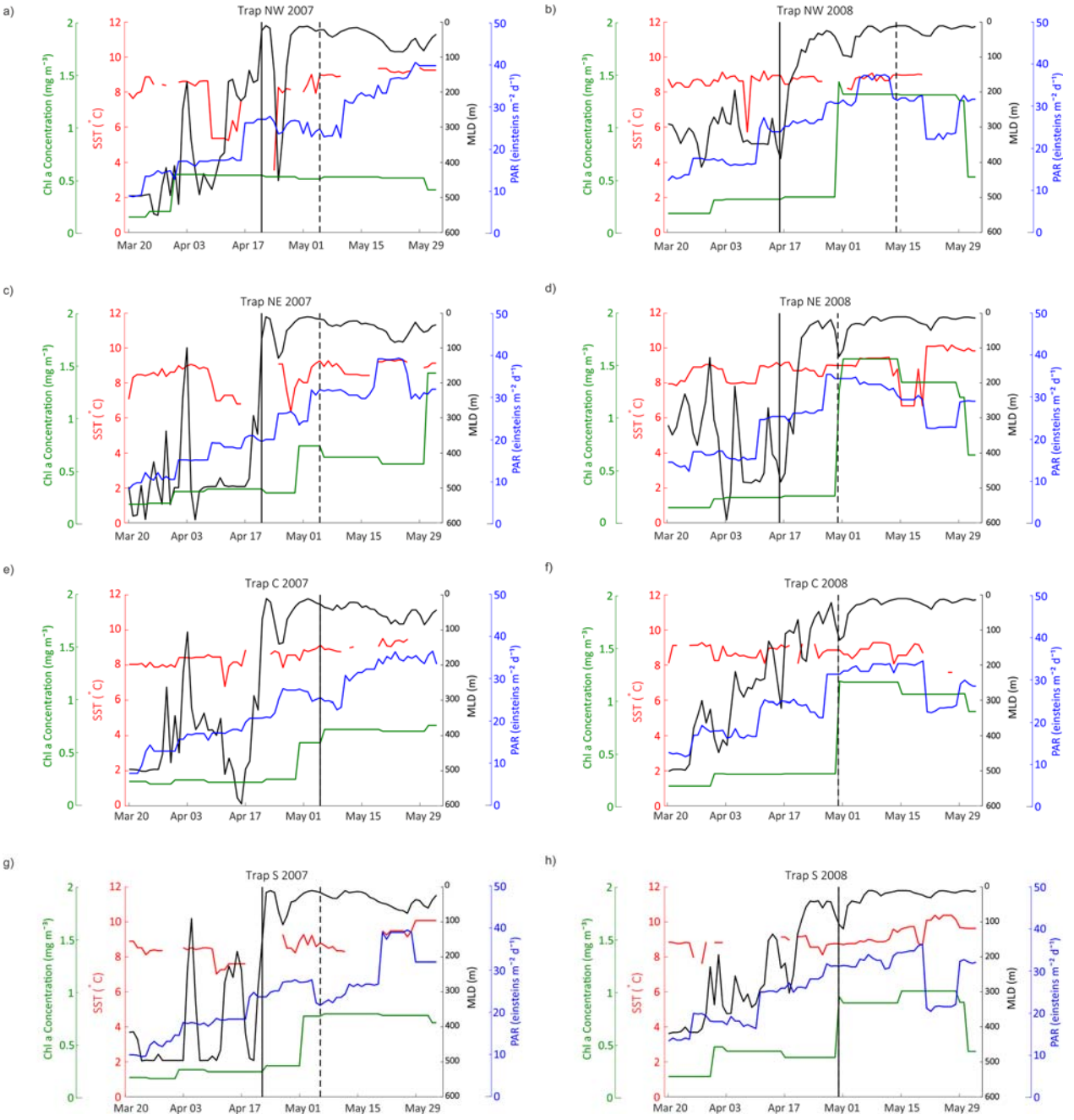

Figure C.4.4 Upper ocean environmental data for the Acantharian cyst predicted source regions using a sinking speed of 960 m d^{-1}. Each panel shows satellite-derived chl a concentration, PAR and SST and physical reanalysis model derivation of MLD. The panels highlight the sedimentation events for 2007 for a) Trap NW, c) Trap NE, e) Trap C and g) Trap S and for 2008 for b) Trap NW, d) Trap NE, f) Trap C and h) Trap S. Each panel highlights the upper ocean date of the first occurrence of Acantharian cysts in a sediment trap sample with a solid black vertical line and the date that the peak abundance of cysts would have been in the upper ocean by a dashed black vertical line. For panels where there is only one line the first occurrence and peak in cyst flux coincide. This method assumes that the mid-point of the two week sediment trap sampling period is the most representative date and assumes that all the cysts would have taken 2 days to reach the deep ocean (960 m d^{-1} sinking rate is equivalent to 2.08 days to 2000 m).

C.5 Variability in the Particle Source Regions

The main difference between the predicted source region for the Acantharian cysts using the Copernicus model output compared to the current meter and OSCAR surface velocity data, for the three sinking speeds, is that the source regions are more localised when using model output, similar to the results from Chapter 3 and Appendix C.2. However, the broad location of the source regions in relation to each trap agree well. The main traps that show different mean locations for the source regions are Trap S 2008 for all sinking speeds, Trap C 2007 for 960 m d^{-1} and Trap C 2008 for 560 m d^{-1}.

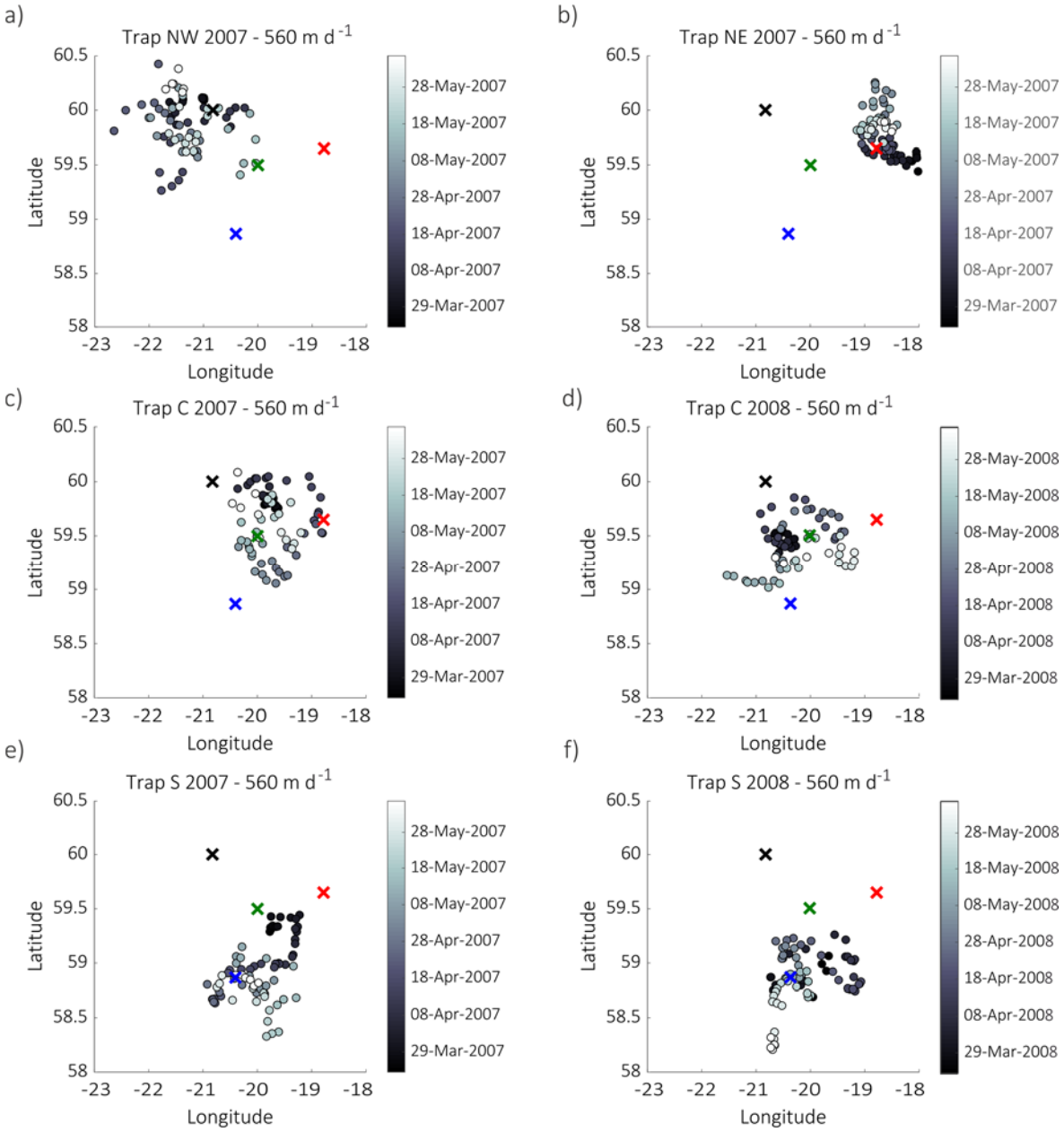

Figure C.5.1 Acantharian cyst source regions estimated using the lower uncertainty estimate of the measured sinking velocity of 560 m d^{-1} using current meter and OSCAR surface velocities. The crosses represent the sediment trap locations: black is Trap NW, red is Trap NE, green is Trap C and blue is Trap S. Panels a), b), c), and e) are the source regions for the 2007 sedimentation event and panels d) and f) are the source regions for the 2008 sedimentation event. There was no current meter data for Trap NW and Trap NE in 2008. The marker colours represent the timing that the cysts reached the sediment traps during the sedimentation event.

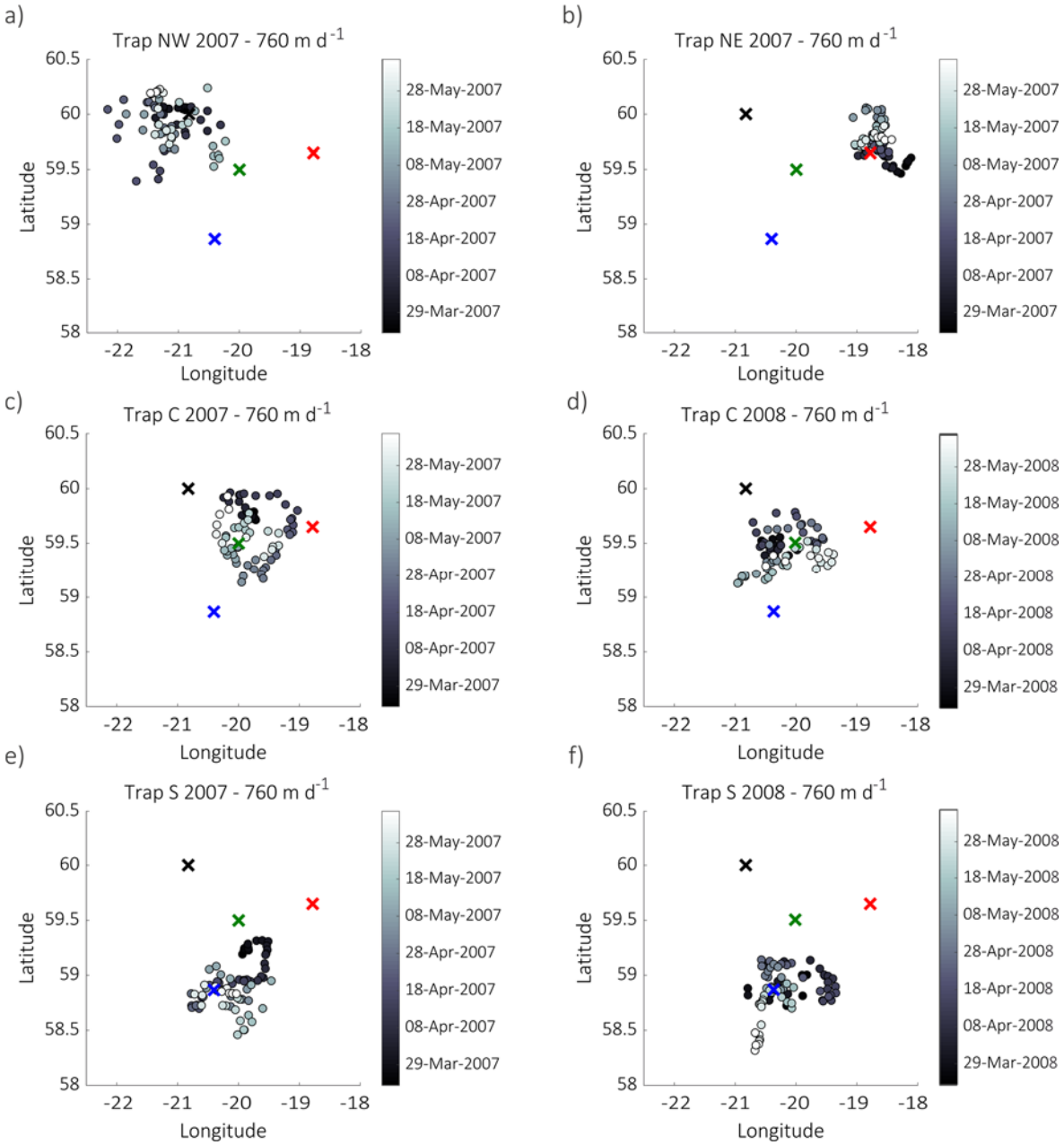

Figure C.5.2 Acantharian cyst source regions estimated using the mean measured sinking velocity of 760 m d^{-1} using current meter and OSCAR surface velocities. The crosses represent the sediment trap locations: black is Trap NW, red is Trap NE, green is Trap C and blue is Trap S. Panels a), b), c), and e) are the source regions for the 2007 sedimentation event and panels d) and f) are the source regions for the 2008 sedimentation event. There was no current meter data for Trap NW and Trap NE in 2008. The marker colours represent the timing that the cysts reached the sediment traps during the sedimentation event.

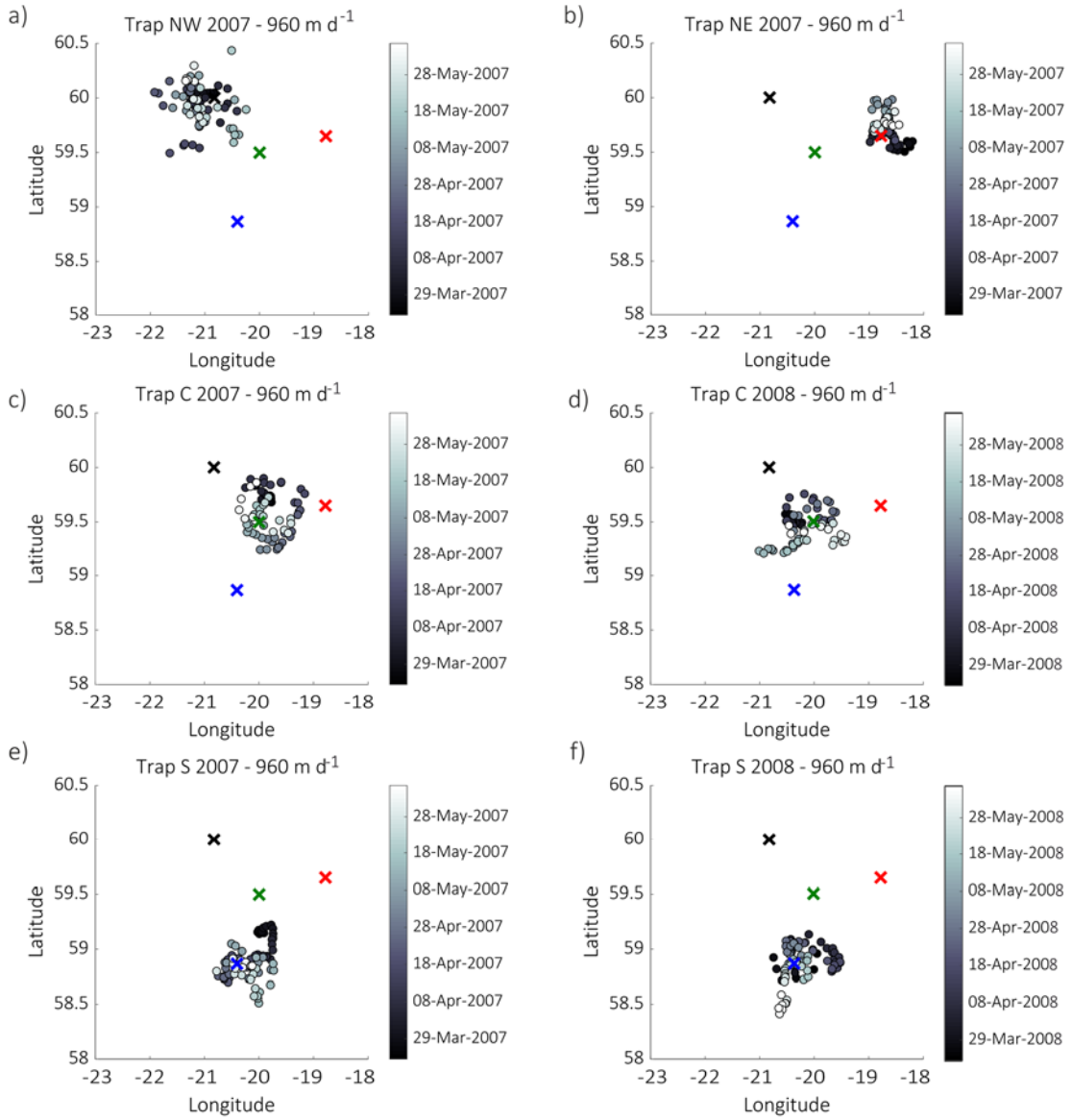

Figure C.5.3 Acantharian cyst source regions estimated using the higher uncertainty estimate of the measured sinking velocity of 960 m d^{-1} using current meter and OSCAR surface velocities. The crosses represent the sediment trap locations: black is Trap NW, red is Trap NE, green is Trap C and blue is Trap S. Panels a), b), c), and e) are the source regions for the 2007 sedimentation event and panels d) and f) are the source regions for the 2008 sedimentation event. There was no current meter data for Trap NW and Trap NE in 2008. The marker colours represent the timing that the cysts reached the sediment traps during the sedimentation event.

Appendix D Particulate Strontium Flux

To calculate the Sr budget for the IB and the contribution that Acantharian cysts make to the budget, the particulate and supernatant Sr flux data were required. As Sr was not measured in the particulate fraction for deployment 1 we have modelled the Sr contribution based on the measured $CaCO_3$ particulate flux. The major contributions to $CaCO_3$ flux are calcite, which mainly originates from organisms such as coccolithophores and foraminifera, and aragonite which is mostly likely to originate from pteropod shells. As part of the swimmer picking procedure, pteropod shells with intact body parts remaining are removed and counted as swimmers. In this case, some broken and empty pteropod shells remain in the sample and will contribute to the $CaCO_3$ flux and therefore the Sr flux. To model the particulate Sr flux we have used the Sr:Ca ratios from Villiers (1999), with a Sr:Ca ratio of 1.5 µmol/mmol for calcite and a Sr:Ca ratio of 8.6 µmol/mmol for aragonite. The deployment 2 measured particulate Sr fluxes were used to validate the assumptions for modelling the deployment 1 Sr flux.

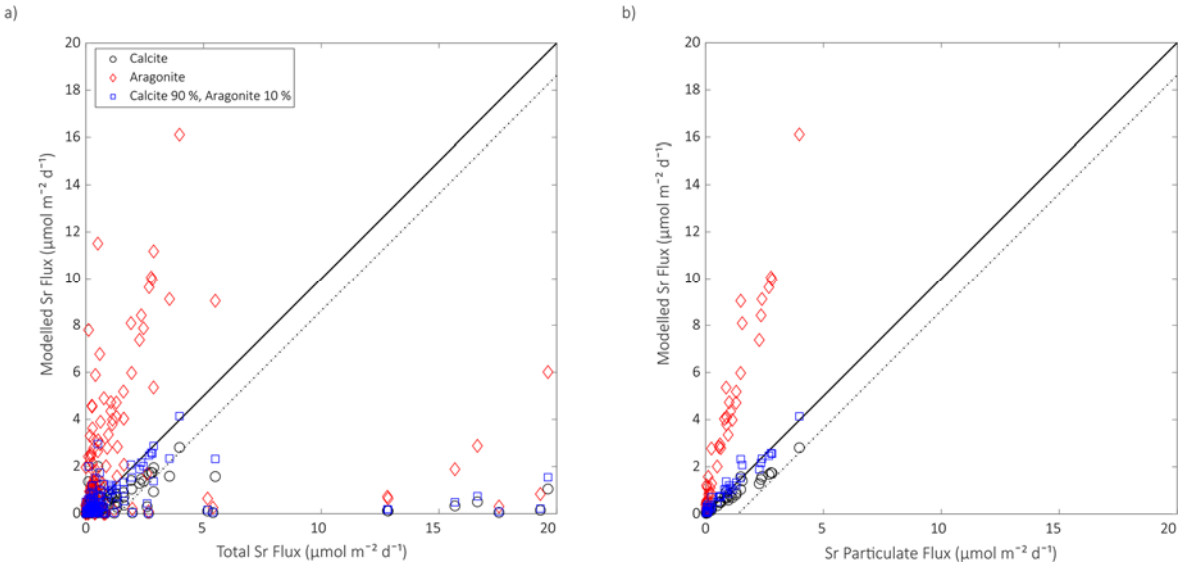

Figure D.1.1 Measured a) total Sr flux and b) particulate Sr flux compared to the modelled Sr flux. The modelled fluxes are estimated by multiplying the measured particulate Ca flux by 1.5 assuming all $CaCO_3$ flux consisted of calcite (black circles, Sr:Ca 1.5 µmol/mmol; Villiers, 1999), by 8.6 assuming all $CaCO_3$ flux consisted of aragonite (red diamonds, Sr:Ca 8.6 µmol/mmol; Villiers, 1999) or by assuming that 90 % of $CaCO_3$ flux is calcite and 10 % is aragonite (blue squares). The solid black line is the 1:1 line and data points that plot below the dashed black line are from samples that included Acantharian cysts and hence had elevated Sr fluxes.

Figure D.1.1 shows that assuming the $CaCO_3$ particulate flux only consists of calcite underpredicts the amount of particulate Sr in the samples, whilst assuming the $CaCO_3$ flux is only made up of aragonite clearly overpredicts the amount of Sr. A $CaCO_3$ flux composition of 90 % calcite and

10 % aragonite models the amount of particulate Sr flux very closely with the modelled Sr fluxes falling very close to the 1:1 line. For each trap the linear models have very strong significant linear relationships approaching an R^2 of 1 (Table C.1.1).

Table D.1.1 Statistical measures, R^2 (*p* value) of the strength of linear models between measured Sr fluxes and modelled Sr fluxes, with and without cysts, relating to Figure D.1. The total Sr flux ($\mu mol\ m^{-2}\ d^{-1}$) is the sum of the cyst Sr flux (unless stated as 'without cysts'), supernatant Sr flux and particulate Sr flux, except for deployment 1 samples in which particulate Sr was not measured. The particulate Sr was measured for deployment 2 and compares very well to the modelled particulate Sr, which assumes the $CaCO_3$ particle flux consists of 90 % calcite and 10 % aragonite.

	Incl. cysts	Without cysts	Without cysts
	Total vs modelled	Total vs modelled	Particulate vs modelled
Trap NW	0.03 (0.33)	0.597 (< 0.001)	0.90 (< 0.001)
Trap NE	0 (0.83)	0.86 (< 0.001)	1.0 (<0.001)
Trap C	0 (0.80)	0.89 (< 0.001)	0.99 (<0.001)
Trap S	0 (0.97)	0.67 (< 0.001)	0.96 (<0.001)

Appendix E Supplementary Work

The author of this thesis worked on two other research projects during the PhD study period which were ineligible to be included in this thesis. The journal articles are outlined below.

Baker, C. A., Henson, S. A., Cavan, E. L., Giering, S. L. C., Yool, A., Gehlen, M., Belcher, A., Riley, J.S., Smith, H. E. K., and R. Sanders. (2017). Slow Sinking Particulate Organic Carbon in the Atlantic Ocean: magnitude, flux and potential controls. Global Biogeochemical Cycles, 31, 1–15. https://doi.org/10.1002/2017GB005638.

This paper was based on initial research completed as part of the MSc Oceanography at the University of Southampton.

Baker, C. A., M. L. Estapa, M. Iversen, R. Lampitt and K. Buesseler (submitted to *Progress in Oceanography*, under review), Are all sediment traps created equal? An intercomparison study of carbon export methodologies at the PAP-SO site.

This paper was based on initial research completed during a 3 month SPITFIRE DTP (NERC) research placement at Woods Hole Oceanographic Institution during which time PhD candidature was suspended.

Appendix F

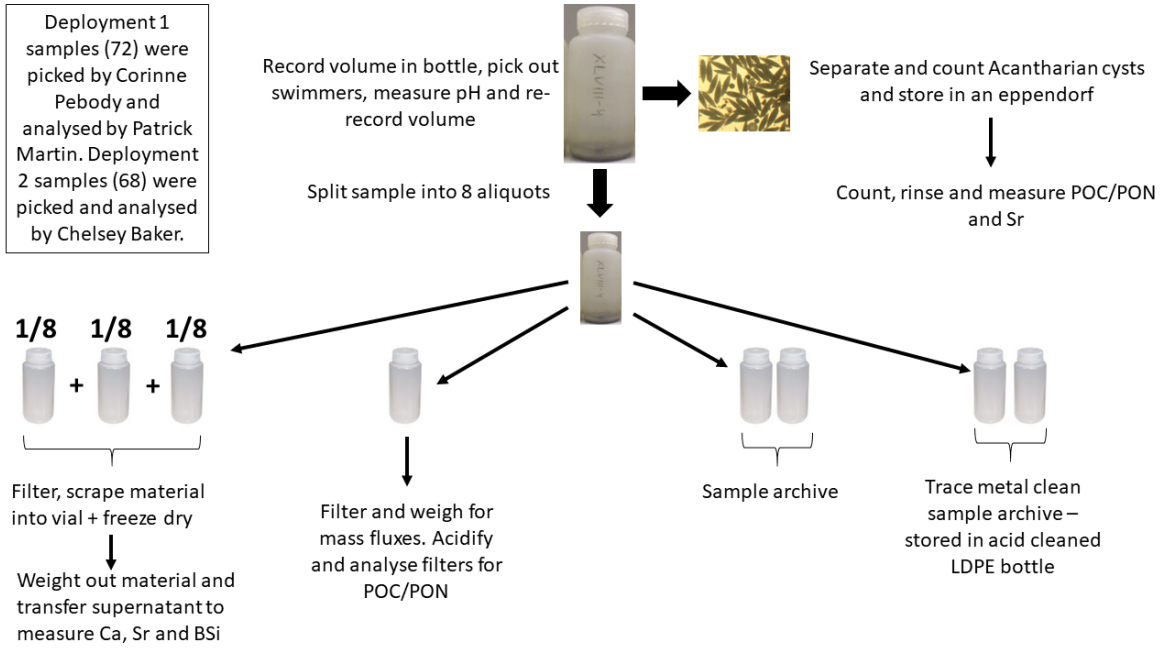

Figure F.1 Sediment trap sample preparation and analysis flowchart.

List of References

Abell, R. E., Brand, T., Dale, A. C., Tilstone, G. H., & Beveridge, C. (2013). Variability of particulate flux over the Mid-Atlantic Ridge. *Deep-Sea Research Part II: Topical Studies in Oceanography*, *98*, 257–268. https://doi.org/10.1016/j.dsr2.2013.10.005

Agusti, S., González-Gordillo, J. I., Vaqué, D., Estrada, M., Cerezo, M. I., Salazar, G., et al. (2015). Ubiquitous healthy diatoms in the deep sea confirm deep carbon injection by the biological pump. *Nature Communications*, *6*(May), 1–8. https://doi.org/10.1038/ncomms8608

Alldredge, A. L., & Gotschalk, C. C. (1989). Direct observations of the mass flocculation of diatom blooms: characteristics, settling velocities and formation of diatom aggregates. *Deep-Sea Research*, *36*(2), 159–171.

Amaral-Zettler, L. A., Sogin, M. L., & Caron, D. A. (1997). Phylogenetic relationships between the Acantharea and the Polycystinea : A molecular perspective on Haeckel's Radiolaria. *PNAS*, *5*(October), 11411–11416. https://doi.org/10.1073/pnas.94.21.11411

Anderson, T. R. (1992). Modelling the influence of food C:N ratio, and respiration on growth and nitrogen excretion in marine zooplankton and bacteria. *Journal of Plankton Research*, *14*(12), 1645–1671. https://doi.org/10.1093/plankt/14.12.1645

Anderson, T. R. (2005). Plankton functional type modelling: Running before we can walk? *Journal of Plankton Research*, *27*(11), 1073–1081. https://doi.org/10.1093/plankt/fbi076

Anderson, T. R., Gentleman, W. C., & Yool, A. (2015). EMPOWER-1.0: An Efficient Model of Planktonic ecOsystems WrittEn in R. *Geoscientific Model Development*, *8*(7), 2231–2262. https://doi.org/10.5194/gmd-8-2231-2015

Antia, A. N. (2005). Solubilization of particles in sediment traps: revising the stoichiometry of mixed layer export. *Biogeosciences*, *2*, 189–204. https://doi.org/10.5194/bg-2-189-2005

Antia, A. N., Bauerfeind, E., Bodungen, B. V., & Zeller, U. (1993). Abundance, encystment and sedimentation of acantharia during autumn 1990 in the East Greenland Sea. *Journal of Plankton Research*, *15*(1), 99–114. https://doi.org/10.1093/plankt/15.1.99

Antia, A. N., Von Bodungen, B., & Peinert, R. (1999). Particle flux across the mid-European continental margin. *Deep-Sea Research Part I: Oceanographic Research Papers*, *46*(12), 1999–2024. https://doi.org/10.1016/S0967-0637(99)00041-2

Antia, A. N., Koeve, W., Fischer, G., Blanz, T., Schulz-Bull, D., Schölten, J., et al. (2001). Basin-wide

particulate carbon flux in the Atlantic Ocean: Regional export patterns and potential for atmospheric CO2 sequestration. *Global Biogeochemical Cycles*, *15*(4), 845–862. https://doi.org/10.1029/2000GB001376

Archer, D., Eby, M., Brovkin, V., Ridgwell, A., Cao, L., Mikolajewicz, U., et al. (2009). Atmospheric Lifetime of Fossil Fuel Carbon Dioxide. *Annual Review of Earth and Planetary Sciences*, *37*(1), 117–134. https://doi.org/10.1146/annurev.earth.031208.100206

Armstrong, R. A., Lee, C., Hedges, J. I., Honjo, S., & Wakeham, S. G. (2002). A new, mechanistic model for organic carbon fluxes in the ocean based on the quantitative association of POC with ballast minerals. *Deep-Sea Research Part II: Topical Studies in Oceanography*, *49*, 219–236. https://doi.org/10.1016/S0967-0645(01)00101-1

Asper, V. L., Deuser, W. G., Knauer, G. A., & Lohrenz, S. E. (1992). Rapid coupling of sinking particle fluxes between surface and deep ocean waters. *Nature*, *357*(6380), 670–672. https://doi.org/10.1038/357670a0

Auffret, G., Khripounoff, A., & Vangriesheim, A. (1994). Rapid post-bloom resuspension in the northeastern Atlantic. *Deep-Sea Research Part I*, *41*(5–6), 925–939. https://doi.org/10.1016/0967-0637(94)90084-1

Bach, L. T., Riebesell, U., Sett, S., Febiri, S., Rzepka, P., & Schulz, K. G. (2012). An approach for particle sinking velocity measurements in the 3-400 µm size range and considerations on the effect of temperature on sinking rates. *Marine Biology*, *159*(8), 1853–1864. https://doi.org/10.1007/s00227-012-1945-2

Bacon, M. P., Spencer, D. W., & Brewer, P. G. (1976). 210Pb/226Ra and 210Po/210Pb disequilibria in seawater and suspended particulate matter. *Earth and Planetary Science Letters*, *32*(2), 277–296. https://doi.org/10.1016/0012-821X(76)90068-6

Baker, C. A., Estapa, M. L., Iversen, M. H., Lampitt, R. S., & Buesseler, K. O. (n.d.). Are all sediment traps created equal? An intercomparison study of carbon export methodologies at the PAP-SO site. *Under Review: Progress in Oceanography*.

Baker, C. A., Henson, S. A., Cavan, E. L., Giering, S. L. C., Yool, A., Gehlen, M., et al. (2017). Slow Sinking Particulate Organic Carbon in the Atlantic Ocean: magnitude, flux and potential controls. *Global Biogeochemical Cycles*, *31*, 1–15. https://doi.org/10.1002/2017GB005638

Baker, E. T., Milburn, H. B., & Tennant, D. A. (1988). Field assessment of sediment trap efficiency under varying flow conditions. *Journal of Marine Research*, *46*(3), 573–592.

https://doi.org/10.1357/002224088785113522

Barange, M., Butenschön, M., Yool, A., Beaumont, N., Fernandes, J. A., Martin, A. P., & Allen, J. I. (2017). The Cost of Reducing the North Atlantic Ocean Biological Carbon Pump. *Frontiers in Marine Science*, *3*(January), 290. https://doi.org/10.3389/fmars.2016.00290

Batchelder, H. P., VanKeuren, J. R., Vaillancourt, R., & Swift, E. (1995). Spatial and temporal distributions of acoustically estimated zooplankton biomass near the Marine Light-Mixed Layers station (59°30'N, 21°00'W) in the North Atlantic in May 1991. *Journal of Geophysical Research*, *100*(C4), 6549–6563. https://doi.org/10.1029/94JC00981

Bauerfeind, E., & Bodungen, B. v. (2006). Underestimation of biogenic silicon flux due to dissolution in sediment trap samples. *Marine Geology*, *226*(3–4), 297–306. https://doi.org/10.1016/j.margeo.2005.11.001

Bauerfeind, E., Nöthig, E. M., Beszczynska, A., Fahl, K., Kaleschke, L., Kreker, K., et al. (2009). Particle sedimentation patterns in the eastern Fram Strait during 2000-2005: Results from the Arctic long-term observatory HAUSGARTEN. *Deep-Sea Research Part I: Oceanographic Research Papers*, *56*(9), 1471–1487. https://doi.org/10.1016/j.dsr.2009.04.011

Beck, J. W., Edwards, R. L., Ito, E., Taylor, F. W., Recy, J., Rougerie, F., et al. (1992). Sea-surface temperature from coral skeletal strontium/calcium ratios. *Science*, *257*(5070), 644–647. https://doi.org/10.1126/science.257.5070.644

Beers, J. R., & Stewart, G. L. (1970). The Preservation of Acantharians in Fixed Plankton Samples. *Limnology and Oceanography*. https://doi.org/10.4319/lo.1970.15.5.0825

Behrenfeld, M. J., & Boss, E. S. (2014). Resurrecting the Ecological Underpinnings of Ocean Plankton Blooms. *Annual Review of Marine Science*, *6*(1), 167–194. https://doi.org/10.1146/annurev-marine-052913-021325

Belcher, A., Iversen, M., Manno, C., Henson, S. A., Tarling, G. A., & Sanders, R. (2016). The role of particle associated microbes in remineralization of fecal pellets in the upper mesopelagic of the Scotia Sea, Antarctica. *Limnology and Oceanography*, *61*(3), 1049–1064. https://doi.org/10.1002/lno.10269

Belcher, A., Manno, C., Thorpe, S., & Tarling, G. (2018). Acantharian cysts: high flux occurrence in the bathypelagic zone of the Scotia Sea, Southern Ocean. *Marine Biology*, *165*(7), 1–11. https://doi.org/10.1007/s00227-018-3376-1

Belcher, A., Henson, S. A., Manno, C., Hill, S. L., Atkinson, A., Thorpe, S. E., et al. (2019). Krill faecal

pellets drive hidden pulses of particulate organic carbon in the marginal ice zone. *Nature Communications*, *10*(1), 1–8. https://doi.org/10.1038/s41467-019-08847-1

Bellacicco, M., Cornec, M., Organelli, E., Brewin, R. J. W., Neukermans, G., Volpe, G., et al. (2019). Global Variability of Optical Backscattering by Non-algal particles From a Biogeochemical-Argo Data Set. *Geophysical Research Letters*, *46*(16), 9767–9776. https://doi.org/10.1029/2019GL084078

Berelson, W. (2001). The Flux of Particulate Organic Carbon Into the Ocean Interior: A Comparison of Four U.S. JGOFS Regional Studies. *Oceanography*, *14*(4), 59–67. https://doi.org/10.5670/oceanog.2001.07

Berelson, W. M. (2001). Particle settling rates increase with depth in the ocean. *Deep-Sea Research Part II: Topical Studies in Oceanography*, *49*(1–3), 237–251. https://doi.org/10.1016/S0967-0645(01)00102-3

Bernstein, R., Stanley, S., & Boltovskoy, D. (1999). Acantharia. In D. Boltovskoy (Ed.), *South Atlantic Zooplankton vol 1* (pp. 75–147). Leiden, The Netherlands: Backhuys Publishers.

Bernstein, R. E., Betzer, P. R., Feely, R. A., Byrne, R. H., Lamb, M. F., & Michaels, A. F. (1987). Acantharian Fluxes and Strontium to Chlorinity Ratios in the North Pacific Ocean. *Science*, *237*(4821), 1490–1494. https://doi.org/10.1126/science.237.4821.1490

Bernstein, Renate E, Byrne, R. H., Betzer, P. R., & Greco, A. M. (1992). Morphologies and transformations of celestite in seawater: The role of acantharians in strontium and barium geochemistry. *Geochimica et Cosmochimica Acta*, *56*(8), 3273–3279. https://doi.org/10.1016/0016-7037(92)90304-2

Biard, T., Stemmann, L., Picheral, M., Mayot, N., Vandromme, P., Hauss, H., et al. (2016). In situ imaging reveals the biomass of giant protists in the global ocean. *Nature*, *532*(7600), 504–507. https://doi.org/10.1038/nature17652

Billett, D. S. M., Lampitt, R. S., Rice, A. L., & Mantoura, R. F. C. (1983). Seasonal sedimentation of phytoplankton to the deep-sea benthos. *Nature*, *302*(5908), 520–522. https://doi.org/10.1038/302520a0

Bishop, J. K. B., Edmond, J. M., Ketten, D. R., Bacon, M. P., & Silker, W. B. (1977). The chemistry, biology, and vertical flux of particulate matter from the upper 400 m of the equatorial Atlantic Ocean. *Deep-Sea Research*, *24*(6). https://doi.org/10.1016/0146-6291(77)90526-4

Bishop, J. K. B., Fong, M. B., & Wood, T. J. (2016). Robotic observations of high wintertime carbon

export in California coastal waters. *Biogeosciences*, *13*(10), 3109–3129. https://doi.org/10.5194/bg-13-3109-2016

Bopp, L., Monfray, P., Aumont, O., Dufresne, J. L., Le Treut, H., Madec, G., et al. (2001). Potential impact of climate change on marine export production. *Global Biogeochemical Cycles*, *15*(1), 81–99. https://doi.org/10.1029/1999GB001256

Bopp, L., Aumont, O., Cadule, P., Alvain, S., & Gehlen, M. (2005). Response of diatoms distribution to global warming and potential implications: A global model study. *Geophysical Research Letters*, *32*, 2–5. https://doi.org/10.1029/2005GL023653

Bottazzi, E. M. (1978). Systematic-ecological aspects of radiolaria with special reference to acantharia. *Bolletino Di Zoologia*, *45*(2), 133–144. https://doi.org/10.1080/11250007809440123

Bottazzi, E. M., & Andreoli, M. G. (1982). Distribution of adult and juvenile Acantharia (Protozoa Sarcodina) in the Atlantic Ocean. *Journal of Plankton Research*, *4*(4), 757–777. https://doi.org/10.1093/plankt/4.4.757

Bourne, H. L., Bishop, J. K. B., Wood, T. J., Loew, T. J., & Liu, Y. (2019). Carbon Flux Explorer optical assessment of C, N and P fluxes. *Biogeosciences*, *16*(6), 1249–1264. https://doi.org/10.5194/bg-16-1249-2019

Bower, A. S., Le Cann, B., Rossby, T., Zenk, W., Gould, J., Speer, K., et al. (2002). Directly measured mid-depth circulation in the northeastern North Atlantic Ocean. *Nature*, *419*(6907), 603–607. https://doi.org/10.1038/nature01078

Boyd, P. W., & Newton, P. P. (1999). Does planktonic community structure determine downward particulate organic carbon flux in different oceanic provinces? *Deep-Sea Research Part I: Oceanographic Research Papers*, *46*, 63–91. https://doi.org/10.1016/S0967-0637(98)00066-1

Boyd, P. W., & Trull, T. W. (2007). Understanding the export of biogenic particles in oceanic waters: Is there consensus? *Progress in Oceanography*, *72*(4), 276–312. https://doi.org/10.1016/j.pocean.2006.10.007

Boyd, P. W., Claustre, H., Levy, M., Siegel, D. A., & Weber, T. (2019). Multi-faceted particle pumps drive carbon sequestration in the ocean. *Nature*, *568*(7752), 327–335. https://doi.org/10.1038/s41586-019-1098-2

de Boyer Montégut, C., Madec, G., Fischer, A. S., Lazar, A., & Iudicone, D. (2004). Mixed layer

depth over the global ocean: An examination of profile data and a profile-based climatology. *Journal of Geophysical Research C: Oceans*, *109*(12), 1–20. https://doi.org/10.1029/2004JC002378

Brass, G. W. (1980). Trace elements in acantharian skeletons. *Limnology and Oceanography*, *25*(1), 146–149. https://doi.org/10.4319/lo.1980.25.1.0146

Breitbarth, E., Bellerby, R. J., Neill, C. C., Ardelan, M. V., Meyerhöfer, M., Zöllner, E., et al. (2010). Ocean acidification affects iron speciation during a coastal seawater mesocosm experiment. *Biogeosciences*, *7*(3), 1065–1073. https://doi.org/10.5194/bg-7-1065-2010

Briggs, N., Perry, M. J., Cetinić, I., Lee, C., D'Asaro, E., Gray, A. M., & Rehm, E. (2011). High-resolution observations of aggregate flux during a sub-polar North Atlantic spring bloom. *Deep-Sea Research Part I: Oceanographic Research Papers*, *58*(10), 1031–1039. https://doi.org/10.1016/j.dsr.2011.07.007

Brix, H., Gruber, N., Karl, D. M., & Bates, N. R. (2006). On the relationships between primary, net community, and export production in subtropical gyres. *Deep-Sea Research Part II: Topical Studies in Oceanography*, *53*(5–7), 698–717. https://doi.org/10.1016/j.dsr2.2006.01.024

Brody, S. R., & Lozier, M. S. (2015). Characterizing upper-ocean mixing and its effect on the spring phytoplankton bloom with in situ data. *ICES Journal of Marine Science*, *72*(6), 1961–1970. https://doi.org/10.1093/icesjms/fsv006

Brown, L., Sanders, R., Savidge, G., & Lucas, C. H. (2003). The uptake of silica during the spring bloom in the Northeast Atlantic Ocean. *Limnology and Oceanography*, *48*(5), 1831–1845. https://doi.org/10.4319/lo.2003.48.5.1831

Buesseler, K. (1991). Do upper-ocean sediment traps provide an accurate record of particle flux? *Nature*, *353*(6343), 420–423. https://doi.org/10.1038/353420a0

Buesseler, K. (1998). The decoupling of production and particulate export in the surface ocean. *Global Biogeochemical Cycles*, *12*(2), 297–310. https://doi.org/10.1029/97GB03366

Buesseler, K., Ball, L., Andrews, J., Benitez-Nelson, C., Belastock, R., Chai, F., & Chao, Y. (1998). Upper ocean export of particulate organic carbon in the Arabian Sea derived from thorium-234. *Deep-Sea Research Part II: Topical Studies in Oceanography*, *45*(10–11), 2461–2487. https://doi.org/10.1016/S0967-0645(98)80022-2

Buesseler, K., Steinberg, D. K., Michaels, A. F., Johnson, R. J., Andrews, J. E., Valdes, J. R., & Price, J. F. (2000). A comparison of the quantity and composition of material caught in a neutrally

buoyant versus surface-tethered sediment trap. *Deep-Sea Research Part I: Oceanographic Research Papers*, *47*, 277–294. https://doi.org/10.1016/S0967-0637(99)00056-4

Buesseler, K., Benitez-Nelson, C. R., Moran, S. B., Burd, A., Charette, M., Cochran, J. K., et al. (2006). An assessment of particulate organic carbon to thorium-234 ratios in the ocean and their impact on the application of 234Th as a POC flux proxy. *Marine Chemistry*, *100*, 213–233. https://doi.org/10.1016/j.marchem.2005.10.013

Buesseler, K., Antia, A. N., Chen, M., Fowler, S. W., Gardner, W. D., Gustafsson, O., et al. (2007). An assessment of the use of sediment traps for estimating upper ocean particle fluxes. *Journal of Marine Research*, *65*, 345–416. https://doi.org/10.1357/002224007781567621

Buesseler, K., Lamborg, C., Cai, P., Escoube, R., Johnson, R., Pike, S., et al. (2008). Particle fluxes associated with mesoscale eddies in the Sargasso Sea. *Deep-Sea Research Part II: Topical Studies in Oceanography*, *55*(10–13), 1426–1444. https://doi.org/10.1016/j.dsr2.2008.02.007

Burd, A. B., Hansell, D. A., Steinberg, D. K., Anderson, T. R., Arístegui, J., Baltar, F., et al. (2010). Assessing the apparent imbalance between geochemical and biochemical indicators of meso- and bathypelagic biological activity: What the @$♯! is wrong with present calculations of carbon budgets? *Deep Sea Research Part II: Topical Studies in Oceanography*, *57*(16), 1557–1571. https://doi.org/10.1016/j.dsr2.2010.02.022

Butman, C. A. (1986). Sediment trap biases in turbulent flows: results from a laboratory flume study. *Journal of Marine Research*, *44*(3), 645–693. https://doi.org/10.1357/002224086788403051

Capo, R. C., & Depaolo, D. J. (1990). Seawater strontium isotopic variations from 2.5 million years ago to the present. *Science*, *249*(4964), 51–55. https://doi.org/10.1126/science.249.4964.51

Van Cappellen, P., Dixit, S., & van Beusekom, J. (2002). Biogenic silica dissolution in the oceans: Reconciling experimental and field-based dissolution rates. *Global Biogeochemical Cycles*, *16*(4), 1–10. https://doi.org/10.1029/2001GB001431

Caron, D. A., & Swanberg, N. R. (1990). The ecology of plankton sarcodines. *Rev Aquat Sci*, *3*, 147–180.

Cavan, E. L., Le Moigne, F. A. C., Poulton, A. J., Tarling, G. A., Ward, P., Daniels, C. J., et al. (2015). Attenuation of particulate organic carbon flux in the Scotia Sea, Southern Ocean, is controlled by zooplankton fecal pellets. *Geophysical Research Letters*, *42*(3), 821–830.

https://doi.org/10.1002/2014GL062744

Cavan, E. L., Henson, S. A., Belcher, A., & Sanders, R. (2017). Role of zooplankton in determining the efficiency of the biological carbon pump. *Biogeosciences*, *14*(1), 177–186. https://doi.org/10.5194/bg-14-177-2017

Cetinić, I., Perry, M. J., D'Asaro, E., Briggs, N., Poulton, N., Sieracki, M. E., & Lee, C. M. (2015). A simple optical index shows spatial and temporal heterogeneity in phytoplankton community composition during the 2008 North Atlantic Bloom Experiment. *Biogeosciences*, *12*(7), 2179–2194. https://doi.org/10.5194/bg-12-2179-2015

Chelton, D. B., Schlax, M. G., & Samelson, R. M. (2011). Global observations of nonlinear mesoscale eddies. *Progress in Oceanography*, *91*(2), 167–216. https://doi.org/10.1016/j.pocean.2011.01.002

Chiswell, S. M., & Nodder, S. D. (2015). Tilt-induced biases in sediment trap functioning. *Journal of Geophysical Research: Oceans*, *120*(12), 8381–8391. https://doi.org/10.1002/2015JC011350

Ciais, P., Sabine, C., Bala, G., Bopp, L., Brovkin, V., Canadell, J., et al. (2013). *Carbon and Other Biogeochemical Cycles. Climate Change 2013: The Physical Science Basis. Contribution of Working Group I to the Fifth Assessment Report of the Intergovernmental Panel on Climate Change*. Cambridge University Press, Cambridge, United Kingdom and New York, NY, USA. Retrieved from http://www.climatechange2013.org/images/report/WG1AR5_Chapter06_FINAL.pdf

Coale, K. H. (1990). Labyrinth of doom: A device to minimize the "swimmer" component in sediment trap collections. *Limnology and Oceanography*, *35*(6), 1376–1381. https://doi.org/10.4319/lo.1990.35.6.1376

Cole, H. S., Henson, S., Martin, A. P., & Yool, A. (2015). Basin-wide mechanisms for spring bloom initiation: How typical is the North Atlantic? *ICES Journal of Marine Science*, *72*(6), 2029–2040. https://doi.org/10.1093/icesjms/fsu239

Conte, M. H., & Weber, J. C. (2014). Particle Flux in the Deep Sargasso Sea The 35-Year Oceanic Flux Program Time Series. *Oceanography*, *27*(1), 142–147. https://doi.org/10.5670/oceanog.2014.17

Conte, M. H., Eglinton, G., & Madureira, L. A. S. (1995). Origin and fate of organic biomarker compounds in the water column and sediments of the eastern North Atlantic. *Philosophical Transactions - Royal Society of London*, *348*(1324), 169–178.

https://doi.org/10.1098/rstb.1995.0059

Conte, M. H., Ralph, N., & Ross, E. H. (2001). Seasonal and interannual variability in deep ocean particle fluxes at the Oceanic Flux Program (OFP)/Bermuda Atlantic Time Series (BATS) site in the western Sargasso Sea near Bermuda. *Deep-Sea Research Part II: Topical Studies in Oceanography*, *48*(8–9), 1471–1505. https://doi.org/10.1016/S0967-0645(00)00150-8

Conte, M. H., Dickey, T. D., Weber, J. C., Johnson, R. J., & Knap, A. H. (2003). Transient physical forcing of pulsed export of bioreactive material to the deep Sargasso Sea. *Deep-Sea Research Part I: Oceanographic Research Papers*, *50*(10–11), 1157–1187. https://doi.org/10.1016/S0967-0637(03)00141-9

Cowles, T. J., & Fessenden, L. M. (1995). Copepod grazing and fine-scale distribution patterns during the Marine Light-Mixed Layers experiment. *Journal of Geophysical Research*, *100*(C4), 6677–6686. https://doi.org/10.1029/94JC02214

d'Ovidio, F., De Monte, S., Alvain, S., Dandonneau, Y., & Levy, M. (2010). Fluid dynamical niches of phytoplankton types. *Proceedings of the National Academy of Sciences*. https://doi.org/10.1073/pnas.1004620107

Dall'Olmo, G., & Mork, K. A. (2014). Carbon export by small particles in the Norwegian Sea. *Geophysical Research Letters*, *41*(8), 2921–2927. https://doi.org/10.1002/2014GL059244

Dall'Olmo, G., Dingle, J., Polimene, L., Brewin, R. J. W., & Claustre, H. (2016). Substantial energy input to the mesopelagic ecosystem from the seasonal mixed-layer pump. *Nature Geoscience*, *9*(11), 820–823. https://doi.org/10.1038/ngeo2818

Daniels, C. J., Tyrrell, T., Poulton, A. J., & Pettit, L. (2012). The influence of lithogenic material on particulate inorganic carbon measurements of coccolithophores in the bay of biscay. *Limnology and Oceanography*, *57*(1), 145–153. https://doi.org/10.4319/lo.2012.57.1.0145

Daniels, C. J., Poulton, A. J., Esposito, M., Paulsen, M. L., Bellerby, R., St John, M., & Martin, A. P. (2015a). Phytoplankton dynamics in contrasting early stage North Atlantic spring blooms: composition, succession, and potential drivers. *Biogeosciences*, *12*(8), 2395–2409. https://doi.org/10.5194/bg-12-2395-2015

Daniels, C. J., Poulton, A. J., Esposito, M., Paulsen, M. L., Bellerby, R., St John, M., & Martin, A. P. (2015b). Phytoplankton dynamics in contrasting early stage North Atlantic spring blooms: Composition, succession, and potential drivers. *Biogeosciences*, *12*(8), 2395–2409. https://doi.org/10.5194/bg-12-2395-2015

Decelle, J., & Not, F. (2015). Acantharia. In *eLS* (pp. 1–10). Chichester, UK: John Wiley & Sons, Ltd. https://doi.org/10.1002/9780470015902.a0002102.pub2

Decelle, J., Probert, I., Bittner, L., Desdevises, Y., Colin, S., de Vargas, C., et al. (2012). An original mode of symbiosis in open ocean plankton. *Proceedings of the National Academy of Sciences*, *109*(44), 18000–18005. https://doi.org/10.1073/pnas.1212303109

Decelle, J., Martin, P., Paborstava, K., Pond, D. W., Tarling, G., Mahé, F., et al. (2013). Diversity, Ecology and Biogeochemistry of Cyst-Forming Acantharia (Radiolaria) in the Oceans. *PLoS ONE*, *8*(1), 1–13. https://doi.org/10.1371/journal.pone.0053598

De Deckker, P. (2004). On the celestite-secreting Acantharia and their effect on seawater strontium to calcium ratios. *Hydrobiologia*, *517*(1–3), 1–13. https://doi.org/10.1023/B:HYDR.0000027333.02017.50

Denman, K. L., Brasseur, G., Chidthaisong, A., Ciais, P., Cox, P. M., Dickinson, R. E., et al. (2007). Couplings Between Changes in the Climate System and Biogeochemistry. *Climate Change 2007: The Physical Science Basis. Contribution of Working Group I to the Fourth Assessment Report of the Intergovernmental Panel on Climate Change*. Retrieved from https://www.globalcarbonproject.org/global/pdf/AR4WG1_Pub_Ch07.pdf

Deuser, W. G. (1986). Seasonal and interannual variations in deep-water particle fluxes in the Sargasso Sea and their relation to surface hydrography, *33*(2), 225–246.

Deuser, W. G., & Ross, E. H. (1980). Seasonal change in the flux of organic carbon to the deep Sargasso Sea [5]. *Nature*. https://doi.org/10.1038/283364a0

Deuser, W. G., Ross, E. H., & Anderson, R. F. (1981). Seasonality in the supply of sediment to the deep Sargasso Sea and implications for the rapid transfer of matter to the deep ocean. *Deep Sea Research Part A, Oceanographic Research Papers*, *28*(5), 495–505. https://doi.org/10.1016/0198-0149(81)90140-0

Deuser, W. G., Muller-Karger, F. E., & Hemleben, C. (1988). Temporal variations of particle fluxes in the deep subtropical and tropical North Atlantic: Eulerian versus Lagrangian effects. *Journal of Geophysical Research*, *93*(C6), 6857–6862. https://doi.org/10.1029/JC093iC06p06857

Deuser, W. G., Muller-Karger, F. E., Evans, R. H., Brown, O. B., Esaias, W. E., & Feldman, G. C. (1990). Surface-ocean color and deep-ocean carbon flux: how close a connection? *Deep Sea Research Part A. Oceanographic Research Papers*, *37*(8), 1331–1343.

https://doi.org/10.1016/0198-0149(90)90046-X

DeVries, T., & Weber, T. (2017). The export and fate of organic matter in the ocean: New constraints from combining satellite and oceanographic tracer observations. *Global Biogeochemical Cycles*, *31*(3), 535–555. https://doi.org/10.1002/2016GB005551

DeVries, T., Primeau, F., & Deutsch, C. (2012). The sequestration efficiency of the biological pump. *Geophysical Research Letters*, *39*(13), 1–5. https://doi.org/10.1029/2012GL051963

Dickey, T., Lewis, M., & Chang, G. (2006). Optical oceanography: Recent advances and future directions using global remote sensing and in situ observations. *Reviews of Geophysics*, *44*(1), RG1001. https://doi.org/10.1029/2003RG000148

Doney, S. C., Glover, D. M., McCue, S. J., & Fuentes, M. (2003). Mesoscale variability of Sea-viewing Wide Field-of-view Sensor (SeaWiFS) satellite ocean color: Global patterns and spatial scales. *Journal of Geophysical Research: Oceans*, *108*(C2), 1–15. https://doi.org/10.1029/2001JC000843

Dove, P. M., & Czank, C. A. (1995). Crystal chemical controls on the dissolution kinetics of the isostructural sulfates: Celestite, anglesite, and barite. *Geochimica et Cosmochimica Acta*, *59*(10), 1907–1915. https://doi.org/10.1016/0016-7037(95)00116-6

Ducklow, H. W. (2008). Long-term studies of the marine ecosystem along the west Antarctic Peninsula. *Deep Sea Research Part II: Topical Studies in Oceanography*, *55*(18–19), 1945–1948. https://doi.org/10.1016/j.dsr2.2008.05.014

Ducklow, H. W., Wilson, S. E., Post, A. F., Stammerjohn, S. E., Erickson, M., Lee, S., et al. (2015). Particle flux on the continental shelf in the Amundsen Sea Polynya and Western Antarctic Peninsula. *Elementa: Science of the Anthropocene*, *3*, 000046. https://doi.org/10.12952/journal.elementa.000046

Eittreim, S., Thorndike, E. M., & Sullivan, L. (1976). Turbidity distribution in the Atlantic Ocean. *Deep Sea Research*, *23*(12), 1115–1127. https://doi.org/10.1016/0011-7471(76)90888-3

Eppley, R. W., Holmes, R. W., & Strickland, J. D. H. (1967). Sinking rates of marine phytoplankton measured with a fluorometer. *Journal of Experimental Marine Biology and Ecology*, *1*(2), 191–208. https://doi.org/10.1016/0022-0981(67)90014-7

Estapa, M., Buesseler, K., Boss, E., & Gerbi, G. (2013). Autonomous, high-resolution observations of particle flux in the oligotrophic ocean. *Biogeosciences*, *10*(8), 5517–5531. https://doi.org/10.5194/bg-10-5517-2013

Estapa, M., Durkin, C., Buesseler, K., Johnson, R., & Feen, M. (2017). Carbon flux from bio-optical profiling floats: Calibrating transmissometers for use as optical sediment traps. *Deep Sea Research Part I: Oceanographic Research Papers*, *120*(December 2016), 100–111. https://doi.org/10.1016/j.dsr.2016.12.003

Estapa, M., Feen, M. L., & Breves, E. (2019). Direct Observations of Biological Carbon Export From Profiling Floats in the Subtropical North Atlantic. *Global Biogeochemical Cycles*, *33*(3), 282–300. https://doi.org/10.1029/2018GB006098

Febvre, J., & Febvre-Chevalier, C. (2001). Acantharia. https://doi.org/10.1038/npg.els.0002102

Fernandez, E., Boyd, P., Holligan, P. M., & Harbour, D. S. (1993). Production of organic and inorganic carbon within a large-scale coccolithophore bloom in the northeast Atlantic Ocean. *Marine Ecology Progress Series*, *97*(3), 271–285. https://doi.org/10.3354/meps097271

Fischer, G., & Karakaş, G. (2009). Sinking rates and ballast composition of particles in the Atlantic ocean: Implications for the organic carbon fluxes to the deep ocean. *Biogeosciences*, *6*(1), 85–102. https://doi.org/10.5194/bg-6-85-2009

Fontela, M., García-Ibáñez, M. I., Hansell, D. A., Mercier, H., & Pérez, F. F. (2016). Dissolved Organic Carbon in the North Atlantic Meridional Overturning Circulation. *Scientific Reports*, *6*, 1–9. https://doi.org/10.1038/srep26931

Foukal, N. P., & Lozier, M. S. (2017). Assessing variability in the size and strength of the North Atlantic subpolar gyre. *Journal of Geophysical Research: Oceans*, *122*(8), 6295–6308. https://doi.org/10.1002/2017JC012798

Francois, R., Honjo, S., Krishfield, R., & Manganini, S. (2002). Factors controlling the flux of organic carbon to the bathypelagic zone of the ocean. *Global Biogeochemical Cycles*, *16*(4), 1–20. https://doi.org/10.1029/2001GB001722

Franks, P. J. S. (2001). Phytoplankton blooms in a fluctuating environment: the roles of plankton response time scales and grazing. *Journal of Plankton Research*, *23*(12), 1433–1441. https://doi.org/10.1093/plankt/23.12.1433

Frigstad, H., Henson, S. A., Hartman, S. E., Omar, A. M., Jeansson, E., Cole, H., et al. (2015). Links between surface productivity and deep ocean particle flux at the Porcupine Abyssal Plain sustained observatory. *Biogeosciences*, *12*(19), 5885–5897. https://doi.org/10.5194/bg-12-5885-2015

Gardner, W. (1980). Sediment trap dynamics and calibration: a laboratory evaluation. *Journal of*

Marine Research, *38*(1), 17–39.

Gardner, W. (1985). The effect of tilt on sediment trap efficiency. *Deep Sea Research Part A, Oceanographic Research Papers*, *32*(3), 349–361. https://doi.org/10.1016/0198-0149(85)90083-4

Gardner, W. (2000). Sediment trap sampling in surface waters. *The Changing Ocean Carbon Cycle: A Midterm Synthesis of the Joint Global Ocean Flux Study*, 240–284.

Gardner, W., Chung, S. P., Richardson, M. J., & Walsh, I. D. (1995). The oceanic mixed-layer pump. *Deep-Sea Research Part II*. https://doi.org/10.1016/0967-0645(95)00037-Q

Gardner, W., Tucholke, B. E., Richardson, M. J., & Biscaye, P. E. (2017). Benthic storms, nepheloid layers, and linkage with upper ocean dynamics in the western North Atlantic. *Marine Geology*, *385*, 304–327. https://doi.org/10.1016/j.margeo.2016.12.012

Gardner, W., Richardson, M. J., & Mishonov, A. V. (2018). Global assessment of benthic nepheloid layers and linkage with upper ocean dynamics. *Earth and Planetary Science Letters*, *482*, 126–134. https://doi.org/10.1016/j.epsl.2017.11.008

Gardner, W. D., & Sullivan, L. G. (1981). Benthic storms: Temporal variability in a deep-ocean nepheloid layer. *Science*, *213*(4505), 329–331. https://doi.org/10.1126/science.213.4505.329

Gehlen, M., Bopp, L., Emprin, N., Aumont, O., Heinze, C., & Ragueneau, O. (2006). Reconciling surface ocean productivity, export fluxes and sediment composition in a global biogeochemical ocean model. *Biogeosciences*, *3*(4), 521–537. https://doi.org/10.5194/bg-3-521-2006

Giering, S. L. C., Sanders, R., Lampitt, R. S., Anderson, T. R., Tamburini, C., Boutrif, M., et al. (2014). Reconciliation of the carbon budget in the ocean's twilight zone. *Nature*, *507*(7493), 480–483. https://doi.org/10.1038/nature13123

Giering, S. L. C., Sanders, R., Martin, A. P., Lindemann, C., Möller, K. O., Daniels, C. J., et al. (2016). High export via small particles before the onset of the North Atlantic spring bloom. *Journal of Geophysical Research: Oceans*, *121*(9), 6929–6945. https://doi.org/10.1002/2016JC012048

Giering, Sarah L.C., Sanders, R., Martin, A. P., Henson, S. A., Riley, J. S., Marsay, C. M., & Johns, D. G. (2017). Particle flux in the oceans: Challenging the steady state assumption. *Global Biogeochemical Cycles*, *31*(1), 159–171. https://doi.org/10.1002/2016GB005424

Gifford, D. J., Fessenden, L. M., Garrahan, P. R., & Martin, E. (1995). Grazing by microzooplankton and mesozooplankton in the high-latitude North Atlantic Ocean: spring versus summer dynamics. *Journal of Geophysical Research*, *100*(C4), 6665–6675. https://doi.org/10.1029/94JC00983

Graham, D. W., Bender, M. L., Williams, D. F., & Keigwin, L. D. (1982). Strontium-calcium ratios in Cenozoic planktonic foraminifera. *Geochimica et Cosmochimica Acta*, *46*(7), 1281–1292. https://doi.org/10.1016/0016-7037(82)90012-6

Gruber, N., & Sarmiento, J. L. (2002). Large scale biochemical-physical interactions in elemental cycles. In *The Sea: biological-physical interactions in the oceans* (Vol. 12, pp. 337–399).

Gruber, Nicolas, Clement, D., Carter, B. R., Feely, R. A., van Heuven, S., Hoppema, M., et al. (2019). The oceanic sink for anthropogenic CO 2 from 1994 to 2007. *Science*, *363*(6432), 1193–1199. https://doi.org/10.1126/science.aau5153

Guidi, L., Stemmann, L., Legendre, L., Picheral, M., Prieur, L., & Gorsky, G. (2007). Vertical distribution of aggregates (>110 μm) and mesoscale activity in the northeastern Atlantic: Effects on the deep vertical export of surface carbon. *Limnology and Oceanography*, *52*(1), 7–18. https://doi.org/10.4319/lo.2007.52.1.0007

Guidi, L., Jackson, G. A., Stemmann, L., Miquel, J. C., Picheral, M., & Gorsky, G. (2008). Relationship between particle size distribution and flux in the mesopelagic zone. *Deep Sea Research Part I: Oceanographic Research Papers*, *55*(10), 1364–1374. https://doi.org/10.1016/j.dsr.2008.05.014

Guieu, C., Roy-Barman, M., Leblond, N., Jeandel, C., Souhaut, M., Le Cann, B., et al. (2005). Vertical particle flux in the northeast Atlantic Ocean (POMME experiment). *Journal of Geophysical Research C: Oceans*, *110*(7), 1–21. https://doi.org/10.1029/2004JC002672

Hahm, D., & Kim, K. R. (2008). Observation of bottom water renewal and export production in the Japan Basin, East Sea using tritium and helium isotopes. *Ocean Science Journal*, *43*(1), 39–48. https://doi.org/10.1007/BF03022430

Hansen, A. N., & Visser, A. W. (2016). Carbon export by vertically migrating zooplankton: An optimal behavior model. *Limnology and Oceanography*, *61*(2), 701–710. https://doi.org/10.1002/lno.10249

Hargrave, B., von Bodungen, B., Stoffyn-Egli, P., & Mudie, P. J. (1994). Seasonal variability in particle sedimentation under permanent ice cover in the Arctic Ocean. *Continental Shelf*

Research, *14*(2–3), 279–293. https://doi.org/10.1016/0278-4343(94)90017-5

Harland, R. (1983). Dsitribution maps of recent dinoflagellate cysts in the bottom sediments from the North Atlantic Ocean and adjacent seas. *Palaeontology*, *26*(2), 321–387.

Harris, R. P., Boyd, P., Harbour, D. S., Head, R. N., Pingree, R. D., & Pomroy, A. J. (1997). Physical, chemical and biological features of a cyclonic eddy in the region of 61°10'N 19°50'W in the North Atlantic. *Deep Sea Research Part I: Oceanographic Research Papers*, *44*(11), 1815–1839. https://doi.org/10.1016/S0967-0637(97)00053-8

Hátún, H., Azetsu-Scott, K., Somavilla, R., Rey, F., Johnson, C., Mathis, M., et al. (2017). The subpolar gyre regulates silicate concentrations in the North Atlantic. *Scientific Reports*, *7*(1), 1–9. https://doi.org/10.1038/s41598-017-14837-4

Hebbeln, D., Marchant, M., & Wefer, G. (2000). Seasonal variations of the particle flux in the Peru-Chile current at 30°S under 'normal' and El Niño conditions. *Deep Sea Research Part II: Topical Studies in Oceanography*, *47*(9–11), 2101–2128. https://doi.org/10.1016/S0967-0645(00)00018-7

Hedges, J. I., & Stern, J. H. (1984). Carbon and nitrogen determinations of carbonate-containing solids1. *Limnology and Oceanography*, *29*(3), 657–663. https://doi.org/10.4319/lo.1984.29.3.0657

Hedges, J. I., Lee, C., Wakeham, S. G., Hernes, P. J., & Peterson, M. L. (1993). Effects of poisons and preservatives on the fluxes and elemental compositions of sediment trap materials. *Journal of Marine Research*, *51*(3), 651–668. https://doi.org/10.1357/0022240933223990

Henson, S. A. (2014). Slow science: the value of long ocean biogeochemistry records. *Philosophical Transactions of the Royal Society A: Mathematical, Physical and Engineering Sciences*, *372*(2025), 20130334. https://doi.org/10.1098/rsta.2013.0334

Henson, S. A., Dunne, J. P., & Sarmiento, J. L. (2009). Decadal variability in North Atlantic phytoplankton blooms. *Journal of Geophysical Research: Oceans*, *114*(4), 1–11. https://doi.org/10.1029/2008JC005139

Henson, S. A., Sanders, R., Madsen, E., Morris, P. J., Le Moigne, F., & Quartly, G. D. (2011). A reduced estimate of the strength of the ocean's biological carbon pump. *Geophysical Research Letters*, *38*(4), n/a-n/a. https://doi.org/10.1029/2011GL046735

Henson, S. A., Sanders, R., & Madsen, E. (2012). Global patterns in efficiency of particulate organic carbon export and transfer to the deep ocean. *Global Biogeochemical Cycles*, *26*(1), 1–14.

https://doi.org/10.1029/2011GB004099

Henson, S. A., Yool, A., & Sanders, R. (2015). Variability in efficiency of particulate organic carbon export: A model study. *Global Biogeochemical Cycles*, *29*(1), 33–45. https://doi.org/10.1002/2014GB004965

Henson, S. A., Beaulieu, C., & Lampitt, R. (2016). Observing climate change trends in ocean biogeochemistry: when and where. *Global Change Biology*, *22*(4), 1561–1571. https://doi.org/10.1111/gcb.13152

Henson, SA, Sanders, R., Holeton, C., & Allen, J. (2006). Timing of nutrient depletion, diatom dominance and a lower-boundary estimate of export production for Irminger Basin, North Atlantic. *Marine Ecology Progress Series*, *313*, 73–84. https://doi.org/10.3354/meps313073

Henson, Stephanie, Lampitt, R., & Johns, D. (2012). Variability in phytoplankton community structure in response to the North Atlantic Oscillation and implications for organic carbon flux. *Limnology and Oceanography*, *57*(6), 1591–1601. https://doi.org/10.4319/lo.2012.57.6.1591

Henson, Stephanie, Le Moigne, F., & Giering, S. (2019). Drivers of Carbon Export Efficiency in the Global Ocean. *Global Biogeochemical Cycles*, 2018GB006158. https://doi.org/10.1029/2018GB006158

Hoffmann, L., Breitbarth, E., Boyd, P., & Hunter, K. (2012). Influence of ocean warming and acidification on trace metal biogeochemistry. *Marine Ecology Progress Series*, *470*, 191–205. https://doi.org/10.3354/meps10082

Holligan, P. M., Fernández, E., Aiken, J., Balch, W. M., Boyd, P., Burkill, P. H., et al. (1993). A biogeochemical study of the coccolithophore, Emiliania huxleyi, in the North Atlantic. *Global Biogeochemical Cycles*, *7*(4), 879–900. https://doi.org/10.1029/93GB01731

Honjo, S., & Manganini, S. J. (1993). Annual biogenic particle fluxes to the interior of the North Atlantic Ocean; studied at 34°N 21°W and 48°N 21°W. *Deep Sea Research Part II: Topical Studies in Oceanography*, *40*(1–2), 587–607. https://doi.org/10.1016/0967-0645(93)90034-K

Honjo, S., Manganini, S. J., & Cole, J. J. (1982). Sedimentation of biogenic matter in the deep ocean. *Deep Sea Research Part A. Oceanographic Research Papers*, *29*(5), 609–625. https://doi.org/10.1016/0198-0149(82)90079-6

Honjo, S., Spencer, D. W., & Gardner, W. D. (1992). A sediment trap intercomparison experiment in the Panama Basin, 1979. *Deep Sea Research Part A. Oceanographic Research Papers*,

39(2), 333–358. https://doi.org/10.1016/0198-0149(92)90112-7

Honjo, S., Dymond, J., Prell, W., & Ittekkot, V. (1999). Monsoon-controlled export fluxes to the interior of the Arabian Sea. *Deep Sea Research Part II: Topical Studies in Oceanography*, *46*(8–9), 1859–1902. https://doi.org/10.1016/S0967-0645(99)00047-8

Honjo, S., Francois, R., Manganini, S., Dymond, J., & Collier, R. (2000). Particle fluxes to the interior of the Southern Ocean in the Western Pacific sector along 170°W. *Deep Sea Research Part II: Topical Studies in Oceanography*, *47*(15–16), 3521–3548. https://doi.org/10.1016/S0967-0645(00)00077-1

Honjo, S., Manganini, S. J., Krishfield, R. a., & Francois, R. (2008). Particulate organic carbon fluxes to the ocean interior and factors controlling the biological pump: A synthesis of global sediment trap programs since 1983. *Progress in Oceanography*, *76*(3), 217–285. https://doi.org/10.1016/j.pocean.2007.11.003

Hosoda, S., Ohira, T., Sato, K., & Suga, T. (2010). Improved description of global mixed-layer depth using Argo profiling floats. *Journal of Oceanography*, *66*(6), 773–787. https://doi.org/10.1007/s10872-010-0063-3

Ikenoue, T., Kimoto, K., Okazaki, Y., Sato, M., Honda, M. C., Takahashi, K., et al. (2019). Phaeodaria: An Important Carrier of Particulate Organic Carbon in the Mesopelagic Twilight Zone of the North Pacific Ocean. *Global Biogeochemical Cycles*, *33*(8), 1146–1160. https://doi.org/10.1029/2019GB006258

IPCC. (2007). *Climate Change 2007 Synthesis Report*. *Intergovernmental Panel on Climate Change [Core Writing Team IPCC*. https://doi.org/10.1256/004316502320517344

Ittekkot, V. (1993). The abiotically driven biological pump in the ocean and short-term fluctuations in atmospheric CO2 contents. *Global and Planetary Change*, *8*(1–2), 17–25. https://doi.org/10.1016/0921-8181(93)90060-2

Iversen, M., & Poulsen, L. (2007). Coprorhexy, coprophagy, and coprochaly in the copepods Calanus helgolandicus, Pseudocalanus elongatus, and Oithona similis. *Marine Ecology Progress Series*, *350*(1990), 79–89. https://doi.org/10.3354/meps07095

Iversen, M. H., & Ploug, H. (2010). Ballast minerals and the sinking carbon flux in the ocean: carbon-specific respiration rates and sinking velocity of marine snow aggregates. *Biogeosciences*, *7*(9), 2613–2624. https://doi.org/10.5194/bg-7-2613-2010

Iversen, Morten H., Pakhomov, E. A., Hunt, B. P. V., van der Jagt, H., Wolf-Gladrow, D., & Klaas, C.

(2017). Sinkers or floaters? Contribution from salp pellets to the export flux during a large bloom event in the Southern Ocean. *Deep Sea Research Part II: Topical Studies in Oceanography*, *138*(December 2016), 116–125. https://doi.org/10.1016/j.dsr2.2016.12.004

Jahnke, R. A. (1996). The global ocean flux of particulate organic carbon: Areal distribution and magnitude. *Global Biogeochemical Cycles*, *10*(1), 71–88. https://doi.org/10.1029/95GB03525

JGOFS. (1994). Protocols for the joint global ocean flux study (JGOFS) core measurements, IOC Manual and guides, (29), 170 p.

Jiao, N., Herndl, G. J., Hansell, D. A., Benner, R., Kattner, G., Wilhelm, S. W., et al. (2010). Microbial production of recalcitrant dissolved organic matter: long-term carbon storage in the global ocean. *Nature Reviews Microbiology*, *8*(8), 593–599. https://doi.org/10.1038/nrmicro2386

Joint, I., Pomroy, A., Savidge, G., & Boyd, P. (1993). Size-fractionated primary productivity in the northeast Atlantic in May–July 1989. *Deep Sea Research Part II: Topical Studies in Oceanography*, *40*(1–2), 423–440. https://doi.org/10.1016/0967-0645(93)90025-I

Jónasdóttir, S. H., Visser, A. W., Richardson, K., & Heath, M. R. (2015). Seasonal copepod lipid pump promotes carbon sequestration in the deep North Atlantic. *Proceedings of the National Academy of Sciences*, *112*(39), 12122–12126. https://doi.org/10.1073/pnas.1512110112

Karl, D. M., & Lukas, R. (1996). The Hawaii Ocean Time-series (HOT) program: Background, rationale and field implementation. *Deep Sea Research Part II: Topical Studies in Oceanography*, *43*(2–3), 129–156. https://doi.org/10.1016/0967-0645(96)00005-7

Karl, D. M., Church, M. J., Dore, J. E., Letelier, R. M., & Mahaffey, C. (2012). Predictable and efficient carbon sequestration in the North Pacific Ocean supported by symbiotic nitrogen fixation. *Proceedings of the National Academy of Sciences*, *109*(6), 1842–1849. https://doi.org/10.1073/pnas.1120312109

Kemp, A. E. S., Pike, J., Pearce, R. B., & Lange, C. B. (2000). The “Fall dump” — a new perspective on the role of a “shade flora” in the annual cycle of diatom production and export flux. *Deep Sea Research Part II: Topical Studies in Oceanography*, *47*(9–11), 2129–2154. https://doi.org/10.1016/S0967-0645(00)00019-9

Khatiwala, S., Tanhua, T., Mikaloff Fletcher, S., Gerber, M., Doney, S. C., Graven, H. D., et al. (2013). Global ocean storage of anthropogenic carbon. *Biogeosciences*, *10*(4), 2169–2191. https://doi.org/10.5194/bg-10-2169-2013

Klaas, C., & Archer, D. E. (2002). Association of sinking organic matter with various types of mineral ballast in the deep sea: Implications for the rain ratio. *Global Biogeochemical Cycles*, *16*(4), 63-1-63–14. https://doi.org/10.1029/2001GB001765

Klein, P., & Lapeyre, G. (2009). The Oceanic Vertical Pump Induced by Mesoscale and Submesoscale Turbulence. *Annual Review of Marine Science*, *1*(1), 351–375. https://doi.org/10.1146/annurev.marine.010908.163704

Knappertsbusch, M., & Brummer, G.-J. A. (1995). A sediment trap investigation of sinking coccolithophorids in the North Atlantic. *Deep Sea Research Part I: Oceanographic Research Papers*, *42*(7), 1083–1109. https://doi.org/10.1016/0967-0637(95)00036-6

Knauer, G. A., Karl, D. M., Martin, J. H., & Hunter, C. N. (1984). In situ effects of selected preservatives on total carbon, nitrogen and metals collected in sediment traps. *Journal of Marine Research*, *42*(2), 445–462. https://doi.org/10.1357/002224084788502710

Kuss, J., & Kremling, K. (1999). Particulate trace element fluxes in the deep northeast Atlantic Ocean. *Deep Sea Research Part I: Oceanographic Research Papers*, *46*(1), 149–169. https://doi.org/10.1016/S0967-0637(98)00059-4

Kwon, E. Y., Primeau, F., & Sarmiento, J. L. (2009). The impact of remineralization depth on the air–sea carbon balance. *Nature Geoscience*, *2*(9), 630–635. https://doi.org/10.1038/ngeo612

De La Rocha, C. L., & Passow, U. (2007). Factors influencing the sinking of POC and the efficiency of the biological carbon pump. *Deep Sea Research Part II: Topical Studies in Oceanography*, *54*(5–7), 639–658. https://doi.org/10.1016/j.dsr2.2007.01.004

Lacour, L., Ardyna, M., Stec, K. F., Claustre, H., Prieur, L., Poteau, A., et al. (2017). Unexpected winter phytoplankton blooms in the North Atlantic subpolar gyre. *Nature Geoscience*, *10*(11), 836–839. https://doi.org/10.1038/NGEO3035

Lacour, L., Briggs, N., Claustre, H., Ardyna, M., & Dall'Olmo, G. (2019). The Intraseasonal Dynamics of the Mixed Layer Pump in the Subpolar North Atlantic Ocean: A Biogeochemical-Argo Float Approach. *Global Biogeochemical Cycles*, *33*(3), 266–281. https://doi.org/10.1029/2018GB005997

Lalande, C., Nöthig, E.-M., Bauerfeind, E., Hardge, K., Beszczynska-Möller, A., & Fahl, K. (2016). Lateral supply and downward export of particulate matter from upper waters to the seafloor in the deep eastern Fram Strait. *Deep Sea Research Part I: Oceanographic Research Papers*, *114*(April), 78–89. https://doi.org/10.1016/j.dsr.2016.04.014

Lam, P. J., & Bishop, J. K. B. (2007). High biomass, low export regimes in the Southern Ocean. *Deep Sea Research Part II: Topical Studies in Oceanography*, *54*(5–7), 601–638. https://doi.org/10.1016/j.dsr2.2007.01.013

Lam, P. J., Doney, S. C., & Bishop, J. K. B. (2011). The dynamic ocean biological pump: Insights from a global compilation of particulate organic carbon, CaCO 3 , and opal concentration profiles from the mesopelagic. *Global Biogeochemical Cycles*, *25*(3), n/a-n/a. https://doi.org/10.1029/2010GB003868

Lampitt, R. S., Noji, T., & von Bodungen, B. (1990). What happens to zooplankton faecal pellets? Implications for material flux. *Marine Biology*, *104*(1), 15–23. https://doi.org/10.1007/BF01313152

Lampitt, R. S., Salter, I., & Johns, D. (2009). Radiolaria: Major exporters of organic carbon to the deep ocean. *Global Biogeochemical Cycles*, *23*(1), n/a-n/a. https://doi.org/10.1029/2008GB003221

Lampitt, R.S. (1985). Evidence for the seasonal deposition of detritus to the deep-sea floor and its subsequent resuspension. *Deep Sea Research Part A. Oceanographic Research Papers*, *32*(8), 885–897. https://doi.org/10.1016/0198-0149(85)90034-2

Lampitt, R.S., & Antia, A. N. (1997). Particle flux in deep seas: regional characteristics and temporal variability. *Deep Sea Research Part I: Oceanographic Research Papers*, *44*(8), 1377–1403. https://doi.org/10.1016/S0967-0637(97)00020-4

Lampitt, R.S., Newton, P. P., Jickells, T. D., Thomson, J., & King, P. (2000). Near-bottom particle flux in the abyssal northeast Atlantic. *Deep Sea Research Part II: Topical Studies in Oceanography*, *47*(9–11), 2051–2071. https://doi.org/10.1016/S0967-0645(00)00016-3

Lampitt, R.S., Boorman, B., Brown, L., Lucas, M., Salter, I., Sanders, R., et al. (2008). Particle export from the euphotic zone: Estimates using a novel drifting sediment trap, 234Th and new production. *Deep Sea Research Part I: Oceanographic Research Papers*, *55*(11), 1484–1502. https://doi.org/10.1016/j.dsr.2008.07.002

Lampitt, R.S., Salter, I., de Cuevas, B. A., Hartman, S., Larkin, K. E., & Pebody, C. A. (2010). Long-term variability of downward particle flux in the deep northeast Atlantic: Causes and trends. *Deep Sea Research Part II: Topical Studies in Oceanography*, *57*(15), 1346–1361. https://doi.org/10.1016/j.dsr2.2010.01.011

Lampitt, R.S, Bett, B. ., Kiriakoulakis, K., Popova, E. ., Ragueneau, O., Vangriesheim, A., & Wolff,

G. . (2001). Material supply to the abyssal seafloor in the Northeast Atlantic. *Progress in Oceanography*, *50*(1–4), 27–63. https://doi.org/10.1016/S0079-6611(01)00047-7

Lampitt, R.S, Achterberg, E. ., Anderson, T. ., Hughes, J. ., Iglesias-Rodriguez, M. ., Kelly-Gerreyn, B. ., et al. (2008). Ocean fertilization: a potential means of geoengineering? *Philosophical Transactions of the Royal Society A: Mathematical, Physical and Engineering Sciences*, *366*(1882), 3919–3945. https://doi.org/10.1098/rsta.2008.0139

Lampitt, Richard S., Sumida, P. Y. G., & Castillo, F. P. (2002). Ophiuroid growth within deep-sea sediment traps: A problem for carbon flux measurements at continental margins. *Limnology and Oceanography*, *47*(2), 571–575. https://doi.org/10.4319/lo.2002.47.2.0571

Laws, E. A., & Maiti, K. (2019). The relationship between primary production and export production in the ocean: Effects of time lags and temporal variability. *Deep Sea Research Part I: Oceanographic Research Papers*, *148*(April), 100–107. https://doi.org/10.1016/j.dsr.2019.05.006

Laws, E. A., D'Sa, E., & Naik, P. (2011). Simple equations to estimate ratios of new or export production to total production from satellite-derived estimates of sea surface temperature and primary production. *Limnology and Oceanography: Methods*, *9*(12), 593–601. https://doi.org/10.4319/lom.2011.9.593

Leblanc, K., Quéguiner, B., Diaz, F., Cornet, V., Michel-Rodriguez, M., Durrieu de Madron, X., et al. (2018). Nanoplanktonic diatoms are globally overlooked but play a role in spring blooms and carbon export. *Nature Communications*, *9*(1), 953. https://doi.org/10.1038/s41467-018-03376-9

Lee, C., Wakeham, S., & Hedges, J. (1988). The Measurement of Oceanic Particle Flux—Are "Swimmers" a Problem? *Oceanography*, *1*(2), 34–36. https://doi.org/10.5670/oceanog.1988.06

Lee, C., Peterson, M. L., Wakeham, S. G., Armstrong, R. a., Cochran, J. K., Miquel, J. C., et al. (2009). Particulate organic matter and ballast fluxes measured using time-series and settling velocity sediment traps in the northwestern Mediterranean Sea. *Deep Sea Research Part II: Topical Studies in Oceanography*, *56*(18), 1420–1436. https://doi.org/10.1016/j.dsr2.2008.11.029

Legendre, L., Rivkin, R. B., Weinbauer, M. G., Guidi, L., & Uitz, J. (2015). The microbial carbon pump concept: Potential biogeochemical significance in the globally changing ocean. *Progress in Oceanography*, *134*, 432–450. https://doi.org/10.1016/j.pocean.2015.01.008

Levy, M., Bopp, L., Karleskind, P., Resplandy, L., Ethe, C., & Pinsard, F. (2013). Physical pathways for carbon transfers between the surface mixed layer and the ocean interior. *Global Biogeochemical Cycles*, *27*(4), 1001–1012. https://doi.org/10.1002/gbc.20092

Lozier, M. S., Li, F., Bacon, S., Bahr, F., Bower, A. S., Cunningham, S. A., et al. (2019). A sea change in our view of overturning in the subpolar North Atlantic. *Science*, *363*(6426), 516–521. https://doi.org/10.1126/science.aau6592

Lutz, M., Dunbar, R., & Caldeira, K. (2002). Regional variability in the vertical flux of particulate organic carbon in the ocean interior. *Global Biogeochemical Cycles*, *16*(3), 11-1-11–18. https://doi.org/10.1029/2000GB001383

Lutz, M. J., Caldeira, K., Dunbar, R. B., & Behrenfeld, M. J. (2007). Seasonal rhythms of net primary production and particulate organic carbon flux to depth describe the efficiency of biological pump in the global ocean. *Journal of Geophysical Research*, *112*(C10), C10011. https://doi.org/10.1029/2006JC003706

Maiti, K., Charette, M. a., Buesseler, K. O., & Kahru, M. (2013). An inverse relationship between production and export efficiency in the Southern Ocean. *Geophysical Research Letters*, *40*(8), 1557–1561. https://doi.org/10.1002/grl.50219

Marra, J., Langdon, C., & Knudson, C. A. (1995). Primary production, water column changes, and the demise of a Phaeocystis bloom at the Marine Light-Mixed Layers site (59°N, 21°W) in the northeast Atlantic Ocean. *Journal of Geophysical Research*, *100*(C4), 6633. https://doi.org/10.1029/94JC01127

Marsay, C. M., Sanders, R. J., Henson, S. A., Pabortsava, K., Achterberg, E. P., & Lampitt, R. S. (2015). Attenuation of sinking particulate organic carbon flux through the mesopelagic ocean. *Proceedings of the National Academy of Sciences*, *112*(4), 1089–1094. https://doi.org/10.1073/pnas.1415311112

Martin, A. P., & Richards, K. J. (2001). Mechanisms for vertical nutrient transport within a North Atlantic mesoscale eddy. *Deep Sea Research Part II: Topical Studies in Oceanography*, *48*(4–5), 757–773. https://doi.org/10.1016/S0967-0645(00)00096-5

Martin, A. P., Wade, I. P., Richards, K. J., & Heywood, K. J. (1998). The PRIME Eddy. *Journal of Marine Research*, *56*(2), 439–462. https://doi.org/10.1357/002224098321822375

Martin, A. P., Richards, K. J., Law, C. S., & Liddicoat, M. (2001). Horizontal dispersion within an anticyclonic mesoscale eddy. *Deep Sea Research Part II: Topical Studies in Oceanography*,

48(4–5), 739–755. https://doi.org/10.1016/S0967-0645(00)00095-3

Martin, A. P., Richards, K. J., Bracco, A., & Provenzale, A. (2002). Patchy productivity in the open ocean. *Global Biogeochemical Cycles*, *16*(2), 9-1-9–9. https://doi.org/10.1029/2001GB001449

Martin, J. H., & Knauer, G. A. (1973). The elemental composition of plankton. *Geochimica et Cosmochimica Acta*, *37*(7), 1639–1653. https://doi.org/10.1016/0016-7037(73)90154-3

Martin, J. H., Knauer, G. A., Karl, D. M., & Broenkow, W. W. (1987). VERTEX: carbon cycling in the northeast Pacific. *Deep Sea Research Part A. Oceanographic Research Papers*, *34*(2), 267–285. https://doi.org/10.1016/0198-0149(87)90086-0

Martin, P. (2011). Particle export and flux through the mesopelagic in the high-latitude North and South Atlantic. *PhD Thesis, University of Southampton*, 168.

Martin, P., Allen, J. T., Cooper, M. J., Johns, D. G., Lampitt, R. S., Sanders, R., & Teagle, D. A. H. (2010). Sedimentation of acantharian cysts in the Iceland Basin: Strontium as a ballast for deep ocean particle flux, and implications for acantharian reproductive strategies. *Limnology and Oceanography*, *55*(2), 604–614. https://doi.org/10.4319/lo.2010.55.2.0604

Martin, P., Lampitt, R. S., Jane Perry, M., Sanders, R., Lee, C., & D'Asaro, E. (2011). Export and mesopelagic particle flux during a North Atlantic spring diatom bloom. *Deep Sea Research Part I: Oceanographic Research Papers*, *58*(4), 338–349. https://doi.org/10.1016/j.dsr.2011.01.006

Martinez-Garcia, A., Sigman, D. M., Ren, H., Anderson, R. F., Straub, M., Hodell, D. A., et al. (2014). Iron Fertilization of the Subantarctic Ocean During the Last Ice Age. *Science*, *343*(6177), 1347–1350. https://doi.org/10.1126/science.1246848

Mayor, D. J., Sanders, R., Giering, S. L. C., & Anderson, T. R. (2014a). Microbial gardening in the ocean's twilight zone: Detritivorous metazoans benefit from fragmenting, rather than ingesting, sinking detritus: Fragmentation of refractory detritus by zooplankton beneath the euphotic zone stimulates the harvestable productio. *BioEssays*, *36*(12), 1132–1137. https://doi.org/10.1002/bies.201400100

Mayor, D. J., Sanders, R., Giering, S. L. C., & Anderson, T. R. (2014b). Microbial gardening in the ocean's twilight zone: Detritivorous metazoans benefit from fragmenting, rather than ingesting, sinking detritus. *BioEssays*, *36*(12), 1132–1137. https://doi.org/10.1002/bies.201400100

McCave, I. N. (1975). Vertical flux of particles in the ocean. *Deep Sea Research and Oceanographic Abstracts*, *22*(7), 491–502. https://doi.org/10.1016/0011-7471(75)90022-4

McDonnell, A. M. P., Lam, P. J., Lamborg, C. H., Buesseler, K. O., Sanders, R., Riley, J. S., et al. (2015). The oceanographic toolbox for the collection of sinking and suspended marine particles. *Progress in Oceanography*, *133*, 17–31. https://doi.org/10.1016/j.pocean.2015.01.007

McGillicuddy, D. J. (2016). Mechanisms of Physical-Biological-Biogeochemical Interaction at the Oceanic Mesoscale. *Annual Review of Marine Science*, *8*(1), 125–159. https://doi.org/10.1146/annurev-marine-010814-015606

McNeil, J. D., Jannasch, H. W., Dickey, T., McGillicuddy, D., Brzezinski, M., & Sakamoto, C. M. (1999). New chemical, bio-optical and physical observations of upper ocean response to the passage of a mesoscale eddy off Bermuda. *Journal of Geophysical Research: Oceans*, *104*(C7), 15537–15548. https://doi.org/10.1029/1999JC900137

Michaels, A. F. (1988). Vertical distribution and abundance of Acantharia and their symbionts. *Marine Biology*, *97*(4), 559–569. https://doi.org/10.1007/BF00391052

Michaels, Anthony F. (1991). Acantharian abundance and symbiont productivity at the VERTEX seasonal station. *Journal of Plankton Research*, *13*(2), 399–418. https://doi.org/10.1093/plankt/13.2.399

Michaels, Anthony F., Silver, M. W., Gowing, M. M., & Knauer, G. A. (1990). Cryptic zooplankton "swimmers" in upper ocean sediment traps. *Deep Sea Research Part A. Oceanographic Research Papers*, *37*(8), 1285–1296. https://doi.org/10.1016/0198-0149(90)90043-U

Michaels, Anthony F., Bates, N. R., Buesseler, K. O., Carlson, C. A., & Knap, A. H. (1994). Carbon-cycle imbalances in the Sargasso Sea. *Nature*, *372*(6506), 537–540. https://doi.org/10.1038/372537a0

Michaels, Anthony F., Caron, D. A., Swanberg, N. R., Howse, F. A., & Michaels, C. M. (1995). Planktonic sarcodines (Acantharia, Radiolaria, Foraminifera) in surface waters near Bermuda: abundance, biomass and vertical flux. *Journal of Plankton Research*, *17*(1), 131–163. https://doi.org/10.1093/plankt/17.1.131

Mignot, A., Ferrari, R., & Claustre, H. (2018). Floats with bio-optical sensors reveal what processes trigger the North Atlantic bloom. *Nature Communications*, *9*(1), 190. https://doi.org/10.1038/s41467-017-02143-6

Millar, R. J., Fuglestvedt, J. S., Friedlingstein, P., Rogelj, J., Grubb, M. J., Matthews, H. D., et al. (2017). Emission budgets and pathways consistent with limiting warming to 1.5°C. *Nature Geoscience*, *10*(10), 741–747. https://doi.org/10.1038/ngeo3031

Le Moigne, F.A.C., Villa-Alfageme, M., Sanders, R. J., Marsay, C., Henson, S., & García-Tenorio, R. (2013). Export of organic carbon and biominerals derived from 234Th and 210Po at the Porcupine Abyssal Plain. *Deep Sea Research Part I: Oceanographic Research Papers*, *72*, 88–101. https://doi.org/10.1016/j.dsr.2012.10.010

Le Moigne, Frédéric A. C., Poulton, A. J., Henson, S. A., Daniels, C. J., Fragoso, G. M., Mitchell, E., et al. (2015). Carbon export efficiency and phytoplankton community composition in the Atlantic sector of the Arctic Ocean. *Journal of Geophysical Research: Oceans*, *120*(6), 3896–3912. https://doi.org/10.1002/2015JC010700

Le Moigne, Frédéric A. C., Henson, S. A., Cavan, E., Georges, C., Pabortsava, K., Achterberg, E. P., et al. (2016). What causes the inverse relationship between primary production and export efficiency in the Southern Ocean? *Geophysical Research Letters*, *43*(9), 4457–4466. https://doi.org/10.1002/2016GL068480

Moore, J. K., Fu, W., Primeau, F., Britten, G. L., Lindsay, K., Long, M., et al. (2018). Sustained climate warming drives declining marine biological productivity. *Science*, *359*(6380), 1139–1143. https://doi.org/10.1126/science.aao6379

Mortlock, R. A., & Froelich, P. N. (1989). A simple method for the rapid determination of biogenic opal in pelagic marine sediments. *Deep Sea Research Part A. Oceanographic Research Papers*, *36*(9), 1415–1426. https://doi.org/10.1016/0198-0149(89)90092-7

Müller, H., & Wünsch, C. (1999). Seasonal dynamics of cyst formation of pelagic strombidiid ciliates in a deep prealpine lake. *Aquatic Microbial Ecology*, *17*(1), 37–47. https://doi.org/10.3354/ame017037

Neter, J., Kutner, M. H., Nachtsheim, C. J., & Wasserman, W. (1996). *Applied Linear Statistical Models* (4th ed.). Chicago.

Newton, P. P., Lampitt, R. S., Jickells, T. D., King, P., & Boutle, C. (1994). Temporal and spatial variability of biogenic particles fluxes during the JGOFS northeast Atlantic process studies at 47°N, 20°W. *Deep Sea Research Part I: Oceanographic Research Papers*, *41*(11–12), 1617–1642. https://doi.org/10.1016/0967-0637(94)90065-5

Nielsdóttir, M. C., Moore, C. M., Sanders, R., Hinz, D. J., & Achterberg, E. P. (2009). Iron limitation

of the postbloom phytoplankton communities in the Iceland Basin. *Global Biogeochemical Cycles*, *23*(3), n/a-n/a. https://doi.org/10.1029/2008GB003410

Nieuwenhuize, J., Maas, Y. E. ., & Middelburg, J. J. (1994). Rapid analysis of organic carbon and nitrogen in particulate materials. *Marine Chemistry*, *45*(3), 217–224. https://doi.org/10.1016/0304-4203(94)90005-1

Nodder, S. D., Chiswell, S. M., & Northcote, L. C. (2016). Annual cycles of deep-ocean biogeochemical export fluxes in subtropical and subantarctic waters, southwest Pacific Ocean. *Journal of Geophysical Research: Oceans*, *121*(4), 2405–2424. https://doi.org/10.1002/2015JC011243

Odum, H. T. (1951). Notes on the Strontium Content of Sea Strontianite Snail Shells. *Science*, *114*, 211–213.

Omand, M. M., D'Asaro, E. A., Lee, C. M., Perry, M. J., Briggs, N., Cetini, I., & Mahadevan, A. (2015). Eddy-driven subduction exports particulate organic carbon from the spring bloom. *Science*, *348*(6231), 222–225. https://doi.org/10.1126/science.1260062

Orr, J. C., Fabry, V. J., Aumont, O., Bopp, L., Doney, S. C., Feely, R. A., et al. (2005). Anthropogenic ocean acidification over the twenty-first century and its impact on calcifying organisms. *Nature*, *437*(7059), 681–686. https://doi.org/10.1038/nature04095

Orvik, K. A., & Niiler, P. (2002). Major pathways of Atlantic water in the northern North Atlantic and Nordic Seas toward Arctic. *Geophysical Research Letters*, *29*(19), 2-1-2–4. https://doi.org/10.1029/2002GL015002

Oschlies, A., & Garçon, V. (1998). Eddy-induced enhancement of primary production in a model of the North Atlantic Ocean. *Nature*, *394*(6690), 266–269. https://doi.org/10.1038/28373

Pabortsava, K., Lampitt, R. S., Benson, J., Crowe, C., McLachlan, R., Le Moigne, F. A. C., et al. (2017). Carbon sequestration in the deep Atlantic enhanced by Saharan dust. *Nature Geoscience*, *10*(3), 189–194. https://doi.org/10.1038/ngeo2899

Palevsky, H., & Nicholson, D. (2018). The North Atlantic Biological Pump: Insights from the Ocean Observatories Initiative Irminger Sea Array. *Oceanography*, *31*(1), 42–49. https://doi.org/10.5670/oceanog.2018.108

Palevsky, H. I., & Doney, S. C. (2018). How Choice of Depth Horizon Influences the Estimated Spatial Patterns and Global Magnitude of Ocean Carbon Export Flux. *Geophysical Research Letters*, *45*(9), 4171–4179. https://doi.org/10.1029/2017GL076498

Parekh, P., Dutkiewicz, S., Follows, M. J., & Ito, T. (2006). Atmospheric carbon dioxide in a less dusty world. *Geophysical Research Letters*, *33*(3), L03610. https://doi.org/10.1029/2005GL025098

Passow, U. (2004). Switching perspectives: Do mineral fluxes determine particulate organic carbon fluxes or vice versa? *Geochemistry, Geophysics, Geosystems*, *5*(4), n/a-n/a. https://doi.org/10.1029/2003GC000670

Passow, U., & Carlson, C. (2012). The biological pump in a high CO<sub>2 world. *Marine Ecology Progress Series*, *470*(2), 249–271. https://doi.org/10.3354/meps09985

Passow, U., Alldredge, A. L., & Logan, B. E. (1994). The role of particulate carbohydrate exudates in the flocculation of diatom blooms. *Deep Sea Research Part I: Oceanographic Research Papers*, *41*(2), 335–357. https://doi.org/10.1016/0967-0637(94)90007-8

Pickart, R. S., Torres, D. J., & Clarke, R. A. (2002). Hydrography of the Labrador Sea during Active Convection. *Journal of Physical Oceanography*, *32*(2), 428–457. https://doi.org/10.1175/1520-0485(2002)032<0428:HOTLSD>2.0.CO;2

Pidcock, R., Martin, A., Allen, J., Painter, S. C., & Smeed, D. (2013). The spatial variability of vertical velocity in an Iceland basin eddy dipole. *Deep-Sea Research Part I: Oceanographic Research Papers*, *72*, 121–140. https://doi.org/10.1016/j.dsr.2012.10.008

Plueddemann, A. J., Weller, R. A., Stramska, M., Dickey, T. D., & Marra, J. (1995). Vertical structure of the upper ocean during the Marine Light-Mixed Layers experiment. *Journal of Geophysical Research*, *100*(C4), 6605. https://doi.org/10.1029/94JC03203

Pollard, R. T. (2004). Water masses and circulation pathways through the Iceland Basin during Vivaldi 1996. *Journal of Geophysical Research*, *109*(C4), C04004. https://doi.org/10.1029/2003JC002067

Pospelova, V., Zonneveld, K. A. F., Heikkilä, M., Bringué, M., Price, A. M., Esenkulova, S., & Matsuoka, K. (2018). Seasonal, annual, and inter-annual Spiniferites cyst production: a review of sediment trap studies. *Palynology*, *42*(sup1), 162–181. https://doi.org/10.1080/01916122.2018.1465738

Poulton, A. J., Charalampopoulou, A., Young, J. R., Tarran, G. A., Lucas, M. I., & Quartlya, G. D. (2010). Coccolithophore dynamics in non-bloom conditions during late summer in the central Iceland Basin (July-August 2007). *Limnology and Oceanography*, *55*(4), 1601–1613. https://doi.org/10.4319/lo.2010.55.4.1601

Poulton, A. J., Charalampopoulou, A., Young, J. R., Tarran, G. A., Lucas, M. I., & Quartly, G. D. (2010). Coccolithophore dynamics in non-bloom conditions during late summer in the central Iceland Basin (July-August 2007). *Limnology and Oceanography*, *55*(4), 1601–1613. https://doi.org/10.4319/lo.2010.55.4.1601

Primeau, F. (2005). Characterizing Transport between the Surface Mixed Layer and the Ocean Interior with a Forward and Adjoint Global Ocean Transport Model. *Journal of Physical Oceanography*, *35*(4), 545–564. https://doi.org/10.1175/JPO2699.1

Primeau, F. (2006). On the variability of the exponent in the power law depth dependence of POC flux estimated from sediment traps. *Deep Sea Research Part I: Oceanographic Research Papers*, *53*(8), 1335–1343. https://doi.org/10.1016/j.dsr.2006.06.003

Qiu, Z., Doglioli, A. M., & Carlotti, F. (2014). Using a Lagrangian model to estimate source regions of particles in sediment traps. *Science China Earth Sciences*, *57*(10), 2447–2456. https://doi.org/10.1007/s11430-014-4880-x

Qiu, Z. F., Doglioli, A. M., & Carlotti, F. (2014). Using a Lagrangian model to estimate source regions of particles in sediment traps. *Science China Earth Sciences*, *57*(10), 2447–2456. https://doi.org/10.1007/s11430-014-4880-x

Quay, P., Stutsman, J., & Steinhoff, T. (2012). Primary production and carbon export rates across the subpolar N. Atlantic Ocean basin based on triple oxygen isotope and dissolved O 2 and Ar gas measurements. *Global Biogeochemical Cycles*, *26*(2), n/a-n/a. https://doi.org/10.1029/2010GB004003

Le Quéré, C., Andrew, R. M., Canadell, J. G., Sitch, S., Korsbakken, J. I., Peters, G. P., et al. (2016). Global Carbon Budget 2016. *Earth System Science Data*, *8*(2), 605–649. https://doi.org/10.5194/essd-8-605-2016

Ragueneau, O., Schultes, S., Bidle, K., Claquin, P., & Moriceau, B. (2006). Si and C interactions in the world ocean: Importance of ecological processes and implications for the role of diatoms in the biological pump. *Global Biogeochemical Cycles*, *20*(4), n/a-n/a. https://doi.org/10.1029/2006GB002688

Read, J. F., & Pollard, R. T. (2001). A long-lived eddy in the Iceland Basin 1998. *Journal of Geophysical Research: Oceans*, *106*(C6), 11411–11421. https://doi.org/10.1029/2000jc000492

Reid, P C. (1987). Mass encystment of a planktonic oligotrich ciliate. *Marine Biology*, *95*(2), 221–

230. https://doi.org/10.1007/BF00409009

Reid, PHILIP C. (1978). Dinoflagellate Cysts in the Plankton. *New Phytologist*, *80*(1), 219–229. https://doi.org/10.1111/j.1469-8137.1978.tb02284.x

Reid, Philip C, Fischer, A. C., Lewis-Brown, E., Meredith, M. P., Sparrow, M., Andersson, A. J., et al. (2009). Chapter 1 Impacts of the Oceans on Climate Change. In *Advances* (Vol. 56, pp. 1–150). https://doi.org/10.1016/S0065-2881(09)56001-4

Richardson, A. J., Walne, A. W., John, A. W. G., Jonas, T. D., Lindley, J. A., Sims, D. W., et al. (2006). Using continuous plankton recorder data. *Progress in Oceanography*, *68*(1), 27–74. https://doi.org/10.1016/j.pocean.2005.09.011

Rii, Y. M., Brown, S. L., Nencioli, F., Kuwahara, V., Dickey, T., Karl, D. M., & Bidigare, R. R. (2008). The transient oasis: Nutrient-phytoplankton dynamics and particle export in Hawaiian lee cyclones. *Deep Sea Research Part II: Topical Studies in Oceanography*, *55*(10–13), 1275–1290. https://doi.org/10.1016/j.dsr2.2008.01.013

Riley, J. S., Sanders, R., Marsay, C., Le Moigne, F. a C., Achterberg, E. P., & Poulton, a. J. (2012). The relative contribution of fast and slow sinking particles to ocean carbon export. *Global Biogeochemical Cycles*, *26*, 1–10. https://doi.org/10.1029/2011GB004085

Robinson, J., Popova, E. E., Yool, A., Srokosz, M., Lampitt, R. S., & Blundell, J. R. (2014). How deep is deep enough? Ocean iron fertilization and carbon sequestration in the Southern Ocean. *Geophysical Research Letters*, *41*(7), 2489–2495. https://doi.org/10.1002/2013GL058799

Rodríguez, J., Tintoré, J., Allen, J. T., Blanco, J. M., Gomis, D., Reul, A., et al. (2001). Mesoscale vertical motion and the size structure of phytoplankton in the ocean. *Nature*, *410*(6826), 360–363. https://doi.org/10.1038/35066560

Rost, B., & Riebesell, U. (2013). Coccolithophores and the biological pump: responses to environmental changes. In *Encyclopedia of Quaternary Science* (pp. 783–794). Elsevier. Retrieved from https://linkinghub.elsevier.com/retrieve/pii/B9780444536433002818

Rushdi, A. I., McManus, J., & Collier, R. W. (2000). Marine barite and celestite saturation in seawater. *Marine Chemistry*, *69*(1–2), 19–31. https://doi.org/10.1016/S0304-4203(99)00089-4

Sabine, C. L. (2004). The Oceanic Sink for Anthropogenic CO2. *Science*, *305*(5682), 367–371. https://doi.org/10.1126/science.1097403

Sabine, C. L., & Tanhua, T. (2010). Estimation of Anthropogenic CO 2 Inventories in the Ocean. *Annual Review of Marine Science*, *2*(1), 175–198. https://doi.org/10.1146/annurev-marine-120308-080947

Salter, I., Kemp, A. E. S., Lampitt, R. S., & Gledhill, M. (2010). The association between biogenic and inorganic minerals and the amino acid composition of settling particles. *Limnology and Oceanography*, *55*(5), 2207–2218. https://doi.org/10.4319/lo.2010.55.5.2207

Sanders, R., Morris, P. J., Poulton, A. J., Stinchcombe, M. C., Charalampopoulou, A., Lucas, M. I., & Thomalla, S. J. (2010). Does a ballast effect occur in the surface ocean? *Geophysical Research Letters*, *37*(8), 1–5. https://doi.org/10.1029/2010GL042574

Sanders, R., Henson, S. A., Koski, M., De La Rocha, C. L., Painter, S. C., Poulton, A. J., et al. (2014). The Biological Carbon Pump in the North Atlantic. *Progress in Oceanography*, *129*, 200–218. https://doi.org/10.1016/j.pocean.2014.05.005

Sanders, R. J., Henson, S. A., Martin, A. P., Anderson, T. R., Bernardello, R., Enderlein, P., et al. (2016). Controls over Ocean Mesopelagic Interior Carbon Storage (COMICS): Fieldwork, Synthesis, and Modeling Efforts. *Frontiers in Marine Science*, *3*(August), 1–7. https://doi.org/10.3389/fmars.2016.00136

Sarmiento, J. L., Slater, R. D., Fasham, M. J. R., Ducklow, H. W., Toggweiler, J. R., & Evans, G. T. (1993). A seasonal three-dimensional ecosystem model of nitrogen cycling in the North Atlantic Euphotic Zone. *Global Biogeochemical Cycles*, *7*(2), 417–450. https://doi.org/10.1029/93GB00375

Savidge, G., Turner, D. R., Burkill, P. H., Watson, A. J., Angel, M. V., Pingree, R. D., et al. (1992). The BOFS 1990 spring bloom experiment: Temporal evolution and spatial variability of the hydrographic field. *Progress in Oceanography*, *29*(3), 235–281. https://doi.org/10.1016/0079-6611(92)90005-K

Schewiakoff, W. T. (1902). Beitrage zur Kentnis der Radiolaria Acanthometra. *Mem. Acad. Imp. Sci. St. Petersbourg*, *XII*, 1–40.

Schewiakoff, W. T. (1926). Die Acantharia. *Fauna e Flora Del Golfo Di Napoli*, *37*, 1–755.

Schiebel, R. (2002). Planktic foraminiferal sedimentation and the marine calcite budget. *Global Biogeochemical Cycles*, *16*(4), 3-1-3–21. https://doi.org/10.1029/2001GB001459

Schmidt, K., De La Rocha, C. L., Gallinari, M., & Cortese, G. (2014). Not all calcite ballast is created equal: differing effects of foraminiferan and coccolith calcite on the formation and sinking of

aggregates. *Biogeosciences*, *11*(1), 135–145. https://doi.org/10.5194/bg-11-135-2014

Scholten, J. C., Fietzke, J., Vogler, S., Rutgers van der Loeff, M. M., Mangini, A., Koeve, W., et al. (2001). Trapping efficiencies of sediment traps from the deep Eastern North Atlantic: *Deep Sea Research Part II: Topical Studies in Oceanography*, *48*(10), 2383–2408. https://doi.org/10.1016/S0967-0645(00)00176-4

Scripps Oceanography. (2019). Carbon dioxide concentration at Mauna Loa Observatory. Retrieved April 16, 2015, from https://scripps.ucsd.edu/programs/keelingcurve

Sherman, A. D., Hobson, B. W., McGill, P. R., Davis, R. E., McClune, M. C., & Smith, K. L. (2011). Lagrangian sediment traps for sampling at discrete depths beneath free-drifting icebergs. *Deep Sea Research Part II: Topical Studies in Oceanography*, *58*(11–12), 1327–1335. https://doi.org/10.1016/j.dsr2.2010.11.008

Siegel, D. A., Buesseler, K. O., Doney, S. C., Sailley, S. F., Behrenfeld, M. J., & Boyd, P. W. (2014). Global assessment of ocean carbon export by combining satellite observations and food-web models. *Global Biogeochemical Cycles*, *28*(3), 181–196. https://doi.org/10.1002/2013GB004743

Siegel, D.A., & Deuser, W. G. (1997). Trajectories of sinking particles in the Sargasso Sea: modeling of statistical funnels above deep-ocean sediment traps. *Deep Sea Research Part I: Oceanographic Research Papers*, *44*(9–10), 1519–1541. https://doi.org/10.1016/S0967-0637(97)00028-9

Siegel, D.A., Fields, E., & Buesseler, K. O. (2008). A bottom-up view of the biological pump: Modeling source funnels above ocean sediment traps. *Deep Sea Research Part I: Oceanographic Research Papers*, *55*(1), 108–127. https://doi.org/10.1016/j.dsr.2007.10.006

Siegel, David A., Granata, T. C., Michaels, A. F., & Dickey, T. D. (1990). Mesoscale eddy diffusion, particle sinking, and the interpretation of sediment trap data. *Journal of Geophysical Research*, *95*(C4), 5305. https://doi.org/10.1029/JC095iC04p05305

Siegel, David A., Buesseler, K. O., Behrenfeld, M. J., Benitez-Nelson, C. R., Boss, E., Brzezinski, M. A., et al. (2016). Prediction of the Export and Fate of Global Ocean Net Primary Production: The EXPORTS Science Plan. *Frontiers in Marine Science*, *3*. https://doi.org/10.3389/fmars.2016.00022

Smetacek, V., von Bröckel, K., Zeitzschel, B., & Zenk, W. (1978). Sedimentation of particulate matter during a phytoplankton spring bloom in relation to the hydrographical regime.

Marine Biology, *47*(3), 211–226. https://doi.org/10.1007/BF00541000

Smith, C. L., Richards, K. J., & Fasham, M. J. R. (1996). The impact of mesoscale eddies on plankton dynamics in the upper ocean. *Deep Sea Research Part I: Oceanographic Research Papers*, *43*(11–12), 1807–1832. https://doi.org/10.1016/S0967-0637(96)00035-0

Smith, K. L., Sherman, A. D., McGill, P. R., Henthorn, R. G., Ferreira, J., & Huffard, C. L. (2017). Evolution of monitoring an abyssal time-series station in the northeast pacific over 28 years. *Oceanography*, *30*(4), 72–81. https://doi.org/10.5670/OCEANOG.2017.425

Smith, K. L., Ruhl, H. A., Huffard, C. L., Messié, M., & Kahru, M. (2018). Episodic organic carbon fluxes from surface ocean to abyssal depths during long-term monitoring in NE Pacific. *Proceedings of the National Academy of Sciences*, *115*(48), 12235–12240. https://doi.org/10.1073/pnas.1814559115

Spindler, M., & Beyer, K. (1990). Distribution, abundance and diversity of Antarctic acantharian cysts. *Marine Micropaleontology*, *15*(3–4), 209–218. https://doi.org/10.1016/0377-8398(90)90011-A

Stange, P., Bach, L. T., Le Moigne, F. A. C., Taucher, J., Boxhammer, T., & Riebesell, U. (2017). Quantifying the time lag between organic matter production and export in the surface ocean: Implications for estimates of export efficiency. *Geophysical Research Letters*, *44*(1), 268–276. https://doi.org/10.1002/2016GL070875

Steinberg, D. K., & Landry, M. R. (2017). Zooplankton and the Ocean Carbon Cycle. *Annual Review of Marine Science*, *9*(1), 413–444. https://doi.org/10.1146/annurev-marine-010814-015924

Steinberg, D. K., Carlson, C. A., Bates, N. R., Goldthwait, S. A., Madin, L. P., & Michaels, A. F. (2000). Zooplankton vertical migration and the active transport of dissolved organic and inorganic carbon in the Sargasso Sea. *Deep Sea Research Part I: Oceanographic Research Papers*, *47*(1), 137–158. https://doi.org/10.1016/S0967-0637(99)00052-7

Steinberg, D. K., Van Mooy, B. A. S., Buesseler, K. O., Boyd, P. W., Kobari, T., & Karl, D. M. (2008). Bacterial vs. zooplankton control of sinking particle flux in the ocean's twilight zone. *Limnology and Oceanography*, *53*(4), 1327–1338. https://doi.org/10.4319/lo.2008.53.4.1327

Stemmann, L., Eloire, D., Sciandra, A., Jackson, G. A., Guidi, L., Picheral, M., & Gorsky, G. (2008). Volume distribution for particles between 3.5 to 2000 µm in the upper 200 m region of the South Pacific Gyre. *Biogeosciences*, *5*(2), 299–310. https://doi.org/10.5194/bg-5-299-2008

Stoll, H. M., & Schrag, D. P. (1998). Effects of Quaternary Sea Level Cycles on Strontium in

Seawater. *Geochimica et Cosmochimica Acta*, *62*(7), 1107–1118. https://doi.org/10.1016/S0016-7037(98)00042-8

Strickland, J. D. H., & Parsons, T. R. (1972). *A Practical Handbook of Seawater Analysis*. *Bulletin 167*. https://doi.org/10.1002/iroh.19700550118

Stukel, M. R., Aluwihare, L. I., Barbeau, K. A., Chekalyuk, A. M., Goericke, R., Miller, A. J., et al. (2017). Mesoscale ocean fronts enhance carbon export due to gravitational sinking and subduction. *Proceedings of the National Academy of Sciences*, *114*(6), 1252–1257. https://doi.org/10.1073/pnas.1609435114

Stukel, M. R., Song, H., Goericke, R., & Miller, A. J. (2018). The role of subduction and gravitational sinking in particle export, carbon sequestration, and the remineralization length scale in the California Current Ecosystem. *Limnology and Oceanography*, *63*(1), 363–383. https://doi.org/10.1002/lno.10636

Suess, E. (1980). Particulate organic carbon flux in the oceans—surface productivity and oxygen utilization. *Nature*, *288*(5788), 260–263. https://doi.org/10.1038/288260a0

Sverdrup, H. U. (1953). On Conditions for the Vernal Blooming of Phytoplankton. *ICES Journal of Marine Science*, *18*(3), 287–295. https://doi.org/10.1093/icesjms/18.3.287

Swanberg, N. R., & Caron, D. A. (1991). Patterns of sarcodine feeding in epipelagic oceanic plankton. *Journal of Plankton Research*, *13*(2), 287–312. https://doi.org/10.1093/plankt/13.2.287

Sweeney, E. N., McGillicuddy, D. J., & Buesseler, K. O. (2003). Biogeochemical impacts due to mesoscale eddy activity in the Sargasso Sea as measured at the Bermuda Atlantic Time-series Study (BATS). *Deep Sea Research Part II: Topical Studies in Oceanography*, *50*(22–26), 3017–3039. https://doi.org/10.1016/j.dsr2.2003.07.008

Takahashi, K., & Be, A. W. H. (1984). Planktonic foraminifera: factors controlling sinking speeds. *Deep Sea Research Part A. Oceanographic Research Papers*, *31*(12), 1477–1500. https://doi.org/10.1016/0198-0149(84)90083-9

Takahashi, K., & Honjo, S. (1983). Radiolarian skeletons: size, weight, sinking speed, and residence time in tropical pelagic oceans. *Deep Sea Research Part A. Oceanographic Research Papers*, *30*(5), 543–568. https://doi.org/10.1016/0198-0149(83)90088-2

Takahashi, T., Sutherland, S. C., Sweeney, C., Poisson, A., Metzl, N., Tilbrook, B., et al. (2002). Global sea–air CO2 flux based on climatological surface ocean pCO2, and seasonal biological

and temperature effects. *Deep Sea Research Part II: Topical Studies in Oceanography*, *49*(9–10), 1601–1622. https://doi.org/10.1016/S0967-0645(02)00003-6

Takahashi, T., Sutherland, S. C., Wanninkhof, R., Sweeney, C., Feely, R. A., Chipman, D. W., et al. (2009). Climatological mean and decadal change in surface ocean pCO2, and net sea–air CO2 flux over the global oceans. *Deep Sea Research Part II: Topical Studies in Oceanography*, *56*(8–10), 554–577. https://doi.org/10.1016/j.dsr2.2008.12.009

Thomalla, S. J., Poulton, A. J., Sanders, R., Turnewitsch, R., Holligan, P. M., & Lucas, M. I. (2008). Variable export fluxes and efficiencies for calcite, opal, and organic carbon in the Atlantic Ocean: A ballast effect in action? *Global Biogeochemical Cycles*, *22*(1), n/a-n/a. https://doi.org/10.1029/2007GB002982

Turner, J. (2002). Zooplankton fecal pellets, marine snow and sinking phytoplankton blooms. *Aquatic Microbial Ecology*, *27*, 57–102. https://doi.org/10.3354/ame027057

Våge, K., Pickart, R. S., Thierry, V., Reverdin, G., Lee, C. M., Petrie, B., et al. (2009). Surprising return of deep convection to the subpolar North Atlantic Ocean in winter 2007–2008. *Nature Geoscience*, *2*(1), 67–72. https://doi.org/10.1038/ngeo382

Valdes, J. R., & Price, J. F. (2000). A Neutrally Buoyant, Upper Ocean Sediment Trap. *Journal of Atmospheric and Oceanic Technology*, *17*(1), 62–68. https://doi.org/10.1175/1520-0426(2000)017<0062:ANBUOS>2.0.CO;2

Villa-Alfageme, M., de Soto, F., Le Moigne, F. A. C., Giering, S. L. C., Sanders, R., & García-Tenorio, R. (2014). Observations and modeling of slow-sinking particles in the twilight zone. *Global Biogeochemical Cycles*, *28*(11), 1327–1342. https://doi.org/10.1002/2014GB004981

Villa-Alfageme, M., de Soto, F. C., Ceballos, E., Giering, S. L. C., Le Moigne, F. A. C., Henson, S., et al. (2016). Geographical, seasonal, and depth variation in sinking particle speeds in the North Atlantic. *Geophysical Research Letters*, *43*(16), 8609–8616. https://doi.org/10.1002/2016GL069233

de Villiers, S. (1999). Seawater strontium and Sr/Ca variability in the Atlantic and Pacific oceans. *Earth and Planetary Science Letters*, *171*(4), 623–634. https://doi.org/10.1016/S0012-821X(99)00174-0

Volk, T., & Hoffert, M. I. (1985). Ocean Carbon Pumps: Analysis of Relative Strengths and Efficiencies in Ocean-Driven Atmospheric CO 2 Changes. In *The carbon cycle and atmospheric CO2: Natural variations archean to present* (Vol. 32, pp. 99–110). Washington,

DC: American Geophysical Union. https://doi.org/10.1029/GM032p0099

Waite, A. M., Stemmann, L., Guidi, L., Calil, P. H. R., Hogg, A. M. C., Feng, M., et al. (2016). The wineglass effect shapes particle export to the deep ocean in mesoscale eddies. *Geophysical Research Letters*, *43*(18), 9791–9800. https://doi.org/10.1002/2015GL066463

Waniek, J., Koeve, W., & Prien, R. D. (2000a). Trajectories of sinking particles and the catchment areas above sediment traps in the northeast Atlantic. *Journal of Marine Research*, *58*(6), 983–1006. https://doi.org/10.1357/002224000763485773

Waniek, J., Koeve, W., & Prien, R. D. (2000b). Trajectories of sinking particles and the catchment areas above sediment traps in the northeast Atlantic. *Journal of Marine Research*, *58*(6), 983–1006. https://doi.org/10.1357/002224000763485773

Waniek, J., Schulz-Bull, D. E., Kuss, J., & Blanz, T. (2005). Long time series of deep water particle flux in three biogeochemical provinces of the northeast Atlantic. *Journal of Marine Systems*, *56*(3–4), 391–415. https://doi.org/10.1016/j.jmarsys.2005.03.001

Waniek, J. J., Schulz-Bull, D. E., Blanz, T., Prien, R. D., Oschlies, A., & Müller, T. J. (2005). Interannual variability of deep water particle flux in relation to production and lateral sources in the northeast Atlantic. *Deep Sea Research Part I: Oceanographic Research Papers*, *52*(1), 33–50. https://doi.org/10.1016/j.dsr.2004.08.008

Waniek, J. J., Schulz-Bull, D. E., Kuss, J., & Blanz, T. (2005). Long time series of deep water particle flux in three biogeochemical provinces of the northeast Atlantic. *Journal of Marine Systems*, *56*(3–4), 391–415. https://doi.org/10.1016/j.jmarsys.2005.03.001

Ward, B. A., Dutkiewicz, S., & Follows, M. J. (2014). Modelling spatial and temporal patterns in size-structured marine plankton communities: top–down and bottom–up controls. *Journal of Plankton Research*, *36*(1), 31–47. https://doi.org/10.1093/plankt/fbt097

Wassmànn, P. (1998). Retention versus export food chains: Processes controlling sinking loss from marine pelagic systems. *Hydrobiologia*, *363*, 29–57. https://doi.org/10.1023/A:100311340

Weber, T., Cram, J. A., Leung, S. W., DeVries, T., & Deutsch, C. (2016). Deep ocean nutrients imply large latitudinal variation in particle transfer efficiency. *Proceedings of the National Academy of Sciences*, *113*(31), 8606–8611. https://doi.org/10.1073/pnas.1604414113

Wekerle, C., Krumpen, T., Dinter, T., von Appen, W.-J., Iversen, M. H., & Salter, I. (2018). Properties of Sediment Trap Catchment Areas in Fram Strait: Results From Lagrangian Modeling and Remote Sensing. *Frontiers in Marine Science*, *5*(November).

https://doi.org/10.3389/fmars.2018.00407

Wilks, J. V., Rigual-Hernández, A. S., Trull, T. W., Bray, S. G., Flores, J.-A., & Armand, L. K. (2017). Biogeochemical flux and phytoplankton succession: A year-long sediment trap record in the Australian sector of the Subantarctic Zone. *Deep Sea Research Part I: Oceanographic Research Papers*, *121*(December 2016), 143–159. https://doi.org/10.1016/j.dsr.2017.01.001

Wong, C. S., Whitney, F. A., Crawford, D. W., Iseki, K., Matear, R. J., Johnson, W. K., et al. (1999). Seasonal and interannual variability in particle fluxes of carbon, nitrogen and silicon from time series of sediment traps at Ocean Station P, 1982–1993: relationship to changes in subarctic primary productivity. *Deep Sea Research Part II: Topical Studies in Oceanography*, *46*(11–12), 2735–2760. https://doi.org/10.1016/S0967-0645(99)00082-X

Woods, J. (1988). Scale Upwelling and Primary Production. In B. J. Rothschild (Ed.), *Toward a Theory on Biological-Physical Interactions in the World Ocean* (pp. 7–38). Dordrecht: Springer Netherlands. https://doi.org/10.1007/978-94-009-3023-0_2

Yashayaev, I., & Clarke, A. (2008a). Evolution of North Atlantic Water masses inferred from Labrador Sea salinity series. *Oceanography*, *21*(SPL.ISS. 1), 30–45. https://doi.org/10.5670/oceanog.2008.65

Yashayaev, I., & Clarke, A. (2008b). Evolution of North Atlantic Water Masses Inferred from Labrador Sea Salinity Series. *Oceanography*, *21*(1), 30–45. https://doi.org/10.5670/oceanog.2008.65

Yool, A., Popova, E. E., & Anderson, T. R. (2011). Medusa-1.0: a new intermediate complexity plankton ecosystem model for the global domain. *Geoscientific Model Development*, *4*(2), 381–417. https://doi.org/10.5194/gmd-4-381-2011

Yool, A., Popova, E. E., & Anderson, T. R. (2013). MEDUSA-2.0: An intermediate complexity biogeochemical model of the marine carbon cycle for climate change and ocean acidification studies. *Geoscientific Model Development*, *6*(5), 1767–1811. https://doi.org/10.5194/gmd-6-1767-2013

Yu, E.-F., Francois, R., Bacon, M. ., Honjo, S., Fleer, A. ., Manganini, S. ., et al. (2001). Trapping efficiency of bottom-tethered sediment traps estimated from the intercepted fluxes of and. *Deep Sea Research Part I: Oceanographic Research Papers*, *48*(3), 865–889. https://doi.org/10.1016/S0967-0637(00)00067-4